Ablation on the ice cap of King George Island (Antarctica)

- an approach from field measurements, modelling and remote sensing -

---

Doctoral thesis

at the

Faculty of Earth Sciences

Albert–Ludwigs–Universität Freiburg i. Br.

submitted by

Matthias Braun

from Riedlingen/Württ.

2001

Dekan: Prof. Dr. J. Behrmann

Referent: Prof. Dr. H. Goßmann

Koreferent: Prof. Dr. G. Menz

Tag der Beschlußfassung des Promotionsausschuses 12. Juli 2001

Acknowledgements

I am greatly indebted to many people who gave advice and support in the course of this study and during the field work in Antarctica.

First of all, I would like to thank my supervisor, Prof. Hermann Goßmann, who provided an unconstrained workaround at the *Institut für Physische Geographie*, giving me all freedom to pursue any question, idea and problem arising during this work. He enabled my participation in four field campaigns on King George Island as well as on the Antarctic Peninsula and supported my attendance of several national and international conferences. I highly appreciate this confidence in autonomous work which was not only extremely motivating and stimulating, but also enabled me to present this study to a broader scientific community and to build up international contacts. Furthermore, I would like to thank the Prof. Gunter Menz who kindly agreed to act as second supervisor of this work.

During the entire course of this work, my colleagues Frank Rau, Steffen Vogt and Dr. Helmut Saurer stimulated my activities. Their scientific advise and refreshing enthusiasm, even over long distances, provided a great deal of motivation and encouragement. Thanks for the many hours of discussion on specific problems of this work, assistance and help in the preparation of and during field work, proof reading or just for having a beer after a long day.

Antarctic field campaigns are always an international business and so I would like to express my gratitude to Dr. Jefferson Simões (*Laboratório de Pesquisas Antárticas e Glaciológicas* (LAPAG), Porto Alegre, Brazil) who not only provided the embedding of this work in the international framework of the SCAR program 'Glaciology of the South Shetland Islands', but also the logistics backbone of this research via his project in the Brazilian Antarctic Program. Moreover, he was always open for a fruitful discussion on glaciological problems on King George Island and helped with his profound knowledge of the island. Continuing with LAPAG personnel, I want to send

a big HUG to Chico and Ulisses, my custom, logistic, communication and data specialists in Porto Alegre or Antarctica. Without their skills and talents many activities would have been a lot more difficult or even impossible. Finally, the nice companionship of Helo, Charlotte, Ferron, Jorge and Dakir completed the favourable LAPAG team and guaranteed for a high degree of Brazilian 'Samba and Ska' atmosphere in the camp. I am very grateful to Dr. Jandyr Travassos (*Observatótio Nacional*, Rio de Janeiro, Brazil) for our open-minded discussions on whatever topic and his efforts to integrate us Germans in the group during the 3 field seasons on King George Island. Dr. Alberto Setzer (*Instituto Nacional de Pequisas Espaciales*, São Jose dos Campos, Brazil), responsible for the meteorological program at the Brazilian Antarctic station Commandante Ferraz, kindly provided data and helped with his weather forecasts during field work.

In particular, I would like to thank my friends, Rosita, Bareta, Marcelo and Bajo from the *Club Alpino Paulista*, who did not only unrestrictedly support any necessary and unnecessary activity in field, but were always open for every alpinistic challenge and excursion and became very good friends. I will always remember the unforgettable hours we spent in the tent, on the skidoo or waiting in the King George Island typical white-out for the GPS to measure only one blooming velocity stake after one hour.

Marion Pfender and Dr. Norbert Blindow from the *Universität Münster* kindly provided data and figures from their detailed DGPS and radio echo sounding surveys and strongly contributed to the charming atmosphere during the 1997/98 field season.

I do not want to end this list before thanking Dr. Regine Hock *(Climate Impact Research Centre*, Kiruna, Sweden) for her tremendous support with her energy balance software package and validation programs. Her critical comments on parts of the manuscript were very helpful and significantly improved this work. Furthermore, I would like to thank her for hosting me during a fortnight in Kiruna and visiting me in Freiburg for a model update and discussion.

I am very grateful to Frank Weber, Andrea Morgan (both Vancouver, Canada), Thomas Püstow (St. Johns, N.F., Canada) and Paul Sterzel (Freiburg) spending lots of time on this manuscript for English proof-reading.

At IPG, another long list of people, too numerous to mention, assisted me in one way or the other and contributed to the pleasant academic environment. I am indebted to Dr. Klaus Braun, who always had an open channel and fast solution for my computer and software problems. I would like to extend my gratitude to Dr. Hans-Peter Thamm for continuously encouraging me, having an open door for any PV-Wave problems and never stopping keeping me at good humour. Similarly, I will not forget the hours preparing and inventorying the DYPAG instruments for field work together with Dirk Beppler in summer 1997. The field season 1999/2000 was facilitated by the assistance of Martin Pichlmaier, who maintained and prepared instrumentation and especially contributed to the warm atmosphere in the glacier camp. Friedemann Heusel patiently responded to my never ending questions while taking my first steps

with ARC/info. Dr. Christoph Schneider kindly provided the source code of his energy balance model and data from his energy balance calculations near the Argentine Station San Martín.

Finally, I would like to thank my parents who continuously encouraged me, although my long stays down under were not always easy for them.

This work was financed by the *Deutsche Forschungsgemeinschaft* under the projects '*Die Erfassung des Schmelzverhaltens der Schneedecke und die Ableitung subglazialer Schmelzwasserströme der subantarktischen Eiskappe King George Islands unter dem Einsatz klimatologischer, schneehydrologischer und EMR-Geländedaten sowie von Fernerkundungsaufnahmen (KIGEIS)'* and '*Gletscher-monitoring auf der Antarktischen Halbinsel und angrenzender Gebiete mit Satelliten-daten (GLAS)'* (contracts # SA 694/1-1/2 and SA 694/2-1). ERS-1/2 satellite imagery was provided within the ESA projects 'Monitoring Dynamic Processes in Antarctic Geosystems' (contract # AO2.148) and 'Midterm monitoring of snow cover characteristics by ERS-SAR imagery on the Antarctic Peninsula' (contract # AO3.196). The *Wissenschaftliche Gesellschaft* of the *Universität Freiburg* partially funded a visit to the libraries and archives of the British Antarctic Survey and the Scott Polar Research Institute as well as a conference attendance in Nice, France.

The Royal Meteorological Society, the British Antarctic Survey, the International Glaciological Society and the European Association of Remote Sensing Laboratories are acknowledged for granting the permission to reprint previously published material in this thesis.

Abstract

Snow and ice melt is a considerable mass balance parameter for glacial systems at the northern margin of the Antarctic continent, in particular on the northern Antarctic Peninsula. On the background of various indications for on-going climatic and glacial changes in this region, such as significant air temperature increase, changes in the precipitation regime, glacier retreat or the disintegration of ice shelves, ablation during summer seasons on the King George Island ice cap was investigated. To achieve these objectives different methodological approaches were combined and the present glaciological and climatological knowledge of the ice cap compiled.

The work focuses on the modelling of the surface energy exchange between the atmosphere and the snow surface. Therefore, the energy balance components were computed from hourly meteorological data obtained during three summer field campaigns in the years 1995/96, 1997/98 and 1999/2000 for sites at different altitudes on the ice cap. Net radiation was measured directly, and turbulent fluxes were calculated according to the aerodynamic bulk approach. The large-scale atmospheric weather patterns were derived from NOAA-IR composites and surface pressure charts. The ablation rates for the entire ice cap were estimated using a sensitivity analysis of a spatially distributed energy balance model. To obtain information on the snowmelt patterns during time periods without direct measurements, a multi-year data archive of ERS-1/2 data was evaluated.

In the period from 02 December 1997 to 12 January 1998, net radiation contributed to snowmelt with a mean value of 22.5 W m^{-2} (AWS1, 85 m a.s.l., 1997/98). Heat supplied by sensible heat flux (9.5 W m^{-2}) was far more important as by the latent heat flux (–1.1 W m^{-2}). A distinct influence of the prevailing synoptic circulation on the energy exchange could be determined. Highest ablation rates were recorded during northerly to northwesterly advection of warm humid air masses. Maximum ablation rates reached more than 20 mm d^{-1} in lowest elevations. Almost no snowmelt

occurred when dry and cold air came from southerly to southeasterly directions. Within the altitude range of the ice cap (0 to 705 m a.s.l.), a strong dependence of energy balance terms on elevation was found. Snow cover in areas higher than 500 m a.s.l. is only wetted by very strong frontal advection events. This is in good agreement with the results from the evaluation of the SAR imagery on which frequent refreezing above this altitude could be observed. Similarly, the outcomes of a comprehensive ground penetrating radar survey show a marked decrease of melt water percolation in areas higher than about 500 m a.s.l..

In comparison to other sites on the Antarctic Peninsula, ablation rates on King George Island are comparably high. Within the 6-weekly measuring periods in 1997/98 and 1999/2000, the snow cover was almost completely depleted. Extrapolating the measured values for these years over the corresponding ablation period (December-March), an ablation rate of 1,100 mm WE would result for the 1997/98 and 1,150 mm WE for the 1999/2000 season. This is almost double the ablation rates reported for the 1970s at similar locations. It has to be kept in mind that the values might be even higher when the ablation increase due to albedo reduction over appearing bare glacier ice were to be considered. This supports the results from the analysis of the satellite imagery on which a rise of the firn line in the 1990s is indicated. Furthermore, the increased mass loss would be a suitable explanation for the enormous retreat of small glaciers on the island since the 1950s.

The spatially distributed modelling showed a high sensitivity towards the choice of air temperature lapse rate. When no concurrent data is used, ablation rates can only be achieved if lapse rates are assumed to be considerably lower than those reported by several authors based on the analysis of station data and snow temperatures. This again reveals that for this area, the strong influences of the prevailing synoptic conditions on the melt process have to be considered. Based on the data set from 1997/98 and the assumption of a 2 K air temperature increase, ablation on the King George Island ice cap would increase by about 60%. This underscores the high sensitivity of the ice cap towards future climatic changes as reported previously by other authors.

The achieved results and the compiled database of this work enable a multitude of future research topics that are summarised in the outlook of this thesis.

Zusammenfassung

Schnee- und Eisschmelze ist für glaziale Systeme am Nordrand der Antarktis, insbesondere im Bereich der nördlichen Antarktischen Halbinsel, ein wichtiger Massenhaushaltsparameter. Im Hinblick auf die vielen Anzeichen für aktuelle klimatische und glaziologische Veränderungen in dieser Region, wie z.B. signifikante Temperaturanstiege, Änderungen im Niederschlagsregime, vielerorts zu beobachtende Gletscherrückzüge sowie dem Zerfall von Eisschelfen, wurde die Ablation während sommerlicher Schmelzperioden auf King George Island unter Einsatz verschiedener Verfahren untersucht. Ferner wurde der aktuelle glaziologische und klimatologische Kenntnisstand über die Eiskappe zusammengestellt.

Der Schwerpunkt der Arbeit liegt auf der Modellierung des Energieaustausches zwischen der Atmosphäre und der Schneeoberfläche. Hierfür wurden aus meteorologischen Datensätzen von sommerlichen Feldkampagnen aus den Jahren 1995/96, 1997/98 und 1999/2000 die Energiebilanzkomponenten und die Schneeschmelze an den Meßstandorten in verschiedenen Höhenlagen berechnet. Die Strahlungsbilanz wurde direkt gemessen und die turbulenten Wärmeströme über die sogenannte ‚aerodynamic bulk approach' bestimmt. Die synoptische Situationen wurden aus NOAA-IR Kompositen und Bodenluftdruckkarten abgeleitet. Mittels einer Sensitivitätsanalyse eines räumliche Energiebilanzmodells konnte die Ablationsmengen der gesamten Eiskappe abgeschätzt werden. Um Informationen über die Schneeschmelze in Zeiträumen, in denen keine Abdeckung mit meteorologischen Feldmessungen vorhanden waren, zu erhalten, wurde ein mehrjähriges Archiv von ERS-1/2 SAR Satellitenbildern ausgewertet.

Im Meßzeitraum vom 02.12.1997 bis 12.01.1998 trug die Strahlungsbilanz im Mittel mit 22.5 W m^{-2} (AWS1, 85 m, 1997/98) zur Schneeschmelze bei. Der Wärmeeintrag über sensiblen Wärmestrom war mit 9.5 W m^{-2} deutlich bedeutsamer als durch den latenten Wärmefluss mit –1.1 W m^{-2}. Es konnte ein bedeutender Einfluß der groß-

räumigen Wetterlage auf den Energiehaushalt und die vertikalen Temperaturgradienten festgestellte werden. Die höchsten Ablationsraten waren während nördlicher bis nordwestlicher Advektion von warmen, maritimen Luftmassen zu verzeichnen. Die maximalen Ablationsraten überstiegen dabei 20 mm d^{-1} in den tiefsten Lagen der Eiskappe. Bei überwiegend südlicher bis südöstlicher Anströmung mit vergleichsweise kalten und trockenen Luftmassen trat hingegen fast keine Schneeschmelze auf. Innerhalb der Höhenausdehnung der Eiskappe (0-705 m) ist eine starke Abhängigkeit der Energiebilanzkomponenten von der Meereshöhe feststellbar. Die Schneedecke in den höheren Lagen (>500 m) wird nur während starker Advektionsereignisse durchfeuchtet. Dies ist in sehr guter Übereinstimmung mit den Auswertungen der Radarbilder, wo in den höheren Bereichen häufig ein Wiedergefrieren der Schneedecke festgestellt werden konnte. Radioecholot-Untersuchungen der internen Strukturen der Eiskappe zeigen ebenfalls eine deutlich geringeren Schmelzwassereinfluß in diesen Höhenlagen.

Im Vergleich zu anderen Meßstandorten auf der Antarktischen Halbinsel zählen die gemessenen Ablationsraten auf King George Island zu den höchsten im Bereich der Antarktischen Halbinsel. Innerhalb der jeweils 6-wöchigen Feldkampagnen in den Südsommern 1997/98 und 1999/2000 wurde die Schneedecke in den tiefsten Lagen der Eiskappe fast komplett abgebaut. Extrapoliert man die gemessenen Werte dieser Jahre auf die gesamte Ablationsperiode, so ergibt sich für das Jahr 1997/98 eine Ablationsrate von 1100 mm WE und für 1999/2000 1150 mm WE. Dies ist etwa das doppelte der in den 70-er Jahren ermittelten Ablationsraten an gleicher Stelle, wobei verstärkte Schmelze durch die geringere Albedo nach der Ausaperung des Gletschers hierbei noch nicht berücksichtigt ist. Diese Resultate stützen die Ergebnisse der Radarfernerkundung, die einen Anstieg der Firnlinie in den 90-er Jahren nahe legen. Ferner würde solch erhöhter Massenverlust eine plausible Erklärung für den starken Rückzug kleiner Gletscher auf King George Island leisten.

Die räumliche Modellierung zeigt eine hohe Sensitivität der Ablationsraten gegenüber der Wahl der vertikalen Temperaturgradienten. Werden keine in-situ Daten verwendet, können die Ablationsraten nur nachgezeichnet werden, wenn deutlich geringere Gradienten als die aus Stationsdaten und Schneetemperaturen abgeleiteten Werte verwendet werden. Hierbei zeigt sich erneut, daß der Einfluß der vorherrschenden Wetterlage auf den Ablationsprozeß in diesem Raum berücksichtigt werden muss. Basierend auf dem Datensatz von 1997/98 und der Annahme, daß sich nur die Lufttemperatur um 2 K erhöhen würde, wurde eine Steigerung der Ablation von etwa 60% für das gesamte Untersuchungsgebiet abgeschätzt. Dies unterstreicht die bereits von anderen Autoren eingestufte hohe Klimasensitivität der Eiskappe.

Die Rahmen dieser Arbeit erzielten Ergebnisse und die Zusammenstellung von Datenmaterial bieten eine Vielzahl von Anknüpfungspunkte für weitere Studien die in einem Ausblick zusammengetragen wurden.

Contents

Index of tables

Index of figures

Abbreviations

AAR	Accumulation Area Ratio
ACC	Antarctic Circumpolar Current
ACW	Antarctic Circumpolar Wave
AMI	Active Microwave Instrument onboard the ERS satellites
AOI	Areas Of Interest
AP	Antarctic Peninsula
AVHRR	Advanced Very High Resolution Radiometer
AWI	*Alfred-Wegener-Institut für Polar- und Meeresforschung*
AWS	Automatic Weather Station
BAS	British Antarctic Survey
BASM	Base Antártica San Martín
BI	bare ice radar zone
CFLA	Climatic Firn Line Altitude
CSIRO	Global Climate Model of the Commonwealth Scientific and Industrial Research Organisation
DEM	Digital Elevation Model
DGPS	Differential Global Positioning System
DI	Deception Island
DS	Dry snow radar zone
EAP	East Antarctic Peninsula
ECHAM4/OPYC3	Global Climate Model of the *Max-Planck-Institut* in Hamburg
ECMWF	European Centre of Medium Range Weather Forecast

ELA	Equilibrium Line Altitude
ENSO	El Niño/Southern Oscillation
ENVISAT	Future SAR remote sensing satellite to be launched by ESA in 2001
ERS-1/2	European Radar Satellites
ESA	European Space Agency
FIDASE	Falkland Island Dependency Aerial Survey Expedition
FLA	Firn Line Altitude
FP	Frozen percolation radar zone
GARS	German Antarctic Receiving Station at the Chilean base O'Higgins on the northern tip of the Antarctic Peninsula
GCM	Global Climate Model
GPR	Ground Penetrating Radar = Radio Echo Sounding (RES)
HADCM2	Global Circulation Model of the U.K. Meteorological Office Hadley Centre
IGM	*Institut für Geophysik* of the *Universität Münster*
IGY	International Geophysical Year
IPCC	Intergovernmental Panel of Climate Change
IPG	*Institut für Physische Geographie* of the *Universität Freiburg*
IS92A	Climate change scenario for sensitivity studies of global climate model runs (2 K temperature increase between 1990 and 2100)
J-ERS	Japanese Radar Satellite
JRI	James Ross Island
KGI	King George Island
LANDSAT MSS	LANDSAT Multi-Spectral Scanner. Optical satellite system operated by the US National Aeronautics and Space Administration (NASA) between 1972 and 1978.
LANDSAT TM	LANDSAT Thematic Mapper. Optical satellite system operated by the US National Aeronautics and Space Administration (NASA) since 1982 onboard various spacecrafts.
LAPAG	*Laboratório de Pesquisas Antárticas e Glaciológicas, Universidade Federal do Rio Grande do Sul*, Porto Alegre, Brazil
LI	Livingston Island
LTER	Palmer Long Term Research study area
M2	Sea level pressure index to measure the strength of the meridional circulation on the west Antarctic Peninsula based on the pressure difference between 75°W and 60°W at 65°S (latitude of Faraday/Vernadsky station)

NCAR/NCEP	National Centers for Environmental Prediction/National Center for Atmospheric Research
NOAA AVHRR	Advanced very high resolution radiometer carried by the American NOAA (National Oceanographic and Atmospheric Administration) series of satellites
	or phase 2 melt radar glacier zone
P2 or M2	metamorphosed wet snow radar zone
PI	Penguin Island
PRI	ERS Precision Image (amplitude image)
RADARSAT	Canadian radar satellite system is funded by the Canadian Space Agency in co-operation with NASA and NOAA
RES	Radio Echo Sounding = Ground Penetrating Radar (GPR)
SAO	Semi-Annual Oscillation
SAR	Synthetic Aperture Radar
SCAR	Scientific Committee on Antarctic Research
SOI	Southern Oscillation Index
SPOT HRV	*Satellite Pour l'Observation de la Terre*, high resolution visible. Multi-spectral, optical satellite system with 20 m ground resolution operated by the French Space Agency
SST	Sea surface temperatures
THIR	Temperature Humidity Infrared Radiometer
TPI	Trans-Polar-Index (pressure difference between Hobbart and Port Stanley)
WAP	West Antarctic Peninsula region
WCRP	World Climate Research Programme [The objectives of the programme are to develop the fundamental scientific understanding of the physical climate system and climate processes needed to determine to what extent climate can be predicted and the extent of man's influence on climate (http://www.wmo.ch/web/wcrp/about.htm, 2000)]
WE	Snow Water Equivalent
WGG	SCAR Working Group on Glaciology
WG-GGI	SCAR Working Group on Geodesy and Geographic Information
WS	wet snow radar zone

Symbols

A	Dimensionless transfer coefficient
a_1=0.005, a_2=-1.1 and a_3=0.02	Coefficients
c_p	Specific heat capacity at constant pressure
c_W	Specific heat of water
D	Diffuse radiation
D_S	Direct part of shortwave radiation
D_t	Diffuse part of shortwave radiation by backscattering
G	Global radiation
h	Solar hour angle
h_{rms}	Average height variations
I	Direct beam short-wave radiation (I), flux density at the surface
I_0	Extraterrestrial solar radiation
I_i	Direct beam short-wave radiation, flux density normal to the beam
I_i	Flux density normal to the beam
K_E	Eddy diffusivity for water vapour
K_H	Eddy diffusivity for heat
K_M	Eddy diffusivity for momentum
L	Monin-Obukhov length
L_f	Latent heat of fusion for ice ($3.34 \cdot 10^5$ J kg^{-1})
L_S	Latent heat of sublimation ($2.849 \cdot 10^6$ J kg^{-1})

L_V	Latent heat of evaporation ($2.514 \cdot 10^6$ J kg^{-1})
L_V	Latent heat of evaporation or sublimation
$L_S^{\downarrow}$	Denoting the longwave sky radiation
$L^{\uparrow}$	Emitted long-wave radiation in W m^{-2}
$L_t^{\downarrow}$	Longwave terrain radiation
M	Melt
n_d	Number of days since snowfall
P	Atmospheric pressure
P_s	Snow precipitation
q	Specific humidity
Q_E	*L*atent heat flux
Q_G	*C*hange of heat in the vertical column of the snow pack
Q_H	*S*ensible heat transfer
Q_M	*E*nergy available for melt
Q_N	*N*et radiation
Q_R	*H*eat supplied by rain
R	Eccentricity correction factor of the earth's orbit
R	Rrainfall rate
Rb	Bulk Richardson number (*Rb*)
S	Solar constant (1368 W m^{-2})
T	Absolute temperature (K)
T	Air temperature,
T	Snow/ice temperature
t	Time
ToA	Top of the atmosphere radiation
T_R	Temperature of rain
T_S	Surface temperature
T_S	Surface temperature
u	Wind speed
u^*	Friction velocity
z	Height

Z	Zenith angle
z_0	Surface roughness length for momentum
z_{0E}	Surface roughness lengths for latent heat
z_{0T}	Surface roughness lengths for sensible heat
α	Albedo
α_{t1}	Starting values of snow albedo (
α_{t2}	Snow albedo
β	Angle between the beam and the normal of the surface
B	Slope angle
γ	Look angle
δ	Declination
ε_s	Emissivity (old snow: 0.82, fresh snow: 0.99; OKE, 1987)
Θ	Angle between the beam and the normal of the surface
Θ	Angle of incidence between the normal to the slope and the solar beam
Θ	Potential temperature
κ	Dimensionless von Kármán constant (0.4)
λ	Wavelength
ρ	Density of air
ρ'	Density of the medium
ρ_w	Density of water
σ	Stefan Boltzmann constant ($5.67 \cdot 10^{-8}$ W m^{-2} K^{-4})
τ	Shear stress in the air above the surface
Φ	Geographic latitude
Ω	Solar azimuth angle

1 Introduction

1.1 Study purpose

In the last years, uncertainties in the determination of the contribution of Antarctic ice to global sea level rise have been subject to intense discussion, not only in the scientific community, but also in public. Complex models, new remote sensing techniques, rapidly increasing computing power and strengthened international co-operations have expanded the understanding of Antarctic ice masses and their role in the global climate system. However, due to its remoteness and the difficult accessibility, still many open questions remain. The problems in determining the actual state and in predicting impacts of global warming on Antarctic ice masses result from the lack of accurate information on surface mass balance terms. For the glaciers on the northern Antarctic Peninsula, ablation is a major mass balance parameter, and hence the knowledge of ablation rates is a prerequisite for sensitivity studies. It is the objective of this work to study the present state of the King George Island ice cap, with special focus on snowmelt dynamics and ablation. The location of King George Island (58°W / 62°S) and the comparably easy accessibility throughout the year led to the selection of this site for a case study for other sub-Antarctic islands and the northern Antarctic Peninsula.

The following questions form the backbone of this work and shall guide through the following chapters:

- *Why is it important to study Antarctica's climate and ice masses? Why in particular small glaciers and ice caps surrounding Antarctica?*
- *Are there any indications for on-going climatic and glacial changes in the study area and adjacent regions?*
- *What is the present state of the King George Island ice masses?*

- *What are the ablation rates in the different elevations of the ice cap, and which processes trigger snowmelt on King George Island?*
- *Can the observed snowmelt patterns and ablation rates be linked to certain synoptic weather types?*
- *Are there any interannual variations in ablation rates and patterns detectable and in case, can they be explained?*
- *What is the ice caps sensitivity towards future climatic changes?*
- *Will increased ablation have any impact on local ecosystems?*

As a consequence of these objectives, the methodological approaches of this study comprise the application of a single location and a spatially distributed surface energy balance model. Synoptic-scale weather patterns and their influence on energy balance components and ablation rates will be analysed based on NOAA-IR composites and sea level pressure charts. Moreover, the interannual variations of ablation rates and snowmelt patterns will be derived from radar remote sensing and snowmelt modelling. To achieve these objectives, ground surveys from field campaigns will be combined with new techniques from satellite remote sensing.

1.2 Structure of the work

Chapter 1.3 reviews the scientific context and the motivation to conduct this study. Special attention is given to new possibilities for snow and glacier research resulting from the developments in remote sensing techniques during the last decades, to the role of Antarctica in the global climate system and its contribution to sea level rise as well as to the observed on-going climatic changes in the region of the Antarctic Peninsula and, in particular, on King George Island. The study area is introduced in the following chapter. Section 3 contains an overview of the database the investigation is based on. Information about the accuracy of the respective meteorological measurements is presented in the same section. A comprehensive summary of the glaciological and climatological knowledge on King George Island will be given in chapter 4, whereas a short theoretical outline on SAR remote sensing and the radar glacier zone concept as well as the theoretical and methodological approaches used for the energy balance modelling are the subjects of chapters 5 and 6. The results (chapter 7) are split in several subchapters on point and spatially distributed energy balance modelling, on the influence of large-scale weather systems on the ablation process, on interannual variations and a sensitivity analysis of ablation rates. Moreover, multi-year snowmelt dynamics and ablation patterns as revealed by active radar remote sensing are discussed in this part. Subsequently, a synthesis on glacier melt dynamics on the King George Island ice cap is presented on the background of the different approaches and combined with results from a detailed radio echo sounding survey and previously published data. The work closes

with an outlook from the presented findings to further potential and future needs for scientific investigations in the area.

1.3 Scientific context and motivation

1.3.1 New signals of snow and glacier melt from satellite imagery

Aerial photography has been used in combination with ground surveys for mapping in remote areas like Antarctica since the early 1930s. However, satellite remote sensing in snow-hydrological and glaciological research is a relatively new technique. Sensor improvements, a larger amount of operating satellites and the rapidly increasing computing power during the last two decades have favoured the application of imagery from spaceborne platforms in a variety of scientific areas.

Availability of optical satellite imagery for the region of the Antarctic Peninsula starts in 1962 with satellite photography from the CORONA missions (a formerly classified spying mission). The launch of the first LANDSAT MSS in 1972 preluded the series of very successfully operating, polar-orbiting systems – LANDSAT TM and SPOT. With the launch of the first polar orbiting European Radar Satellite (ERS-1) in 1991 and the operation of the German Antarctic Receiving Station (GARS) on the Antarctic Peninsula near the Chilean base O'Higgins, cloud and sun azimuth independent image acquisition became reality (REINIGER & ZIMMER, 2000). However, as the physical interaction between the active radar beam of a synthetic aperture radar system (SAR) with the surface differs from the signal observed in imagery from optical sensors, these systems reveal complementary information.

In the following, two case studies demonstrate the capabilities of optical and active microwave satellite imagery for snow-hydrological and glaciological investigations. Early applications of this kind of remote sensing data on King George Island formed the initial motivation to observe the snow melt dynamics on the island in more detail (WUNDERLE, 1996).

Melt water originating from glaciers and snow fields induces sediment plumes in the adjacent fjords and bays. These can be detected in the shortwave channel of SPOT XS imagery (e.g. BISHOP ET AL., 1995; NELLIES ET AL., 1998; WUNDERLE, 1996; WUNDERLE & GOßMANN, 1995). Figure 1.1 displays sediment loads as classified from a SPOT scene from 19 February 1988. The spatial distribution of the suspended sediment concentrations is clearly visible. Even very small melt water currents and their related sediment loads can be determined in the images as shown in figure 1.2 for a subset of Potter Cove. As fresh water and sediment loads impact the marine ecosystems, a detailed knowledge of the snowmelt process and the seasonal dynamics is mandatory for coastal ecological research. However, the application of this technique for sub-Antarctic regions has certain restrictions. The reflection recorded at the sensor is an integrated signal over the entire water column of the first decameters. As a consequence the determination of quantitative sediment concen-

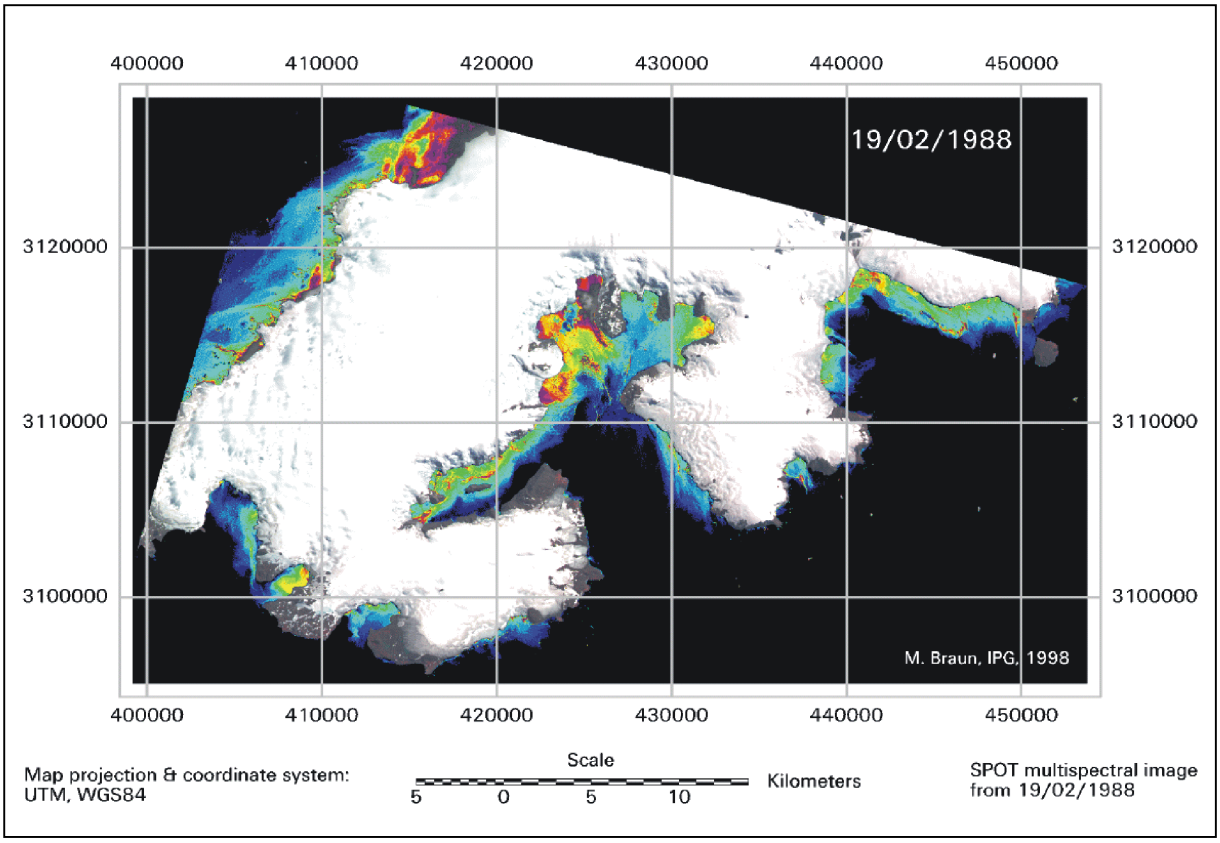

Figure 1.1: *Sediment loads in the coastal ecosystems of King George Island as revealed from a SPOT XS satellite image from 19 February 1988. The location of the island on the Antarctic continent is marked in red colour in the inset map. The coordinates refer to UTM system, Zone 21, WGS84.*

trations is strongly reduced. The frequent cloud coverage in this region inhibits a regular acquisition of high quality imagery and a consequent monitoring of seasonal dynamics. Furthermore, illumination conditions, brash and sea ice concentrations, wind and hydrographic conditions as well as the appropriate choice of sensor gain settings may counteract a proper determination of sediment plumes.

In contrast to optical imagery, the backscatter signal of active microwave sensors is highly sensitive toward the liquid water content and other properties of a snow cover. As a consequence, radar imagery enables the monitoring of seasonal and multi-year snow cover dynamics (e.g. BERNIER, 1987; MÄTZLER, 1987; ROTT & MÄTZLER, 1987; SHI & DOZIER, 1993, 1995; JEZEK ET AL., 1993; ROTT & NAGLER, 1993; DOWDESWELL ET AL., 1994; STROZZI & MÄTZLER, 1995; FORSTER ET AL., 1996; HALLIKAINEN, 1996; WUNDERLE, 1996; MÄTZLER ET AL., 1997; PARTINGTON, 1998; SAURER ET AL., 1998; RAU & SAURER, 1998; KÖNIG ET AL., 2001a). Figure 1.3 shows a multi-temporal colour composite from SAR data of the glacier mass balance year 1996/97 for King George Island. The different colours express changing surface properties between the three acquisition dates. The green colours denote permafrost areas and bare glacier ice in the summer image, blue colours indicate a wetted snow cover in the spring and summer imagery, whereas pink colours can be attributed to a wetting of the snow

cover only in the mid-summer image. Areas with no changes in the backscatter signal are displayed in white colours. A more detailed discussion on the seasonal and multi-year snowmelt dynamic as observable in ERS SAR imagery and how this data can be used to complement ground observations will be given in the chapters 6 and 7.3. Problems in C-band SAR remote sensing of snow and ice covers still exist in the exact determination of glacier mass balance related parameters such as the equilibrium line altitude or the dry snow line (MARSHALL ET AL., 1995; KELLY ET AL., 1997; HALL ET AL., 2000; RAU & BRAUN , submitted; KÖNIG ET AL., 2001b; RAU ET AL., 2001). Here, further methodological approaches will have to be developed.

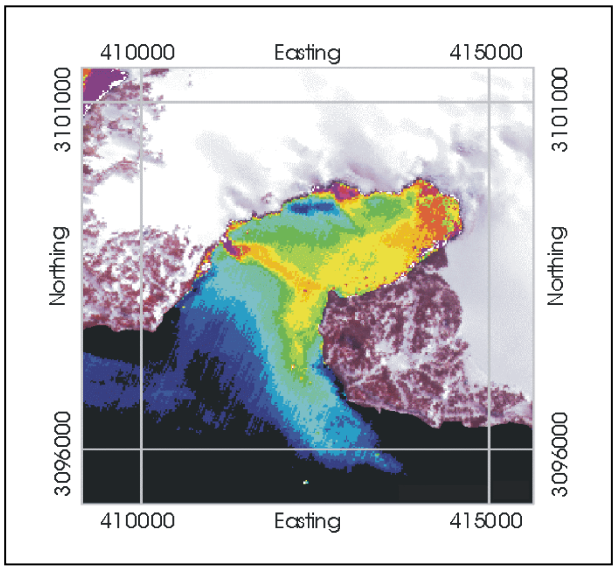

Figure 1.2: *Melt water induced sediment plumes can be determined accurately using the shortwave channel of SPOT XS mutli-spectral scenes. Shown is a subset of Potter Cove for an image from 26 November 1994.*

Moreover, for King George Island the following questions arose form the figures above

- *Can the observed snowmelt dynamics be quantified by ground observations?*
- *Is it possible to explain the amount and locations of the meltwater induced sediment plumes by snowmelt modelling?*

Summary 1.3.1:
Since the mid 1980's, the available high resolution satellite imagery has significantly improved the monitoring of snowmelt dynamics. SPOT imagery enables the detection of sediment loads as a visible consequence of melt processes. However, comparability of the derived results is reduced e.g. due to cloudiness, the lack of compensation for differences in the sensor gain settings during image acquisition, variations in the illumination conditions or ice brash and sea ice concentrations. A calibration to absolute sediment concentrations contains enormous difficulties as a consequence of the integrated signal over the entire superficial water column and other environmental factors. SAR data enables the monitoring of the seasonal development of ablation patterns independent of cloud or illumination influences. However, further research is still required concerning a definite separation of the various snow zones in SAR imagery. The question arose, if the observed melt patterns can be explained by snowmelt modelling and ground observations.

1.3.2 The significance of Antarctica in the global climate system and its representation in global circulation models

The knowledge about the significance of the polar regions in the global climate system has risen since the late 1980s (SCAR, 1993; WCRP, 1998; AWI, 1999). Differences in the land-sea-distribution between the southern and the northern hemisphere lead to strong disparities in the corresponding climatic processes.

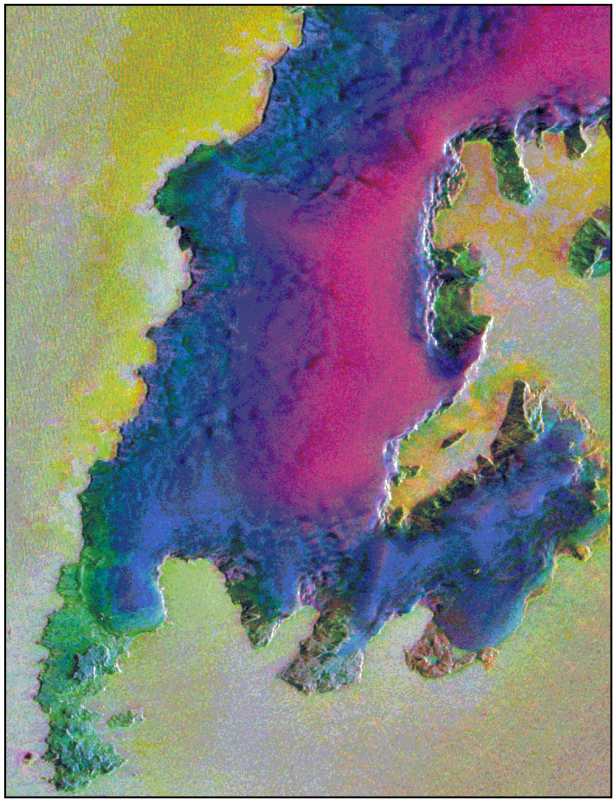

Figure 1.3: *Multi-temporal SAR composite of the western part King George Island with an image showing winter conditions (19 October 1996) in the blue channel, an image starting snow melt in early spring (4 November 1996) in the red channel and a summer scene (29 January 1997) in the green one. The different colours express mainly temporal changes in the liquid water content of the snow cover or changes from snow covered to bare glacier ice or periglacial areas.*

Antarctica is one of the most important heat sinks in the general circulation of the atmosphere. The high elevation of central Antarctica combined with the high albedo of the snow and ice surfaces as well as the enormous extent of sea ice induce a completely different thermal and radiation regime as compared to the northern high latitudes. Stronger equator-pole temperature and pressure gradients in the frontal zone as well as higher wind speeds are a result of this. The gradients lead to an exchange of momentum and energy between the polar and extra-tropical regions. This happens mainly at the polar front via ocean currents and atmospheric circulation. Teleconnections with the extra-polar regions as well as interactions and feedback mechanisms between the atmospheric circulation, the oceans and the cryosphere within Antarctica bring about the high degree of complexity of this climate system and account for Antarctica being one of the key regions triggering global climate.

El Niño/Southern Oscillation (ENSO) is perhaps the most pronounced natural climatic variation on Earth and one of the teleconnections also found in Antarctic climate records. Anomalies of the Southern Oscillation Index (SOI) - the standardised sea level pressure between Tahiti and Darwin (Australia) – involve fluctuations of atmospheric mass across the tropical pacific. These fluctuations are closely linked with ocean currents and sea surface temperatures on the west coast of South America. Resulting cold phases are called “La Niña” and warm phases “El Niño”. Evidence of ENSO teleconnections in the South Pacific extratropical circulation and climate has been ambiguous. In austral winter, raised pressures in the low- and mid-

troposphere west of the Antarctic Peninsula with associated increased blocking have been recorded (e.g. VAN LOON & SHEA, 1987; SINCLAIR, 1996). However, such signatures fail to appear during all ENSO warm events, including the strongest in 1982 (KAROLY, 1989). The statement of KING & TURNER (1997) that during warm ENSO events, a greater exchange of air between the Antarctic and mid-latitudes with warm moist air penetrating into the interior takes place fits in this context. Such situations seem to be responsible for many major precipitation events over the Antarctic plateau and the rapid rise of surface temperatures at the South Pole.

Further mechanisms and teleconnections driving interannual climate variability in Antarctica comprise, i.e.

- seasonal and interannual variations of the sea ice coverage. For instance, sea ice is closely linked to surface air temperatures, cyclogenesis, or Antarctic bottom water formation.
- the *Semi-Annual Oscillation* (SAO) – semi-annual, anti-synchronous run in the sea level pressure and temperature differences between the mid-latitudes and Antarctica. In pressure, the half-yearly wave attains its greatest amplitudes in the mid-latitudes ocean basins and on the Antarctic periphery, with a minimum near 55°S. The SAO of the temperature gradient is strongest near 60°S, where it explains typically 50% of the mean annual variance of monthly data (SIMMONDS & JONES, 1998; SIMMONDS ET AL., 1998; VAN DEN BROEKE, 2000a, b, c, d, e).
- the *Antarctic Circumpolar Current* (ACC) – an ocean current around the Antarctic continent
- the recently discovered *Antarctic Circumpolar Wave* (ACW) – a coupled atmospheric phenomenon of an oscillation in surface pressure, wind, temperature, and sea ice extent that propagates around Antarctica with a time-scale of four to six years (MOTOI ET AL., 1998; HOFMANN & PRIDDLE, 2000). The analysis of satellite time series confirms the influence of the ACW on surface temperatures and sea ice cover as well as the resulting variability of these factors (WHITE & PETERSON, 1996; COMISO, 2000).

Figure 1.4 illustrates the time sequence of global change and feedback responses in Antarctica. However, many details of the processes and feedback mechanisms are not yet well understood. Some of these feedback mechanisms, interactions and teleconnections will be taken up again in one of the next sub-chapters (1.3.5). Their characteristics and possible role in the observed signals of interannual climate variability and climate change along the Antarctic Peninsula will be discussed.

In the following, a brief overview of the predictions and limitations of global climate models in Antarctica will be given. Global circulation models (GCMs) predict a short-term rise in global sea level (mainly due to thermal expansion). This is a direct reaction to increased warming as a consequence of antropogenic emissions of greenhouse gases. However, many high latitude regions are not captured well by these

models and hence the confidence in such predictions and in the timing of the expected changes is not high (WELLER, 1998). For instance, HINES ET AL. (in press) and MARSHALL & HARANGOZO (2000) validated NCEP/ NCAR reanalysis against station records and discovered that only the period from the 1970s on is modelled reliably. They could show that the availability of input data plays a significant role in the accuracy of the model runs. Similarly, TURNER ET AL. (1998a) and MARSHALL ET AL. (1998) analysed precipitation from ECMWF reanalysis for the Antarctic Peninsula and stated that the major discrepancies originate from the poor representation of the Antarctic Peninsula mountain chain in the orography of the model. SINCLAIR (1994) found the data sets produced by the ECMWF GCM being highly sensitive towards model changes from his analysis of twice daily geopotential height fields during the time period 1980-86. He attributed the sudden increase in the total cyclone number in 1983 to the change in the ECMWF model topography.

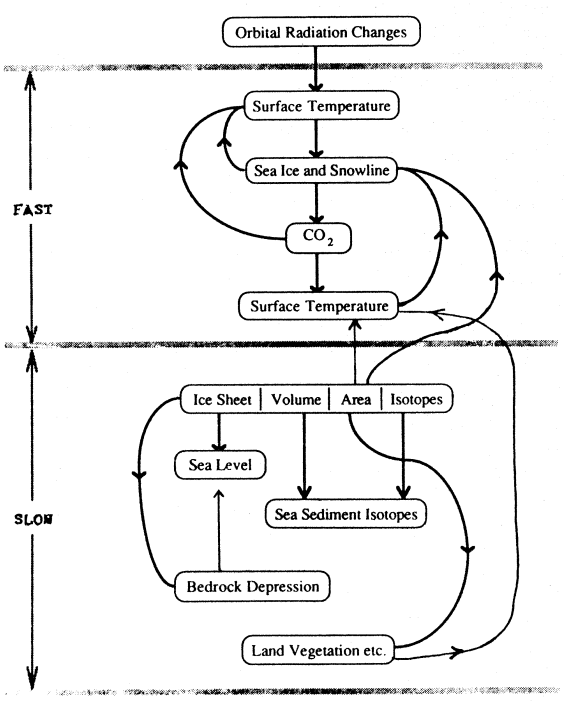

Figure 1.4: *Time sequence of global change and feedback responses (BUDD, 1991).*

In addition to these problems on data availability and grid size, CONNOLLEY & O'FARRELL (1998) clearly pointed out based on the analysis of three GCM outputs (HADCM2, CSIRO, ECHAM4/OPYC3) that

> *"despite some regions of agreement, in general, the GCM runs appear to be incompatible with each other and with the observations, although the short observational record and high natural variability make verification difficult."*

In particular, none of the GCMs could reproduce the observed extraordinary high temperature rise on the Antarctic Peninsula where the longest data records for Antarctica exist. Running the HADCM2 model with the increment of effective CO_2 concentration that matched the rates seen in the last century and then with the IS92A emission scenario for increasing concentrations for the next century, the model predicted a warming of 5 K in the Bellingshausen Sea near the peninsula. However, there was no temperature maximum near the Antarctic Peninsula, with a winter temperature increase of 3-4 K, whilst several other regions showed changes >6 K. Similarly, the warming over the Peninsula was modest in the CSIRO model runs. The air temperature response in the models was correlated strongly with changes in ice compactness (O'FARRELL & CONNOLLEY, 1998). They concluded that the warming in

the Antarctic Peninsula is possibly regional in character and not linked to any large-scale warming. If so, the distribution of trends from coupled transient and control runs showed that the models failed to capture whatever anthropogenic or natural processes are responsible for this warming. Moreover, the coarse grid size and a too smooth topography of the Antarctic Peninsula in the models did not allow to simulate the processes in sufficient detail in this region.

Summary 1.3.2:
Antarctica plays a central role in the global climate system. Several teleconnections and feedback mechanisms make the system complicated and highly sensitive to changes. Many processes, interrelations and regional changes are not always represented well by GCM and have to be further investigated. The warming in the Antarctic Peninsula region is not captured by the GCMs and its possible causes and links to any large-scale warming still have to be determined.

1.3.3 Snow cover and glaciers as indicators for global change and their expected contribution to global sea level rise

The retreat and advance of glacier fronts has probably been used as a measure of climatic variations as long as humans have lived close to glaciated environments (NESJE & DAHL, 2000). Climate is characterised by annual fluctuations superimposed on long-term trends. Such climatic changes are reflected in variations in the glacier extent and ice volume as glacier mass balance is determined by the difference of mass gain (accumulation) and mass loss (ablation). The time lag a glacier takes to adjust to a change in mass balance is defined as response time (PATERSON, 1994), or, in other words, the response time is the time the mass balance perturbation takes to remove the differences between the steady-state volumes of the glacier before and after the change in mass balance (JOHANNESSON et al., 1989). The response time is therefore determined by the mass balance parameters and the glacier flow. Small glaciers and snow patches have short response times to climate change and are therefore powerful instruments for detecting climatic changes at a variety of temporal and spatial scales, e.g. BIKENMAJER (1999):

> *"Glaciers of all types are among the most sensitive instruments of nature immediately responding to and registering regional and global climatic change, its cooling or warming. They naturally become one of the major fields of coordinated scientific research in an attempt to construct models of present and future climatic trends on the earth."*

Glacier length changes have also been used in the opposite way to verify the observed warming trend in long-term meteorological records as done by OERLEMANS (1994). He determined the world-wide warming rate from observed historic glacier front positions of 48 glaciers to +0.66 ± 0.2 K per century. This value is quite close to

the global temperature trend of +0.41 K per century observed in meteorological time series compiled by JONES ET AL. (1999). In a further study, OERLEMANS ET AL. (1998) used ice-flow modelling to estimate the sensitivity of 12 glaciers and ice caps towards climatic changes. They concluded that for a warming rate of 0.04 K a^{-1}, without an increase in precipitation, few glaciers would survive until 2100. On the other hand, if the warming rate was to be limited to 0.01 K a^{-1} with an increase in precipitation of 10% per degree warming, they predict a restriction of the overall loss to 10 to 20% of the 1990 volume.

OERLEMANS ET AL. (1998) stated further that

> *"... the distribution of glaciers over classes of area size would be very helpful, but exist only for a few glaciated regions."*

This is consistent with the claims by WELLER (1992), BAHR (1997), BAHR & MEIER (2000) for a world-wide glacier inventory in order to assess the magnitude of changes in glaciers and their contribution to global sea level rise that will occur during the 21st century. Due to the lack of in-situ measurements, no glaciers from Antarctica are included in the existing glacier inventories, e.g. the database of the World Glacier Monitoring Service (WGMS). To overcome this problem, an attempt is made in the international framework *"Global Land Ice Measurements from Space"* (GLIMS) based on routinely acquired satellite imagery.

In the report of the Intergovernmental Panel of Climate Change (IPCC), HOUGHTON ET AL. (1996) emphasised the need of a better understanding of the reactions of inland ice masses and glaciers for an improvement of GCM predictions of global sea level rise. They gave a rise of global mean air temperature of about +2 K from 1990 to 2100 as best estimate. As a consequence thereof, a global sea level rise of +50 cm would be expected, mainly as a result of thermal expansion but also due to melt water input from snow and ice covered areas. The average rate of global sea-level rise over the past century has been 1-2 mm a^{-1}, with higher values (2.3-2.4 mm a^{-1}) over the past 50 years (JACOBS, 1990 in BIRKENMAJER, 1999). ZUO & OERLEMANS (1997) estimated the ice melt of glaciers in the period 1965-1990 in terms of sea level change equivalent to 5.7 cm (2.7 cm for glaciers and 3 cm for the Greenland ice sheet). Using a heuristic model, WIGLEY & RAPER (1995) predicted a sea level rise of 12 to 19 cm as contribution from small glaciers and ice caps for a global warming of +2.2 K between 1990 to 2100. GREGORY & OERLEMANS (1998) took the effects of regional and seasonal temperature variations from a GCM (HADCAM2) into account. From their calculations they predicted a glacier melt equivalent of 13.2 cm of sea level rise over the period 1990-2100, with a further 7.6 cm from the melting of the Greenland ice sheet. Other authors estimate the high mass balance sensitivities of the Greenland ice sheet to range between +0.235 to +0.355 mm K^{-1} a^{-1} (JANSSENS & HUYBRECHTS, 2000). The expected compensation by increased accumulation on the central Antarctica was already included, the marginal regions of Antarctica were excluded from these model runs. In a further study, DE WOLDE ET AL. (1997) compared different projections of global sea level rise calculated with a two-

dimensional energy balance climate model and dynamic ice sheet models. The largest inter-model differences in individual sea-level contributions were found for thermal expansion and for the Antarctica ice sheet. Sensitivity experiments showed the importance of different assumptions about the temperature forcing of the glacier and ice sheet models and about the weakening of the ocean circulation. Furthermore, uncertainties in thermal expansion caused by uncertainties in ocean heat mixing are considerable.

The limited number and accuracy of in-situ measurements makes the determination of the current mass balance for the Antarctic ice sheet on a basin-scale as well as on a continental-scale very difficult. In contrast to the large ice sheets, the *"local glaciers surrounding the continental ice sheets"* (WEIDICK & MORRIS, 1998) react with a mass decrease on the actual recorded global warming. Their location at the border between terrestrial and marine ecosystems, as well as in the transition of various climatic systems results in a high sensitivity towards changes and regional shifts in these systems. Hence, WEIDICK & MORRIS (1998) specified for the Antarctic Peninsula in their review on existing mass balance studies for this region, that

> *"... further work is needed to establish mass-balance curves for the region, but the primary need is mapping on a sufficiently detailed scale to resolve the form of local glaciers and enable more precise estimates of their area to be made".*

Estimation of the contribution of the Antarctic Peninsula ice masses to global sea level rise have been given by DREWRY & MORRIS (1992). Based on the sea-level isotherms and temperature lapse rates determined by REYNOLDS (1981), they estimated the area of the Antarctic Peninsula, where surface ablation occurs (mean annual temperature >-11°C) to some 20,000 km² (2% of the entire Antarctic Peninsula). The IPCC (HOUGHTON ET AL., 1990) suggested an ablation increase of 0.5 m ice a^{-1} K^{-1} for warm glaciers. DREWRY & MORRIS (1992) considered this value too high and only fitting to the conditions in northernmost parts of the Peninsula, and used a more conservative melt rate of 0.25 m ice a^{-1} K^{-1} instead. Data to support this assumption were, however, almost completely lacking. A surface air temperature increase of 2 K over 40 years would then contribute to at least 1.0 mm of sea level rise, offsetting the fall of 0.5 mm caused by increased accumulation (This is a lot less than the expected reduction of sea level rise of 0.4 mm $a^{-1}K^{-1}$ due to precipitation increase for entire Antarctica (SMITH ET AL., 1998)). In a more recent study based on observations of the Moraine Corrie Glacier on Alexander Island, MORRIS (1999) determined an ablation sensitivity of 1.3±0.3 m WE a^{-1} K^{-1}, which is three times the value suggested by the IPCC and almost five times the values used by DREWRY & MORRIS (1992). Thus, she suggested to revise the rate of contribution of Antarctic Peninsula glaciers to sea level rise used by DREWRY & MORRIS (1992) of 0.012 mm a^{-1} K^{-1} upwards by at least a factor of two. She further stated:

> *"Ideally, of course, many more direct measurements of ablation at different sites should be made, but in the interim the result from Moraine Corrie suggest that DREWRY & MORRIS (1992) were over-cautious."*

Furthermore, the ablation area of 20,000 km² given by DREWRY & MORRIS (1992) has to be treated with some caution. They delineated the area where surface melt has to be considered in mass balance estimations to coincide with areas where the mean annual surface air temperature is higher than –11°C. This threshold is also frequently used as a rough estimation of the lower boundary of the dry snow zone. They used the well-known map of REYNOLDS (1981) to identify such areas on the Antarctic Peninsula. ERS-1/2 SAR mosaics of the Antarctic Peninsula presented by RAU ET AL. (2000) and RAU & BRAUN (submitted) reveal a considerably larger area where summer ablation occurs. Together with a possibly higher ablation sensitivity, this would result in a considerable upward shift of the contribution of the Antarctic Peninsula ice masses to sea level rise as previously suggested by DREWRY & MORRIS (1992).

However, it has to be kept in mind, that the expected contribution of the Antarctic Peninsula is small in regard of the positive mass balance of the entire Antarctic ice sheet due to an expected increase in accumulation in the central Antarctic continent (BUDD, 1991). This is valid for almost all other glaciated regions as well except Greenland. On the other hand, the glacerized area of e.g. King George Island comprises about a third of the area covered by glaciers in Scandinavia or in the Alps. Hence, considering latter regions for estimations of global sea level rise, refined estimations for the Antarctic Peninsula are mandatory as well.

Summary 1.3.3:
Small glaciers and ice caps can be used as indicators for climatic changes. So far, the estimates of their contribution to global sea level rise do not include the glaciers at the margin of Antarctica. Concerning the ice masses of the Antarctic Peninsula, considerable uncertainty still exists on the present ablation rates, their ablation sensitivity and the extent of areas potentially contribution to global sea level rise.

1.3.4 Interannual climatic variability and actual signals of climate change along the Antarctic Peninsula

The Antarctic Peninsula is the region with the densest station network and longest meteorological records in Antarctica which reach back to the beginning of the 20th century (e.g. Orcadas station since 1903). Several authors have analysed the existing data series in regard to surface temperature increase, changes in the precipitation patterns and their causes linked to interactions with sea ice and large

scale circulation as well as from teleconnections with extra-polar regions. Figure 1.5 summarises indicators for a climatic change on the Antarctic Peninsula.

1.3.4.1 Surface air temperature trends

A statistically significant warming trend can be drawn from various data sets, revealing a warming of up to 3 K in the last 50 years in mean surface air temperature (e.g. JONES, 1990; KING, 1994; STARK, 1994; SMITH ET AL., 1996; HARANGOZO ET AL., 1997; SKVARCA ET AL., 1998; COMISO, 2000; MARSHALL & LAGUN, submitted). The increase is even higher if single months or seasons are regarded; e.g. SMITH ET AL. (1996) gave a mid-winter temperature rise of 4-5 K in the period 1944-91. As a consequence many studies focus on winter air temperatures in relation to sea ice extent and ENSO as will be outlined later. Similarly, the highest rise is also observed in winter in the Bellingshausen record, although this is not statistically significant (Table 1.1). CONNOLLEY & O'FARRELL (1998) reported that the warming at Esperanza station (Hope Bay), on the eastern side of the Antarctic Peninsula, is smaller and not significant except in summer. Further north, at Orcadas, trends are less significant and less seasonally distinct, since this station is subject to a highly maritime climate and is less influenced by sea ice. Other proxy data on temperature through this period, such as the expansion of vascular plants, also indicate continuous warming (GROBE ET AL., 1997). The air temperature rise seems to span over the Drake Passage (HOFFMANN ET AL., 1997), and the warming rates are among the highest found outside of urban areas on the world. VAN DEN BROEKE (2000b) argues that northerly circulation anomalies in combination with decreased sea ice cover have regionally enhanced low-level warming, for instance in the region of the Antarctic Peninsula. Based on this, he proposes a background Antarctic warming trend of 1.30 ± 0.38 K per century, representative for the period 1957-1995

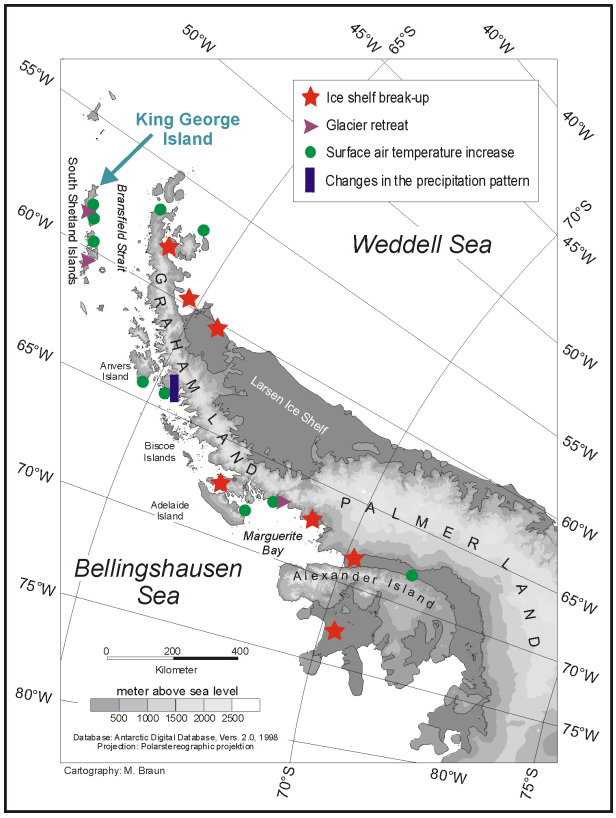

Figure 1.5: *Indicators for a climatic change along the Antarctic Peninsula.*

The analysis of early expedition records and the long-term record at Orcadas station indicated a warming between 0.3 to 3.0 K since the early years of the 20th century (JONES, 1990). This conflicts with the temperatures deduced from oxygen isotope ratios in ice cores from the Peninsula (James Ross Island, Dolleman Island) and from

Table 1.1: *Surface air temperature trends at four Antarctic stations. The values refer only to the data measured at the station itself, extensions of the data sets with data from adjacent stations are not taken into account. Therefore and due to the extent of the data records, differences in the observed trends to previous published data are possible. Percent values in brackets denote the significance level. Auto-correlation has been considered in the trend analysis. Data source: BAS Sept. 2000, http://www.nerc-bas.ac.uk/icd/gjma/temps.html.*

Parameter	Orcadas	Bellingshausen	Faraday/Vernadsky	Rothera
Lat/Lon	60°45'S / 44°43'W	62°15'S / 58°58'W	61°15'S / 64°15'W	67°34'S / 68°08'W
Period	1903-2000	1968-2000	1950-2000	1976-2000
Annual mean	-4.1°C	-2.4°C	-4.0°C	-4.7°C
Annual trend	+0.0198 (99%)	+0.0319 (90%)	+0.0552 (99%)	+0.1134 (90%)
Trend in autumn	+0.0208 (99%)	+0.0504 (-)	+0.0624 (95%)	+0.1218 (95%)
Trend in winter	+0.0268 (95%)	+0.0501 (-)	+0.1089 (99%)	+0.1742 (-)
Trend in spring	+0.0169 (99%)	-0.0093 (-)	+0.0228 (-)	+0.1139 (90%)
Trend in summer	+0.0149 (99%)	+0.0296 (99%)	+0.0244 (99%)	+0.0361 (90%)

the Ronne Ice Shelf. Latter data sets revealed a cooling from the mid nineteenth century to the 1940s and a succeeding warming (ARISTARAIN ET AL., 1987; PEEL, 1992a, b; PEEL ET AL., 1996; JONES ET AL., 1993; THOMPSON ET AL., 1994). PEEL (1992a), JONES ET AL. (1993) and KING & TURNER (1997) attributed these discrepancies to a greater fraction of open water in the Weddell Sea as a result of a rather different prevailing atmospheric circulation pattern. The latter leads to a different origin of air masses and isotope concentrations in the cores. Furthermore, based on the chloride record of the Dolleman Island ice core, PEEL ET AL. (1996) concluded that the exceptionally low chloride levels seen in the mid-19th century imply a generally weaker atmospheric circulation. Finally, they stated that ice core evidence from higher elevations on the Antarctic Peninsula might be better representative for the detection of true temperature changes.

Western Antarctic Peninsula air temperatures show not only a significant warming trend in recent years, they are also subject to a considerable interannual variability, especially during winter months (KING, 1994; SAMSON, 1989). KING & TURNER (1997) observed a high degree of persistence in temperature anomalies from one year to the next. The dominating factor for this is the sea ice extent (WEATHERLY ET AL., 1991). KING (1994) found a strong association between sea ice and temperature, but could not conclusively link these together. He stated that atmosphere-ocean interactions in the Bellingshausen Sea and Drake Passage were likely to be responsible for the temperature anomalies at Faraday/Vernadsky. Winter temperatures on the Antarctic Peninsula are strongly anticorrelated with sea ice extent in the Bellingshausen Sea, with low winter temperatures associated with anomalously extensive sea ice and vice versa (CARLETON ET AL., 1998; KING & HARANGOZO, 1998). SMITH ET AL. (1996) and SMITH & STEARNS (1993) performed lead/lag correlations

between Faraday/Vernadsky surface air temperature and sea ice extent as well as with the Southern Oscillation Index (SOI) and observed a significant seasonal relationship and a significant low frequency coherence which underscores the complexity of the interconnections in the system. Similarly, the highest level of correlation of local West Antarctic Peninsula (WAP) winter sea ice extent with winter air temperature was found by standardising and lowpass filtering the monthly ice edge position data and then forming winter averages, taking May positions paired with the temperatures of the winter months for the years 1973-93 (HARANGOZO, 2000). Using the average of the May and August monthly sea ice data yields an improved correlation coefficient of 0.92 (Figure 1.6a). This average is referred to as the winter baseline ice extent. Furthermore, it correlates significantly with the pressure index M2 at >1% level, yielding a value of r=-0.75 (Figure 1.6b). Lag correlation analysis confirms highest r values at lag 0 (M2 June-August) and lag –1 (M2 May-July) with r=-0.79 (HARANGOZO, 2000). M2 is a measure for the strength of the meridional circulation on the west Antarctic Peninsula based on the pressure difference between 75°W and 60°W at 65°S (latitude of Faraday/Vernadsky station). It thus appears that the Antarctic Peninsula winter ice extent is systematically perturbed by the local meridional atmospheric circulation and hence by ENSO which affects this circulation. Several studies have indicated a weakening of the westerlies during ENSO warm events and increased southerlies over southern South America and the Antarctic Peninsula (summarized in HARANGOZO, 2000). Furthermore, King (1994) and KING & HARANGOZO (1998) were able to show that Antarctic Peninsula winter air temperatures are strongly correlated with the meridional component of the atmospheric circulation. Anomalous northern circulation is associated with warmer winters and vice versa.

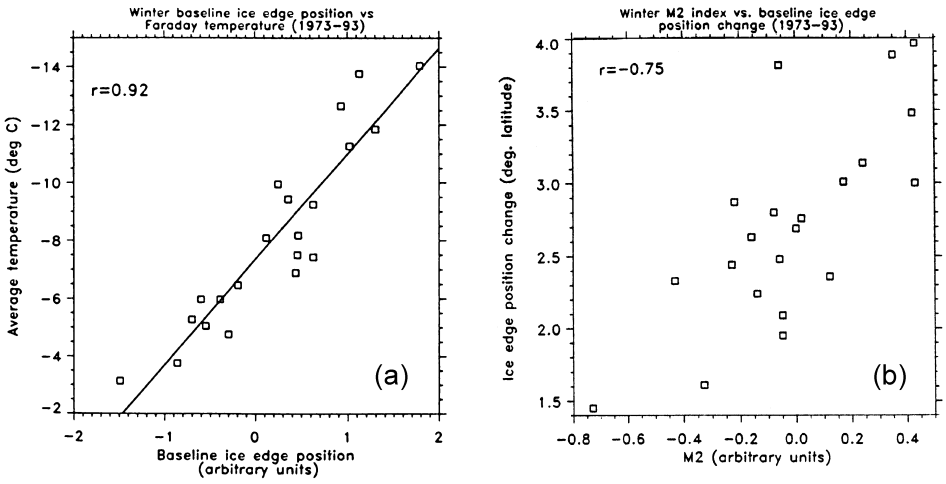

Figure 1.6: a) *Scatter plot of austral winter (JJA) baseline ice edge position (arbitrary units based on standardised monthly sea ice edge position) against WAP surface air temperature (°C) for 1973-1993. The line of best fit obtained from a least squares regression analysis is superposed;* ***b)*** *scatter plot of winter (JJA) M2 meridional flow index (based on seasonally averaged standardized units of SLP) against the winter change in baseline ice edge position. Southerly flows are shown by positive M2 values (HARANGOZO, 2000).*

Reasons for this strong influence of sea ice on air temperature are the reduction of the heat fluxes from the ocean to the atmosphere and changes in surface albedo. Since higher air temperatures will promote the decline of sea ice, there is potential for a positive feedback mechanism, and it would seem likely that the extreme climatic sensitivity of the region results, at least in part, from the effects of this feedback. Further insight in the spatial and temporal variation of surface temperature and its relation to sea ice coverage and ENSO has to be gained in future from spatial data sets as demonstrated by COMISO (2000) for the years 1979-98 with data from the Temperature Humidity Infrared Radiometer (THIR) and the Advanced Very High Resolution Radiometer (AVHRR).

1.3.4.2 Precipitation records

Shallow ice cores from the plateau area of the Antarctic Peninsula indicated an increase in accumulation in the last decades (PEEL, 1992). Reconstructed annual layer thickness suggests an increase in net accumulation beginning in the early 19th century and continuing to the present (THOMPSON ET AL., 1994). Similarly, the meteorological record from Faraday/Vernadsky station reveals an increase in precipitation events by about 20% for the period 1956-93. In comparison with the 1950s, during the last years the amount of rain events rose by about 50% (TURNER ET AL., 1997). In the same period, significant warming has been observed, however, there is little correlation between year to year variations in precipitation frequency and air temperature. This suggests that other factors than temperature changes contribute to the observed variability in precipitation on the west coast of the Antarctic Peninsula (KING & TURNER, 1997). A more vigorous or increased cyclone activity is identified as a reason for these precipitation changes by TURNER & COLWELL (1995). This is further supported by the fact that the observed accumulation increase in ice cores (+15.2% K^{-1}) is significantly higher than the rate of change of saturation vapour pressure (10% K^{-1}) at the average temperature of the core site (-19°C). Hence, concurrent changes in the circulation can be plausibly to be associated with the temperature increase. TURNER ET AL. (1997) further consolidate this hypothesis and it is also consistent with the findings of KING & HARANGOZO (1998). They used the M2 east-west pressure index to describe the strength of the meridional atmospheric circulation. Faraday/Vernadsky monthly mean air temperatures are anticorrelated with this index at a level of 99%. Furthermore, a regression shows that this index has decreased in winter, indicating a more frequent air mass advection from northerly directions. The studies of SCHWERDTFEGER (1976) already showed that the average speed of the boundary-layer winds from the northwest sector towards the west coast of the Peninsula had increased. This statement is supported by statistics of the sea-level pressure differences between the stations Bellingshausen (King George Island), Faraday/Vernadsky (Argentine Islands) and Rothera (Adelaide Island), with a probability of 95% for the years 1947-76.

1.3.4.3 Sea ice extent

The sea ice coverage in the Southern Ocean varies annually between $4*10^6$ km² and $20*10^6$ km², a larger area than covered by the Antarctic ice sheet itself (STAMMERJOHN & SMITH, 1996). Sea ice exhibits a strong interaction with other climatic factors as e.g. KING & TURNER (1997) state:

> *"The extent of the sea ice around the continent, for example, and the track and location of synoptic-scale depressions are closely connected, but the exact quantitative nature of the link has yet to be fully resolved*."

No homogenous trend could be determined in the long-term sea ice records for various sectors of Antarctica, however, several studies indicate a marked decrease of the sea ice extent in the Amundsen and Bellingshausen Sea, in particular during summer months (STAMMERJOHN & SMITH, 1997; JACKA & BUDD, 1998; PARKINSON, 1994). This corresponds with the statement of SCHWERDTFEGER (1976) who observed a great decrease of the duration of the ice cover in Marguerity Bay in earlier years. An increase could be determined for the eastern Weddell Sea region (BIAN ET AL., 1997 (1973-92); STAMMERJOHN & SMITH, 1996 (1978-95); JACKA & BUDD, 1998 (1973-96); PARKINSON, 1994 (1988-94)). These differences can be explained by the climatic settings – depression centres in the Weddell Sea and Barrier Winds direct cold southerly winds to the eastern side of the Antarctic Peninsula and help to maintain the permanent ice fields in this sector. On the western side of the Peninsula, longitudinal variability in location and frequency of lows is considerably higher. The location of these synoptic-scale weather systems may influence whether the Bellingshausen Sea experiences a high or low ice year. The pattern of the maximum and minimum extents shows a yearly displacement of about 40° in easterly direction, which coincides with the Antarctic Circumpolar Wave. As surface air temperature and sea ice extent are closely correlated, it is not surprising that in the sea ice records an ENSO signal could be discovered as well. SMITH ET AL. (1996) determined a strong anti-correlation of sea ice extent and SOI for the Palmer Long Term Research study area (LTER). For the El-Niño event of 1982, an above average sea ice coverage was noticed, whereas during La-Niña events the sea ice coverage is reduced in the years 0 and +1. This coincides with results presented by CARLETON (1988).

SIMMODS ET AL. (1998) studied the influence of sea ice on the SAO using GCM runs and discovered that a reduction of the sea ice extent leads to an amplification of the SAO amplitude. In a previous study, SIMMONDS & WU (1993) suggested that the observed decrease of mean sea level pressure results essentially from an increase in the number of cyclones rather than from the possibility that the cyclones are more intense. The negative circumpolar trend of summer mean sea level pressure (MSLP) with a concurrent increase in the Northern Oceans induces a strengthening of the pressure differences and thus leads to an increased cyclone activity. A close association between sea ice limit and the location of the south polar trough was described by ENEMOTO & OHMURA (1990). The fact that the interannual variations of the Trans-Polar-Index (TPI, pressure difference between Hobbart, Tasmania and

Port Stanley, South Georgia) correlate with the sea ice variations in the Scotia Sea and the maximum frequency of depressions also fits in this context.

1.3.4.4 Ice shelf disintegration and glacier retreat

Perhaps the most spectacular process that not only drew scientific attention but also public interest to the Antarctic Peninsula was the break-up of various ice shelves in the last decades. Three ice shelves on each side of the Antarctic Peninsula (Wordie, Wilkins and George IV Shelf Ice on the west side as well as the ice shelf in Prinz-Gustav Channel, Larsen A and Larsen B on the east side) have disintegrated or shown signs of break-up (DOAKE & VAUGHAN, 1991; SKVARCA, 1993, 1994; VAUGHAN ET AL., 1993; BINDSCHADLER ET AL., 1994; ROTT ET AL., 1996, 1998; VAUGHAN & DOAKE, 1996; DOAKE ET AL., 1998; LUCCHITTA & ROSANOVA, 1998; SKVARCA ET AL., 1998, 1999a, 1999b; RACK ET AL., 1999, 2000; DOMACK ET AL., 2000; SCAMBOS ET AL., 2000). The very small ice shelves (<50 km²) on the west coast of the Antarctic Peninsula, Muller and Jones Ice Shelf, are said to survive only because of their sheltered fjord environment.

MERCER (1978) noted that the distribution of ice shelves might be climatically controlled, with the 0°C summer isotherm marking the limit of occurrence. The –5°C annual isotherm is often used as a proxy for the mean monthly 0°C January isotherm. Comparison of air temperature data (REYNOLDS, 1981) with the pattern and magnitude of ice shelf retreat shows that this isotherm can be associated with the abrupt thermal limit on ice shelf variability. The warming observed around the Antarctic Peninsula corresponds to a southward migration of the –5°C isotherm of 200 km on the west side of the Peninsula but only about 50 km on the east side due to the influence of the perennial pack ice of the Weddell Sea. However, this observation lacks a physical explanation of the processes controlling the limit (VAUGHAN, 1992).

HULBE (1997) and SCAMBOS ET AL. (2000) showed that surface melting which is extensive enough to form ponds of liquid water on the ice-shelf surface is an important contributor to the break-up of ice shelves. Thus, the marginal ice shelves of the Antarctic Peninsula provide a large scale indicator of changes in certain climatic parameters (VAUGHAN 1992). From the studies on the Wordie Ice shelf

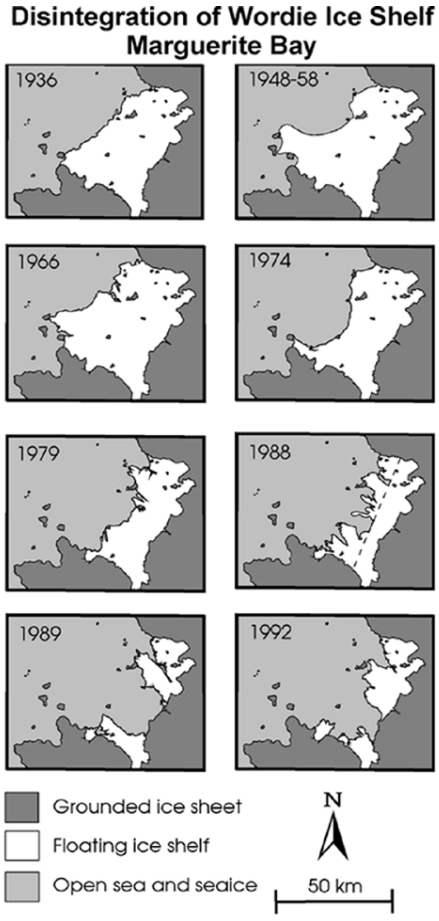

Figure 1.7: *Disintegration of the Wordie Ice Shelf (VAUGHAN & DOAKE, 1996).*

(Figure 1.7), VAUGHAN (1992) determined several factors that influence the ice shelf dynamics:

(1) Ice rises: (i) when embedded, they created broken waves downstream and zones of compression upstream – and hence helped to stabilise the ice shelf, (ii) during retreat, they temporarily pinned the local ice front position and also acted as nucleating points for rifting – thus enhancing the decay.

(2) Increased ablation and amount of melt water as a consequence of several consecutive warm summers destabilize the ice shelves (HULBE, 1997; SCAMBOS ET AL., 2000). The fracture toughness of ice is reduced at higher temperatures and possibly by the presence of water. Rifts might grow due to the increasing pressure from percolating melt water at the bottom of crevasses.

Parallel to the enormous ice shelf disintegration, glacier retreat and advance have been documented for many regions in Antarctica. In a study focusing on Marie Byrd Land and Ellsworth Land in West Antarctica, FERRIGNO ET AL. (1998) determined an overall small average advance since the early 1970s. However, no clear trend could be found. Contrasting to this, retreat seems to prevail in the region of the Antarctic Peninsula. CALVET & CORBERA (1993) and CALVET ET AL. (1992, 1999) documented the fluctuations of ice masses on Livingston Island. Moreover, the disappearance of the ice ramp between Stonington Island and the adjacent glacier was reported by SPLETTSTOESSER (1992). In Marguerite Bay, a significant lowering was measured for the ice ramp at Rothera station by BAS personnel as well (mean annual mass loss 0,32 m WE, SMITH ET AL., 1998). FOX & COOPER (1998) analysed the extent of small snow patches in the northern Marguerite Bay using aerial photography and discovered a significant shrinkage of these areas within the last 40 years. They attributed this to the significantly increasing number of degree-days as observed at Rothera station. Satellite imagery, as well as historic aerial photography and maps have also been used to determine the glacier retreat rates near the Argentine station San Martín (WUNDERLE, 1996; WUNDERLE & SCHMIDT, 2000).

1.3.4.5 Local signals of climate change from King George Island

Perhaps the most obvious sign for local climatic and glacial changes is the immense glacier retreat since the mid 1950s. First observations were made by Polish scientists based on field studies (e.g. PAULO & TOKARSKI, 1982; MARTIANOV & RAKUSA-SUSZCZEWSKI, 1989). Analysis of aerial photography and satellite imagery then revealed a retreat of about 89 km² for the entire King George Island (SIMÕES ET AL., 1999). Several studies refined this observations (e.g. BRAUN & GOßMANN, in press; KEJNA ET AL., 1998; MUSER, 1995; PARK ET AL., 1998; WUNDERLE, 1996). Figure 1.8 shows the retreat areas of glaciers in Admiralty Bay on King George Island in the period 1956 to 1992/95. In total, almost 16 km² of ice have disappeared. A review on

the different stages of glacier retreat and possible explanations are given in chapter 4.5.1. Using a two-dimensional vertical flow model, KNAP ET AL. (1996) estimated the sensitivity of the King George Island ice cap towards climatic changes. They calculated a reduction of the present-day ice volume by 36% if temperatures increase by 1 K. The ice loss would mainly occur on the southern side, a finding which coincides with the retreat observed via satellite imagery. However, the model suggested that the ice cap seems to be insensitive to precipitation increase.

As shown in figure 1.9, a pronounced temperature increase is also detectable in the King George Island climatic records. Apart from spring, all seasons and the yearly

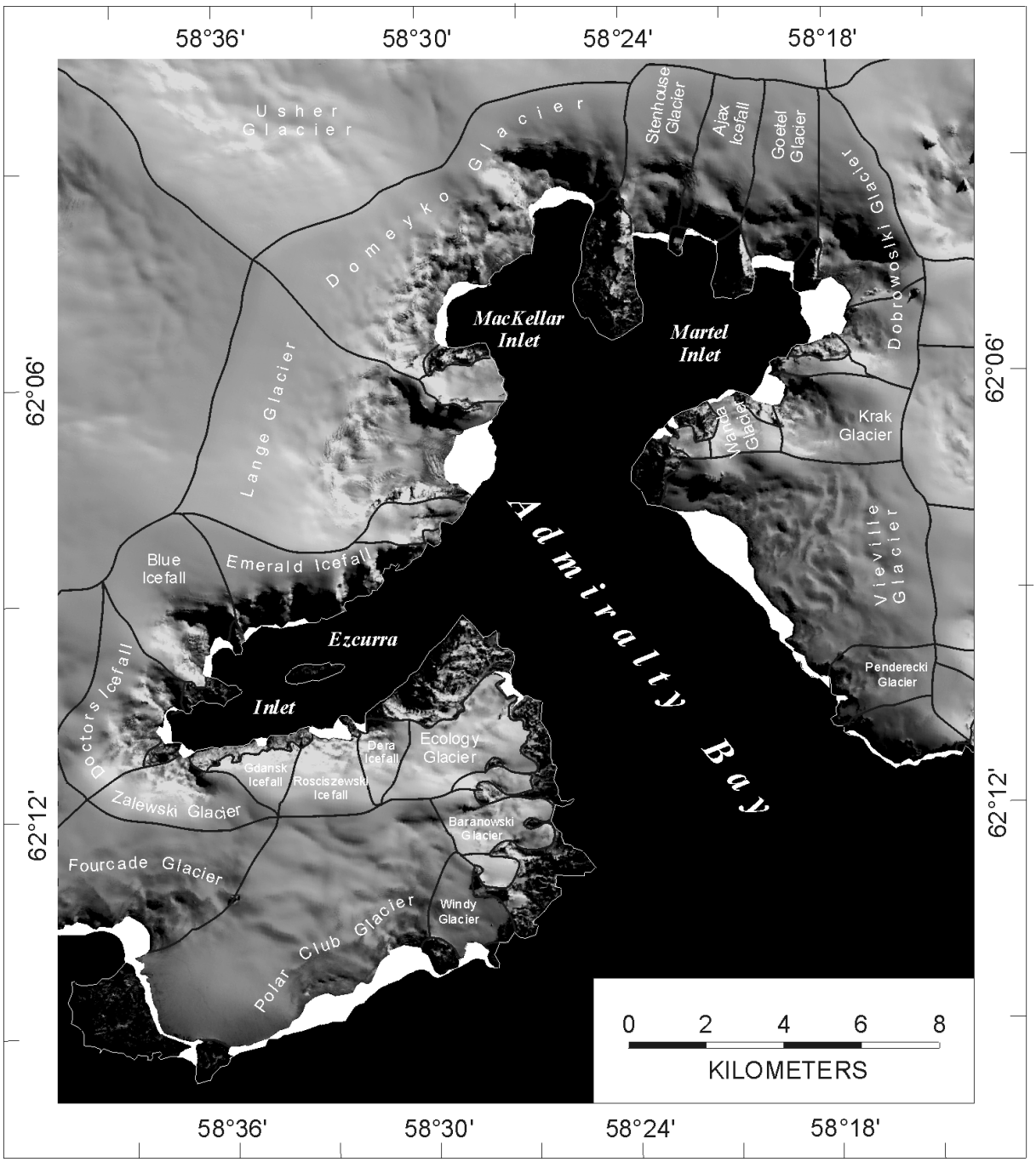

Figure 1.8: *Glacier retreat between 1956 and 1995 in Admiralty Bay and adjacent areas.*

means indicate a positive trend. In particular, the trend of the summer season is statistically significant. This is of special importance and deserves particular attention, as the present work focuses on summer ablation. Moreover, OERLEMANS & REICHERT (2000) show that summer air temperatures and, for wetter climates spring and fall temperatures as well have a considerable influence on glacier mass balance.

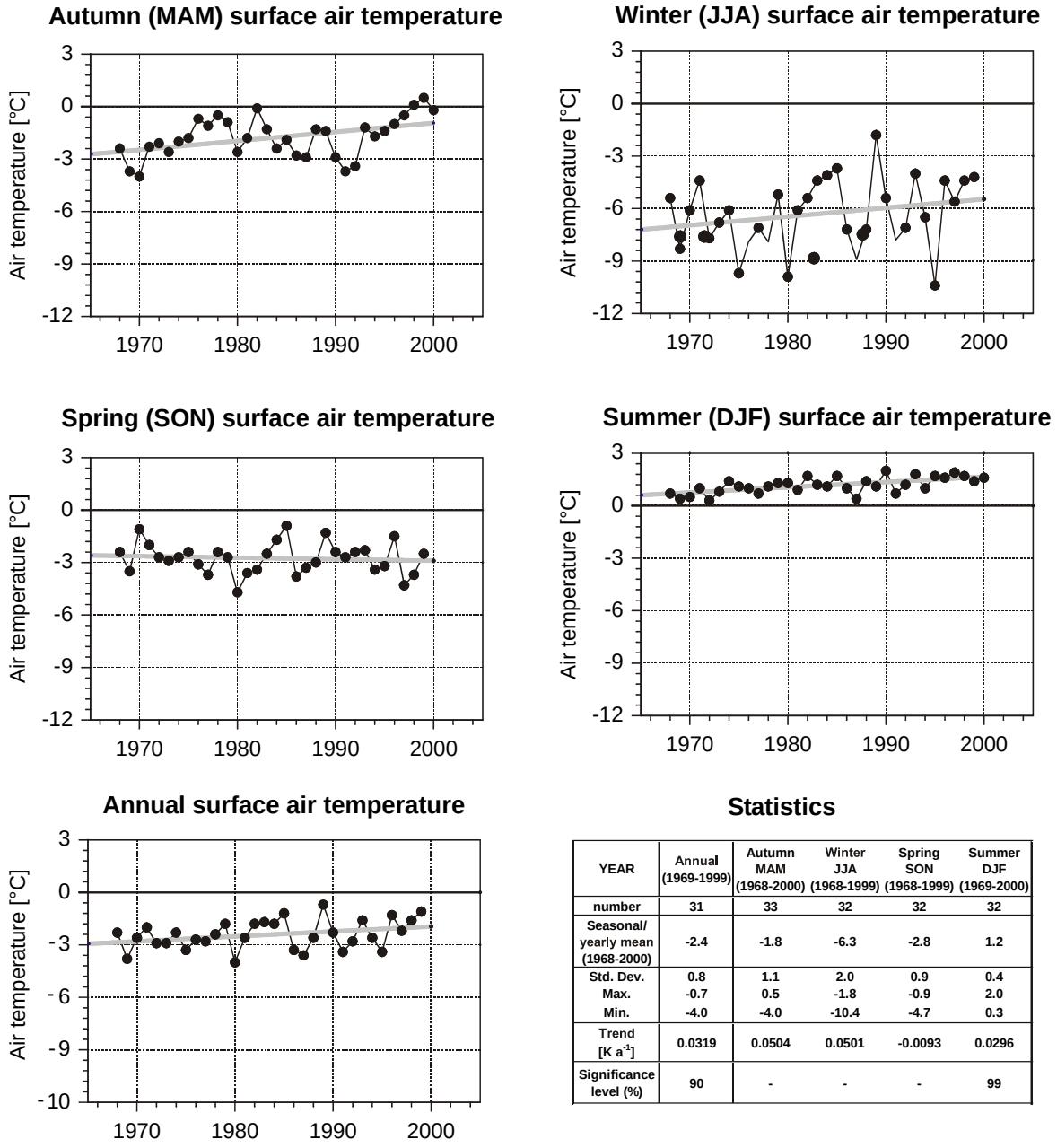

Statistics

YEAR	Annual (1969-1999)	Autumn MAM (1968-2000)	Winter JJA (1968-1999)	Spring SON (1968-1999)	Summer DJF (1969-2000)
number	31	33	32	32	32
Seasonal/ yearly mean (1968-2000)	-2.4	-1.8	-6.3	-2.8	1.2
Std. Dev.	0.8	1.1	2.0	0.9	0.4
Max.	-0.7	0.5	-1.8	-0.9	2.0
Min.	-4.0	-4.0	-10.4	-4.7	0.3
Trend [K a^{-1}]	0.0319	0.0504	0.0501	-0.0093	0.0296
Significance level (%)	90	-	-	-	99

Figure 1.9: *Seasonal and annual mean air temperatures as well as linear trends from Bellingshausen station, King George Island (Data source: BAS Sept. 2000, http://www.nerc-bas.ac.uk/icd/gjma/temps.html, MARSHALL & LAGUN, submitted).*

Summary 1.3.4:
The signals of on-going climatic and glacial changes in the region of the Antarctic Peninsula range from extraordinary warming trends, changes in the sea ice extent to variations in the precipitation pattern. The disintegrations of the ice shelves in this region are now linked directly with rising summer air temperatures and consequent increase in summer snowmelt. Local signals from King George Island comprise a significant trend in summer air temperature and distinct glacier retreat. Model results indicate a very high sensitivity of the King George Island ice masses towards a further air temperature increase.

1.3.5 The impact of glacial sediments and melt water on the marine ecosystems

In chapter 1.3.1 it was demonstrated that large amounts of sediment are transported into the coastal zones of King George Island. These melt water induced sediment loads cause considerable impact on the marine life cycle and, in second order, on the terrestrial ecosystems. These connections will be briefly reviewed as one example where increased ablation may impact the local ecosystems.

In Admiralty Bay, RAKUSA-SUSZCZEWSKI (1993) observed that the availability of nutrients and their seasonal variation is controlled more by the hydro-dynamical rather than by the biological processes. He further stated, the highest variability was induced by the melt water supply from glaciers (e.g. visibility depth in Admiralty Bay in summer is 2-3 m compared to about 32 m in winter (LIPSKI, 1987; GURGUL, 1993)). Hence, a profound knowledge of the abiotic factors is mandatory for the understanding of many biological process studies. In the following the interaction between melt water from glaciers and snow fields, suspended anorganic matter and coastal ecosystems is briefly outlined.

Terrestrial ecosystems strongly depend on the productivity of the marine ecosystems and the transport of organic material within the sea. Especially the near coastal marine ecosystems experience changes in the hydrodynamic conditions by the adjacent land and ice masses (e.g. upwelling and water gyres on the lee sides, the stability of the water column and the circulation within the bay). WÄGELE & BRITO (1990), for instance, observed higher phytoplankton concentrations in the interior of Admiralty Bay than in the various inlets. This impact of fresh water and sediments on the marine ecosystems was pointed out by KLÖSER & ARNTZ (1994), stating that the formation of large phytoplankton concentrations will be inhibited by the stable, low-saline surface waters with high anorganic particle concentrations. Moreover, the optical properties are modified by fresh water input and anorganic suspended material. The latter shows a remarkable seasonal cycle (LIPSKI, 1987; RAKUSA-SUSZCZEWSKI, 1993). Suspended sediment reduces the penetration depth of light to 5 m (RAUSCHERT, 1991) which makes it to limiting factor for the abundance of the algae

Mimantothallus grandifolius. The hydro-optical conditions directly affect the photosynthesis by the available amount of energy (SCHLOSS ET AL., 1998). LIGOWSKI & KOPCYZYŃSKA (1993) determined the highest phytoplankton concentrations in the uppermost 10 m during stable synoptic situations characterised by high pressure, when the water column is not mixed.

KÜHNE (1997) observed that in Potter Cove *Ascidiacea* (sessile filterers) were dominant at the sea floor in depths below 20 m in contrast to sponges in similar depth in the McMurdo Sound. He concluded that differences in anorganic matter might be the reasons for these distribution discrepancies. In McMurdo Sound, visibilities range between 60-100 m. These physical settings do not exist in Potter Cove, where sediment-rich melt waters drain (KLÖSER ET AL., 1994). However, the sediment concentrations vary strongly with time and location (SCHLOSS ET AL., 1994; SCHLOSS ET AL., 1998). Additional anorganic matter input is caused by the sea circulation from Marian Cove (CHANG ET AL., 1990; HONG ET AL., 1991). *Ascidiacea* are better adapted to high sediment concentrations than various other benthic organisms (KÜHNE, 1997; MOORE, 1977; REISWIG, 1971) whereas the slowly growing sponges are endangered of being buried by high sedimentation rates (DAYTON, 1989). Similar findings have been reported by JAZDZEWSKI ET AL. (1986) and WÄGELE & BRITO (1990) for Admiralty Bay on King George Island as well as by RAMOS ET AL. (1987) and SAIZ-SALINAS ET AL. (1997) for the Antarctic Peninsula. Many studies proved that high sediment loads occur as a consequence of melt water and wind-induced re-suspension in these regions as well (e.g. JAZDZEWSKI ET AL., 1991; RAKUSA-SUSZCZEWSKI, 1993; GURGUL, 1993; RAKUSA-SUSZCZEWSKI, 1995; PLATT, 1979; PEDDERSEN ET AL., 1995; DOMACK, 1990; DOMACK & WILLIAMS, 1990; DOMACK ET AL., 1989, 1993; PUDSEY ET AL., 1994). PECHERZEWSKI (1980) estimated the sediment load in Admiralty Bay to about 2000 t per day. This corresponds to measured sediment concentrations in Matías creek draining into Potter Cove by VARELA (1998) in 1996/97. She observed values ranging between 5 g s^{-1} and 60,000 g s^{-1}, but most frequently below 5,000 g s^{-1} (0.432 to 5184 t d^{-1}, 432 t d^{-1} respectively).

SICINSKI ET AL. (1996) outlined the significance of mineral suspensions for the zoobenthos on examples from Herve Cove on King George Island. They reported a yearly mean of 46 mg l^{-1} as sediment concentrations. Using cluster analysis, they were able to distinguish four major benthic communities which occur in dependence of the distance from the glacier tongue. Similar findings are reported by RAKUSA-SUSZCZEWSKI ET AL. (1993) for these coves which developed as a consequence of the intense glacier retreat in the last decades. Concurrently, the glacier retreat was accompanied by an increase in sediment supply (RAKUSA-SUSZCZEWSKI, 1993). Finally, RAKUSA-SUZSCZEWSKI (1995) reports the observation of mass mortality of krill (*Euphausia superba*) in front of glaciers during several occasions. He speculated that the contact of krill with fresh water or high concentrations of anorganic material may cause interference with the ability of the animal to feed or swim.

Summary 1.3.5:

The penetration depth of sun light into the sea is one major limiting factor in the marine ecosystem. In the fjords and bays of King George Island, sediment plumes induced by snow and glacier melt strongly control the hydro-optical conditions and hence the marine life cycle. Moreover, the hydro-dynamic conditions are modified by the fresh water supply from the glacierised areas. Consequently, increasing melt water supply due to higher ablation rates will alter the environmental settings and hence influence the coastal ecosystems.

2 Topography and place names

With about 1,250 km², King George Island is the largest of the South Shetland Islands. 92.7 % of the island are ice covered (SIMÕES ET AL., 1999). The major ice free areas are located on the western tip (Fildes Peninsula) and southern shore of the island (Barton and Potter Peninsula, Admiralty Bay, Penguin Island). On the northern shore exist only small rock outcrops.

The surface topography of King George Island is strongly influenced by the sub-glacial relief (Figure 2.1). The highest elevations of the island (about 705 m a.s.l.) are located along a major geological ridge, extending almost in ENE-WSW direction. In contrast to the gently inclined northern slopes of King George Island, the southern part is deeply incised with fjord-like inlets.

King George Island can be subdivided into the following major geographical units:

- The *Arctowski Icefield* consists of several unnamed ice domes reaching the highest elevations of the island with about 705 m a.s.l.. It is drained by numerous outlet glaciers to the south, whereas a smooth glacier surface dominates the appearance of the northern side.
- Near Fildes Peninsula a small ice dome called *Bellingshausen Dome* (also “Dome A” or “Collins Dome“) forms the connection to the main ice cap.
- Two separate icefields border Admiralty Bay*. Krakow* and *Warzawa Icefield* do not exceed 450 m a.s.l. and are characterised by an ice cover whose topography is strongly dominated by bedrock.

The study area of the present work covers the western part of King George Island ice cap, extending from Fildes Peninsula in the west to one of the major ice domes of the

Arctowski Icefield at about 58°25' W. The ice masses of Warzsawa Icefield are also included in the analysis.

Place names mentioned in the text are shown on the satellite image map (Figure 2.1) and are used in agreement with the Gazetteer Antarctica (WORKING GROUP OF GEODESY & GEOGRAPHIC INFORMATION, 1999). In cases of multi-naming, the suggestions of SIEVERS & THOMPSON (1995) were followed giving priority to the first naming. Name ambiguities are quite frequent on King George Island, since 9 nations operate permanent research stations, and several other countries perform research based on small refuges or field camps. The history of place names was mainly obtained from HATTERSLEY-SMITH (1991). Further information on names and locations were taken from BIRKENMAJER (1980a, 1984), the ANTARCTIC PLACE NAMES COMMITTEE OF FOREIGN AND COMMONWEALTH (1986), and the Gazetteer Antarctica (WORKING GROUP OF GEODESY AND GEOGRAPHIC INFORMATION, 1999; CERVELLATI ET AL., 2000). A more detailed description of the island's topography can be found in SIMÕES ET AL. (1999) and BRAUN ET AL. (2001).

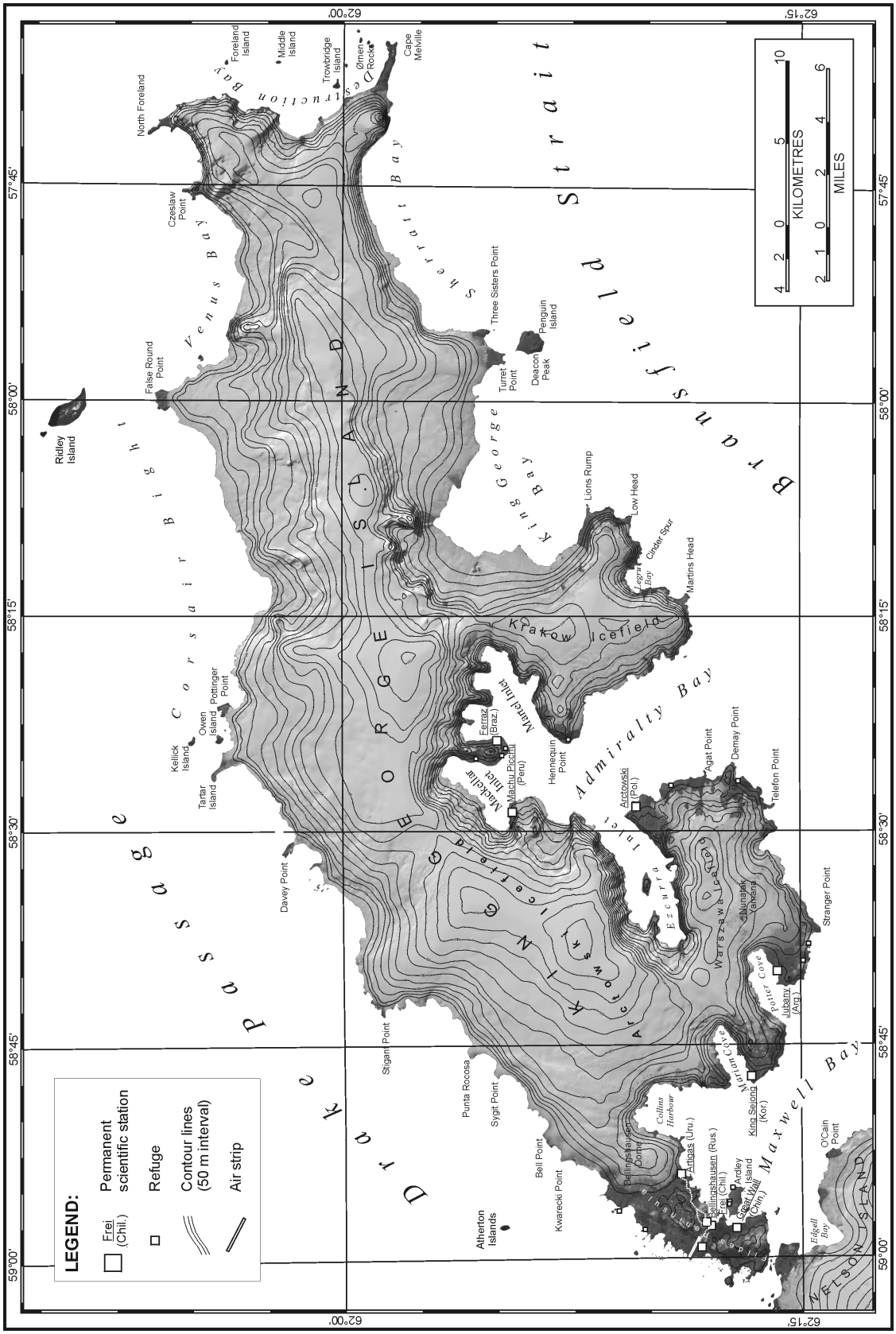

***Figure 2.1**: Map of King George Island. The major place names, permanent research stations and refuges referred to in the text are indicated. Contour interval is 50 m.*

3 Database and data preparation

For this study, data from standard meteorological observations at permanent research stations were available as e.g. mean monthly air temperatures from Bellingshausen station or radio sounding data. The energy balance calculations are based on data from automatic weather stations (AWS) operated during several consecutive field campaigns on the King George Island ice cap. Remote sensing data generally available for King George Island and in particular as used in this study are outlined in the following chapter as well.

3.1 Field campaigns on King George Island

Meteorological and snow-hydrological data on the King George Island ice cap were collected during 3 joint field expeditions of the *Laboratório de Pesquisas Antárticas e Glaciológicas (LAPAG), Universidade Federal do Rio Grande do Sul*, Porto Alegre, Brazil and the *Institut für Physische Geographie* (IPG), *Universität Freiburg*, Germany during the austral summers 1995/96, 1997/98 and 1999/2000. After a first reconnaissance study during 1995/96, extended measuring programs were carried out in the following austral summers. Figure 3.1 shows the location of the AWS and table 3.1 gives an overview of the periods of their operation.

During all expeditions, AWS instrumentation and data sampling techniques kept consistent. Details on sensor types and instrument accuracies are compiled in table 3.2. Sensors were sampled every 10 seconds and data was stored as 10-minute and hourly averages. In addition to the AWS data, synoptic weather observations were performed as often as possible.

Before and after each field campaign, the combined temperature-humidity-sensors were carefully calibrated. Anemometers were recalibrated once in a wind channel. An intercomparison of the shortwave radiation sensors at a test site near Freiburg

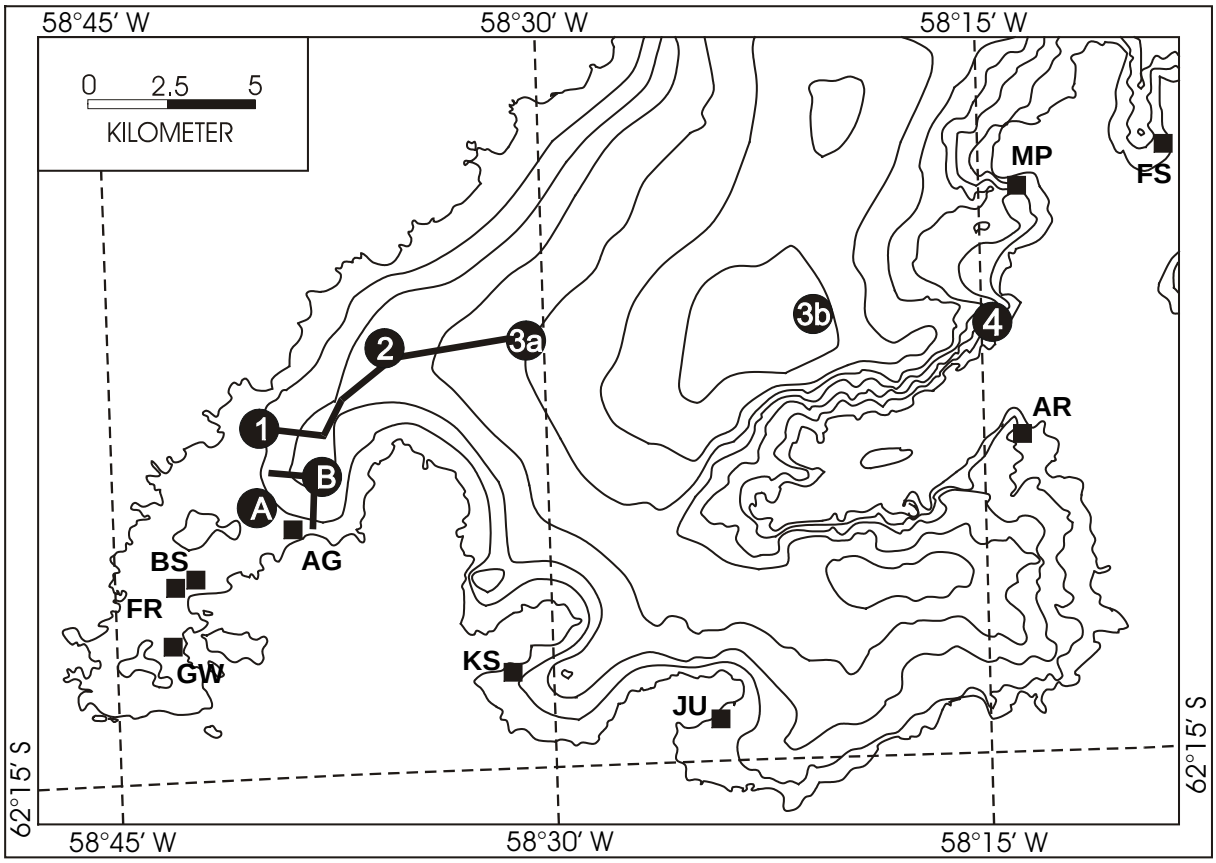

Figure 3.1: *Location of the different AWS and profiles of snow measurements on the King George Island ice cap. Permanent research stations are denoted as follows: FR: Frei, BS: Bellingshausen, GW: Great Wall, AG: Artigas, KS: King Sejong, JU: Jubany, AR: Arctowski, MP: Machu Picchu, FS: Ferraz.*

revealed no considerable deviations. The measured deviations were within the measuring accuracy. Generally, all AWS data was checked and calibrated after each maintaining in the basecamp during field campaigns. Moreover, plausibility tests were applied before performing any further analysis. Where instrument failures occurred, data gaps were filled by regression analysis with values from the other AWS. However, such cases were scarce, amounting to less than 3% in the total measuring time period.

3.1.1 International Glaciological Expedition 1995/1996

During this expedition, two AWS were operated in the vicinity of Fildes Peninsula, one over permafrost (AWS A), the other on top of Bellingshausen Dome (AWS B) over snow. The Latter AWS was equipped with three measuring levels (0.5, 2.0 and 6.0 m) of temperature, humidity and wind speed. AWS A was installed only with one level of the respective sensors. No automatic snow depth sensor was usedduring this field campaign.

Furthermore, snow depth and density measurements were carried out along two profiles on Bellingshausen Dome, one extending from Artigas station to the top of the

dome, another on the northwestern slopes of the dome. However, the positions of the sampling points could be determined only with a single handhold GPS resulting in an accuracy of the site determination within a range of about 100 m. The altitude of the sampling points was measured by multiple readings of two altimeters to a vertical precision of about 10 m.

3.1.2 Brazilian-German Expeditions 1997/1998 and 1999/2000

During the expeditions in 1997/98 and 1999/2000 comprehensive measurement programmes were run including the installation of 3 to 4 AWS at various altitudes on the ice cap. Along 2 transect lines between 45 and 300 m a.s.l., direct ablation measurements at stakes and snow pits were performed. The wooden ablation stakes were drilled both times several decimetres into the glacier ice using a HEUCKE ice drill and read in 2 to 7 day intervals. In similar time steps, snow pits were dug near the AWS. All AWS were instrumented with temperature, humidity and wind speed sensors at two levels (0.5 and 2 m). During both expeditions, AWS 1 was equipped with a sonic ranging sensor (SR50) to continuously measure snow depletion and, in 1997/98, with an additional tipping bucket rain gauge. In 1999/2000, AWS 2 was supplied with a SR50 sensor as well. AWS 3a was moved on December 17th 1997 from 385 m a.s.l. to 619 m a.s.l (AWS 3b) as weather conditions proved to be better than expected and hoarfrost on the sensors rarely occurred even in altitudes greater than 400 m a.s.l.. However, during the expedition in 1999/2000, the data from AWS 3b was not reliable due to frequent rime and ice formation on the sensors. Hence, the data from this AWS could not be used for energy balance computations. Generally, the AWS were maintained in the same intervals as the ablation stake readings were performed. The locations of AWS 3b close to the advanced camp enabled shorter service intervals. Data was checked and calibrated immediately after collection.

Table 3.1: *Summary of the locations and operation times of the AWS during the different field campaigns.*

Austral summer	AWS ID	Latitude / Longitude	Altitude [m a.s.l.]	Operation time
1995-1996	AWS A	62°10’17.4” S 58°55’14.2” W	35	07/12/1995-15/01/1996
	AWS B	62°09’56.2” S 58°53’03.4” W	250	16/12/1995-15/01/1996
1997-1998	AWS 1	62°09’13.90” S 58°54’57.95” W	85	02/12/1997-12/01/1998
	AWS 2	62°08’25.31” S 58°51’12.95” W	255	02/12/1997-13/01/1998
	AWS 3a	62°07’45.5” S 58°46’07.2” W	385	05/12/1997-17/12/1997
	AWS 3b	62°07’10.02” S 58°36’00.00” W	619	19/12/1997-11/01/1998
1999-2000	AWS 1	62°09’13.90” S 58°54’57.95” W	85	24/11/1999-08/01/2000
	AWS 2	62°08’25.31” S 58°51’12.95” W	255	30/11/1999-09/01/2000
	AWS 3b	62°07’10.02” S 58°36’00.00” W	619	17/12/1999-07/01/2000
	AWS 4	62°07’44.4” S 58°29’11.4” W	45	31/12/1999-21/02/2000

The snow density measurements revealed only a very small variability between 480 and 510 kg m^{-3}. Thus, a mean density value of 500 kg m^{-3} was used to convert the SR50 snow depth into a continuous record of snow water equivalent (WE) decrease. The location of the ablation stakes and AWS was determined by differential Global Position System (DGPS) with an accuracy better than 1 m in horizontal and vertical dimension.

In both years, mobile DGPS techniques could be applied to determine surface topography in the central part of the ice cap. This data was later combined with additional information from topographic maps to build a digital elevation MODEL (BRAUN ET AL., 2001). Concurrently with this survey, a detailed radio echo sounding (RES) survey was carried out by the Institut für Geophysik (IGM) of the Universität Münster in 1997/98. Glacier velocities in the drainage basin of Lange Glacier and on Bellingshausen Dome were determined by re-measuring the stake positions in an interval of about 3 weeks in cm-accuracy. From this data, 2-dimensional movement vectors were compiled.

Table 3.2: *Sensor types and their nominal accuracy and range as used at the AWS. Errors resulting from mounting or other factors as solar radiance are not considered here.*

Meteorological arameter	Sensor	Instrument accuracy	Range
Air temperature	VAISALA HMP35C	±0.4 K	-23 to +48°C
Relative humidity	VAISALA HMP35C	±2 %	0 to 90 %
		±3 %	90 to 100 %
Wind speed	VECTOR INSTRUMENTS A100R	1 % ± 0.1 ms^{-1}	0.25 to >75 ms^{-1}
Wind direction	VECTOR INSTRUMENTS W200P	±2°	>75 ms^{-1}
Net radiation	CAMPBELL Q7	n.a.	0.25 to 60 µm
Shortwave radiation	SKYE SP1110 Pyranometer	±5 %	0.35 to 1.1 µm
Snow temperature	CAMPBELL 107 temperature probe	±0.4 K	-23 to +48°C
Snow depth	CAMPBELL SR50 Sonic Ranging Sensor	±1 cm or 4 %	0.5 to 10 m

3.1.3 Complementary meteorological and snow-hydrological data sets not originating from IPG field work

For the analysis of the large-scale synoptic situation, NOAA-IR composites and sea level pressure charts for all three measuring periods were supplied by the University of Wisconsin, Madison, USA,. Additionally, NOAA imagery received at Ferraz station and synoptic weather charts compiled by the Chilean Station Eduardo Frei were used for the year 1997/98 and 1999/2000 respectively. The meteorological section of the Brazilian station supplied their records as hourly or 3-hourly values for the time of

AWS operation as well as for periods before and after the field work. New definite, long-term monthly mean air temperatures of Bellingshausen station for the time period February 1968 to July 2000 were downloaded from the British Antarctic Survey website (MARSHALL & LAGUN, in press; http://www.nerc-bas.ac.uk/icd/gjma/temps.html).

3.2 Remote sensing data

The satellite data used in this study consist of SPOT and ERS-1/2 imagery. Generally, the availability of remote sensing data on King George Island is very good in comparison to other regions in Antarctica. Figure 3.2 illustrates the large amount of aerial photography and optical satellite imagery available. In particular, the increasing amount of satellite imagery since the mid 1980s (including SAR data since the 1990s) as stated in chapter 1.3 is noteworthy. For the derivation of glacier drainage basin boundaries and sediment plumes, several SPOT scenes were available (see also figures 1.1 and 1.2). The acquisition dates range between February 1988 and February 2000. To determine the sediment loads, grey values of channel 1 of each SPOT images were classified. This channel has the deepest penetration depth in water and hence reveals the best signal of sediment concentrations.

In total, 40 ERS-1/2 precision images (PRI) were analysed using data from both ascending and descending orbits (Figure 3.3).. The imagery covers the time period

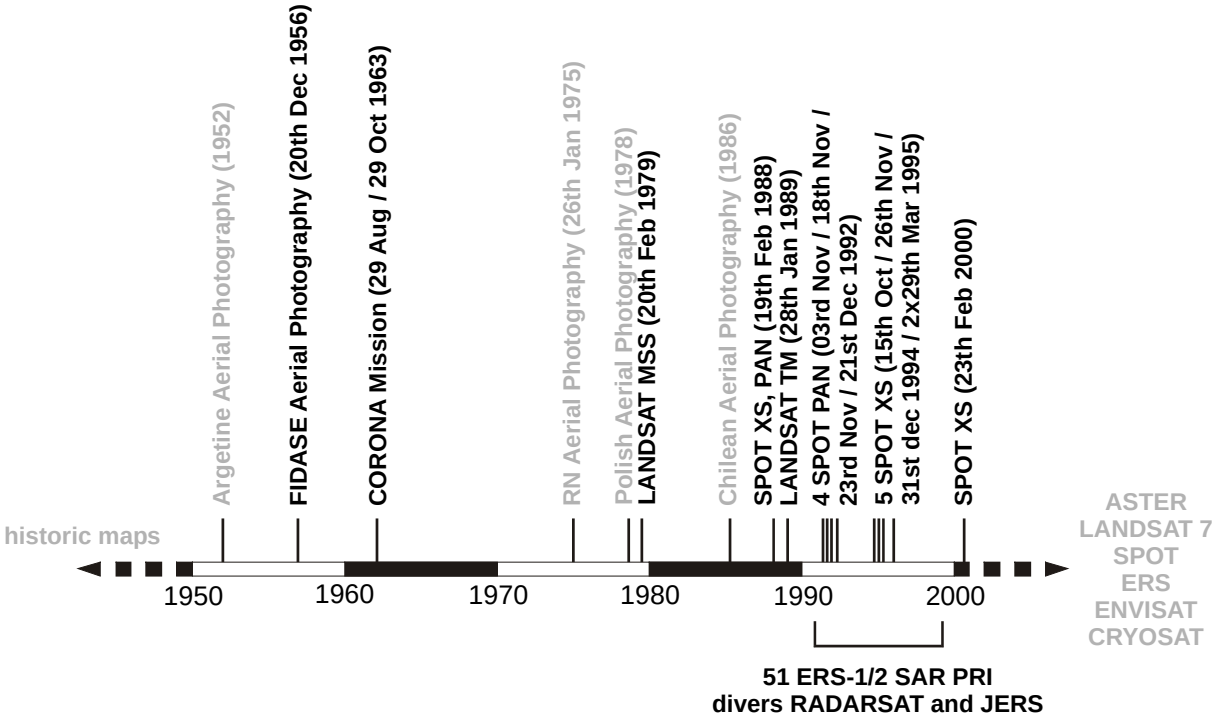

Figure 3.2: *Remote sensing data for King George Island. Black text: available at IPG, grey text: not available at IPG, but existence known to come.*

between July 1992 and November 1999. For almost all mass balance years, at least one winter scene and several summer images were available to monitor the seasonal development of the melt process. The timing of the melt onset in November could only occasionally be determined using SAR data due to the limitation in the operation of German Antarctic Receiving Station near the Chilean base O'Higgins.

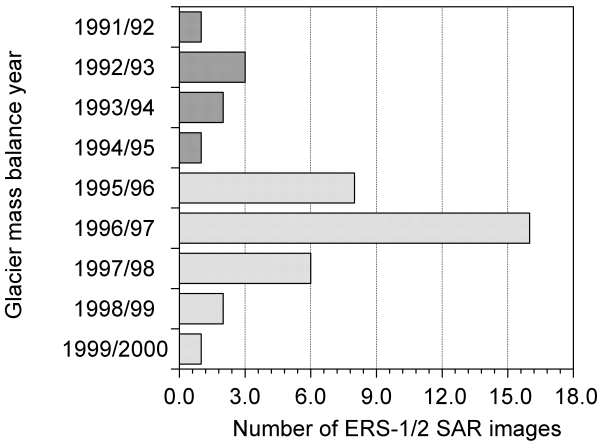

Figure 3.3: *Distribution of the ERS-1/2 SAR imagery in the different glacier mass balance years.*

4 Environmental settings

4.1 Geology

As bedrock strongly influences surface topography and subsurface drainage characteristics, a short overview of the geological settings on King George Island is given in the following.

The geological evolution of the South Shetland Islands was closely linked to the formation of the Antarctic Peninsula. King George Island was situated in the middle of the magmatic island arc of the South Shetland Islands. The latter was formed during the subduction of the Pacific Oceanic crust beneath the Antarctic lithospheric crustal edge during the late Mesozoic up to the late Tertiary times (BIRKENMAJER 1997a, GROENEWEG & BEUNGK, 1992, PANKHURST & SMELLIE, 1983). The deep sea trough of the South Shetland Trench in the northwest of the island group can be regarded as a remainder of the subduction which ended about 4 Ma years ago. In the late Pliocene to early Pleistocene, the island group was separated from the Antarctic Peninsula by the opening of the Bransfield Strait (BIRKENMAJER, 1997a). The spreading resulted in a thinning and fractionating of the continental crust.

King George Island consists mainly of Upper Cretaceous through Oligocene terrestrial, basaltic and andesitic lavas, pyroclastic rocks and plant-bearing volcanoclastic deposits, small-size andesitic and basaltic hypabyssal plugs as well as moderate-size granodioritic through gabbroic plutons (BIRKENMAJER, 1997a). During the period from the Eocene to the Lower Miocene, terrestrial glacial and fossiliferous glacio-marine deposition associated with basaltic volcanics occured along the southeast coast of the island (BIRKENMAJER, 1989).

King George Island consists of several tectonic blocks that are separated by eastnortheast-westnorthwest extending strike-slip faults (Figure 4.1). These blocks may represent terrane displaced with respect to one another at an unknown distance

(DALZIEL, 1989; BIRKENMAJER, 1997a). They are traversed by a system of younger strike-slip faults trending northwest-southeast (BIRKENMAJER, 1982a, 1989).

The following main geological units can be distinguished on King George Island:

- Barton Horst
- Fildes Block
- Warsawa Block
- Krakow Block
- Penguin Island Group

The **Barton Horst** forms the highest parts of the island and consists primarily of calc-alcaline volcanics and intervening sediments affected by low-grade metamorphism (TOKARSKI, 1987). These rocks are mainly of terrestrial origin with very restricted marine influence (BIRKENMAJER, 1982a). Its age was determined to between 66.7 and 26 Ma years (BIRKENMAJER, 1997a).

The **Fildes Block** consists of only weekly unfolded terrestrial lawa, tuff, basaltic and andesitic agglomerates as well as some dacitic compositions, with several fossil-bearing horizons. K-Ar dating suggests an Upper Paleocene (59 Ma) through Middle/Upper Eocene (43-42 Ma) age (SMELLIE ET AL., 1984; TOKARSKI, 1987; BIRKENMAJER, 1997a; JIN ET AL., 1983). A detailed outline of stratigraphy and volcanism on Fildes Peninsula was given by ZHENG & LIU (1990).

The rocks of **Warsawa Block** are unfolded and generally unmetamorphosed volcanics and subordinary sediments (TOKARSKI, 1987). This Block is also referred to as King George Island Supergroup (BIRKENMAJER, 1980b). Its age was dated between 77 and 37 Ma years (GROENEWEG & BEUNGK, 1992).

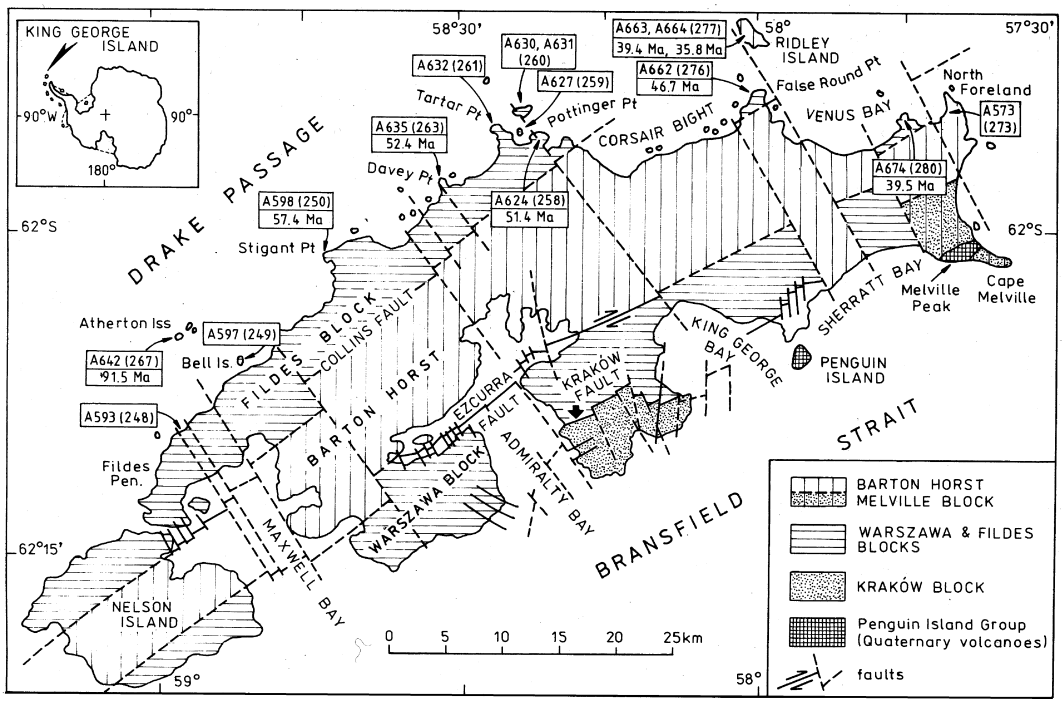

Figure 4.1: *Main tectonic units of King George Island (BIRKENMAJER, 1997a).*

Additionally, BIRKENMAJER (1982b) and TOKARSKI (1987) distinguished the **Krakow Block** which, in contrast to the other blocks, consists of volcanics and glacial-interglacial deposits. It was originally considered of Pliocene age but radiometric dating revealed an Cretaceous age. The superimposed Polonez Cove Formation appears to be latest Oligocene in age.

The last major tectonic group, **Penguin Island Group**, is marked by the Pleistocene to recent stratocones of the Melville Peak and Penguin Island volcanoes. These rocks are devoid of any traces of metamorphism, tectonic joints or mineralisation (TOKARSKI, 1984). BIRKENMAJER & KELLER (1990) recognised two volcanic phases at Melville Peak volcano. One dating back to the Middle and Late Pleistocene; the other was tentatively correlated with the Deacon Peak Formation on Penguin Island. Two volcanic craters are still visible on Penguin Island. BIRKENMAJER (1979a) used the lichenometric method to date the principle stratocone of Deacon Peak to an age of more than 300 years and the explosion of Petrel Crater (maar) to about 1905 A.D. Some of the reported volcanic activity of Bridgeman Island was attributed to the formation of the stratocones of Deacon Peak on Penguin Island (BIRKENMAJER, 1979a; LEMASURIER & THOMSON, 1990). BIRKENMAJER (1979a), Paulo & TOKARSKI (1982) and BIRKENMAJER & KELLER (1990) considered it a „sleeping volcano“. The proximity of recent volcanic activity is important for the ice core studies undertaken on King George Island since several ash layers could be identified in the cores (HAN ET AL., 1999).

Summary 4.1:
King George Island consist of several geological units that origin from the Mesozoic to Tertiary tectonic evolution of the magmatic island arc of the South Shetland Islands. The morphology of the bedrock strongly influences the surface topography of the ice cap.

4.2 Glacial history and sea level rise in the area of the South Shetland Islands

information on former glaciations in the area are of great importance for analysing the present climate-glacier-interaction and for estimations of the glacier response to future climate changes. This chapter contains a brief summary of geomorphological studies focusing on glacial history and sea level rise in the region of the South Shetland Islands.

On King George Island, evidence of four Tertiary cold and three warm climatic epochs has been reported by BIRKENMAJER (1996, 1999) from strata of the Kraków Block. He distinguished:

1. *Krakow Glaciation* (early/mid Eocene, 50 Ma)
2. *Arctowski Interglacial* (mid Eocene – early Oligocene, 50-32 Ma)
3. *Polonez Glaciation* (early Oligocene, 32-30 Ma), which was the largest Cenozoic glaciation in Antarctica. The West Antarctic ice cap crossed Bransfield Strait and reached King George Island
4. *Wesele Interglacial* (mid Oligocene, ca. 30 Ma)
5. *Legru Glaciation* (late Oligocene, 30-26 Ma), local glaciation of King George Island
6. *Wawel Interglacial* (Oligocene/Miocene transition, 26-22 Ma), temperate rain forest, opening of the back-arc Bransfield Rift with tectonic dislocations
7. *Melville Glaciation* (early Miocene, 22-20 Ma)

The dating of Polonez Glaciation was supported by the work of DINGLE ET AL. (1997). However, they obtained indications that the chronology presented by BIRKENMAJER (1996, 1999) is not conform with the Ocean Drilling Program (ODP) data. Herein, only three Oligocene glacial events were reported. DINGLE ET AL. (1997) dated interglacial beds at Polonez Cove with 28-31 Ma, which is in accordance with the ODP data.

Little is known about the Pleistocene glaciations although many raised beaches and moraines give indications (Table 4.1). CLAPPERTON (1990) explained the extraordinary number of raised marine features with the presence of a relatively young, thin hot crust beneath the South Shetland block and with the probability of con-

Table 4.1: *Raised marine beaches on King George Island as reported by several authors. Note that not all age datings were reservoir corrected (-850 years or –1200 years) as suggested by CLAPPERTON (1990) or HJORT ET AL. (1998) or were derived with the lichenometric method.*

Location	Altitude [m a.s.l.]	Age [years B.P.]	Authors
Fildes Peninsula	9	1,310	LIU ET AL. (1992)
	10	1,310	
	14	2,180	
	18	3,200	XIE (1988)
	18	5,800	BARSCH & MÄUSBACHER (1986a)
	24	ca. 84,000	BARSCH & MÄUSBACHER (1986b)
	35-45	>85,000	
Maxwell Bay	2.5-3	ca. 350	CURL, 1980
	6	ca. 550	
Barton Peninsula	6	540	SUDGEN & JOHN (1971)
Admiralty Bay	2-2.5	250	BIRKENMAJER (1981a)
	4	407	
	5	333	
	6-7.5	296	
	16-16.5	518	
	45	800	TATUR (1986) in LIU ET AL. (1992)
	54	15,000	CLAPPERTON (1990)
	45-50	1,000	BIRKENMAJER ET AL. (1985)
	52-54	5,000	
	65	4,950 ±140	
	105-115	probably	BIRKENMAJER (1981b), BIRKENMAJER (1997b)
	120-125	Eamian	
	130-135		
	180	Pleistocene	
	205	interglacials	
	225		
	255		
Lions Rump	5-8	approx. 500	BIRKENMAJER (1994)
	10	late to middle	
	15-25	Holocene	
Three Sisters Point	20	late to middle	BIRKENMAJER (1995)
	25	Holocene	
	30		
	35		
	40		
	45		
Penguin Island	15-18		BIRKENMAJER (1979A)
	25-28		

tinuing tectonic uplift. However, dating seems to be somewhat difficult since ages obtained by several authors differ widely. One reason may be that not all C^{14}-datings are reservoir-corrected. CLAPPERTON & SUDGEN (1988) and HJORT ET AL. (1998) made an attempt to homogenise these data. JOHN & SUDGEN (1971) distinguished two intervals of Quaternary glaciation. They proposed a single ice cap, connecting the islands between King George Island and Livingston Island. From their studies, BARSCH & MÄUSBACHER (1986a) concluded that the Riss (Illinoian) glaciation did not extend further than the last glaciation (Würm / Wisconsin). The pronounced marine abrasion platform on Fildes Peninsula was considered to originate from at least earlier than the Eem interglacial or even before the Illinoian glaciation. BIRKENMAJER (1997b) named the latest Pleistocene or early Holocene glaciation *Warszawa Glaciation*. Its maximum ice cap extent has been suggested to have occurred before approximately 20,000-18,000 years, and it was correlated with the 130-135 m beach level (BIRKENMAJER, 1981b). The measurements of HONG ET AL. (1991) suggest that the glacier retreat in Maxwell Bay started about 15,000-14,000 B.P.. Figure 4.2 shows a schematic diagram of the relationship between Holocene glacier readvance moraines and raised beaches. From the dating of the strand walls, BARSCH & MÄUSBACHER (1986a) concluded that deglaciation in West Antarctica began approximately 6,000 B.P. with a fast glacier retreat that lasted until about 5,000 B.P.. Early on, JOHN (1972) proposed a rapid deglaciation caused by a combination of global warming and rising sea level. This is supported by the finding and radiocarbon-dating of a subfossil peat in Admiralty Bay by BIRKENMAJER ET AL. (1985) as well as by research undertaken by DEL VALLE & TATUR (1993) and SCHMIDT ET AL. (1990) on King George Island and, finally, by studies from the Antarctic Peninsula region (PUDSEY ET AL., 1994). BARSCH & MÄUSBACHER (1986a) assumed that glacier retreat was triggered by the northern hemisphere climate. From the analysis of lake sediments, they furthermore distinguished a period of higher glacial activity between 3,000 and 1,000 B.P. where the ice masses originated from the still present ice caps (Figure 4.3). This roughly corresponds with the findings of LEVENTER ET AL. (1996) who set the end of the elevated productivity cycle due to a Holocene climatic optimum at 2,500 B.P. No close chronological correlation with the northern hemisphere was suggested by HJORT ET AL. (1998). They compiled evidence for a slow retreat in the first half of the Holocene, approximately 9,000 to 5,000 B.P.. A distinct, but rather brief glacial readvance took place around 5,000 B.P., which was probably caused by a period of renewed cooling. HJORT ET AL.'s (1998) results suggest that it was followed by the Holocene climatic optimum, about 4,000 to 3,000 B.P..

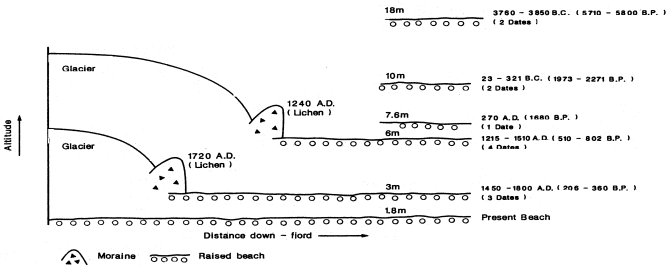

***Figure 4.2**: Schematic diagram showing the relationship of Holocene glacier re-advance moraines with radiocarbon dated raised beaches, South Shetland Islands, Antarctica (CLAPPERTON & SUDGEN, 1988).*

Ages of elevated beaches and rebound rates differ in dependence of authors, dating method and location. BIRKENMAJER (1981b) and LEE (1992) separated the Holocene (2-65 m) from the Pleistocene (105-255 m) levels, whereas BARSCH & MÄUSBACHER (1986a) did this separation between the levels 18 and 24 m. CLAPPERTON (1990) and HJORT ET AL. (1998) argued for a separation at 18 m as well.

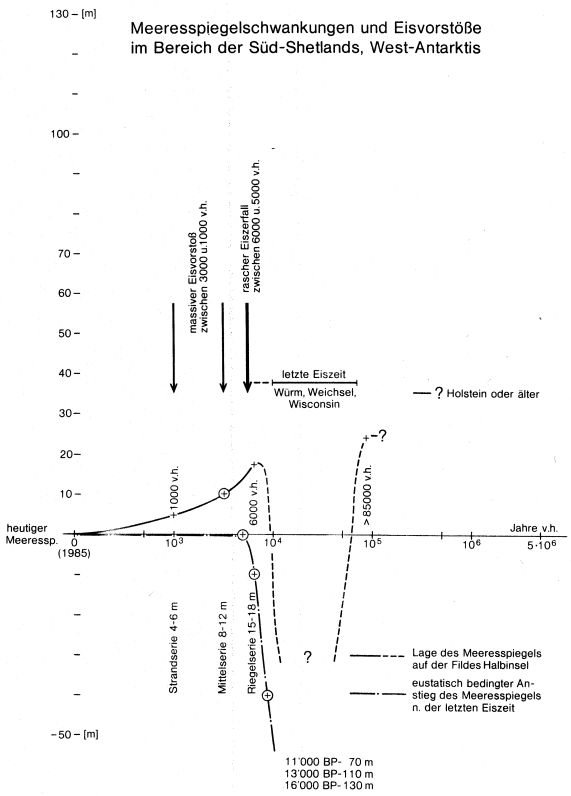

***Figure 4.3**: Sea level changes and ice advances in the area of the South Shetland Islands (BARSCH & MÄUSBACHER, 1986a).*

HOCHSCHILD (1995) reported that the moraines on Potter Peninsula are all ice-cored. The analysis of Delta-O^{18} and Delta-H^2 revealed no differences to values of recent glacier ice. This may be explained by similar climatic conditions during the formation in the middle Holocene (6,000 B.P.), during the glacier retreat or by the infiltration of melt water. The superimposed glacial deposits are possibly of an age between 3,000 and 1,000 B.P.. Moraines of similar type and probably age border Bellingshausen Dome on Fildes Peninsula. However, some of the datings are doubted by BARSCH & MÄUSBACHER (1986a) and only partially corrected, as e.g. the False Bay Glacial Event on Livingston Island to 2,400 B.P. ("Maximum False Bay") and 1,000 B.P. ("Post False Bay"). Using marine sediment cores, HONG ET AL. (1991) determined the Holocene glacier retreat in Marian Cove. They observed that the glacier was already at its present location during Early Holocene. Readvance occurred only during a climatic cooling in the late Holocene (1,500 B.P.), and, since then, the glaciers retreated continuously to their present position (HONG ET AL., 1991; YOON ET AL., 1994).

Recent glacier retreat was investigated at several locations on the southern shore of King George Island by BIRKENMAJER (e.g. 1979b, 1981a,b, 1994, 1995, 1997b). He mainly used the lichenometric method based on growth rates obtained on Livingston Island by CURL

***Table 4.2:** Latest Holocene glacial events in the South Shetland Islands after various sources.*

Name of glacial advance	Age (A.D.)	Author
Ferguson Glacial Event	1,240	BIRKENMAJER 1979b
Potter Cove Glacial Event	1,450	CURL 1980
False Bay Glacial Event	1,720	CURL 1980
Red Corrie Glacial Event	1,780	BIRKENMAJER 1981a
Loggia Corrie Glacial Event	1,825	BIRKENMAJER 1981a
Ecology Glacial Event	1,880	BIRKENMAJER 1981b
Suszczewski Cove	1,905-25	BIRKENMAJER 1981b
Staszek Cove	1,950-60	BIRKENMAJER 1981b

(1980) and stratigraphy to date glacier retreat in Admiralty Bay, Lions Rump and Three Sisters Point. Neo-glacial ice advances in the area of the South Shetland Islands are summarised in table 4.2. Ice core data indicate that the coldest period of the past 300 years occurred around 1760-1780 (PEEL ET AL., 1996). This is consistent with the data from BIRKENMAJER (1981b), statements of HJORT ET AL. (1998) and with the most reliable evidence for advanced glacier positions on Signy Island given by SMITH (1990).

Summary 4.2:
Evidence on the glacial history of the South Shetland Islands is provided by elevated beaches and moraines encountered at several locations. However, the dating is sometimes difficult due to the frequent application of relative dating methods (e.g. lichenometry) instead of absolute dating. As a consequence, published relations between age and corresponding elevated beach height are often ambiguous.

4.3 Climatology

4.3.1 Some aspects of climatology of the Antarctic Peninsula region

It is not the aim of this subchapter to give a full description of the climatology of the Antarctic Peninsula. Detailed description can be found in KING & TURNER (1997) or SCHWERDTFEGER (1970, 1975, 1984). SCHNEIDER (1998), SCHNEIDER & GOßMANN (1999) as well as WUNDERLE (1996) gave climatological summaries for this region. However, for the understanding of the local climatic conditions of King George Island and the meteorological phenomenons observed during the field work, some aspects of the climatic characteristics of the Antarctic Peninsula and of King George Island will be addressed in more detail.

4.3.1.1 General characteristics

The mountain crest of the Antarctic Peninsula acts as a major obstacle in the southern hemisphere circumpolar west wind drift. Moreover, it lies close to one of the most important sea ice producing areas of Antarctica – the Weddell Sea (PEEL, 1992). As a consequence, climate conditions along the Antarctic Peninsula are characterised by strong latitudinal and longitudinal gradients (REYNOLDS, 1981). In general, temperatures on the east coast are approximately 8 K lower than on the west coast of the peninsula. The differences of mean annual temperature between 62°S and 72°S exceed 12 K on the east side of the mountain ridge and about 7 K on the west side.

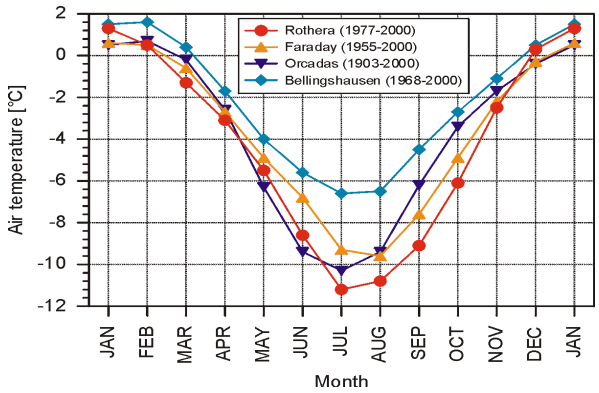

Figure 4.4: *Yearly cycle of the monthly mean air temperatures at four sites on the west coast of the Antarctic Peninsula and the sub-Antarctic islands (Data source: British Antarctic Survey, http://www.nerc-bas.ac.uk/icd/gjma/ temps.html).*

The climate of the northwestern part of the Antarctic Peninsula and the South Shetland Islands is dominated by the frequent succession of low pressure systems which leads to a highly maritime climate (JONES & SIMMONDS, 1993; WEN ET AL., 1994). Further south on the west coast, stable synoptic situations are reported more often (PEPPER, 1954). The run of the yearly cycle of the mean monthly air temperatures does not differ much along the west coast, although the data sets shown in figure 4.4 cover different time spans (e.g. the Oracadas record includes the colder period in the beginning of the 20th century). However, a north–south differentiation can be revealed from the correlation coefficients between the various west coast air temperature records. Farraday (65.4°S/64.4°W) and Rothera (67.5°S/68.1°W) as well as Bellingshausen and Orcadas (60.7°S/44.7°W) show good correlations, whereas the values for the correlations between the sub-Antarctic and the Antarctic Peninsula stations are lower (JONES ET AL., 1993).

The east coast climate is characterised far more by the occurrence of surface inversions. During such situations, cold, dry air masses originating in the central Antarctic are transported along the mountain crest of the Antarctic Peninsula to the North where they spread. This phenomenon is known as “barrier winds” (PARISH, 1983; SCHWERDTFEGER, 1984), and the comparably low summer temperatures of the South Shetland Islands are attributed to this fact (SMITH et al., 1996). The latter authors further state that the proximity of regions with maritime and continental climate results in a stronger regional differentiation of large-scale climatic trends as in other regions. Hence, they consider the Antarctic Peninsula a highly suitable area to detect climatic changes.

4.3.1.2 Synoptic-scale weather systems

Extra-tropical cyclones and anticyclones are the main atmospheric systems found in the Antarctic coastal region. They typically have a length scale of 1,000 to 6,000 km in diameter and a lifetime of between one day and one week (TURNER & LEONARD, 1996). Synoptic-scale cyclones are important for the delivery of moisture as clouds and precipitation, as well as microparticles to the coastal and lower-lying portions of the Antarctic ice sheet (KING & TURNER, 1997). Moreover, the meridional transport of heat is affected predominantly by these systems migrating into Antarctica from their genesis areas over mid-latitudes (CARLTON, 1992). Since the interannual variability of

synoptic processes over higher southern latitudes is large, precipitation and heat flux regimes are also thought to be similarly variable.

Synoptic-scale depressions mainly form at baroclinic zones and grow through baroclinic instability. The polar front, usually found between 40°S and 50°S and separating the temperate mid-latitude from the cold polar air masses, and is hence one of the major regions for the development of cyclones (cyclogenesis) in the Southern Hemisphere (STRETTEN & TROUP, 1973; KING & TURNER, 1997). Below the Antarctic convergence, three main mechanisms of cyclogenesis were summarised by KING & TURNER (1997):

(i) baroclinic instability on frontal cloud bands,

(ii) thermal instability resulting in cold air cyclogenesis and

(iii) topographic forcing.

Frontal developments often occur at the sea ice edge or near ocean fronts (e.g. to the east of South America at the convergence of the Falkland and Brazilian ocean). Coastal regions where katabatic outbreaks of cold, continental air masses meet relatively temperate, maritime air masses (TURNER ET AL., 1998) are another area of cyclogenesis. The developing mesoscale and large-scale disturbances track eastwards or occasionally northwards over the Southern Ocean (KING & TURNER, 1997). Extensive studies on mesoscale cyclone activity in the sector of the Antarctic Peninsula have been performed by WARREN & TURNER (1989), TURNER & ROW (1989), TURNER & THOMAS (1994), CARRASCO & BROMWHICH (1993) and CARRASCO ET AL. (1997). Lee-side cyclogenesis only occurs in the western Weddell Sea where the Antarctic Peninsula spans the belt of strong westerly flow.

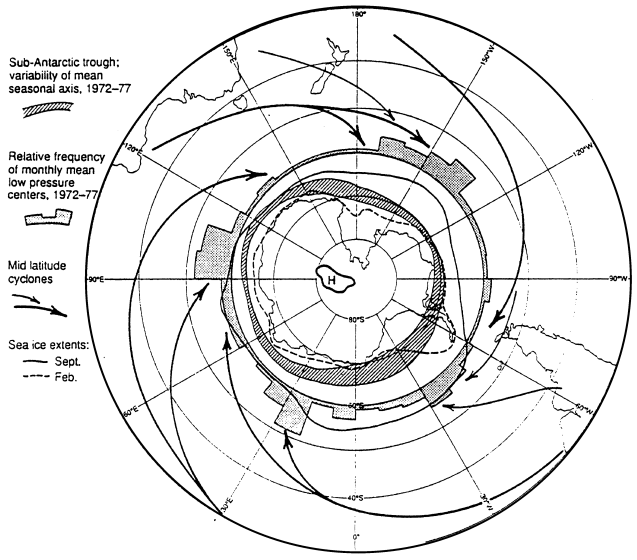

Figure 4.5: *Schematic summarising of dominant features of the synoptic climatology of higher southern latitudes, compiled from various sources (CARLTON, 1992).*

Cyclone dissipation (cyclolysis) most frequently takes place between 60 to 70°S, the circumpolar trough. Stronger winds and more frequent precipitation in the mid-latitude of the Southern Hemisphere are a consequence of the stronger latitudinal gradients in comparison to the Northern Hemisphere. A comprehensive analysis of cyclone and anticyclone tracks based on GCM outputs over several years was performed by JONES & SIMMONDS (1993, 1994). The dominant features of synoptic climatology in the southern latitudes are given in figure 4.5.

Low pressure centres that originate west of 120° move southeast through the Drake Passage and consequently influence the weather on the Antarctic Peninsula by a change from northwesterly to southeasterly advection of air masses (JONES & SIMMONDS, 1993; KING & TURNER, 1997). CHEN ET AL. (1990) distinguished 3 major depression paths in this sector from the analysis of synoptic weather charts from the years 1985-87

(i) tracks moving towards the northern tip of the Antarctic Peninsula,

(ii) southern tracks (south of 65°S) and

(iii) northern tracks (north of 60°S).

They observed that the southern track is the most frequent situation found throughout the year, whereas the northern track is of importance only in summer and autumn months. This is consistent with findings by TURNER & LEONARD (1996) for the year 1993/94.

4.3.2 Local climatic characteristics of King George Island

Although King George Island is one of the most populated and studied places in Antarctica, local climatology is the subject of only very few studies. Most of these concentrate on the area around the Polish Arctowski station in Admiralty Bay.

4.3.2.1 General climatic characteristics

In the region of the South Shetland Islands, the prevailing air mass transport occurs from northwest, westnorthwest, southsouthwest and southwest (RAKUSA-SUSZCZEWSKI ET AL., 1993). The mean monthly air temperatures during summer months (Figure 4.6) reach values well above 0°C. Highest interannual variability can be observed in winter months with the largest standard deviation and a difference between maximum and minimum temperatures of almost 13 K. In contrast, this

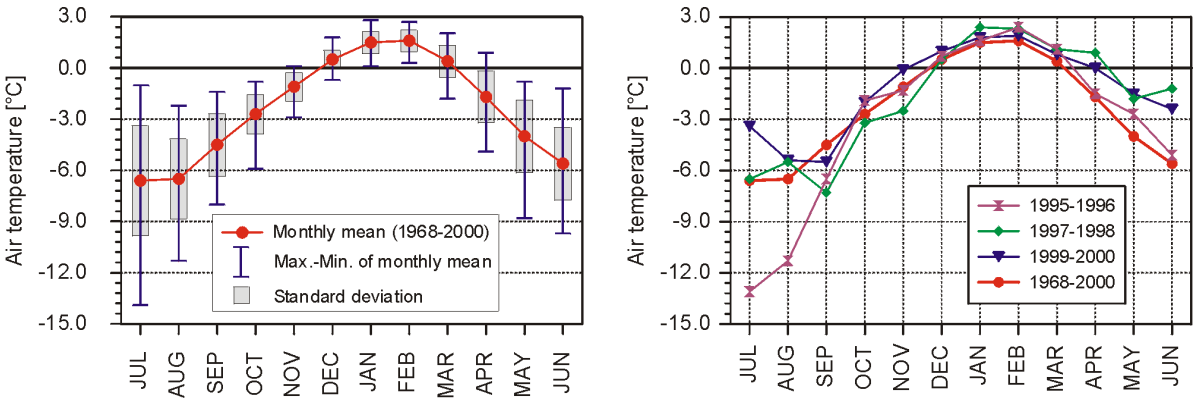

Figure 4.6: *Mean monthly air temperatures at Bellingshausen station (Data source: British Antarctic Survey, http://www.nerc-bas.ac.uk/icd/gjma/ temps.html; see also MARSHALL & LAGUN (submitted).*

difference during summer months amounts only to about 3 K. Snowmelt can also occur during winter months due to the advection of warm, humid air masses from northerly directions (RACHLEWICZ, 1995, 1997; RAKUSA-SUSZCZEWSKI et al., 1993). Mean air temperatures in the southern part of King George Island (Arctowski Station) are in general 0.7 K higher than on the northwestern coast represented by the Bellingshausen station (KEJNA, 1998, RAKUSA-SUSZCZEWSKI, in press). This can be explained by the occurrence of foehn-type effects due to the predominant north and northwest advection (MARTIANOV & RAKUSA-SUSZCZEWSKI, 1989). Furthermore, the authors reported a reduced cloud amount in comparison with the stations on Fildes Peninsula which led to higher solar radiation measured in Admiralty Bay. This was confirmed by BINTANJA (1995) and by own observations during the field campaigns. During the expedition, a continuous cloud cover over the northern part of the ice cap was a frequent phenomenon; while in the Admiralty Bay the cloud cover was at least 7/8. This can be explained by the forced orographic up-lift of humid and relative warm air masses from the Drake Passage. When they reach the cold surface of the ice cap a dense cloud cover is formed. Subsequently, dry adiabatic warming with concurrent reduction in cloud amount occurs when the air masses descend into Admiralty Bay.

Evaluating balloon soundings at Arctowski station during good visibility conditions, KRATKE & WIELBINSKA (1987) found indications for the existence of an orographic wave over the island during southwest, west and northwest advection. These findings are further supported by the occasional observations of *altocumulus lenticularis* clouds over Admiralty Bay during the field work. Despite these foehn-type effects, the high cloud amount of this region was demonstrated by PROSEK ET AL. (1996, 2000) for Arctowski station. On a one year average, they observed only 26.2% of the astronomically possible sunshine hours in 1994/95 with only one day reaching 81.1% as maximum. They therefore concluded, that the main energy input is provided by diffuse radiation. KEJNA (1998) estimated that the amount of hours of sunshine in Admiralty Bay is still 20-30% higher than at the northern coast. BINTANJA (1995) pointed out that his measurements on Ecology Glacier revealed a high variability of global radiation during totally overcast sky which indicated strong differences in the transmissivity and thickness of the cloud cover. The radiation balance measurements of PROSEK ET AL. (1996) over a dense *Deschampsia antarctica* cover near Arctowski station revealed the that longwave radiation balance was almost negligible for energy fluxes since it was near balance. Longwave radiation balance was negative only during days with low cloud amount. They observed a mean of 322 Wm^{-2} for longwave irradiance and 390.7 W m^{-2} and 262 W m^{-2} as the respective maximum and minimum values. Only few information on precipitation is available for the island, and due to the predominant association of high wind speed, the data is less reliable. For Bellingshausen station, a long-term average of about 500 mm was reported (KNAP ET AL., 1996). Accumulation records from ice coring on the ice cap will be reviewed in more detail in the glaciology chapter 4.4.2.

4.3.2.2 Synoptic climatology of the area of King George Island

A first detailed classification scheme of the atmospheric circulation patterns in the area of King George Island was introduced by KEJNA (1993) based on synoptic maps of the years 1986 to 1989 (1,419 days). However, for the application on further data set, it remained unclear how the separation between the different circulation patterns was done in detail. KEJNA (1993) distinguished 21 circulation patterns using the type of pressure centre and air mass transport as major parameters for his classification. Moreover, the central situations anticyclone, cyclone, at the border of an high pressure centre or low pressure trough were distinguished. A summary of the frequency of the different advection directions is given in table 4.3. Advection from north and northeast occurs when a high pressure centre is situated in the northern Weddell Sea area. An anticyclone over the Antarctic Peninsula causes advection of cold air masses from east to southeast ("barrier winds"). SCHWERDTFEGER (1984) presented evidence that a branch of the cold eastern barrier winds frequently sweeps the South Shetland Islands, accounting for the colder air temperatures observed there from November to July in comparison to other peninsula stations. Air mass transport from the south takes place when the centre of the anticyclone is located over the southern Antarctic Peninsula. Relatively high pressure over King George Island is most often encountered with this synoptic situation. In contrast, a high pressure centre in the north of King George Island leads to the advection of air masses from southwest, west and northwest. North and northwest advection occurs in particular when a low pressure centre approaches in the west of King George Island over the Bellingshausen Sea. Northeast and east advection are associated with a cyclone in the Drake Passage. Southeast, south and southwest advection can be caused by a depression centre in the Weddell Sea. Air mass transport from the west is observed when the low pressure centre is located to the South of King George Island. A low pressure centre passing directly over the island is observed very frequently. In general, synoptic situations associated with cyclonic activity dominated the observation period with 990 cases (69%), whereas anticyclones dominated the atmospheric circulation only in 389 cases (27.4 %). However, the quotas of cyclonic and anticyclonic circulation varied from year to year. Generally, during summer months, circulation types with advection from west to north were more frequent due to the movement of the circum-Antarctic low pressure trough further to the

Table 4.3: *Distribution of synoptic situations during 1986 to 1989 (KEJNA 1993). The values given in the table are percentages of each synoptic situation to the total amount of observations (1419 days).*

Direction of air mass advection	Type of synoptic situation	
	Anticyclonic (27,4%)	Cyclonic (69%)
North		4,7
Northeast	3,2	3,6
East	1,1	0,7
Southeast		1,5
South	1,0	4,8
Southwest	4,8	17,8
West	2,7	13,7
Northwest	3,2	13,2
Depression centre		5,7
Low pressure trough		4,0
Anticyclonic centre	5,6	
Margin of an Anticyklone	2,0	
Saddle	2,8	

south (KEJNA, 1998). Only in 40 observations (2.8 %) a high pressure ridge could be observed. During these occasions, the zonal circulation was blocked by the anti-cyclonic ridge.

A further study of synoptic conditions in the area was given by KOWALSKI & WIELBINSKA (1989). They analysed the reasons for the severe winter in 1986 on King George Island and found that predominant meridional circulation led to colder climatic conditions in the area. These situations are predominantly associated with a high pressure ridge over the Antarctic Peninsula causing a cold air flow from the Weddell Sea as mentioned above. In general, these situations with cold air masses and comparably low wind speeds lasted between 2 to 5 days, whereas advective weather situations could last up to 9 days. However, in all years, advection in association with low pressure centres passing to the north of the island led to intense snowmelt in all months at lower altitudes on King George Island.

The different origins of the air masses lead to a significant differentiation in air temperature, relative humidity, wind speed and radiation. The foehn-type effect of north- to west-advection was already mentioned in the previous chapter. WIELBINSKA & SKRZYPCZAK (1988) studied the influence of the direction of air mass advection on air temperature at Arctowski station based on a data set from the years 1978-81, 1983 and 1985. They observed that the highest air temperatures occurred during southerly air mass flow, while westerly to north-westerly wind directions seemed to be coupled with lower air temperatures. These results are in contrast to the observations during the field campaign in 1997/98. Table 4.4 shows the classification of the temperature values at the AWS 3b and the temperature lapse rates between AWS 3b and AWS 1 according to the prevailing air mass transport. Clearly, southerly and south-easterly advection lead to lowest air temperatures. This is confirmed by results from BINTANJA (1995), who observed 1 K lower air temperatures during southeast advection in comparison to the average. He attributed this to the origin of the air masses from the Weddell Sea which reach the island during barrier wind situations. MARTIANOV & RAKUSA-SUSZCZEWSKI (1989) stated that the main ice cap of King George Island acts as a

Table 4.4: *Classification of air temperatures (84 m a.s.l.) and temperature lapse rates (619-84 m a.s.l.) according to predominant wind direction as observed during the field campaign 1997/98.*

Wind direction (619 m NN)	Parameter	Value
north	Frequency	2,3 %
	Lapse rate	-0,38 K
	Air temperature	0,33 °C
northeast	Frequency	1,2 %
	Lapse rate	-0,81 K
	Air temperature	-0,69 °C
east	Frequency	12,9 %
	Lapse rate	-0,85 K
	Air temperature	-2,22 °C
southeast	Frequency	14,5 %
	Lapse rate	-0,85 K
	Air temperature	-2,06 °C
south	Frequency	6,8 %
	Lapse rate	-0,80 K
	Air temperature	-0,91 °C
southwest	Frequency	27,6 %
	Lapse rate	-0,55 K
	Air temperature	0,60 °C
west	Frequency	20,1 %
	Lapse rate	-0,71 K
	Air temperature	0,22 °C
northwest	Frequency	14,7 %
	Lapse rate	-0,41 K
	Air temperature	1,13 °C

barrier for the cold air masses from southeast which these cannot overcome. This is quoted by BINTANJA (1995). However, the obvious differentiation of air temperatures and temperatures lapse rates at the AWS sites shows that this is not the case. Despite the fact that data of WIELBINSKA & SKRZYPCZAK (1988) spans over different years there may be two explanations for these discrepancies:

a) the topography leads to changes in wind direction and therefore measured wind direction at Arctowski station and the AWS site do not represent the general air mass flow. As a result, classified wind direction and associated air temperatures would differ;

b) the site of the standard meteorological observations at Arctowski station is located over permafrost where the AWS measured over a snow surface. Due to lower cloud amount in Admiralty Bay during southerly advection, the radiation conditions over permafrost and the snow surface in 620 m a.s.l. will widely differ. The error of air temperature readings due to solar irradiance during this situation has to be considered and might be the reason for the differences.

4.3.2.3 Hypsometric temperature lapse rates

For the Antarctic Peninsula, only few data on hypsometric temperature lapse rates are available because regular radio and balloon soundings are scarce. However, since many mass balance and snow melt models use temperature as a basic input variable, the knowledge of such lapse rates and its variability is a fundamental requirement. Table 4.5 gives an overview of the published temperature lapse rates in the region of the Antarctic Peninsula. The values obtained from 10-m snow temperature measurements are long-term annual averages. They were derived on the basis of multivariate statistic analysis to describe the latitudinal, longitudinal, altitudinal and temporal variance. In general, these values coincide very well with the average lapse rates obtained from AWS data during summer field campaigns. However, considering the origin of the air masses and short-term changes, considerable differences can be observed. Table 4.4 shows a classification of the temperature lapse rates according to the prevailing wind direction at AWS 3b during the expedition in 1997/98. The highest gradients could be observed during southerly to easterly advection of cold, dry air masses during “barrier wind situations”. In contrast, small lapse rates generally occur during northerly and north-westerly air mass transport. The latter situations result in considerable snowmelt as will be shown in chapter 7 of this work, whereas, during barrier wind conditions, snowmelt is almost negligible since air temperatures are below the freezing point. Hence, it becomes crucial for snowmelt and mass balance calculations which temperature lapse rates are used. Applying a mean hypsometric lapse rate derived from 10-m snow temperatures results in an underestimation of snowmelt in such models. It is therefore suggested to use a lapse rate smaller than the long-term mean in melt

models to properly capture the altitudinal distribution of the melt process. Inversions are negligible due to the predominant cyclonic weather types in this region. Local effects like nocturnal cold surface winds cold not be observed at the AWS. In the radio sounding data of the adjacent Bellingshausen station, no indications of different air masses in the lowermost 1,000 m of the atmosphere could be detected during the entire observation period.

Table 4.5: *Air temperature lapse rates along the Antarctic Peninsula as reported by various authors. AP: Antarctic Peninsula, WAP: West Antarctic Peninsula, EAP: East Antarctic Peninsula, JRI: James Ross Island, PRI: Primavera, BASM: Base Antártica San Martín, KGI: King George Island.*

Location	Temperature lapse rate [K per 100 m]	Database	Author
AP	-0.68	10-m snow temperatures	MARTIN & PEEL (1978)
WAP	-0.57	10-m snow temperatures (0-1,060 m)	REYNOLDS (1981)
WAP	-0.61	(0-2,160 m)	
EAP	-0.57	(0-1,060)	
JRI	-0.58	10-m snow temperatures	ARISTARAIN ET AL. (1987)
AP	-0.57	10-m snow temperatures, station data	MORRIS & VAUGHAN (1992)
WAP	-0.82		
EAP	0.008		
KGI	-0.79 (summer) -0.66 (winter)	Meteorol. observations	WEN ET AL. (1994)
KGI	-0.62	23 baloon soundings	BINTANJA (1995)
PRI	-0.66 (summer) -0.64 (autumn)	Meteorol. observations	BETGEN (1998)
KGI	-0,58 (84-255 m a.s.l.) -0,66 (84-619 m a.s.l.)	Average of AWS data 1997/1998	this study
JRI	0,47 K (200-300 m a.s.l.) -0,42 K (100-550 m a.s.l.) -0,74 K (300-555 m a.s.l.)	Average of AWS data	RAU (pers. communication 1998)
BASM	-0,51 K (20-720 m a.s.l.) -0,58 K (20-540 m a.s.l.)	Average of AWS data	RAU (pers. communication 1998)

4.3.2.4 Altitudinal differentiation of other meteorological variables on the King George Island ice cap

Comparisons of the different AWS data sets from the summer 1997/98 field campaign give some first impressions of the altitudinal variation of the major meteorological parameters (Figure 4.7). Generally, correlations are best between the lowermost AWS sites, and a tendency of decreasing correlation with altitude and distance can be distinguished. Wind velocity, global radiation and air temperature have the best correlation coefficients. Air temperature show very little scatter and follows a clear altitudinal regression. Similar results were obtained from the analysis of temperature lapse rates as outlined in more detail in the next section of this paper. Wind speed reveals no significant altitudinal increase with elevation, and global

radiation increases with altitude as has to be expected from the thinning of the atmosphere. The larger scatter for this variable in the plot from AWS 1 against AWS 3 can be explained by differences in cloud coverage as a consequence of the distance between the two AWS (about 20 km). Shading caused by the topographic settings can be excluded due to the location of the AWS sites. For net radiation, good correlations can be found only for the lowermost areas. This is not surprising, since

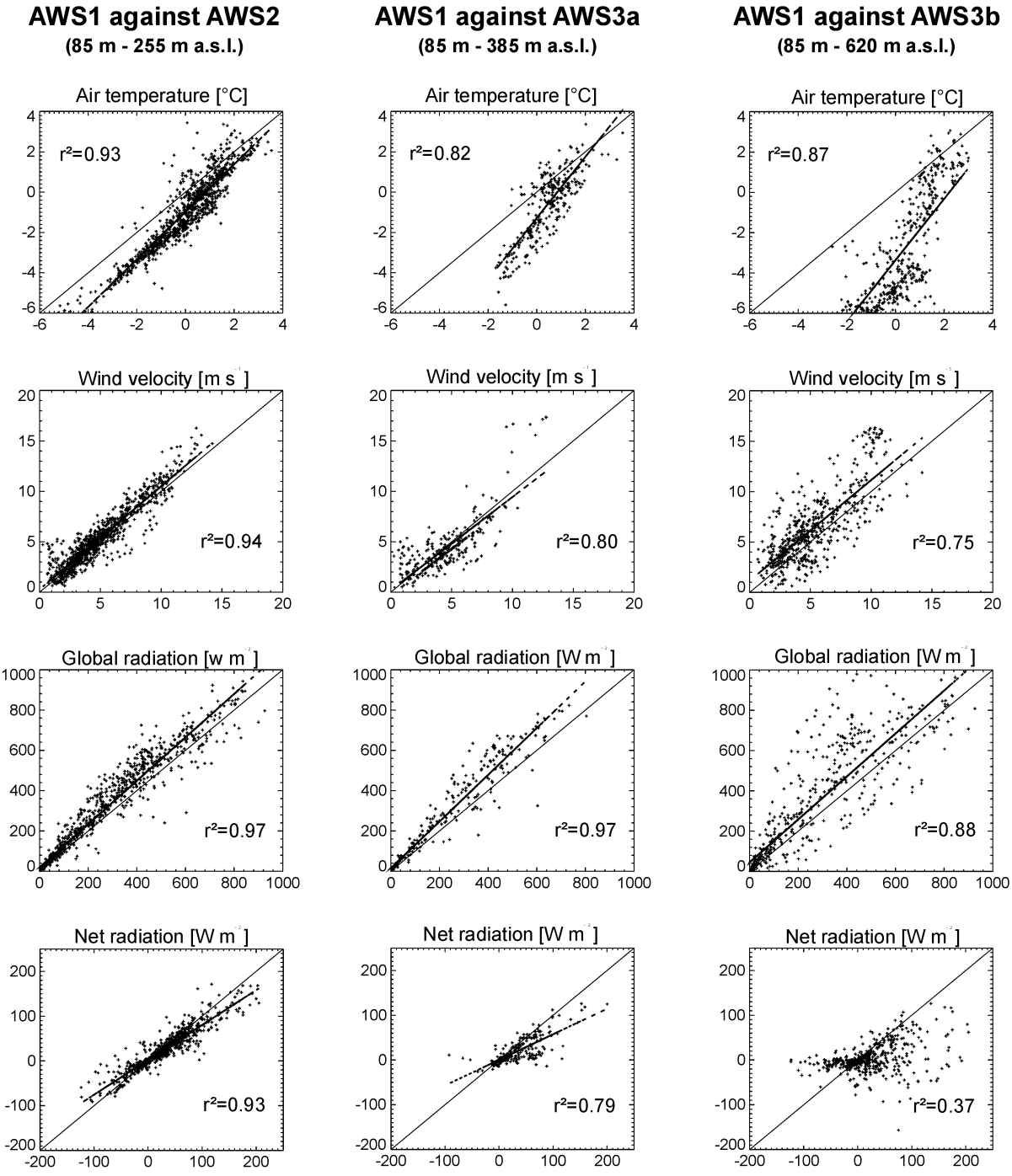

Figure 4.7: *Scatter plots and regressions of the major meteorological variables measured at the AWS during the field campaign in 1997/98. Correlation coefficients are given in the figures. The x-coordinate is always AWS 1, the y-coordinate is AWS 2 in the first column of the Figure and AWS 3a and b in the following ones.*

radiation balance is calculated from shortwave radiation and longwave radiation terms. Hence, spatial variations of one of these parameters causes decorrelation. Global radiation and albedo show comparablly little spatial variation as can be revealed from the data set. The scatter in the plots AWS 1 against AWS 3a and AWS 1 against AWS 3b can be attributed to differences in surface temperature, resulting in differences of longwave outgoing radiation, and longwave incoming radiation as a function of cloud coverage and moisture content of the air masses. This interpretation is further supported by field observations where a condensation level at about 400 m a.s.l. was frequently encountered.

Although this analysis is only based on a small data set of 4 AWS sites on the main ice cap, some general characteristics can be derived. It can be stated that it is important to consider the lapse rates of air temperature and relative humidity for any kind of climatic or hydrological modelling. Spatial variation of net radiation balance is considerable and also has to be incorporated in such models. On the other hand, variance of global radiation and wind velocity seem to be small on the main ice cap. Low effects of shading on global radiation is supported by first results of the application of a spatially distributed energy balance model. However, it has to taken into account that local topographic influence on the wind conditions (e.g. in fjord-like inlets) can not be analysed on the basis of this data set since the AWS were located on ideal sites on flat terrain.

Summary 4.3:
King George Island is subject to a highly maritime climate, characterised by the frequent succession of low pressure centres. Air temperatures during summer months reach well above 0°C. Cyclonic activity is higher in summer as a consequence of the shift of the circum-Antarctic low pressure trough. High pressure in the region of the Antarctic Peninsula is commonly associated with cold air temperatures on King George Island whereas northerly and north-westerly advection lead moist and warm air masses to the South Shetland Islands. Latter advection situation can last up to 9 days whereas situations with cold air masses are considerably shorter in duration. Analysis of the AWS data reveal a strong dependence on altitude for most meteorological variables. Air temperature lapses are particularly dependent on the prevailing synoptic weather situation.

4.4 Glaciology

4.4.1 Glacier retreat

The glacier retreat and ice shelf disintegration along the Antarctic Peninsula and on King George Island have already been introduced in chapter 1.3.4. In this subchapter, the different stages of glacier front positions in the Admiralty Bay are addressed to in more detail, and possible explanations are given.

Two major glacier types can be distinguished in Admiralty Bay: glaciers terminating on land and tidewater glaciers whose glacier fronts terminate in the sea. As previous extensive glaciological studies have shown, most parts of the King George Island ice cap can be regarded as temperate glaciers (e.g. WEN ET AL., 1998; MACHERET & MOSKALEVSKY, 1999). According to WARREN (1992), the terminus of temperate tidewater glaciers does not float.

Figure 1.8 illustrates the glacial basins draining into Admiralty Bay as delineated by SIMÕES ET AL. (1999). The major retreat areas as derived from aerial photography from 1956 and SPOT satellite imagery from 1988, 1992 and 1995 have been highlighted in white. In table 4.6, the drainage basin characteristics as obtained from a digital elevation model (BRAUN ET AL., 2001) and glacier retreat rates between the different acquisition dates (MUSER, 1995) are summarized. Over the entire observation period, all glaciers in Admiralty Bay showed area loss, however, large differences between the various drainage basins can be found. Highest retreat rates were measured in the first two periods, followed by variable retreat and advance in the period 1988 to 1992. Regarding the absolute retreat values in table 3.6, the seasonal oscillation of the glacier front position has to be considered. Some of the small glacier advances during the observation period may be attributed to that fact.

4.4.1.1 Tidewater Glaciers

As can be seen in figure 1.8, not all tidewater glaciers in Admiralty Bay behave alike. Some huge tidewater glaciers, as e.g. Polar Club Glacier, Lange Glacier, Dobrowolski Glacier or Vieville Glacier, show remarkable retreat, whereas smaller tidewater glaciers hardly changed their glacier front positions. The mean altitudes range between 195 m a.s.l. and 443 m a.s.l. Highest retreat rates are encountered in the first two periods - 1956 to 79 and 1979 to 1988. This is in good agreement with the observations by KEJNA ET AL. (1998). Over the entire observation period, the largest glacier area was lost by Polar Club Glacier (2.9 km²), followed by Vieville Glacier (2.0 km²) and Lange Glacier (1.7 km²). The glaciers with highest mass loss also show the largest drainage basin areas. A first idea on reasons for the glacier changes would be climatologically induced changes in mass balance parameters. Normally the accumulation area ratio (AAR) would be a correct measure for this purpose, but it is not available for the glaciers on King George Island. As a first approach, glaciers with different altitudinal characteristics should be affected differently. However, no obvious differences between strongly and less retreating glaciers can be found in the altitudinal range (Table 4.6). Lange Glacier shows highest elevations and a high mean altitude (442 m a.s.l.), whereas Polar Club Glacier reaches only a maximum altitude of 460 m and a mean altitude of 243 m a.s.l.. The smaller tidewater glaciers as e.g. Ajax Icefall, Doctors Icefall or Zalewski Glacier show a small retreat/area ratio and are located in different parts of the ice cap. These differences are illustrated in a subset of Martel Inlet (Figure 4.8). Krak and Dobrowolski Glacier retreated constantly since 1956 with the largest areal

Table 4.6: *Characteristics of glacier drainage basins and ice front retreat rates for the major glaciers in the area of Admiralty Bay, King George Island. Basin characteristics were obtained from a digital terrain model (BRAUN ET AL., 2001). Retreat rates for the period 1956-92 were taken from MUSER (1995). Negative values denote a glacier advance, positive values glacier retreat. T denotes tidewater glacier, L denotes glacier terminating on land, n.a.: not analysed.*

	Drainage Basin Characteristics					Glacier Retreat Rates [km²]					
Glacier Name	**Type of Glacier**	**Area [km²]**	**Mean Altitude [m]**	**Maximum Altitude [m]**	**Minimum Altitude [m]**	**1956-79**	**1979-88**	**1988-92**	**1992-95**	**1956-1992/95**	**Ratio Retreat area 1956-1992/95 to catchment area [%]**
Ajax Icefall	T	6.0	443	583	0	-0.09	0.07	0.04	0.06	0.02	0.3
Baranowski Glacier	L	3.7	195	366	2	-0.06	0.10	0.05	n.a.	0.09	2.4
Dera Icefall	L	2.0	287	455	51	0.02	0.04	0.00	n.a.	0.06	3.0
Dobrowolski Glacier	T	13.2	343	402	0	0.56	0.70	-0.25	0.21	1.22	9.2
Doctors Icefall	T	8.7	289	620	0	0.02	0.10	0.01	n.a.	0.13	1.5
Domeyko Glacier	T	36.1	359	627	0	-0.43	0.60	0.64	0.53	1.34	3.7
Dragon Glacier	L	0.5	212	305	69	0.04	0.17	-0.03	n.a.	0.18	36.0
Ecology Glacier	L	6.3	210	450	0	0.08	0.19	0.10	n.a.	0.37	5.9
Emerald Icefall	T	17.9	395	679	0	0.14	0.37	-0.10	n.a.	0.41	2.3
Gdansk Icefall	L	2.0	324	455	135	0.03	0.03	0.00	n.a.	0.06	3.0
Goetel Glacier	T	7.3	425	583	0	0.04	0.04	0.11	0.09	0.28	3.8
Krak Glacier	T	7.0	324	410	0	0.80	0.50	0.07	0.09	1.46	20.9
Lange Glacier	T	31.7	442	677	0	1.19	0.57	0.02	0.11	1.89	6.0
Pandereski Glacier	T	4.0	234	357	0	1.03	0.18	-0.08	n.a.	1.13	28.3
Rosciszewski Icefall	L	3.8	319	458	0	0.16	0.06	0.00	n.a.	0.22	5.8
Stenhouse Glacier	T	8.2	423	573	0	-0.10	0.09	0.05	0.09	0.13	1.6
Vieville Glacier	T	24.7	260	409	0	0.64	0.81	0.58	0.38	2.41	9.8
Wanda Glacier	L	2.0	236	361	0	0.11	0.15	0.05	n.a.	0.31	15.5
Zalewski Glacier	T	5.7	309	453	8	0.01	0.01	0.03	n.a.	0.05	0.9
Polar Club Glacier	T	28.9	243	460	0	2.29		0.61	n.a.	2.90	10.0
Fourcade Glacier	T	18.0	261	450	0	0.55		0.16	n.a.	0.71	3.9
Sum						***11.73***		***2.06***	***1.56***	***15.35***	

loss in the first period. However, in the 1990s significant ice cliff retreat could still be observed.

The different retreat phases and difficulties in determination of glacier front position due to seasonal changes will be outlined at the example of Lange Glacier (Figure 4.9). A first phase of retreat (440 m) is recorded for the period between 1956 and 1975. Even more striking is the retreat in the short time period between 1975 and 1979. Together, these two periods led to an ice cliff retreat of about 880 m, i.e., a loss of approximately 1.1 km². This process continued between 1979 and 1988, when the glacier retreated additional 280 m, thus losing another 0.56 km². Between 1988 and 1995, the glacier retreated further 180 m, i.e. an area loss of 0.13 km². In total, the glacier retreated about 1,380 m from 1956 to 1995, thus losing approximately 1.7 km². It should be noted that a comparison of the satellite images of February 1988 (late summer) and November 1994 (spring) does not indicate a significant glacier retreat for this period. However, one has to be cautious when interpreting these data as steady state or advance of the glacier terminus. When comparing ice front states of Stenhouse Glacier during 1957/58 and 1959 a strong oscillation of the glacier terminus position depending on the season could be observed (NOBLE, 1965; STANSBURY, 1961a). In February/March 1957, massive calving led to ice front retreat, while during winter the glacier terminus advanced 150 m until the next spring. This

was followed again by a retreat of the terminus in the summer months. STANSBURY (1961a) showed the inter-annual variations of glacier front resulting in a slight advance of the glacier front of Stenhouse Glacier in the period from 1957 to 1960 (Figure 4.10). Keeping this yearly cycle in mind, the acquisition date of aerial and satellite images becomes crucial when small changes in glacier extent are monitored. As a consequence, comparisons of only two dates may only reflect small annual changes and not enable a direct statement on a general glacier retreat. For this purpose, a continuos monitoring over several years/decades is required if retreat rates are small.

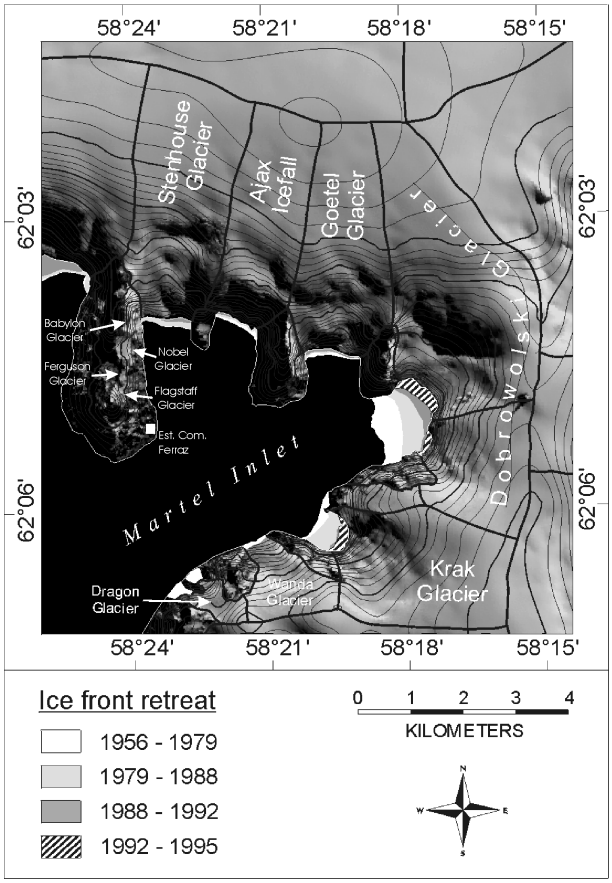

Figure 4.8: *Subset of Martel Inlet in Admiralty Bay. The different glacier retreat phases are indicated in grey levels.*

4.4.1.2 Glaciers terminating on land

Regarding the retreat area, glaciers terminating on land show the smallest absolute values. However, considering the ratio between retreat area and basin area they exhibit the largest percentages (e.g. Dragon Glacier or Wanda Glacier). These glaciers show the lowest altitudinal extends and mean altitudes. Therefore it has to be expected that the AAR is smallest for this glacier type in Admiralty Bay area.

Since ice front changes are very small the accuracy in the determination of glacier borders has to be considered. The estimation of an absolute error of ice front positioning is difficult since there are various influencing factors such as pixel size, errors resulting from co-registration or mixed pixels. MUSER (1995) used residual images to determine glacial changes. Using this technique snow cover on ice free areas can

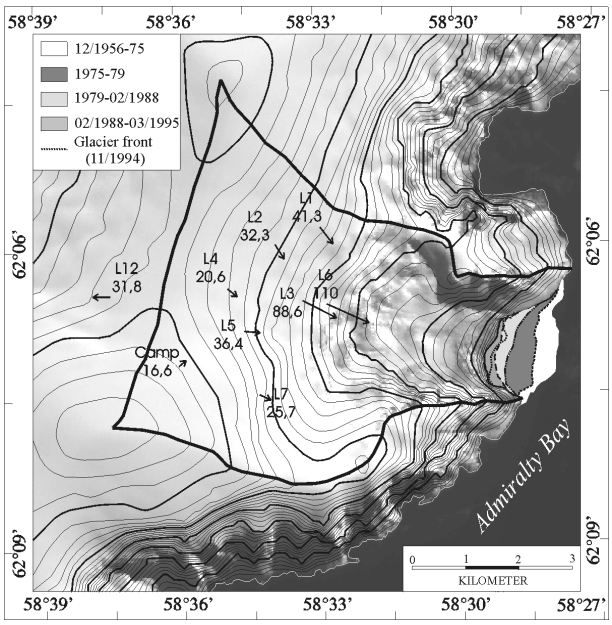

Figure 4.9*: Glacier retreat and velocity vectors in the Lange Glacier drainage basins, one of the largest outlet glaciers of the ice cap.*

lead to errors. However, as he based his work on several panchromatic scenes from the year 1992, he could minimise these errors. Nevertheless, the absolute retreat values have to be treated with some caution. Ecology Glacier showed a retreat of about 0.37 km² between 1956 and 1995. This value comprises mainly the retreat in the central glacier front with a maximum recession of about 270 m between 1956 and 1992.

4.4.1.3 Possible reasons for the differences in glacier retreat of the tidewater glaciers in Admiralty Bay

The results presented above indicate that different mechanisms seem to drive glacier retreat in Admiralty Bay. The calving speed and calving flux of tidewater glaciers are controlled by water depth, sub-glacial runoff, ice velocities, ice thickness and ice cliff height, water temperature, topography, buoyancy forces and accumulated strain (WARREN, 1992). Calving is suppressed during the winter freeze-up and highest in autumn. This is in good coincidence with the observations on Lange and Stenhouse Glacier as mentioned above. However, WARREN (1992) pointed out that the relation water depth to calving rate as well as the fjord or outlet geometry is most important for the explanation of the often drastic retreat of tidewater glaciers. Higher water depth seem to enforce the calving process. The terminus of many stable tidewater glaciers is often grounded on a final moraine. Once the glacier retreats from this moraine, the glacier ends in deep water and enforced calving has to be expected until a stabilisation occurs further to the interior of the drainage basin due to more favourable valley or fjord geometry. Lange Glacier may be regarded as a good example for this situation. It showed an immense retreat in the beginning and now an almost stagnant glacier front position in a more protected part of the outlet. This hypothesis is supported by the fact that all glaciers showing strong ice front retreat ended in a shallow inlet or bay. Many of these tidewater glacier seemed to have been grounded on sub-aquatic moraines during the 1956 image acquisition. These moraines are still visible in recent satellite imagery (e.g. at Vieville Glacier). Re-advance can only occur when the glacier provides sufficient sediment to lower the water depth in front of its ice cliff (WARREN, 1992). Finale moraines are absent in front of small glaciers such as Ajax Icefall or Emerald Icefall. It is supposed that bedrock and glacier

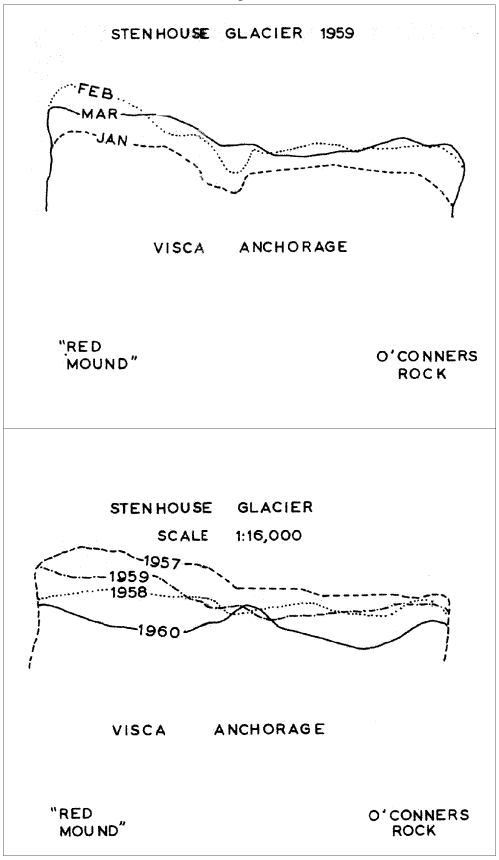

Figure 4.10: *Annual and interannual variations of glacier front positions of Stenhouse Glacier, Admiralty Bay (STANSBURY, 1961a).*

directly rise over sea level so that the influence of water depth is minimised. This demonstrates for tidewater glaciers that the trigger initiating the glacier fluctuation cycle may be climatic such as a rise in the equilibrium line altitude (ELA), but once the cycle is in progress, internal mechanisms can over-ride external forcing (WARREN, 1992; PATERSON, 1994; BENN & EVANS, 1998).

However, the significant retreat of glaciers terminating on land indicates that changes in mass balance parameters have occurred and still do occur. Since ablation is the prevailing mass loss at these glaciers types, increasing air temperatures as observed along the Antarctic Peninsula will affect the glacier mass balance considerably. The low mean altitude of these small glaciers terminating on land together with their small altitudinal range favour their sensitivity against mass balance changes. This has been demonstrated using sensitivity analysis of an energy balance model by BINTANJA (1995). Indications for a rise in ELA since the first measurements on King George Island are given in table 4.7. ELAs observed during the 1990s reveal considerably higher values than the ones measured in the 1970s. This is in good agreement with the higher mean air temperatures recorded during this decade. The data on Deception Island (ORHEIM & GOVORUKHA, 1982) can not be regarded as representative for the entire South Shetland Islands since the data was recorded short after the volcanic eruptions in 1967, 1969 and 1970. Moreover, the island has only a small ice cover. The suggestion that glacier retreat is climatically induced coincides with the observations by PARK ET AL. (1998) for Marian Cove. They concluded from their analysis that the sea ice conditions in Marian Cove did not seem to be responsible for the observed ice front position changes. Both, PARK ET AL. (1998) and KEJNA ET AL. (1998) attributed the glacier retreat to the observed increasing mean air temperatures in the region.

4.4.2 Mass balance parameters, firn-ice transition and glacier velocities

Glaciological investigations in the area of the South Shetland Islands can be subdivided into three major phases. In the 1950's, personnel of the Falkland Island Dependency Survey (FIDS) performed first mass balance measurements on the glaciers near the former Base G on Keller Peninsula (HATTERSLEY-SMITH, 1949; NOBEL, 1965 and STANSBURY, 1961b). A second phase started with the studies by OHRHEIM (1972), ORHEIM ET AL. (1972) and ORHEIM & GOVORUKHA (1982) in the early 1970s. The last phase, starting at about 1985, was introduced by extensive research on the ice caps of Nelson Island and King George Island by Chinese, Russian, Brazilian and German scientists.

4.4.2.1 Accumulation

In comparison to other regions of Antarctica, many accumulation measurements are available for the glaciers on the South Shetland Islands. KNAP ET AL. (1996) used data published by ZAMORUYEV (1972) with 2000 mm water equivalent (WE) for his ice flow

model and a linear accumulation gradient from 500 mm at Bellingshausen station to 2000 mm WE on top of the ice cap. Similar accumulation rates were measured by WEN ET AL. (1998). However, the dating of the ice core on the summit of the ice cap was strongly affected by percolating melt water. This makes a dating by isotopes or snow chemistry difficult (HAN & YOON, 1990; HAN ET AL., 1995, 1999; YAN, 1997), and consequently, they used stratigraphy for dating. Only ice layers exceeding 5 cm thickness were recognised as summer layers, all others as intermediate snow melt events during the year. Using their published data, an altitudinal accumulation gradient of 420 mm WE per 100 m could be determined for the elevation range 250 to 700 m a.s.l. on Arctowski Icefield, excluding data from Bellingshausen Dome (Figure 4.11).

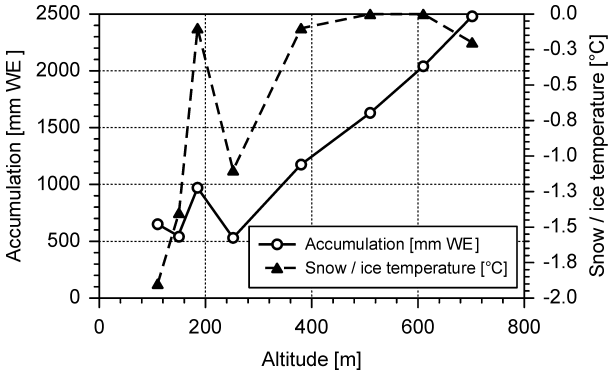

Figure 4.11: *Accumulation and snow / ice temperature in relation to altitude (after data published BY WEN ET AL., 1998).*

These net accumulation rates contrast to the data from a second ice core drilled by an international team in 1995/96 (SIMÕES pers. com., 1999). There a net accumulation rate of 500 to 600 mm WE was obtained for the last years on top of the ice cap using stable isotopes and a Cs^{137} peak at 7.5 m depth which supposedly originated from the French atomic tests in 1978 (POURCHET pers. com, 1996, SIMÕES pers. com., 1999).

ORHEIM & GOVORUKHA (1982) gave a net accumulation between 500 and 700 mm WE at 240 m a.s.l. on Bellingshausen Dome for the years 1957-70. This is in good agreement with a mean value of 700 mm WE obtained from stratigraphic dating of a 80.2 m ice core in 1991 (HAN ET AL. 1999) and unpublished data from several shallow ice cores at various sites on King George Island in this elevation range (SIMÕES pers. com., 2000). SIMÕES ET AL. (1995) gave net accumulation rates on Noble Glacier of 700 to 900 mm WE and 800 to 900 mm WE for Livingston Island based on shallow ice cores. On the adjacent Nelson Island ice cap, JIAWEN (1995) measured accumulation rates of 790 mm WE at 230 m a.s.l., and 1,050 mm WE at 200 m a.s.l. from February 1988 to February 1989. They obtained a mean accumulation rate of 1,200 mm WE (1970-88) for the top of the ice cap since they encountered ash layers of the Deception Island eruptions. POURCHET (pers. com., 1996) obtained a mean accumulation rate of 590 mm WE in an elevation range between 160 and 330 m a.s.l.from Pb and Cs radio-isotope measurements in 11 snow pits on Hurd Glacier, Livingston Island.

4.4.2.2 Ablation

The detailed glaciological program run during the operation of Base G on Keller Peninsula in the years 1957 to 1960 included mass balance and glacier velocity measurements. STANSBURY (1961a) observed a mean ablation of 544 mm WE on Flagstaff Glacier in the period from 03 February to 21 April 1959. Furthermore, he already attributed the interannual variations in the summer ablation rates and the resulting mass balance differences to the varying frequency of northerly gales. In the year 1960 the path of depressions was further south and hence led warmer air masses from lower latitudes to the island. As a consequence, higher ablation rates were recorded during this summer.

In the austral summer 1990/91, BINTANJA (1992, 1995) performed comprehensive energy balance calculations from meteorological measurements on Ecology Glacier. He obtained an ablation rate of 750 mm in one month (Dec-Jan.) at an altitude of about 100 m a.s.l. Extrapolating this value for the entire ablation season (assuming a duration of 2.5 momth at 100 m a.s.l.) an ablation rate (1.5 to 2.0 m WE) of almost twice as much as reported by ORHEIM & GOVORUKHA (1982) would result. However, his measuring period was about 1.5 K warmer than the long-term average. Adding 1 K on his data set, he obtained 15 % higher ablation rates and concluded that the ice masses on King George Island were highly sensitive to climatic changes. Considerably smaller ablation values have also been reported by WEN ET AL. (1998) with 1,430 mm WE (45 m a.s.l.) to 410 mm WE (252 m a.s.l.). A summer ablation gradient of -500 WE mm $100m^{-1}$ can be calculated from their data. They also show how the ablation periods vary with altitude (Figure 4.12).

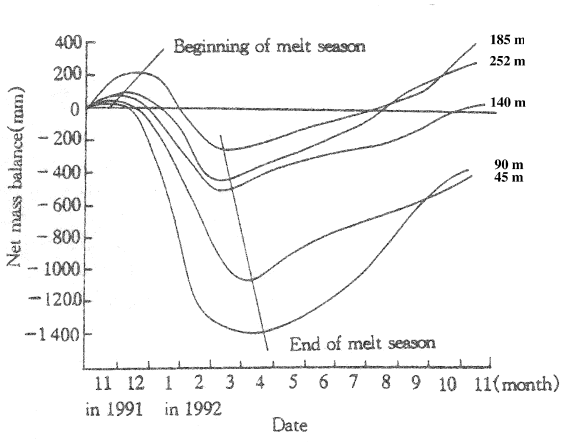

Figure 4.12: *Length of the ablation period on King George island as revealed by stake measurements in the period 1985 to 1991 (WEN ET AL., 1998).*

4.4.2.3 Mass balance / ELA variation

During the International Geophysical Year (IGY, 1957/58), NOBEL (1959, 1965) calculated the specific mass balance of Flagstaff Glacier as –0.53 m WE, i.e. it was undernourished. This compares with a specific budget of –0.76 m WE in the mass balance year 1959/60 (STANSBURY, 1961a). The same author established a relation between his measured mass budgets and observed mean air temperature at the base. He concluded that in the period 1948-60 Flagstaff Glacier had five strong negative budget years and four slightly positive mass balance years that, however, only compensate two of the negative years. The remaining years showed only slightly

negative balances. These negative mass balance years seem to have continued and led to retreat of the small cirque glaciers on Keller Peninsula as subsequent studies by SIMÕES & DANI (1994) revealed. They observed the ice front retreat on Noble Glacier of about 100 m as well as a considerable volume loss between 1959/60 and 1993/94. The mass loss appears to have lasted throughout the warm summer seasons of the late 1990s resulting in a further loss of a glacier lobe (BREMER pers. com., 2000). He also visually observed in February 2000 that the nearby small Ferguson Glacier had completely disappeared. Flagstaff Glacier was reduced to about 50% of its areal extent of 1994.

ORHEIM ET AL. (1972) stated that the annual variations in mass balance are controlled by summer temperatures in the South Shetland Islands. This underscores the importance of ablation measurements in this region. A steep mass balance gradient, typical for glaciers in maritime climates (OERLEMANNS, 1993), is revealed from the observations of ORHEIM & GOVORUKHA (1982). WEN ET AL. (1994) give a mass balance gradient of 840 mm WE per 100 m altitude difference for Bellingshausen Dome. This is double the net accumulation gradient calculated from the data the same authors published in 1998 for the main ice cap. Similarly, a high mass balance gradient was mentioned by BINTANJA (1995) for King George Island and POURCHET (pers. comm. 1996) for Livingston Island.

Equilibrium line elevations (ELA) for Bellingshausen Dome, Rotch Ice Dome (Livingston Island) and Deception Island were first given by ORHEIM & GOVORUKHA (1982). They concluded from their observations that mass balance curves on the South Shetlands were quite well correlated. Furthermore, WEN ET AL. (1994) applied a very simple mass balance model for Bellingshausen Dome where ablation is approximated by a rough formula using 3-monthly mean summer air temperatures. The type of precipitation events was not considered. They concluded from these calculations that Bellingshausen Dome was in a stable mass balance during the period 1971/72 to 1991/92. This is in contrast to the glacier retreat observed by SIMÕES ET AL. (1999). Table 4.7 summarizes the values of ELA, firn line altitudes (FLA) and the estimated climatic firn line altitude (CFLA) for the South Shetland Islands. The data show a wide scatter of ELA/FLAs that possibly reflect the interannual variation and the different local climatic conditions on the study sites. Direct comparisons are therefore very difficult, however, using data only from the same area (e.g. Bellingshausen Dome or Admiralty Bay), a rise of the ELA/FLA in the beginning of the 1990s seems to have occurred.

Tephra layers which can serve as markers (isochrones) in ice cores and ground penetrating radar studies (GPR) have been identified and are still visible on various ice cliffs on King George Island. However, dating and the determination of their origin has caused problems so far and could not be conclusively linked to the GPR results. ZHANG ET AL. (1997) and HAN ET AL. (1999) were able to date at least several of the layers using data from a 80.2 m ice core on Bellingshausen Dome and the Dansgaard-Johnson flow model for age determination. Table 4.8 shows the correla-

Table 4.7: *Summary of equilibrium line altitudes (ELA), firn line altitude (FLA) and climatic firn line altitudes as reported for the South Shetland Islands. DI: Deception Island, KGI: King George Island, LI: Livingston Island*

Balance year	Location	ELA / FLA / CFLA [m]	Authors
1957	Flagstaff Glacier, Admiralty Bay (KGI)	198 (FLA)	STANSBURY (1961a)
1959		130 (FLA) 200 (CFLA)	
1960	Admiralty Bay (KGI)	300 (FLA)	
1968-69	G1 (DI)	275 (ELA)	ORHEIM & GOVORUKHA (1982)
1969-70	G1 (DI) / Bellingshausen Dome (KGI)	290 / 140 (ELA)	ORHEIM & GOVORUKHA (1982)
1970-71	G1 (DI) / Bellingshausen Dome (KGI)	325 / 170 (ELA)	ORHEIM & GOVORUKHA (1982)
1971-72	G1 (DI) / Rotch Ice Dome (LI)	370 / 140 (ELA)	ORHEIM & GOVORUKHA (1982)
1972-73	G1 (DI) / Rotch Ice Dome (LI)	330 /170 (ELA)	ORHEIM & GOVORUKHA (1982)
1973-74	G1 (DI) / Rotch Ice Dome (LI)	280 /150 (ELA)	ORHEIM & GOVORUKHA (1982)
1985-86	Bellingshausen Dome (KGI)	150 (ELA)	JIAWEN ET AL. (1995)
1985-89	Nelson Island	110 (ELA)	JIAWEN ET AL. (1995)
	South Shetland Islands	<100 (ELA)	CLAPPERTON (1990)
1991/92	Bellinsghausen Dome (KGI)	140 (ELA)	WEN ET AL. (1994)
1991/92	Ecology Glacier, Admiralty Bay (KGI)	ELA about 100	BINTANJA (1995)
1992/93	Hurd Dome (LI)	235 (ELA)	VILAPLANA & PALLOS (1994)
1965-93	Hurd Dome (LI)	ca. 200 (ELA)	PERS. COMM. POURCHET 1996
1993	Noble Glacier, Admiralty Bay (KGI)	350	SIMÕES ET AL. (1995)
1993-95		450 (FLA)	
1988	Admiralty Bay (KGI)	350 (FLA)	SIMÕES ET AL. (1999)

tion between their dating and reported eruptions of the adjacent volcanoes of Penguin and Deception Island.

4.4.2.4 Firn-ice transition

The firn-ice transition on the highest elevation on King George Island was measured in both ice cores at about 37-39 m (WEN ET AL., 1994; SIMÕES pers. comm, 1998). This is in good agreement with data obtained by the ground penetrating radar (GPR) survey in 1997/98 (PFENDER, 1999). However, in a second publication, WEN ET AL. (1998) described the firn-ice transition at 45 m depth and a water table often encountered at about 50 m. On Bellingshausen Dome (250 m a.s.l.), the firn-ice transition was determined at a depth between 12 to 20 m by ORHEIM & GOVORUKHA (1982) in the years 1969-71. WEN ET AL. (1998) also report the firn-ice transition on top of that dome to be located at 7 m depth in the years 1985-91. This would indicate decrease of accumulation of at least 5 m in about 15 to 20 years. On top of the adjacent Nelson Island ice cap (330 m a.s.l.), the firn-ice transition was measured at 25-26 m depth and at 250 m a.s.l. at 15 m depth (JIAWEN ET AL., 1995). In a further drilling at 240 m a.s.l., the water table was located at 15 m depth.

Table 4.8: *Visible volcanic deposits along a 80.2 m ice core from Bellingshausen Dome and their possible origins. The Dansgaard-Johnson flow model was used for the age determination (modified after HAN ET AL, 1999). DI and PI denote eruptions at Deception Island and Penguin Island respectively. The "?" indicates eruptions where no assured report is available.*

No.	Depth [m]	Thickness [mm]	Visible feature	Age [AD]	Historical record
1	21.29	10	Brown, dispersed particles	1955	DI 1956
2	40.39	5	Lignite-like, homogeneous particles	1907	PI 1905?; DI 1909?, 1912
3	44.26	>5	Lignite-like, homogeneous particles	1893	
4	45.40	50	Brown, discontinuous slice of scatter particles	1888	
5	47.01	10	Dark-brown, discontinuous layer of particles	1882	
6	48.12	5	Lignite-like, homogeneous particles	1878	
7	48.76	5	Dark-brown, discontinuous layer of particles	1876	1871
8	56.44	>5	Dark-brown, homogeneous particles	1841	DI 1842
9	60.92	5	Dark-brown, homogeneous particles	1817	DI 1812

4.4.2.5 Glacier flow velocities

NOBLE (1965) measured glacier velocities for Stenhouse Glacier in the International Geophysical Year 1957/58. His values (20 to >365 m a^{-1}) are comparable to the flow rates obtained from DGPS measurements during the field campaigns in 1997/98 and 1999/2000 in the upper drainage area of Lange Glacier (Figure 4.10, table 4.8). Both glaciers are heavily crevassed and show steep slopes, in the middle part of Lange Glacier where velocities are highest. Moreover, Noble's observations revealed no significant change with temperature and season. JIAWEN ET AL. (1995) and DAHE (1989) reported glacier velocities for the Nelson Island ice cap with flow rates of 2 to 20 m a^{-1} in the upper parts of the ice cap for the years 1985 to 1989. These lower values are in good agreement with the 18.3 m a^{-1} measured by Hattersley-Smith at a cite called "Camp Glacier" (62°05'S/58°21'W) on the east side of Admiralty Bay in 1949 (STANSBURY, 1961a) as well as with DGPS measurements on Bellingshausen Dome during the field season 1999/2000 (Table 4.9). Both the Nelson Island ice cap as well as the Bellingshausen Dome show only smooth slopes.

4.4.3 Ice thickness, bedrock topography and internal ice structures

Along a major transect line from Fildes Peninsula to the main dome of the ice cap and 3 short cross profiles, first GPR measurements were performed by GOVORUKHA ET AL. (1975) in April 1970. They used a slow-power RV-10 radar set with a SI-20 oscillograph and high resolution frame antenna, and an operating frequency of f=4.4 MHz. Measurements were taken every 50 to 100 m. With these experiments they revealed a mean ice thickness of about 100 m (ORHEIM & GOVORUKHA, 1982), a maximum ice thickness of 326 m and a large subglacial transverse valley in the middle of the profile. Furthermore, they observed that the King George Island ice cap is a temperate glacier, and that the warm firn zone covers most of the accumulation

region. Further spot ice thickness soundings were done during British Antarctic Survey (BAS) flight no. 38 in 1975 and revealed a maximum thickness of 357 m (SIMÕES ET AL., 1999). Concurrent with shallow drillings on the ice cap by a Chinese expedition, radar soundings were performed between Bellingshausen Dome and half-way up to the main dome of the ice cap. Again the 150 point measurements using 300 MHz revealed a mean thickness of 109 m (ZHU ET AL. 1994). However, the data did not include ice thickness over the subglacial valley as obvious from the BAS and Russian studies. In 1995 and 1996/97, a third GPR survey was undertaken by a Russian team (MACHERET ET AL. 1997, 1998; MACHERET & MOSKALEVSKY, 1999). This data set comprises point measurements (every 500 m) along the major ice divide of the ice cap and in the upper part of the Lange Glacier drainage basin. From that data they estimated a mean ice thickness of 180-230 m and a total ice volume of about 236-302 km². All these surveys lack a reliable positioning and altitude reference (the Russian surveys in the 1990s were the most accurate, using a single handheld GPS (±200 m) for the determination of UTM coordinates as well as a combination of map data and barometric measurements for altitude reference).

The most comprehensive GPR survey was carried out by the University of Münster during the joint field work of IGM, IPG and LAPAG on King George Island in 1997/98. The survey covered an area of about 200 km² in a 1 km grid with continuous digital data record (PFENDER, 1999). The study revealed a maximum ice thickness of 397 m

***Table 4.9**: Glacier flow vectors as obtained during the field campaign 1999/2000.*

Stake ID	Latitude [DD MM SS.SS]	Longitude [DD MM SS.SS]	Altitude [m a.s.l.]	Velocity [m a-1]	Direction [°]
Collins Dome:					
B09	62 10 31.61763 S	58 53 18.64 W	152.0	1.8	203
B10	62 10 14.41476 S	58 53 13.11 W	196.3	2.8	185
B11	62 09 58.90171 S	58 53 2.96 W	241.7	1.8	229
B12	62 10 16.45220 S	58 52 57.93 W	190.8	2.1	247
B13	62 10 15.96753 S	58 53 34.69 W	174.1	3.5	213
Lange Glacier:					
L01	62 05 45.62687 S	58 33 3.51 W	479.1	50.0	112
L02	62 05 54.93064 S	58 33 59.53 W	514.0	38.9	105
L03	62 06 31.12303 S	58 33 33.37 W	446.9	89.4	102
L04	62 06 23.25528 S	58 34 58.93 W	547.2	38.0	85
L05	62 06 50.30456 S	58 34 40.60 W	533.5	55.6	76
L06	62 06 40.91500 S	58 33 13.30 W	407.5	111.9	95
L07	62 07 27.52014 S	58 34 24.81 W	544.6	43.2	83
L08	62 07 52.99013 S	58 34 40.88 W	575.8	23.6	79
L09	62 07 43.60913 S	58 35 13.23 W	609.1	16.9	75
L10	62 07 20.93448 S	58 35 38.37 W	615.3	19.9	64
L11	62 06 40.08042 S	58 36 15.91 W	600.4	11.9	52
L13	62 06 29.67117 S	58 33 49.58 W	471.8	77.0	99
L15	62 05 17.67938 S	58 33 38.85 W	537.8	32.0	106
L16	62 05 2.17968 S	58 33 2.23 W	523.1	36.6	102
L20	62 08 15.38993 S	58 33 10.70 W	494.1	7.6	33
L21	62 08 2.48372 S	58 32 59.26 W	437.2	21.6	31
L22	62 07 56.39788 S	58 32 51.83 W	417.7	36.5	35
CAMP1	62 07 15.63762 S	58 36 6.39 W	626.9	15.6	50

in the northwest of the main ice dome. Figure 4.13 shows the bedrock elevation in a 3D-view. The main tectonical structure of Fildes Block and Barton Horst is clearly visible. Two major basins which are not visible in the surface topography drain to the northwest. Note that the coastline (0 m) was used for interpolation in areas where no GPR data could be obtained due to crevasses. Two examples of the radargrams with the most remarkable internal features of the ice cap are given in figure 4.14. Part a) of this figure shows a phenomenon called “Raymond-Bumps”, which has previously only been observed below the ice divide of big ice sheets. They form in areas where surface inclination is close to 0° and often when the ice is frozen to the bed. The horizontal velocities on the ice divide disappear and the vertical velocities are reduced. Consequently, the snow and ice masses are transported slower to deeper parts, and the isochrones show the respective ridging. This coincides with the interpretation of temperature measurements by REN (1990) who infers that the ice in the highest elevations of the King George Island ice cap is frozen to the bed. In the same figure, the water table is well marked in the lateral areas, and left of the “Raymond-Bumps”, a reduced bedrock reflection is visible. MACHERET & MOSKALEVSKY (1999) were able to identify a bedrock signal in only 65% of their GPR sites. In lower elevations, strong water inclusions in the ice body were present (Figure 4.14). Figure 4.15 shows features related to the internal water content of the ice cap. While figure 4.15a displays the distribution of GPR-sections where the ice body shows the strongest water inclusions, figure 4.15b focuses on the water table which forms at the snow-ice transition. It is remarkable that in the highest elevations (>550 m a.s.l.) the water table seem not to be as well developed as in lower elevations (340-550 m a.s.l.).

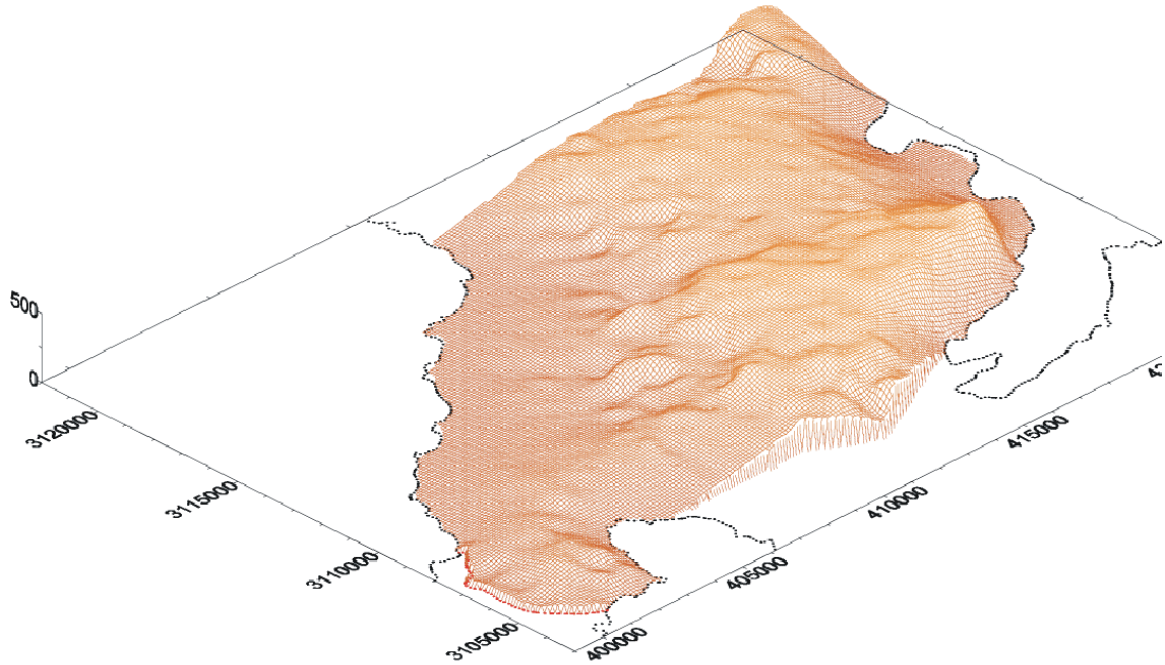

Figure 4.13: *3D-view from southwest of the bedrock topography (PFENDER, 1999).*

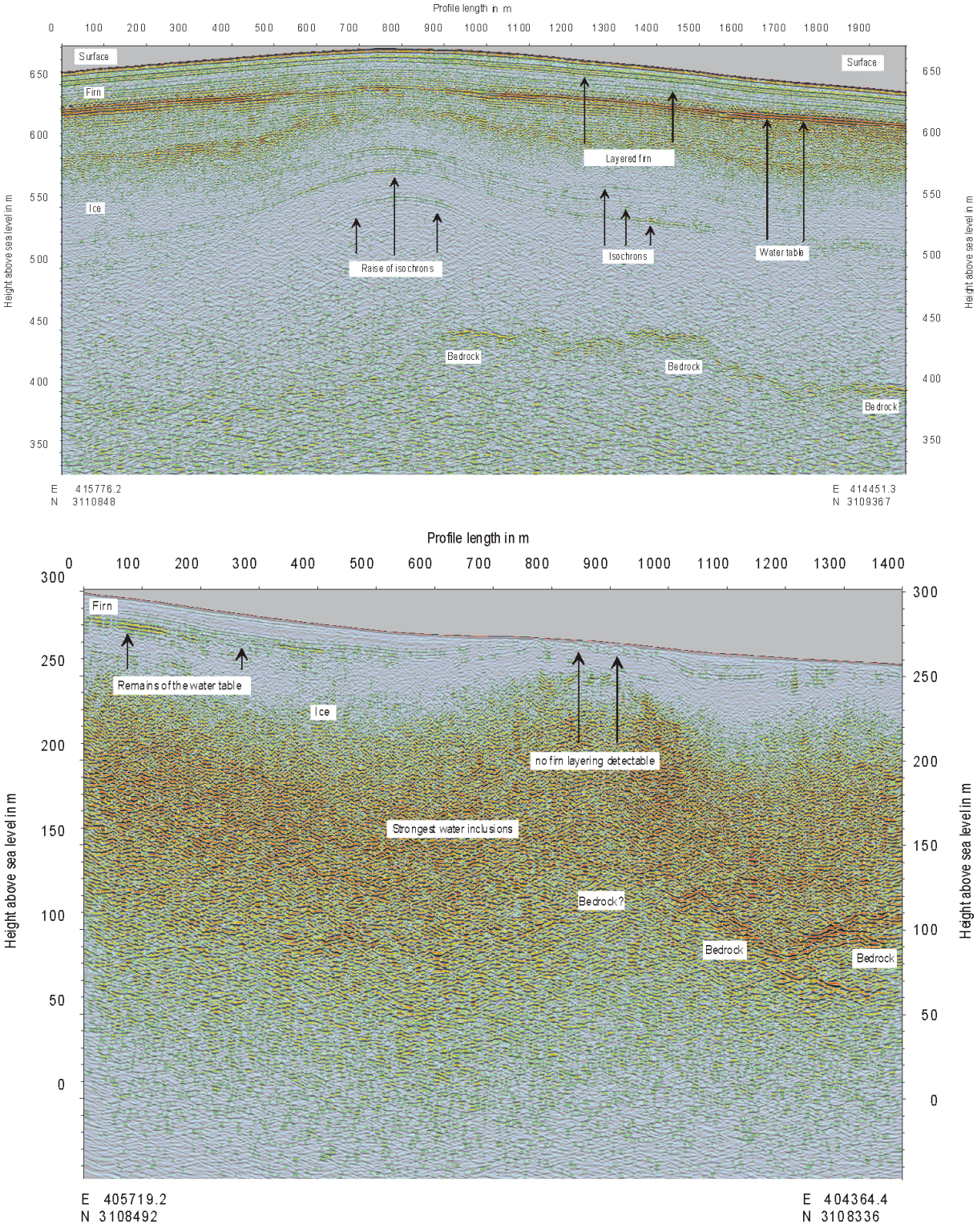

Figure 4.14: *Two radargrams for selected parts of the GPR survey in 1997/98 (from PFENDER, 1999).* ***a)*** *Section of the highest elevation of King George Island. Note the water table, internal isochrones and the reduced bedrock reflection at the highest parts of the ice cap. The raised isochrones below the ice divide are also called "Raymond-Bumps".* ***b)*** *Section from the lower part of the ice cap with very strong water inclusions. The water table and firn layering disappear at about 250 m a.s.l.. Bedrock reflection is reduced due to the high water content in the ice.*

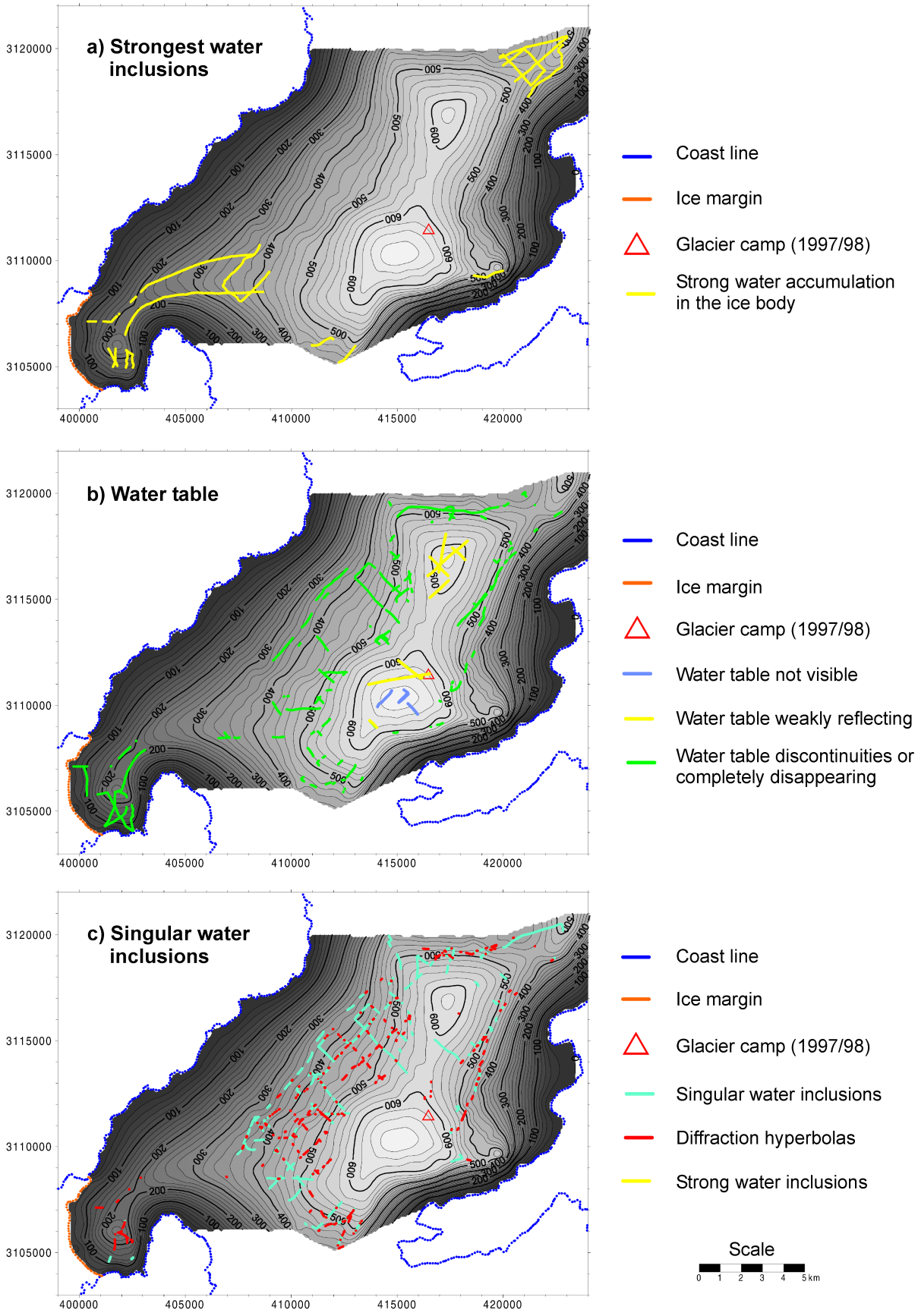

Figure 4.15: *Distributions of GPR-sections with water inclusions and of features of the water table. Diffraction hyperbolas and singular water inclusions which are interpreted as accumulation of melt water in crevasses and small fissures as a consequence of ice distortions (from PFENDER, 1999).*

Discontinuities in the water table are marked in green colour. They are attributed to ice distortions where melt water percolates to lower parts of the ice body. Finally, figure 4.15c displays the distribution of diffraction hyperbolas and singular water inclusions which are interpreted as accumulations of melt water in crevasses or fine fissures. In the GPR-profiles from the lowest elevations of the King George Island ice cap (<150 m a.s.l.), no firn layering and water table could be observed. This is the area which is snow free during the summer months. Consequently, PFENDER (1999) interprets the absence of firn layering as a result of melt-refreeze which leads to a homogenous ice body. This is further supported the finding of HAN ET AL. (1995) who observed colder ice temperatures in the ablation and 0°C-isothermy in the firn body of the accumulation area.

Summary 4.4:

On King George Island, drastic glacier retreat can be traced back to the 1950s. Indications for a change in glacier mass balance exist, but for tidewater glaciers a strong component of dynamic adjustment has to be considered as well. The equilibrium line altitudes in the 1970s and 1980 ranged at about 140 m a.s.l., whereas observations from the 1990 indicate an upward shift to about 200 m a.s.l. on Bellingshausen Dome. Most plausible accumulation for the ice cap rates range between 500 and 1,000 mm WE depending on the location. However, values upt to 2400 mm WE were reported. At lower elevations, the ablation season starts in November and lasts until March. A large altitudinal mass balance gradient was reported by several authors. The firn-ice transition was encountered at about 37 m on the main ice cap, whereas on Bellingshausen Dome, values range between 12 (1969-71) and 7 m (1985-91). GPR surveys and ice core drilling proved the existence of a definitive water table at the firn-ice transition induced by the extensive summer melt. Only in the highest areas of the ice cap, indications for an absence of such melt features were encountered in the GPR data.

5 Modelling snow and glacier melt

5.1 Surface energy balance of a snow cover

One fundamental method to determine snow melt is the calculation of the surface energy budget. Energy balance models can be subdivided into point and spatially distributed studies. Furthermore, single location studies can be subdivided by the approach used to determine the turbulent fluxes:

1. direct measurements via the eddy correlation method, which require intense equipment and maintenance, and
2. indirect calculations from standard meteorological or slightly extended observations.

For an already melting surface, any further energy gain is assumed to be directly used for melting. In glaciology, energy fluxes directed towards the surface are generally defined as positive and those from the surface as negative. The energy balance of a snow surface is then given by the equation

$$Q_N + Q_H + Q_E + Q_G + Q_R + Q_M = 0 \quad (1)$$

Q_N is the net radiation, Q_H the sensible heat transfer, Q_E the latent heat flux, Q_G the change of heat in the vertical column of the snow pack, Q_R the heat supplied by rain, and Q_M the energy available for melt.

In a second step, the available melt energy is then commonly transformed in melt rates (M) via the formula

$$M = \frac{Q_M}{\rho_w L_f} \quad (2)$$

ρ_w *is* the density of water and L_f the latent heat of fusion for ice ($3.34 \cdot 10^5$ J kg^{-1}).

A brief compilation of single location energy balance studies on glaciers and the corresponding distribution of heat fluxes is given in table 5.1. In general, most of the energy balance calculations revealed that net radiation supplies most energy used for melt followed by the sensible heat flux. At selected sites, values of sensible heat flux up to twice the net radiation have been reported (MORRIS, 1989), whereas the latent heat flux frequently is a heat sink or of minor size. The importance of net radiation relative to the turbulent fluxes increases with altitude. This has to be expected from the vertical lapse rates of air temperature and vapour pressure (RÖTHLISBERGER & LANG, 1987 cited in HOCK, 1998; BRAITHWAITE, 1981). Moreover, radiation balance as a heat source seems to gain importance with increasing continentality of the climate (BRAITHWAITE, 1981).

Caution has to be taken when comparing the various studies. Some were more precise than others, in some cases the instruments were unreliable or one or more terms were estimated rather than measured. Furthermore, most studies were carried out over short periods of days to a few weeks, rather than for the entire ablation period. The value of each heat flux term depends strongly on weather conditions, and even during similar conditions, their relative importance changes during the summer. Thus the relative frequency of different weather conditions, and the respective values of the heat budget terms must be determined. Additionally, interannual variations in large-scale atmospheric circulation have strong influence on the energy balance components and ablation rates. As a consequence, the studies are rather restricted in their representativeness. To understand which energy sources dominate the ablation process, the heat budget for the entire ablation season and its variation from year to year should be determined.

There are regions where one heat flux dominates the entire surface energy balance so that only its variations are of importance. In other cases, however, particularly in polar regions where ablation is small, the different terms interact in a complex way and small deviations from the average values may change the annual mass balance significantly. Values from energy balance studies in the area of the Antarctic Peninsula and sub-Antarctic islands will be given later in chapter 7.1.4 when the results of this work are discussed in a broader context.

Distributed energy balance models are the only mean to investigate temporal and spatial variations of the surface balance components. However, their applications are rather scarce as major problems exist in the inter- and extrapolation of the input data, the model validation as well as in the only recently available computing power to handle such data sets in an appropriate time and spatial resolution. HOCK (1998) gives an overview of grid-based energy balance models applied to snow covered and glacerized areas.

Table 5.1: *Overview of the results from surface energy balance studies over snow and ice. Values denoted by *) were derived from figures in the respective publications.*

Location, altitude, surface type	Period [DD/MM/YY]	Net radiation [W m^{-2}]	Sensible heat flux [W m^{-2}]	Latent heat flux [W m^{-2}]	Ground heat flux [W m^{-2}]	Albedo	Reference
Dry Valley glacier, Antarctica, 250 m, ice	21/12/94-21/01/95	30.7	-6.2	-22.0	-0.6	0.68	LEWIS ET AL. (1998)
Dry Valley glacier, Antarctica, 250 m, ice	22/01/95-10/01/96	48.5	3.0	-19.8	1.5	0.64	LEWIS ET AL. (1998)
Filchner Schelfeis, Antarctica, snow	01/02-02/02/1984	-19.7	11.4*)	-	-6.1	0.80-0.85	HEINEMANN & ROSE (1990)
Berkner Island, Antarctica, 886 m, snow	12/02/95-31/12/97	-9.1	10.8	-1.7	0	-	REIJMER ET AL. (1999)
Heimefrontfjella, Dronning Maud Land, Antarctica, 1170 m, blue ice	01/01-10/02/93	47.2	-1.0	-23.9	-22.2	0.56	BINTANJA & VAN DEN BROEKE (1994)
Heimefrontfjella, Dronning Maud Land, Antarctica, 1250 m, snow	01/01-10/02/94	7.7	8.7	-15.1	-1.2	0.81	BINTANJA & VAN DEN BROEKE (1994)
Heimefrontfjella, Dronning Maud Land, Antarctica1150 m, snow	01/01-10/02/96	4.5	18.5	-22.1	-1.0	0.80	BINTANJA & VAN DEN BROEKE (1994)
Kronprins Christian Land, North Greenland, 380 m, ice	08-27/07/93	122	88	0	-	0.3	BRAITHWAITE ET AL. (1998)
Hans Tausen Ice Cap, North Greenland, 540 m, ice	02/07-05/08/94	84	27	0	-	0.48	BRAITHWAITE ET AL. (1998)
Nordbogletscher, West Greenland, 880 m, ice/snow	415 d	79	32	2	-	-	BRAITHWAITE & OELSEN (1990)
Qamanârssûp sermia, West Greenland, 790 m, ice/snow	512 d	103	62	-6	-	-	BRAITHWAITE & OELSEN (1990)
ETH Camp, West Greenland, 1155 m, snow	03/06-13/08/91	28	16	-6	-8	0.77	OHMURA ET AL. (1994)
Søndre Strømfjrod, Southwest Greenland, 341 m, ice	10/06-31/07/91	120	-34	11	-	-	DUYNKERKE & VAN DEN BROEKE (1994)
Søndre Strømfjrod, Southwest Greenland, 519 m, ice	10/06-30/07/91	-	-14	-	-	-	DUYNKERKE & VAN DEN BROEKE (1994)
Søndre Strømfjrod, Southwest Greenland, 1028 m, ice	10/06-24/07/91	-	-44	-	-	-	DUYNKERKE & VAN DEN BROEKE (1994)
Søndre Strømfjrod, Southwest Greenland, 1519 m, snow	05/07-24/07/91	22.5	-30	29	-	-	DUYNKERKE & VAN DEN BROEKE (1994)
Camp IV, EGIG, Greenland, 1013 m, ice	26/05-07/08/59	81.7	-28.7	17.7	-	-	AMBACH (1977A)
Carrefour station, Greenland, 1850 m, snow	20/05-28/07/67	6.7	-15.1	12.4	-	-	AMBACH (1977B)
VU-Camp, Southwest Greenland, 1510 m, snow	08/07/91	26	14	-1	-16	0.70	HENNEKEN ET AL. (1994)
VU-Camp, Southwest Greenland, 1510 m, ice	17/07/91	21	14	-10	-8	0.68	HENNEKEN ET AL. (1994)
Devon ice cap, 1320 m, snow	05-08/62, 63	16	10	-4	-12	-	HOLMGREN (1971)
White Glacier, Axel Heiberg Island, 210 m	16 periods, 08/07-10/08/60	78.7	62.5	37.3	-13.0	-	ANDREWS (1964) IN BRAITHWAITE (1981)
White Glacier, Axel Heiberg Island, 210 m	63 d, 12/06-18/08/61	62.4	48.1	0.5	22.0	-	MÜLLER & ROSKIN-SHARLIN (1967, MÜLLER & KEELER (1969) in BRAITHWAITE (1981)
White Glacier, Axel Heiberg Island, 210 m	11 periods, 16-31/07/62	100.5	44.4	9.1	-17.9	-	HAVENS ET AL. (1965) in BRAITHWAITE (1981)
Sverdrup Glacier, Devon Island, 300 m	33 d, 09/07-10/08/63	51.3	32.1	14.2	-11.2	-	KEELER (1964) in BRAITHWAITE (1981)
Worthington Glacier, South central Alaska, ice	16/07-01/08/67	126.9	68.3	47.0	-	0.19	STRETEN & WENDLER (1968)
McCall Glacier, Brooks Range, Alaska, 1730 m, ice	21/07-01/08/72	75.5	32.4	0.5	-1.4	0.35	WENDLER & ISHIKAWA (1973)
Mueller Glacier, New Zealand, 1780 m, snow	19/10-25/11/95	25.5	10.4	1.2	1.2		NEALE & FITZHARRIS (1997)
Ivory Glacier, New Zealand, 1500 m	53 d in Jan.-Feb. 72/73	76	44	23			HAY & FITZHARRIS (1988)
Franz Josef Glacier, New Zealand, 500 m, ice	15-17/12/81	78*)	97*)	81*)	-	-	OWEN ET AL. (1984) in TAKEUCHI ET AL. (1999)
Soler Glacier, Northern Patagonia, 400 m, ice	15-29/12/83	81*)	135*)	78	-	-	KOBAYASHI & SAITO (1985) IN TAKEUCHI ET AL. (1999)
San Rafael Glacier, Northern Patagonia, 103 m, ice	29/12/83-01/01/84	136*)	104*)	39*)	-	-	OHATA ET AL. (1985) in TAKEUCHI ET AL. (1999)
Moreno Glacier, Southern Patagonia, 330 m, ice, ice	12-27/11/93	140*)	123*)	12*)	-	-	TAKEUCHI ET AL. (1995) in TAKEUCHI ET AL. (1999)
Tyndall Glacier, Southern Patagonia, 700 m, ice	9-17/12/93	136*)	110*)	16*)	-	-	TAKEUCHI ET AL. (1995) in TAKEUCHI ET AL. (1999)
Storglaciären, northern Sweden, 1370 m, ice	19/07-27/08/94	73	33	5	-3.4	0.42	HOCK & HOLMGREN (1996)
Aletsch Gletscher, Alps, 2220 m, ice	02-27/08/73	129	38	14	-	-	RÖTHLISBERGER & LANG (1987)
Aletsch Gletscher, Alps, 3366 m, snow	03-09/08/73	44	4	-3	-	-	RÖTHLISBERGER & LANG (1987)
Glacier de Saint-Sorlin, Alps, 2712 m, ice	11 d, Aug.-Sep. 69	31.9	24.2	-3.5	-	-	MARTIN (1975)

5.1.1 Radiative fluxes

The net all-wave radiation is the balance of the long-wave and short-wave radiation components. The shortwave radiation fluxes cover a spectrum of 0.15 to 3 µm originating from the sun, whereas the longwave fluxes refer to the spectrum of 3 to 100 µm as a result of thermal radiation of terrestrial origin (OKE, 1987). Atmosphere, slope, aspect and shading have considerable influence on the radiation components as will be discussed below.

The instantaneous solar radiation on a horizontal surface without atmosphere and topographical obstructions can be expressed by the extraterrestrial solar radiation (I_0) in the following manner (KONZELMANN, 1994):

$$I_0 = SR(\cos\phi\cos\delta\cosh + \sin\phi\sin\delta) \tag{3}$$

S denotes the solar constant (1368 W m^{-2}), R the eccentricity correction factor of the earth's orbit, Φ the latitude, δ the declination and h the solar hour angle.

In the atmosphere, the solar radiation experiences energy loss by diffuse reflection and selective absorption. Diffuse reflection occurs e.g. at air molecules, water droplets, ice crystals and aerosol (WEISCHET, 1979). Ozone is mainly responsible for the absorption at the wavelengths less than 0.3 µm, and water vapour becomes increasingly important at wavelengths greater than 0.8 µm, but in the intervening band where the intensity of solar radiation is greatest the atmosphere is relatively transparent (OKE, 1987). The atmospheric attenuation of short-wave radiation is proportional to the distance travelled in the atmosphere and the initial flux of radiation. This process is therefore often parameterised in atmospheric models by using transmission coefficients of the most important molecules (HOCK, 1998). Transmissivities vary with season and latitude as a consequence of atmospheric conditions. The portion of the incoming solar radiation that is reflected and scattered in the atmosphere, plus the part that is multi-reflected between the surface and the atmosphere, add up to the diffuse short-wave radiation (D_S). The ratio between diffuse and total shortwave radiation varies again considerably with latitude and season. KONZELMANN (1995) measured 40% of diffuse radiation at the ETH camp in Greenland. Surrounding slopes do not only affect the incoming short-wave radiation by shading, they increase the diffuse part by backscattering (D_t). The amount depends on the surface albedo of the slopes. As a consequence, the incoming short-wave radiation can be split in direct, diffuse and the part that is reflected from the surrounding terrain. Together they form the global radiation. Finally, the portion of incoming solar radiation that arrives at the earth's surface without being absorbed or diffused is called the direct beam short-wave radiation (I). Since it can be approximated as a parallel beam, the irradiance of an exposed surface depends on its orientation to the beam as follows (OKE, 1987):

$$I = I_i \cdot \cos\beta \tag{4}$$

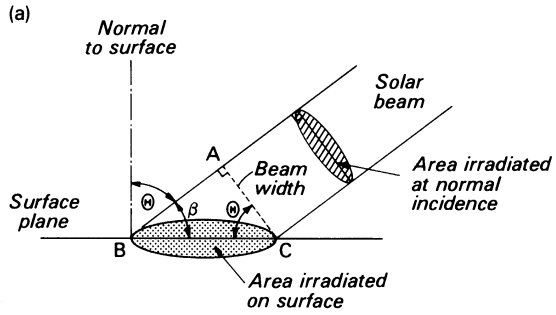

Figure 5.1: *Areas irradiated by a circular beam on planes placed normal to and at an angle of Θ to the beam. The radiant energy flux(J s^{-1}) is spread over unit area (=π(0.5AC)²) at normal incidence but over a larger area (=π(0.5BC)²) on the surface. The flux (W m^{-2}) on the surface is less than that at normal incidence (S_i) by the ration AC/BC=cos Θ or sin β (OKE, 1987).*

I is the flux density at the surface, I_i the flux density normal to the beam and β the angle between the beam and the normal of the surface (Figure 5.1).

Part of the global radiation is reflected from the surface. The ratio between reflected and incoming radiation in the spectrum from 0.35 to 2.8 µm is commonly referred to as albedo (α). The values can range from 0.1 over dirty glacier ice to more than 0.9 over freshly fallen snow. As a consequence, albedo strongly controls the radiation exchange at the glacier surface and hence triggers one of the major energy inputs. Reflection of solar shortwave radiation occurs from the surface and internal structures of the snow cover as snow is a porous media. The specular reflection at the surface increases with decreasing sun elevation whereas only diffuse reflection occurs in the snow pack. Factors influencing albedo are the zenith angle, grain size, impurity content, snow/ice depth and the surface roughness (HOCK, 1998). Moreover, albedo considerably depends on the wavelength – albedo is lower for infrared radiation than for visible light (WARREN, 1982). The portion of visible wavelength (0.36-0.76 µm) in total albedo is increased by cloudiness. This effect is enhanced by a shift of the spectral composition of the global radiation towards visible light by multiple reflection between the cloud base and the surface.

Since snow undergoes a continuous metamorphism according to the prevailing meteorological conditions, albedo changes as well. Therefore, energy balance models which do not incorporate direct measurements of net radiation (e.g. distributed energy balance models), need adequate parameterisations of the albedos of the various surface types. Several models of different complexity have been suggested. An overview of such functions, often in dependence of snow depth, density, melt, air temperature or days after snow fall, can be found in HOCK (1998).

The process of longwave radiative exchange in the atmosphere is very complex. At all levels, the atmosphere absorbs long-wave radiation emitted from the surface and lower layers of air and cloud, and from higher layers of air and cloud. Generally, the atmosphere is a relatively good absorber in the longwave band. This is particularly due to the absorptivities of water vapour, carbon dioxide and ozone. The long-wave radiation balance is composed of the energy gain from longwave sky radiation and the surrounding terrain as well as from the energy loss by thermal emission. Longwave emission in the atmosphere depends on the temperature and the column of water vapour. If the sky is totally overcast and the cloud is both optically thick and low enough for absorption in the sub-cloud layer to be neglected, the downward long-

wave radiation will be close to the blackbody radiation. Thus it is often parameterised by the Stefan Boltzmann Law (KING, 1996; KÖNIG-LANGLO & AUGSTEIN, 1994) or by using empirical formulas like the one suggested by Brunt (BRUTSAERT, 1982). For low-level clouds, the cloud base temperature might be reasonably close to the screen temperature. Outgoing longwave radiation from the surface is consistent with the temperature and can therefore be described by the Stefan Boltzmann Law (WEISCHET, 1979):

$$L^{\uparrow} = \varepsilon_s \cdot \sigma \cdot T^4 \tag{5}$$

$L^{\uparrow}$ denotes the emitted longwave radiation in W m^{-2}, ε_s is the emissivity (old snow: 0.82, fresh snow: 0.99; OKE, 1987), T the absolute temperature (K) and σ the Stefan Boltzmann constant ($5.67 \cdot 10^{-8}$ W m^{-2} K^{-4}).

As a melting snow and glacier surface cannot exceed 0°C, the long-wave outgoing radiation of the snow cover has an upper limit of 315.8 W m^{-2}.

Summarising the radiative fluxes outlined above, the radiation balance of a snow or glacier surface can thus be described with the formula

$$Q_N = (I + D_S + D_t)(1-\alpha) + L_S^{\downarrow} + L_t^{\downarrow} + L^{\uparrow} \tag{6}$$

with $L_S^{\downarrow}$ denoting the longwave sky radiation and $L_t^{\downarrow}$ the longwave terrain radiation.

5.1.2 Turbulent heat fluxes

The turbulent fluxes of sensible and latent heat are driven by temperature and humidity differences between the surface and the air, and by the turbulence in the lower atmosphere. The heat exchange between the atmosphere and the surface can be described by a complicated, non-linear differential equation system (BRUTSAERT, 1982) that can not be solved consistently. To solve the differential equations of momentum, sensible and latent heat simplifications, as the similarity principle suggested by PRANDTL (1934) and first applied over snow by SVERDRUP (1936), have to be maded. It is assumed that the exchange of energy in vertical dimension is considerably larger than the lateral exchange and that isotropic conditions in horizontal dimension exist. As a consequence, the three dimensional problem can be reduced to a one dimensional formulation. The turbulent fluxes are proportional to the time averaged gradients of potential temperature (Θ) and specific humidity (q) in the surface boundary layer – in practice often replaced by the vapour pressure (HOCK, 1998).

The following outlines refer to the classical aerodynamic approach for the calculations of turbulent heat fluxes. In this method, heat transfer by convection is treated as conduction, with eddies playing the part of molecules. The vertical fluxes of sensible and latent heat due to convection are therefore written in terms of vertical gradients

$\partial\Theta/\partial z$ and $\partial e/\partial z$ and a coefficient specifying the effectivity of the transfer process, the eddy diffusivities for heat and water vapour K_H and K_E:

$$Q_H = K_H \rho c_p \frac{\partial \Theta}{\partial z} \tag{7}$$

$$Q_E = -K_E \frac{0.623\rho}{P} \frac{\partial e}{\partial z} \tag{8}$$

where ρ denotes the density of air, c_p the specific heat capacity at constant pressure, P the atmospheric pressure. When the surface is melting, the pressure of water vapour is fixed to 0.611 hPa, as the surface temperature cannot rise over 0°C. In the case that the vapour pressure in the air above the surface is less than this value, ice is evaporated from the surface. Conversely, if the vapour pressure gradient is positive, water vapour condenses at the surface which gains heat as a result. The sensible heat flux will increase with increasing $\partial\Theta/\partial z$ (PATERSON, 1994).

The transfer of heat by the turbulent fluxes also depends on the turbulence of the air. This is measured by the eddy viscosity of momentum K_M defined by the equation

$$\tau = K_M \rho \frac{\partial u}{\partial z} \tag{9}$$

τ is called the shear stress in the air above the surface and u is the wind speed at height z.

This formulation is similar to equations (7) and (8) as the shear stress can be regarded, as a vertical flux of horizontal momentum (PATERSON, 1994). To calculate the fluxes, the gradients of $\partial\Theta/\partial z$, $\partial q/\partial z$ and $\partial u/\partial z$ have to be known from measurements of air temperature and specific humidity at several levels. As a consequence, this method is sensitive against measuring errors, in particular when data from only two levels can be used. Moreover, K_H, K_E and K_M have to be determined if no direct measurements are available. In a near neutral atmosphere (the temperature gradient is equal to the dry adiabatic lapse rate which is about 1 K per 100 m) these eddy diffusivities are assumed to be equal (this is also called Reynolds analogy). Some evidence exists to prove this assumption (GRAINGER & LISTER, 1966), however, it is still a major point of discussion (e.g. KRAUS, 1973; HAY & FITZHARRIS, 1988; MUNRO, 1989; OERLEMANS, 2000). K_M can be determined from wind profile measurements assuming that it varies with height z and that the shear stress is constant. The square root of the ratio τ/ρ is also called the friction velocity u^*. Using equation (9), it can be written as

$$u^* = \sqrt{\frac{\tau}{\rho}} = \sqrt{K_M \frac{\partial u}{\partial z}} \tag{10}$$

u^* also appears in the logarithmic wind profile which is assumed to be valid in the lowermost meters of the atmosphere as well. It is written

$$\frac{u}{u^*} = \frac{1}{\kappa \cdot \ln\left(\frac{z}{z_0}\right)} \tag{11}$$

where κ denotes the dimensionless von Kármán constant (0.4) and z_0 is called the surface roughness length for momentum. The latter determines the height above the mean surface at which the wind speed is zero. z_0 can be used as a tuning parameter of the calculations or determined from measurements (GREULL & OERLEMANS, 1987; KONZELMANN & BRAITHWAITE, 1995) either from surface roughness itself or by measuring the wind velocities at different heights. The value range of published roughness lengths for ice span between 0.003 mm over smooth Antarctic blue ice (BINTANJA & VAN DEN BROEKE, 1995) to >40 mm over glacier ice (DUYNKERKE & VAN DEN BROEKE, 1994). Moreover, surface roughness lengths vary in space and time as reviewed by HOCK (1998). Some distributed energy balance models do already consider this (e.g. BROCK ET AL., 2000). Surface roughness lengths tend to decrease as the snowmelt season proceeds (ANDERSON, 1976). HOLMGREN (1971) observed an increase in z_0 with decreasing wind speed.

If two measurements of wind velocity exist z_0 can be determined by the formula

$$\ln z_0 = \frac{u(z_1) \cdot \ln z_2 - u(z_2) \cdot \ln z_1}{u(z_1) - u(z_2)} \tag{12}$$

z_1 and z_2 denote the height above the snow surface and $u(z_1)$ as well as $u(z_2)$ the respective wind speeds at these levels. If a third measurement of wind speed is available equation (11) can be used to obtain u^* and to determine the eddy diffusivity of momentum from

$$K_M = u^* \kappa \cdot z \tag{13}$$

If air temperature and water vapour pressure are also measured at several levels, the fluxes of heat and water vapour can be calculated from the equations (7) and (8), assuming that K_H, K_E and K_M are equal at each height. This assumption is only plausible if wind speed, air temperature and vapour pressure vary logarithmically with height.

After inserting equations (11) and (13) in (7) and (8) and integration, it can be written

$$Q_H = \rho c_p \kappa^2 u \frac{\Theta(z_1) - \Theta_0}{\left[\ln\left(\frac{z_1}{z_0}\right)\ln\left(\frac{z_1}{z_{0T}}\right)\right]^2} \tag{14}$$

$$Q_E = 0.623 L_V \rho \kappa^2 u(z_1) \frac{e(z_1) - e_0}{P \cdot \left[\ln\left(\frac{z_1}{z_0}\right) \ln\left(\frac{z_1}{z_{0E}}\right) \right]^2} \quad (15)$$

L_V denotes the latent heat of evaporation or sublimation, $\Theta(z_1)$ is the potential temperatures at height z_1, z_2, Θ_0 is the potential temperature at the snow surface (0°C), $e(z_1)$ is the water vapour pressure at height z_1, e_0 is the water vapour pressure at the snow surface (6.1 hPa) and z_{0E} and z_{0T} the surface roughness lengths for sensible and latent heat. The expression $A = \kappa^2/(\ln(z/z_0))^2$ is called the dimensionless transfer coefficient. The values range between 0.002 and 0.004 m over melting snow and ice surfaces (PATERSON, 1994). Various authors use different transfer coefficients for latent and sensible heat than for momentum. A summary of the determination of turbulent fluxes over snow and ice was given by MORRIS (1989) and MOORE (1989). The roughness lengths for latent heat transfer are then chosen in the order of one to two magnitudes smaller than those for sensible heat (SVERDRUP, 1936; HOLMGREN, 1971; AMBACH, 1985; MOORE, 1989). On the other hand, KING & ANDERSON (1994) observed that the variation of heat and water vapour fluxes with stability is well described by the Monin-Obukhov similarity theory (see below), but the scalar roughness lengths for heat and water vapour appeared to be much larger than the momentum roughness length. This result from eddy correlation measurements over a smooth Antarctic ice shelf are in contrast with the choice of roughness lengths reported above. Similarly, MORRIS ET AL. (1994) reported considerably higher values of roughness lengths for heat and water vapour transport (0.05 m) than the aerodynamic roughness length (0.001 m) at the same test site. This discrepancy is further supported by the statement of PATERSON (1994), referring to ablation nomographs of AMBACH (1986), that the use of different coefficients for heat transfer seems to be an unnecessary refinement. Hence, MORRIS & HARDING (1991) as well as BRAITHWAITE (1995) suggested the use of an effective roughness length $z_0 = z_{0T} = z_{0E}$, as the roughness lengths for sensible and latent heat appear in the same mathematical term anyway when the classical bulk approach (equation (14) and (15)) is used. Some of the uncertainties in the magnitude of z_{0E} probably result from the difficulties of accurate measurements of humidity profiles.

As previously outlined, this aerodynamic bulk approach is only valid under neutral or near neutral conditions. However, over snow and ice surfaces this is not always the case (e.g. HOLMGREN, 1971). Due to the temperature fixation at a melting surface to 0°C, temperature gradients are often larger than the dry adiabatic lapse rate. As a consequence, stable conditions exist and turbulence is reduced. To compensate for this, stability functions have been introduced. Two methods are commonly applied:

a) the Monin-Obukhov length (L)

b) the bulk Richardson number (Rb).

The Monin-Obukhov length is given by the equation (BINTANJA & VAN DEN BROEKE, 1995):

$$L = \frac{u_*^{\,2}}{\kappa \frac{g}{\Theta_0}\left(\frac{-Q_H}{\rho c_p u_*} + 0.62\Theta_0 \frac{-Q_E}{\rho L_v u_*}\right)} \tag{16}$$

where g is the acceleration due to gravity. In a stable boundary layer, the Monin-Obukhov length can be interpreted as the height in the boundary layer at which the rate of turbulent energy production by shear stress balances the energy consumption by buoyancy forces (OBUKHOV, 1946 cited in HOCK, 1998). The quantity of the Monin-Obukhov stability parameter depends, among other factors, on sensible heat flux, thus an iterative loop is required to compute the turbulent fluxes.

The bulk Richardson number is a convenient means of categorising atmospheric stability and the state of turbulence in the lowest layers:

$$Rb = \frac{g\left(\Theta(z_2) - \Theta(z_1)\right)\left(z_2 - z_1\right)}{\frac{\Theta(z_2) + \Theta(z_1)}{2}\left(u(z_2) - u(z_1)\right)^2} \tag{17}$$

It relates the relative roles of buoyancy to mechanical forces (i.e. free to forced convection) in turbulent flow. Hence, in strong lapse (unstable) conditions, the free forces dominate and Rb is a negative number, which increases with the size of the temperature gradient but is reduced by an increase in the wind speed gradient. In neutral condition, Rb is zero, where during an inversion (stable) the bulk Richardson number is positive (OKE, 1987).

The application of such corrections for turbulence is also widely discussed, and several authors refrained from applying such formulas (e.g. HOLMGREN, 1971; HOGG ET AL., 1982; KONZELMANN & BRAITHWAITE, 1995; HOCK & HOLMGREN, 1996). HOLMGREN (1971) concluded from his measurements that the Monin-Obukhov theory did not apply under stable conditions as measured by him on an arctic ice cap in summer. BRAITHWAITE (1995) pointed out that the uncertainties in surface roughness might cause larger errors than those of neglecting stability correction. Finally, MOORE (1989) argued that the ratio of the stability corrections tends to compensate for the possible overestimation caused by assuming $z_{0T}=z_{0E}=z_0$. In the range where turbulent exchange is most significant as an energy source for snowmelt, the positive bias due to variations from $z_{0T}=z_0$ would average on the order of 10% and could be masked by instrument errors or uncertainty in the value of z_0. Some of the discrepancies between the various investigators may arise partly because the Monin-Obukhov theory was developed for homogenous conditions above a horizontal flat surface, the bulk Richardson number for a Tundra surface. Glaciers have sloping surfaces, and horizontal homogeneity can hardly be expected on valley glaciers (PATERSON, 1994).

A further possible error source are the assumptions of logarithmic profiles and homogeneous surface. Surface inhomogeneities may cause horizontal flux divergence, thus violating one of the assumptions of the aerodynamic approach (MOORE, 1989). DE LA CASINIÈRE (1974) observed temperature and wind profiles within the lowermost 2 m of the boundary layer that did not reveal a logarithmic shape. Consequently, their assumption would lead to serious errors in an estimation of the turbulent heat fluxes based on standard meteorological measurements at 2 m. Similarly, MUNRO & DAVIES (1977) advise to use measurements of the first meter above ground for calculations based on logarithmic wind profiles, and MOORE (1989) reported that in particular during weather situations characterised by light winds, the profiles of wind, temperature and humidity deviate markedly from logarithmic forms due to radiative flux divergence and the lack of mixing. However, under these conditions, the sensible and latent heat fluxes are less important than radiation, so inaccuracies in their estimation should not be critical to snowmelt computations (MOORE, 1989).

As a consequence of the uncertainties about the applicability of logarithmic profiles, the equality of eddy diffusivities has to be regarded with caution, and some studies already support a ration of K_H/K_M of 1.35 under neutral conditions and a van Kármán constant of 0.35 (BUSINGER ET AL., 1971). Even the equality of K_E and K_H are doubted to some extent and MALE & GRANGER (1981) reported values of 0.5. However, the evidence against equality of eddy diffusivities in stable range is inconclusive, so the assumption $K_H=K_E=K_M$ is as reasonable as any other, but caries some degree of uncertainty (MOORE, 1989).

5.1.3 Ground heat flux

PATERSON (1994) reviewed that the rate heat gain of a vertical column extending from the surface to the depth z, at which seasonal variations in temperature are negligible (usually about 10 m), is

$$\Delta G = -\int_0^z \rho' c \left(\frac{\partial T}{\partial t} \right) dz \tag{18}$$

Here ρ' is the density of the medium, c its specific heat capacity, T snow/ice temperature and t time. With continuous measurements of temperature and snow density in several depths, this term can be evaluated. However, conduction is not the only means of heat transport. Melt water percolating into lower layers of the snowpack can release considerable heat when it refreezes in layers where the snow temperature is still below 0°C. The refreezing of 1 g of water produces enough latent heat to raise the temperature of 160 g of snow by 1 K (PATERSON, 1994). Moreover, short-wave radiation can penetrate into lower layers of the snow cover and result in heat gain. WELLER & SCHWERDTFEGER (1970) reported penetration depths of up to 1 m in Antarctic snow. Finally, heat transfer can also occur by circulation of water vapour and air within the snowpack.

5.1.4 Heat supplied by rain

The energy gain of the snowpack during rain events can be calculated following the approach:

$$Q_R = c_W \cdot R \cdot (T_R - T_S) \quad (19)$$

where c_W is the specific heat of water, **R** the rainfall rate T_R the temperature of rain, and T_S the surface temperature.

5.2 The bulk approach method used for point energy balance calculation

In the following, the model which was applied for the energy balance calculations on King George Island will be specified in more detail on the basis of the review given in chapter 5.1.

Generally, the term 'ablation' refers to surface ablation only. Refreezing of melt water in deeper snow layers is not considered in this investigation; the usage of the term 'ablation' therefore differs from the expression used in glaciological mass balance calculations. Ground heat flux was neglected since temperature profiles in the snow pits revealed a 0 °C isotherm snow cover in the uppermost 2 m. Likewise, a previous study by BINTANJA (1995) reported a very low conductive heat flux for King George Island, since surface temperatures were nearly constant at 0 °C. SCHNEIDER (1998) showed that ground heat flux contributed only with 0.3 W m^{-2} in case a 1 K temperature gradient exists in the uppermost 2 m of the snow pack. During the field campaign 1997/98, a minimum temperature of -3.8°C (22 December 1997) was observed at about 3.5 m in a 10-m temperature profile in the snow cover at the site of AWS 3b. This low temperature can be attributed to the penetration of the winter cold front. During the research period, the minimum snow temperatures at this level increased to about –1.7°C (11 January 1998) as a result of the heat release of refreezing percolating melt water. In the uppermost 1 m, 0°C-isothermy was observed. Heat supplied by rain was calculated after equation (19). Since net radiation was measured directly, only the turbulent heat fluxes had to be computed from the hourly meteorological data. Therefore, a bulk approach model (SCHNEIDER, 1999) was performed to compute latent and sensible heat flux, following the equations given by OKE (1987) and MOORE (1983). This method was discussed in more detail by BRAITHWAITE (1995) and BLACKADAR (1997). When the air temperature was above 0 °C, values from both the lower measuring level and the surface were used to ensure that all calculations were performed within the surface boundary layer. This assumed the snow surface temperature to be 0 °C and postulated the occurrence of saturation conditions with respect to ice:

$$Q_H = \frac{\rho c_p \kappa^2 u(z_1)}{\left[\ln\left(\frac{z_1}{z_0}\right)\ln\left(\frac{z_1}{z_{0T}}\right)\right]}\left(\Theta(z_1)-\Theta_0\right)(1-5Rb)^2 \tag{20}$$

$$Q_E = \frac{\rho L_v 0.622 \kappa^2 u(z_1)}{p\left[\ln\left(\frac{z_1}{z_0}\right)\ln\left(\frac{z_1}{z_{0E}}\right)\right]}\left(e(z_1)-e_0\right)(1-5Rb)^2 \tag{21}$$

In the case of negative temperatures, turbulent fluxes were calculated from the gradients between the two measuring levels. This led to the following formulas:

$$Q_H = \frac{\rho c_p \kappa^2 \left(u(z_2)-u(z_1)\right)}{\left[\ln\left(\frac{z_2}{z_1}\right)\right]^2}\left(\Theta(z_2)-\Theta(z_1)\right)(1-5Rb')^2 \tag{22}$$

$$Q_E = \frac{\rho L_v 0.622 \kappa^2 \left(u(z_2)-u(z_1)\right)}{p\left[\ln\left(\frac{z_2}{z_1}\right)\right]^2}\left(e(z_2)-e(z_1)\right)(1-5Rb')^2 \tag{23}$$

Correction for stable stratification was performed using the bulk Richardson number. The correction terms were applied only for $Rb < 0.2$. In case of stable conditions ($Rb \geq 0.2$), the turbulent fluxes would be forced to zero. However, such conditions occurred in less than 5% of all measurements. The bulk Richardson number was calculated according to equation (17) in case of positive air temperatures; for negative air temperature the following formula was applied:

$$Rb' = \frac{g\left(\Theta(z_2)-\Theta(z_1)\right)(z_2-z_1)}{\frac{\Theta(z_2)+\Theta(z_1)}{2}\left(u(z_2)-u(z_1)\right)^2} \tag{24}$$

Surface roughness lengths were used as tuning parameters since no direct measurements of this parameter were available. All roughness lengths were assumed equal ($z_0=z_{0T}=z_{0E}$), resulting in an effective roughness length. A z_0-value of $5.0\cdot10^{-4}$ m was used for the AWS 1, whereas a value of $z_0=1.0\cdot10^{-3}$ m was used for the remaining sites. These roughness lengths over snow are well within the range published in the literature.

Due to insufficient power supply, radiation shields of the temperature and humidity probes could not be ventilated. This may result in biased measurements due to radiative heating. However, mean wind speed on the ice cap was almost 5 m s^{-1}, and periods of low wind speed rarely occurred. Errors resulting from insufficient ventilation of the temperature and humidity readings are therefore expected to be small and

deemed negligible. This conclusion is supported by an error estimation given by SCHNEIDER (1998). He used a similar data set for energy balance calculations at a test site further to the south in Marguerite Bay and determined the errors summing up to a maximum of about 25% of the sum of energy balance terms. A detailed study on the accuracy of HMP35 humidity probes at temperatures below the freezing point was done by ANDERSON (1994).

5.3 Spatially distributed energy balance modelling

The model for the spatially distributed energy balance estimates was designed by HOCK (1998) and first applied to Storglaciären in Swedish Lapland. It is a physically based model and enables the computation of short-term mass balance variations of ice and snow in subdiurnal temporal resolution. The model is grid based and needs a digital elevation model, derived slope and aspect grids as well as grids of the glacierised area, the firn area and a start grid with the initial snow water equivalent. Point data from AWS provide input of the major meteorological variables. For the application on King George Island, a cell size of 100 m² was considered appropriate, an hourly time resolution was chosen and meteorological input was used from the lowermost AWS 1 as well as altitudinal air temperature lapse rates between AWS 1 and AWS 2. Several options for the parameterisation of the energy balance components can be combined in the model. In the following, only the parameterisations finally applied are described in more detail according to the program documentation and user manual (HOCK, 2000). The interpolation and computation methods of the various input variables and energy balance components are summarised in table 5.2. A flow chart including the demanded input and tuning parameters is displayed in figure 5.2.

Global radiation was calculated by separating measured global radiation into its ***direct*** and ***diffuse parts*** and spatially interpolating these components individually. First, potential clear sky solar radiation on an unobstructed flat surface was computed for each grid cell in subintervals of 10 minutes. Only the geographical coordinates of the centre of the study area were used for these computations. This approach assumes that for all other grid cells latitude and longitude were deemed invariant. Such a simplification is only valid if the study area is sufficiently small as it is the case for the study area. For mountainous regions, the effects of shade, slope and exposition have to be corrected for each grid cell and time step. As a consequence, a correction factor due to slope, shading and aspect of each grid cell was applied. For each grid cell and each time step the correction factor was calculated as a function of slope, aspect, solar azimuth, slope azimuth angle, zenith angle and elevation. The correction factor for slope and aspect is given by the equations:

Table 5.2: *Modelled and interpolated meteorological and surface variables as used in the distributed energy balance model.*

Energy balance components	**Method of computation**
Diffuse global radiation	**Separated from measured global radiation applying an empirical formulation and extrapolated including topographic effects**
Direct global radiation	**Separated from measured global radiation applying an empirical formulation and extrapolated including effects of topography, slope and aspect**
Longwave incoming radiation	Assumed spatially constant, computed as remaining term from measured net radiation at AWS 1 and calculated global and longwave outgoing radiation
Longwave outgoing radiation	Computed from modelled surface temperature
Sensible heat flux	Bulk aerodynamic approach
Latent heat flux	Bulk aerodynamic approach
Ground heat flux	Neglected
Rain heat flux	Equation 19
Meteorological and surface parameters	**Method of parameterisation, interpolation**
Air temperature	Actual lapse rates derived from AWS data
Relative humidity	Assumed to be spatially constant
Wind speed	Assumed to be spatially constant
Rain	Measurements, corrected with assumed 25% gauge undertake
Surface temperature	Computed iteratively, when energy balance was negative
Ice albedo	constant (from measured average)
Firn albedo	constant
Snow albedo	function of time and air temperature after the last snowfall
Input Grids	**Method of interpolation**
Initial snow cover	Linear regression in dependence of altitude from measurements at the beginning of the field campaign
Ice and firn area	Derived from an ERS-1 SAR image from February 25th 1997

$$cor = \frac{\cos\Theta}{\cos Z} = \frac{\cos\beta\cos Z + \sin\beta\sin z\cos(\Omega - \Omega_{slope})}{\cos Z}$$

with

$$\cos\Omega = \frac{(\sin\delta\cos\Phi - \cos\delta\sin\Phi\cos h)}{\sin Z} \qquad t < 12$$

$$\cos\Omega = 360 - \frac{(\sin\delta\cos\Phi - \cos\delta\sin\Phi\cos h)}{\sin Z} \qquad t > 12 \qquad (25)$$

Θ denotes the angle of incidence between the normal to the slope and the solar beam, β the slope angle, Ω the solar azimuth angle, Ω_{slope} the slope azimuth angle, h the hour angle (angle through which the earth must turn to bring the meridian of the site considered directly under the sun) and Z the zenith angle. When a grid cell is shaded the correction factor was set to zero. Subsequently, for each hourly step weighted means of the direct radiation correction factors from the 10-minutes sub-interval data were computed per grid cell. The beam solar radiation was then integrated over the entire hourly time step. Generally, the accuracy of the solar

radiation increases with the number of subintervals, in particular during times of fast change in the sun elevation.

Measured global radiation was then split into direct and diffuse radiation using an empirical relationship between the ratio of global radiation (*G*) to top of the atmosphere radiation (*ToA*) and diffuse radiation (*D*) to global radiation. The following function was derived by a least-square fit from daily radiation data from Kiruna:

$$\frac{D}{G} = \begin{cases} 0.15 & : \quad \frac{G}{ToA} \geq 0.8 \\ 0.929 + 1.134\frac{G}{ToA} - 5.111\left(\frac{G}{ToA}\right)^2 + 3.106\left(\frac{G}{ToA}\right)^3 & : \quad 0.15 < \frac{G}{ToA} < 0.8 \\ 1.0 & : \quad \frac{G}{ToA} \leq 0.15 \end{cases} \quad (26)$$

This function is in very good agreement with the relationship derived by COLLARES-PEREIRA & RABL (1979, cited in HOCK, 1998) from daily data at 5 US sites. The direct radiation at the AWS is obtained from the difference between global and diffuse radiation. Four cases of sun-shade for the grid cell to be calculated and stations grid cell are distinguished: E.g. if the AWS is shade and grid cell not, dIf the AWS is shaded all measured global radiation is assumed to be diffuse. Diffuse radiation was then extrapolated spatially variable by considering additional diffuse radiation reflected from adjacent slopes using a sky view factor relationship and mean albedo of the area.

Snow and ice albedo were treated individually. Snow albedo (α_{t2}) was modelled internally using a function depending on the number of days since the last snowfall and on the air temperature for each grid cell (HOCK 1998):

$$\alpha_{t2} = \begin{cases} \alpha_{t1} - a_1 \cdot \ln(T+1) \cdot e^{(a_2\sqrt{n_d})} & : n_d > 0, T > 0 \\ \alpha_{t1} - a_1 \cdot 0.1 \cdot e^{(a_2\sqrt{n_d})} & : n_d > 0, T < 0 \\ \alpha_{t1} + a_3 \cdot P_S & : n_d = 0 \end{cases} \quad (27)$$

where T is air temperature, P_s is snow precipitation, and n_d is the number of days since snowfall. The coefficients a_1=0.005, a_2=-1.1 and a_3=0.02 were determined by HOCK (1998) from daily averages of snow albedo in the accumulation area of Storglaciären. This method requires the knowledge of the firn and glacierized area as well as starting values of snow albedo (α_{t1}). The latter were determined from the shortwave radiation measurements at the AWS 1.

Major boundary conditions are determined by the ***initial snow cover*** grid. For King George Island it was obtained via a linear regression with altitude from the ablation stake readings starting on 09 December 1997. The melted water equivalent between

02 December 1997 and 09 December 1997 was derived from the measurements at AWS 1 and 2. The final regression with altitude (x) for the initial water equivalent (WE) was then given by the equation

$$WE = 0.8041\,x + 211.0 \tag{28}$$

Using this regression, a initial value of 670 mm WE was obtained for the top of the ice cap at 680 m. This corresponds to the observations of SIMÕES (pers. com., 2000) discussed in chapter 4.4.2. Special attention had to be attributed to the initial snow cover grid (initial water equivalent) as this spatial data set triggers together with the firn area grid according to the modelled energy input the appearance of bare ice in lower elevations and hence, a large part of the calculated melt. Ice albedo (0.39), firn

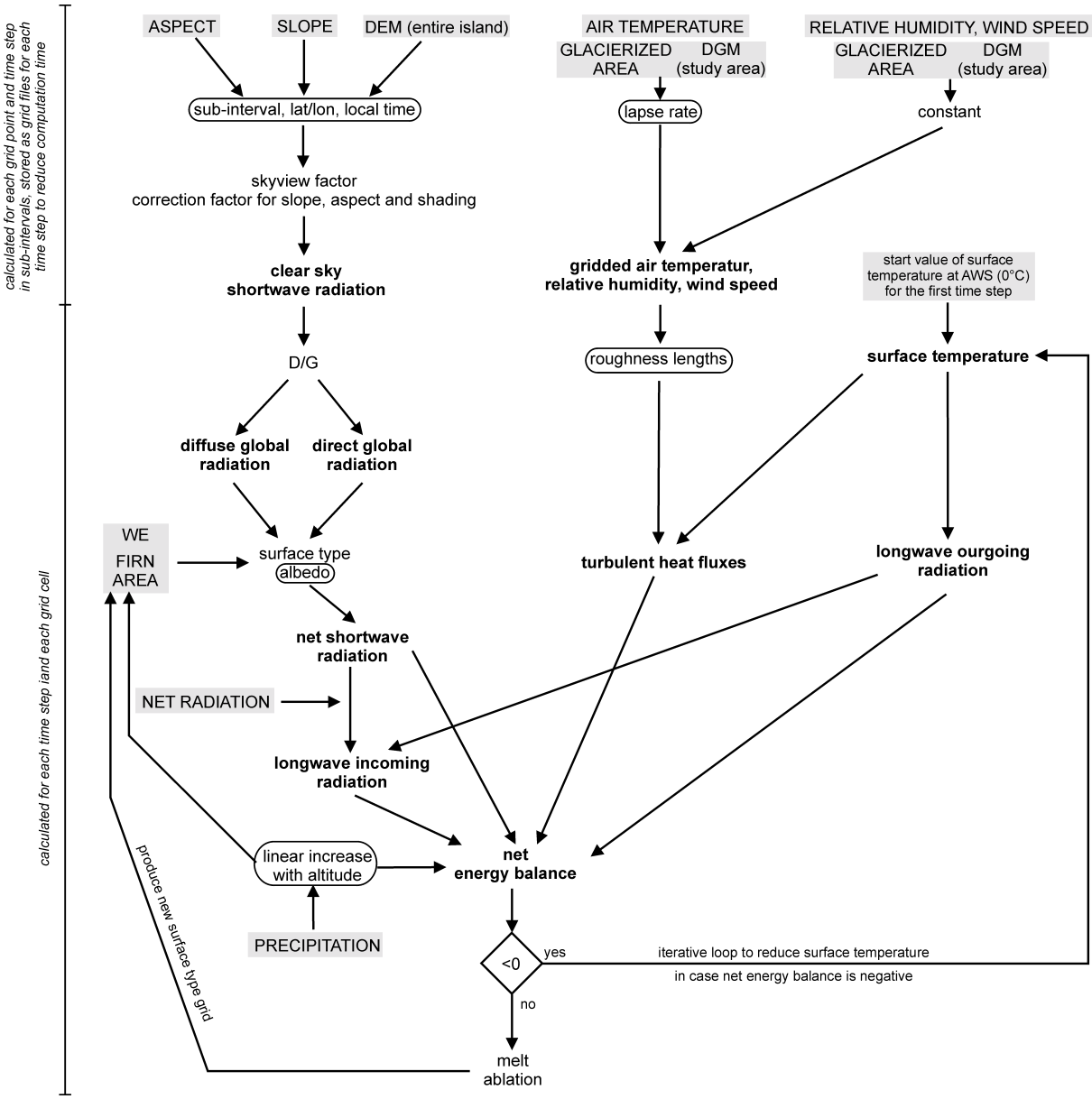

Figure 5.2: *Flow chart of the spatially distributed energy balance modelling. The required input is highlighted in grey, tuning parameters are marked by rounded boxes.*

albedo (0.70) and the starting value of snow albedo (0.81) were taken from measured values from AWS data in December 1997 and single measurements in February 1998, respectively. Snow and firn albedo in the study area were not influences by ash or dust layers as frequently encountered in alpine areas.

Small stones or dust particles were only observed on bare ice areas close to the periglacial sites. The ***distribution of bare glacier ice in the previous summer*** was derived from a ERS-2 SAR images of 25 February 1997. For each time step, new surface type grids were computed according to the ablation rates.

The values of ***longwave outgoing radiation*** depend on the surface temperature as outlined in chapter 5.1. For the first time step, this parameter was determined for the grid cell of the AWS. Subsequently, surface temperature and longwave outgoing radiation were computed using an iterative procedure as outlined below.

Longwave incoming radiation was calculated as the residual from measured net radiation, shortwave radiation balance and outgoing longwave radiation. Applying this methodology implies that errors in the calculations of all other radiation terms cumulate in longwave incoming radiation. Consequently, the model includes a numerical control for to low longwave radiation values originating from measuring errors. If incoming longwave radiation drops below 150 W m^{-2} it is set to 150 W m^{-2} to avoid unrealistic values. However, this case never occurred in the present calculations. In order to reduce computation time, the distribution of longwave incoming radiation was assumed spatially constant. First test runs had shown no significant influence of topography on this radiation term.

The ***turbulent heat fluxes*** were computed by the bulk aerodynamic approach using air temperature, relative humidity and wind speed from the 2 m level at the AWS 1 as well as computed surface temperatures. Roughness lengths for momentum, latent and sensible heat flux were 0.001 m, 0.001 m, 0.001 m. They were used as tuning parameters to optimise the correlation between measured and modelled melt. Relative humidity was assumed to be constant with altitude as first results showed that latent heat flux was of minor importance. Since no information on the spatial variation of wind speed was available despite the point measurements at the AWS, this parameter was assumed to be constant with altitude as well. Hourly air temperatures lapse rates were derived from screen level measurements between AWS 1 and AWS 2. Moreover, a fixed lapse rate was used. Figure 3.8 shows scatter plots of the meteorological parameters at the AWS. The model does not include a correction term for stability. Full account was given for phase changes in the latent heat flux:

condensation:	$Q_E > 0, T_S = 0$	==>	$L = L_V$
resublimation:	$Q_E > 0, T_S < 0$	==>	$L = L_S$
sublimation:	$Q_E < 0$	==>	$L = L_S$

where T_S denotes the surface temperature, L_V the latent heat of evaporation ($2.514 \cdot 10^6$ J kg^{-1}) and L_S the latent heat of sublimation ($2.849 \cdot 10^6$ J kg^{-1}).

In the methods applied, the compilation of longwave outgoing radiation, the turbulent heat fluxes and the rain heat flux required a value of ***surface temperature*** for each grid cell. It was determined iteratively for each grid cell. In case of negative energy balance, the surface temperature was lowered by a step of 0.25 K until the energy balance drops below zero.

The ***ground heat flux*** was neglected, and ***heat supplied by rain*** was calculated after equation (19).

Precipitation was corrected using a fixed percentage (25%) of gauge undertake; a linear increase of rain with altitude (10 %) was assumed. A threshold temperature (T_0=1.5°C) determines when rain or snow precipitation occurs. Either one degree below/above T_0, all precipitation was supposed to fall as snow or rain respectively. Within that range, the percentages of rain and snow were obtained from a linear interpolation (Figure 5.3). In case of snowfall, the water equivalent was added to the snow cover grid of the previous time step.

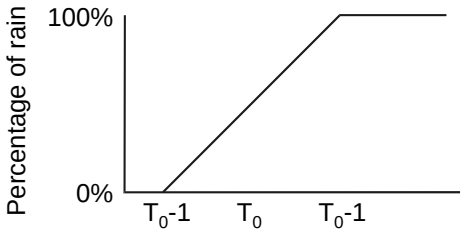

Figure 5.3: *Linear interpolation of percentages of rain and snow.*

5.4 Model validation

5.4.1 Single location energy balance study

Model performance was validated by comparing modelled snow depletion against the measured ablation at AWS 1 and 2, as well as versus the continuous snow height record obtained from the SR50 sensor at AWS 1. For AWS 3b, located near the highest point of the ice cap, no concurrent ablation record was available. Therefore, the respective z_0-values of the AWS 2 and the former AWS 3a sites were used. An evaluation of a 10-m snow temperature profile suggested that refreezing conditions are likely to occur in deeper layers of the snow cover at maximum altitudes. Hence, not all meltwater resulting from the available energy input would be transformed into discharge at this elevation.

Over the entire measuring period during the 1997/98 field campaign, the calculated snowmelt agrees well with the measured water equivalent decrease. The correlation between measured and modelled snow depletion at AWS 1 is

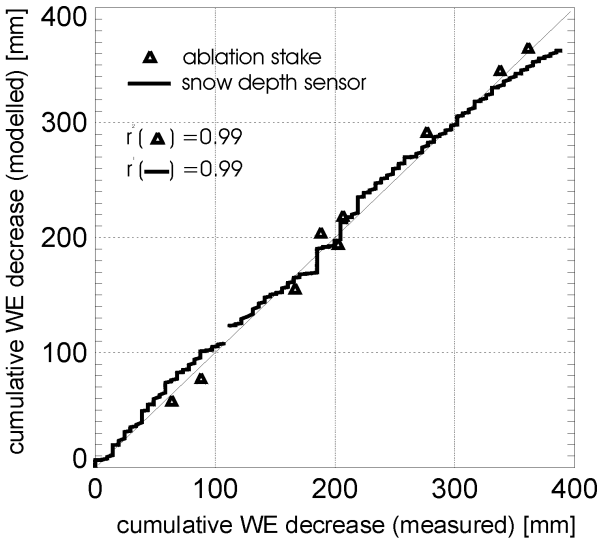

Figure 5.4: *Validation of the single location energy balance calculations. Measured against modelled water equivalent depletion at AWS 1.*

shown in figure 5.4. Correlation coefficients (r^2=0.99) for both validations, modelled ablation against ablation stakes and modelled ablation against the snow depth sensor, are extraordinarily high. Even the marked daily cycle in snowmelt as observed with the continuous snow depth sensor could be reproduced in the model run. For the AWS 2, similar agreements between modelled and measured ablation were achieved (r^2=0.99). Over the measured 42 days, the model underestimated snowmelt at AWS 1 by 3 % (383 mm WE compared to a measured WE decrease of 394 mm). This ablation rate equalised the encountered winter accumulation at the test site. Continuous ice melt occurred until the end of February 1998 (VOGT pers. com., 1998).

It should be noted that the observed model performance resulted from adjustments via the roughness lengths and that the accuracy of temperature and humidity readings are influenced by unventilated radiation shields. Therefore, a sensitivity analysis was performed to estimate the error owing to these factors. A detailed outline of the results of this study will be given in chapter 7.1.3.

5.4.2 Distributed modelling

Due to the operation of several AWS, various validation possibilities of the results and parameterisations of the spatially distributed model runs exist. As for the single location calculations, A direct comparison between modelled and measured values is facilitated. Moreover, albedo parameterisation and radiation terms can be checked using data from AWS. Validation on base of other meteorological variables as e.g. air temperature or wind speed would be possible as well. However, as the chapters 4.3.2.3 and 4.3.2.4 already contain a detailed analysis of the altitudinal variation of the major meteorological input data, these variables will not be discussed further in the present chapter.

5.4.2.1 Melt calculations

As the stake readings started at different dates (02, 09 and 25 December 1997), three initial snow cover grids were generated for the respective date, and the values of the grid cells with the stake readings were substituted with the measured initial water equivalent values of the respective measurements. This facilitated the direct comparison of cumulative modelled against measured melt rates. Thus, possible discrepancies in the comparison of modelled and measured ablation rates due to errors by the interpolation of the water equivalent are avoided. The final model runs were then performed using the initial snow cover from 2 December 1997. Figure 5.5 displays measured against modelled melt for the various ablation stakes and the continuous readings of the SR50 snow depth sensor. As for the single location calculations, the agreements between measured and modelled melt are extraordinarily high for the chosen parameter set. The correlation coefficient between the SR50 data and the model results is 0.9932 and for the 65 stake readings 0.9433. The slight

deviations for the SR50 graph in figure 5.5 result from an overestimation of melt during the cold phase in the central part of the measurement period. This is compensated by an underestimation during the last phase of the field campaign. The largest scatter in the stake array results from the underestimations of melt in the last phase of the measuring period. Ice melt occurred at the stake line from Artigas station to Bellingshausen Dome and this was not reproduced well by the model. For the entire measuring period, the model reveals 409.6 mm WE of snowmelt, whereas the measurements amount to 384.8 mm WE. This is an overestimation of melt of 6.4 %.

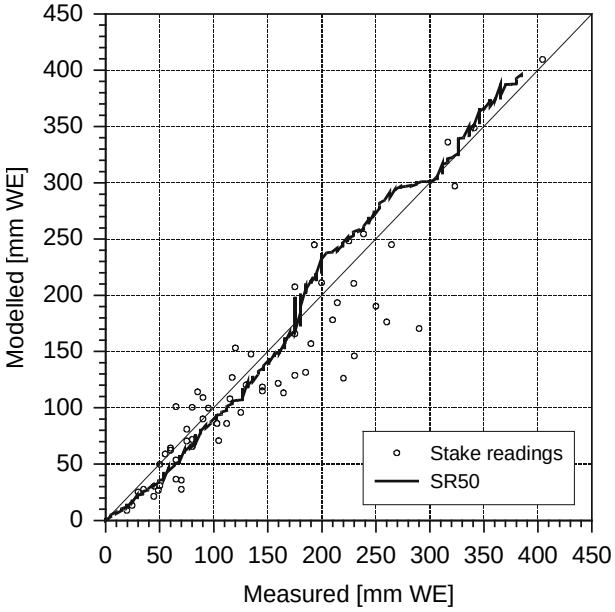

Figure 5.5: *Cumulative measured against modelled melt at the Sonic Ranging Sensor (SR50) and the various ablation stakes over the entire measuring period (03/12/97 to 11/01/98).*

5.4.2.2 Albedo parameterisation

As outlined previously, albedo is a crucial parameter for melt modelling as it controls the radiative energy gain. A comparison of daily modelled and measured albedo values for the three AWS is shown in figure 5.6. The values range between 0.78 and 0.90. Best results were achieved for the uppermost AWS. In lower elevations (AWS 1), modelled albedo is lower than the observed values. This can be attributed to the fact that dust and impurities from periglacial areas are of minor importance in higher elevations. Moreover, bare ice did not appear at the higher AWS sites during the observation period. In contrast to this, small snow precipitation events lead to significant variations of surface albedo in the lowermost areas. It has to be pointed out that small snow fall events are hardly represented in the precipitation record, or that a rain signal is recorded after several hours when the snow in the gauge has melted. Disagreements between modelled and measured albedo are the result. As a consequence, the correlation of measured and modelled daily albedo tends to improve with altitude.

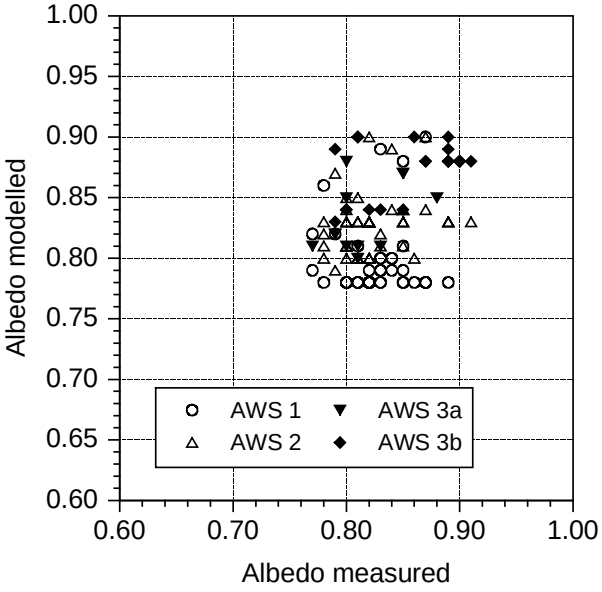

Figure 5.6: *Comparison of measured against modelled daily albedo at the three AWS sites.*

However, the data and the field observations did not show many of these events. Errors resulting from inaccurate albedo parameterisation are highest on days with clear sky conditions. From the albedo deviations in figure 5.6, a maximum hourly error of shortwave radiation balance of about 9.5 W m^{-2} can be estimated. However, clear sky conditions predominately occur during cold southerly advection were snowmelt is reduced due to low air temperatures. Consequently, melt rates are less affected by these errors, however, the general flux determination is. Thus, the general error due to wrong albedo parameterisation has to be considered as smaller.

5.4.2.3 Radiation terms

Radiation is the major energy source for ablation at many locations. Hence, an adequate parameterisation and modelling of this energy fluxes is required. Figure 5.7 displays measured against modelled global radiation, shortwave radiation balance as well as net radiation for the different AWS sites. Generally, results are best for the lowermost AWS, in particular, the measured values at AWS 1 data are reproduced very well which can be attributed to the choice of AWS 1 as major meteorological input. Only little scatter exists in the global radiation, whereas the values of shortwave radiation balance show larger variations. Slightly too high energy gain by shortwave radiation is modelled. This indicates, that the albedo is sometimes too low as already stated above. Measured and modelled net radiation at AWS 1 show very good agreements, only some outliers exist, where too much energy gain is modelled.

Table 5.3: *Correlation between measured and modelled melt as well as radiation terms.*

		Global radiation	Shortwave radiation balance	Net radiation
AWS 1	*Number of data points*	960	960	960
	Correlation coefficient	0.99	0.90	0.81
	Standard deviation of residua	25.68	21.10	26.57
AWS 2	*Number of data points*	960	960	960
	Correlation coefficient	0.90	0.88	0.74
	Standard deviation of residua	98.89	18.69	25.02
AWS 3a	*Number of data points*	287	287	287
	Correlation coefficient	0.86	0.77	0.55
	Standard deviation of residua	111.97	24.49	27.00
AWS 3b	*Number of data points*	547	547	547
	Correlation coefficient	0.88	0.64	0.11
	Standard deviation of residua	105.25	25.32	30.10

The correlation between measured and modelled radiation terms decreases with altitude as can be seen in figure 5.7 and as expressed by the lower correlation coefficients in table 5.3. The results for AWS 2 are still satisfying although scatter is larger than for AWS 1. Similarly, still reasonable correlations are obtained for AWS 3a, whereas the AWS 3b shows large scatter, in particular for net radiation. The increasing scatter with altitude results mainly from spatial variations in cloud coverage, albedo parameterisation and, hence, changes in the radiation terms.

This cannot be reproduced using only data from AWS 1. Moreover, the assumptions of constant wind velocity and relative humidity influence the surface air temperature by the iteration procedure and thus the calculated longwave outgoing radiation. As longwave incoming radiation is assumed spatially constant, spatial variations in cloudiness and errors in surface temperature modelling are the major reasons for the observed discrepancies between modelled and measured terms. As a consequence, the reliability of the model results in higher altitudes above 400 m a.s.l. is reduced. This has to be considered when interpreting the results in chapter 7.2.

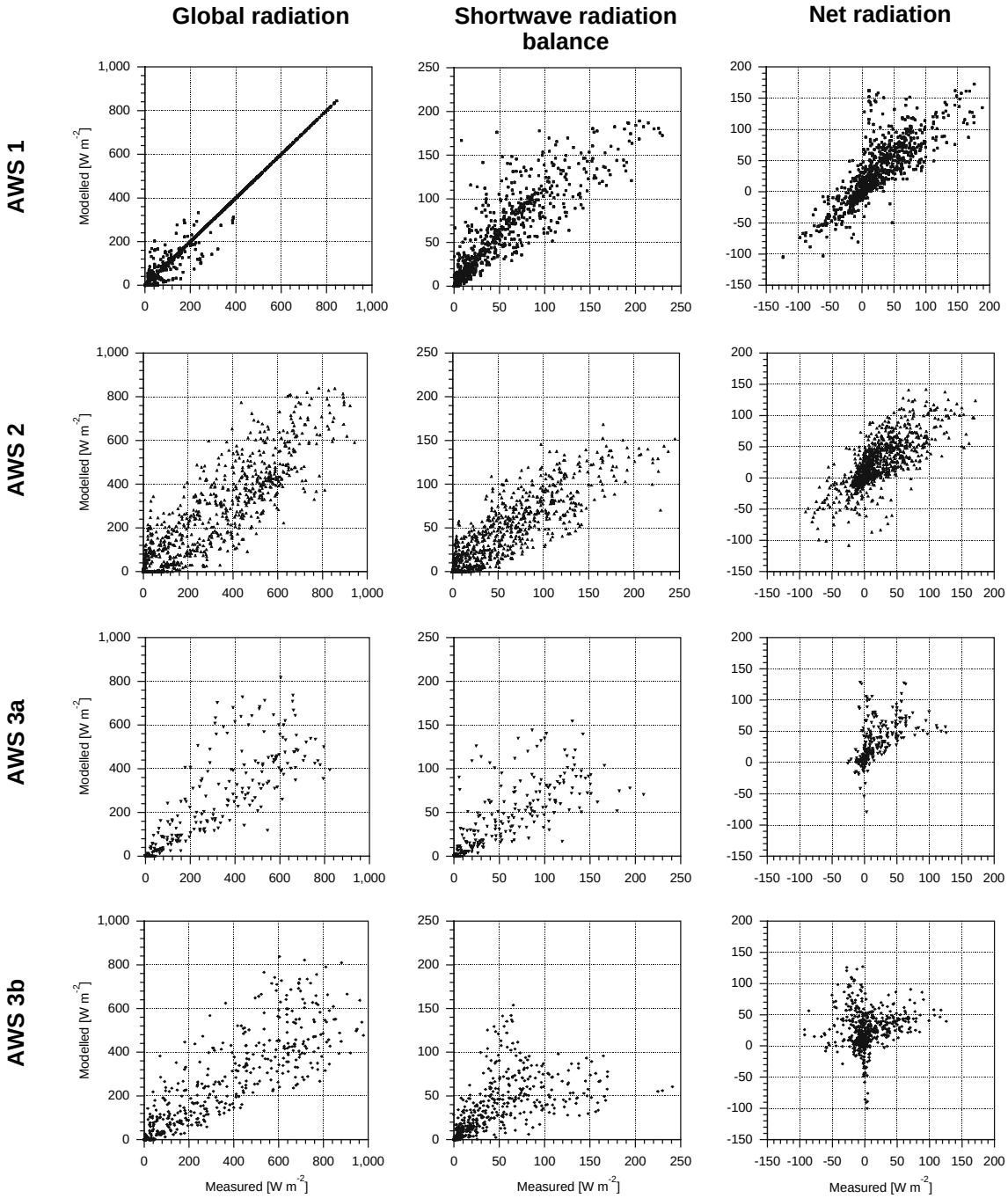

Figure 5.7: *Comparison of measured against modelled hourly radiation fluxes at the three AWS sites for the entire measuring period (03/12/97 to 11/01/98).*

6 Active microwave remote sensing of snow and ice surfaces

6.1 Sensor and platform specifications

Two spaceborne SAR systems are in operation – the European Radar Satellite ERS-2 and the Canadian RADARSAT-1 (Table 6.1). The well known JERS-1 and ERS-1 satellites terminated operation in 1992 and 2000, respectively. ENVISAT is the planed successor of ERS-2 and will continue the European Space Agency (ESA) SAR missions run since the beginning of the 1990s with the largely identical systems of ERS-1 and ERS-2. A continuation of the RADARSAT mission by RADARSAT-2 is expected by the launch of this platform in 2003. As for the present study, only ERS-1/2 SAR data is used, details are given only for these two satellite systems. More information on SAR sensors and processing, radar fundamentals as well as SAR applications can be found e.g. in ULABY ET AL. (1986), HENDERSON & LEWIS (1998) or, specifically, for the study of polar snow covers in BINDSCHADLER (1998), WUNDERLE (1996). The ERS-1/2 platforms carry an active microwave instrument (AMI) consisting of a synthetic aperture radar (SAR) and a wind scatterometer (both in the C-band).

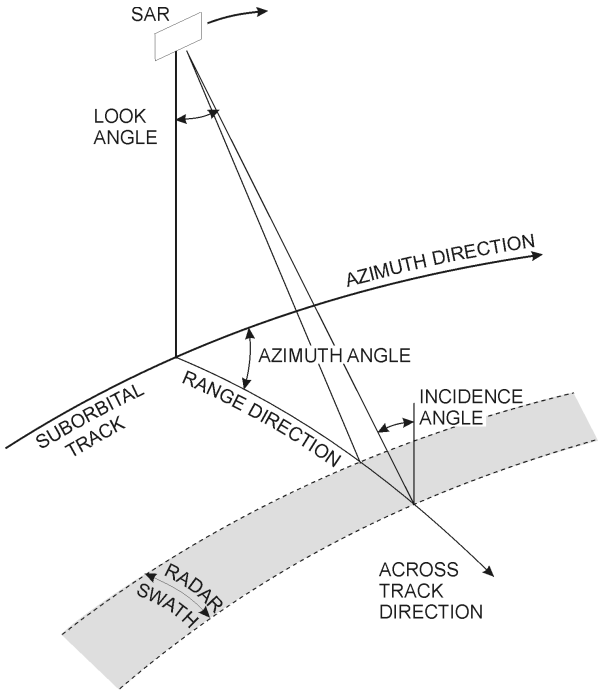

Figure 6.1: *SAR sensor geometry. Azimuth angle is the angle described between the track of the spacecraft and the across track or look direction (modified after HENDERSON & LEWIS, 1998).*

ERS-1/2 have a polar orbit which enables image acquisition over high latitudes. The rectangular antenna of the SAR is aligned along the satellite's line of flight (azimuth direction) to direct a narrow beam sideways and downwards onto the Earth's surface to obtain strips of high resolution imagery of about 100 km swath width. Imagery is built up from the time delay and strength of the return signals which depend primarily on the roughness and dielectric properties of the surface and its range from the satellite. In image mode the ERS SAR provides two-dimensional images with a spatial resolution of 26 m in range (along track) and between 6 and 30 m in range (across track or look direction) (Figure 6.1). As an explanation of the SAR principle, ESA states:

"The SAR's high resolution in the range direction is achieved by phase coding the transmitted pulse with a linear chirp and compressing the echo by matched filtering; range resolution being determined by means of the pulse travel time; and the azimuth resolution is achieved by recording the phase as well as the amplitude of the echoes along the flight path" (http://earth1.esrin.esa.it/).

The amplitude imagery used in this study is multi-look (for speckle-reduction), ground range (projected to a plain assuming a geoid) and system corrected images. These products can be calibrated and corrected for the SAR antenna pattern and range-spreading losses. The resulting values are addressed to in the following as backscatter coefficient sigma nought (σ°). They are defined as the average reflectivity of horizontal material, normalized with respect to a unit area on a horizontal ground plane. The values are fractions which describe the amount of backscatter power compared to the power of the incident field. They depend further on the physical and dielectric properties of the reflected material, as well as on the wavelength, polarization and illumination angle. Strictly speaking, these normalized backscatter values in the imagery are not corrected for topographic effects and hence still depend on the local incidence angle (the orientation of the surface slope towards the

Table 6.1: *Major spaceborne SAR systems with polar coverage (modified after HENDERSON & LEWIS, 1998).*

Parameter	ERS-1	JERS-1	ERS-2	RADARSAT-1	ENVISAT
Operating country	Europe	Japan	Europe	Canada	Europe
Agency	ESA	(MITI/NASDA)	ESA	CSA	ESA
Launch date	Jul. 1991	Feb. 1992	Apr. 1995	Nov. 1995	Jun 2001
operation end	Mar. 2000	Oct. 1998	still operating	still operating	
Band (wave length)	C (5.6 cm)	L (23.5 cm)	C (5.6 cm)	C (5.6 cm)	C (5.6 cm)
Polarisation	VV	HH	VV	HH	VV + HH
Incident angle	23°	39°	23°	<20° - >50°	20° – 50°
Range resolution	26 m	18 m	26 m	10 – 100 m	~25 m
Azimuth resolution	28 m	18 m	28 m	9 – 100 m	~25 m
Number of looks	6	3	6	1-8	~4
Swath width	100 km	75 km	100 km	10 – 500 km	100 (500) km
Nominal altitude	~780 km	568 km	~780 km	~800km	~700 km
Inclination	98.5°	97.7°	98.5°	98.6°	98.5°
Repeat cycle	3, 35, 176	44	35	24	-

radar). These effects are superimposed on differences in sigma nought due to material properties, as e.g. liquid water content of a snowpack which will be outlined in the following (HENDERSON & LEWIS, 1998).

ERS-1/2 acquire image data for a maximum duration of 12 minutes per orbit. As the data rate (100 Mbits/s) is too high for on-board storage it is only acquired within the reception zone of a suitably equipped ground receiving station. Hence, in Antarctica, image acquisition is restricted to the operation of GARS (REINIGER & ZIMMER, 2000).

6.2 A brief overview on radar geometry and backscatter mechanisms

As a consequence of the side looking SAR system and the fact that surface points are localised in the image by the pulse travel time, topography causes distortions. The emitted wave front reaches the surface at different travel times. Figure 6.2 shows examples for topographic influences on the mapping of the surface. Radar shadows form where a mountain inhibits the radar beam to reach the ground. Foreshortening is also a typical phenomenon of reliefed terrain. The wave front reaches the summit earlier than the surrounding lower areas, and, as a consequence of the pulse travel time coding, the slopes towards the sensor are mapped perspectively shorter. Some areas in nature may even disappear in the image when very steep slopes towards the sensor induce the mountain crest of summit to be hit first by the radar beam – this situation is called layover.

The dielectric properties, the density and structure of a medium interacting with a radar wave, strongly influence the reflectance, refraction and absorption characteristics as well as the penetration depth of the radar beam. The signal which is received by the SAR sensor is hence a function of the surface properties on the ground and may consist only of a directly reflected wave or a complex composition of multiple reflections at various surfaces and in the volume of the medium (Figure 6.3).

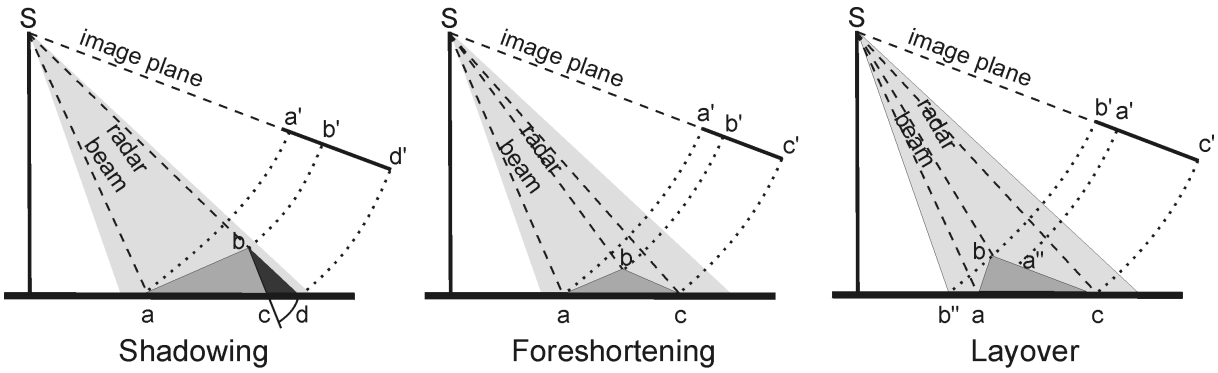

Figure 6.2: *Influence of surface topography on the imaging of a radar system. Displayed are shadowing, foreshortening and layover effects. S denotes the SAR sensor and a, b, c and d the mapped points/areas on the surface.*

Generally, the refraction angle of an electromagnetic wave penetrating a medium is larger, the larger the difference of the dielectric constants of the two mediums is. This is a direct consequence of the proportionality between the dielectric constant of the media and the refraction index.

Furthermore, the strength and direction of the reflection and transmission of a microwave is determined by the roughness as well as by the relief and exposition of the surface. The surface roughness is characterised by the ratio of altitude differences within a certain distance. As a first rough approximation, a surface can be regarded as smooth when the differences in z-dimension are less than the tenth of the wavelength and when specular reflection occurs. A more accurate definition is given by the Ryleigh Criterion where the surface irregularities are expressed as average height variations (h_{rms}), and categorisation is dependent on wavelength (λ) or look angle (γ) (HENDERSON & LEWIS, 1998). The roughness values can be estimated by the equations:

$$\begin{array}{lll} \textit{smooth} & h_{rms} < \dfrac{\lambda}{25\cos\gamma} & h_{rms}\,(ERS\text{-}1/2) < 0{,}25cm \\ \textit{intermediate} & \dfrac{\lambda}{25\cos\gamma} > h_{rms} < \dfrac{\lambda}{4\cos\gamma} & 0{,}25 > h_{rms}\,(ERS\text{-}1/2) < 1{,}52cm \\ \textit{rough} & h_{rms} > \dfrac{\lambda}{4\cos\gamma} & h_{rms}\,(ERS\text{-}1/2) > 1{,}52cm \end{array} \qquad (28)$$

In case of a smooth surface, the reflection angle is the local incidence angle (Figure 6.3). When the surface roughness increases to the value range of the wavelength or larger, diffuse scattering occurs. Moreover, slope, orientation of the surface to the

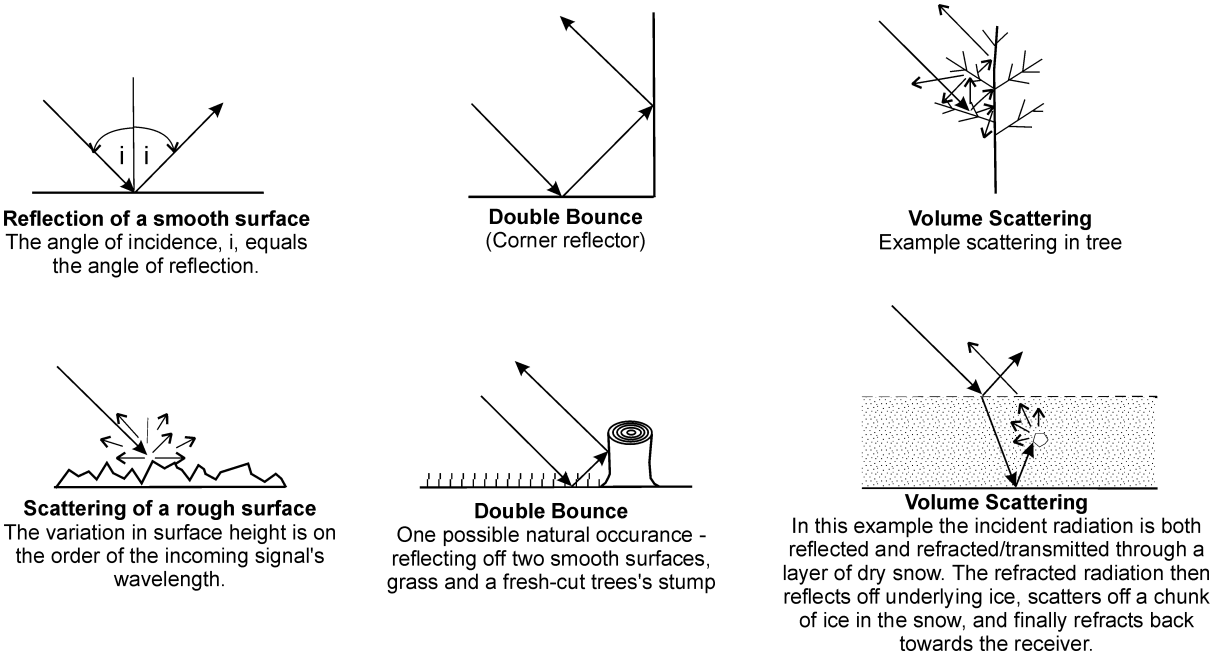

Figure 6.3: *Different radar scattering and reflection mechanisms of a radar wave with a medium.*

sensor or local incidence angle in azimuth and range direction may strongly influence the strength of the signal received at the SAR sensor.

The absorption and penetration depth of a radar wave are determined by the dielectric constant which can be split into a real and imaginary part. The real part is a measure of the reflection, whereas the imaginary part stands for the damping of the wave in the medium. For volume scattering, the particle size becomes of principle importance for the interaction of the wave with the medium. In the case that the particles are of equal size or even larger than the wave length, the scattering coefficients of Mie have to be applied. If the particles are considerably smaller than the wave length, then an incoherent scattering occurs which is described by the Rayleigh Law (the emitted power is proportional to the fourth power of the wave frequency).

Due to its high dielectric constant, the presence of water in the medium strongly alters the reflection and transmission properties of the medium in the microwave spectrum. It can be generally stated for the microwave spectrum: the larger the wave length, the smaller the absorption coefficient, and the higher the amount of liquid water in the medium, the higher the absorption.

6.3 The radar glacier zone concept

Based on the backscatter mechanisms briefly outlined above, snow cover and glacier parameters, such as liquid water content, grain size, snow density, ice layers, and surface roughness, determine the appearance of glacier and snow surfaces in SAR imagery.

Due to its sensitivity to liquid water within the snowpack, SAR-data offer the possibility to discriminate the actual zones of wet and dry snow on a glacier. Since SAR-data furthermore provide information on the deeper layers of a dry snow cover, a more detailed classification of glacier snow zones or glacier facies compared to by optical imagery (WILLIAMS ET AL., 1991) is achievable. Depending on the prevailing meteorological conditions before and during image acquisition, these snow zones on a glacier are dynamic on a time scale of days to weeks and show remarkable seasonal variations. As a consequence, the spatial and temporal evolution as well as the delimitation of snow zones identifiable in SAR images do not necessarily coincide with the characteristics of the classical glaciological snow zones given by BENSON (1996) or PATERSON (1994) which refer to an entire mass balance year. As such, FORSTER ET AL. (1996) introduced the terminology of radar glacier zones in a study on the Patagonian Icefields using SIR-C/X-SAR data in order to distinguish the temporal appearance of a snow cover in a radar image from the glacier mass balance terminology. This radar glacier zone concept was further expanded and refined by SMITH ET AL. (1997), RAMAGE & ISACKS (1998), RAMAGE ET AL. (2000), BRAUN ET AL. (2000) and RAU ET AL. (2000).

The classification given by SMITH ET AL. (1997) from the Stikine Icefields, Canada, comprises dry, melt, phase 2 melt (P2 or M2) and bare ice radar glacier zones. However, this terminology leads to ambiguities with the terminology commonly used to describe glaciological snow zones. The proposed dry radar glacier zone is e.g. assigned to a frozen snowpack and corresponds to a percolation glacier snow zone. Therefore, this work refers to the modified classification scheme proposed by RAU ET AL. (2000) which comprises all radar glacier zones that can be detected in SAR imagery.

The subdivision includes

(1) a dry snow radar zone (DS)

(2) a frozen percolation radar zone (FP)

(3) a wet snow radar zone (WS)

(4) a metamorphosed wet snow radar zone (P2 or M2)

(5) a bare ice radar zone (BI)

A comparison of the radar glacier zone concept and the classical glacier mass balance terminology is given in figure 6.4. Typical backscatter values of these radar glacier zones are given in table 6.2.

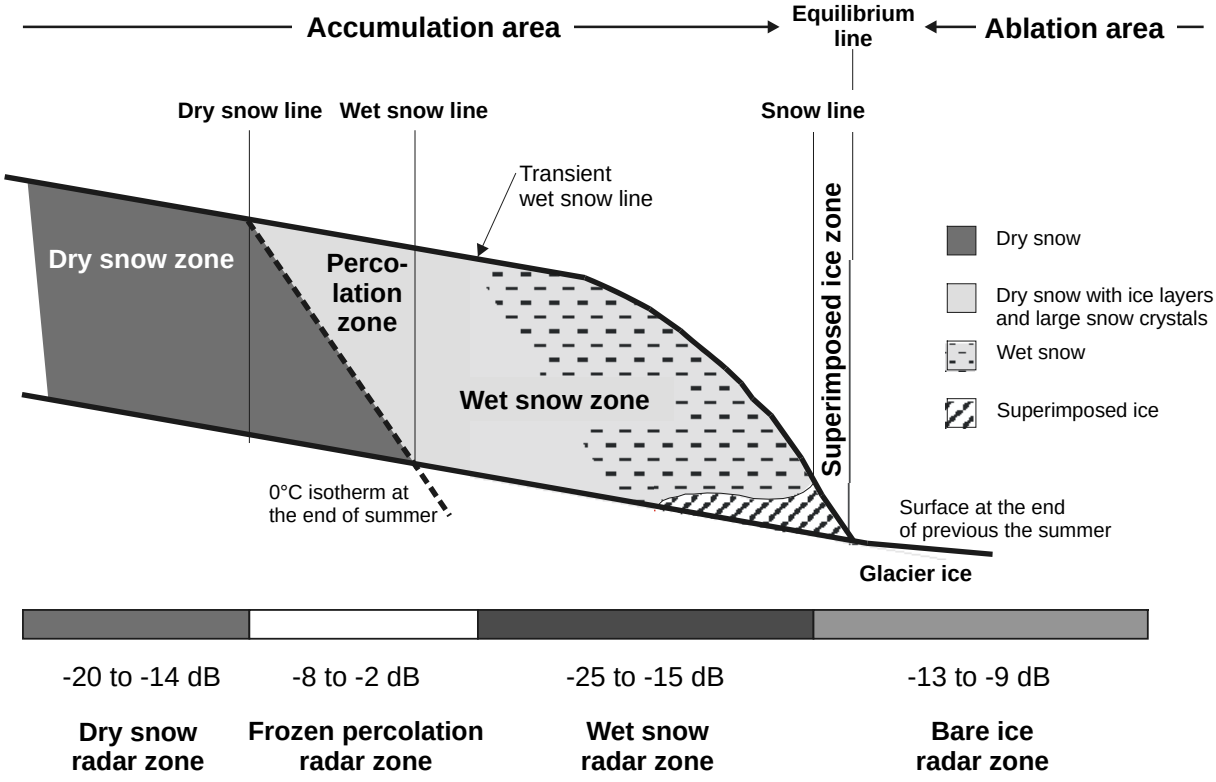

Figure 6.4: *Glacier snow zones and corresponding radar glacier zones with typical backscatter values (C-band, VV; RAU ET AL., 2000).*

6.3.1 Dry snow radar zone

The dry snow radar zone is restricted only to the highest areas where the temperatures never rise above the melting point. The lack of melt events and the predominating dry snow metamorphism result in small grain sizes (< 5 mm; PARTINGTON, 1998) and the absence of ice layers. The snow is gradually compacted under its own weight and metamorphosed under the effect of wind or depth-hoar development. Due to the high penetration depth of the radar beam of up to 20 m (ULABY ET AL., 1986) and dominating volume scattering, the dry snow radar zone is characterised by low backscatter values. Any variation in sigma nought can be expected to derive largely from differences in grain-size (PARTINGTON, 1998) and is attributed to regional differences in patterns of accumulation and wind as visible in imagery from Greenland (FAHNESTOCK ET AL., 1993) and Antarctica (JEZEK, 1998).

6.3.2 Frozen percolation radar zone

Here, frequent or occasional melt-freeze-cycles lead to the formation of numerous pipes, ice lenses, ice layers and large grain sizes in the snowpack. The large snow grains in this zone act as strong scatterers of the radar beam and hence produce considerable volume scattering. Moreover, the presence of pipes and ice lenses can reach dimensions comparable to the wavelength of the SAR and thus lead to high radar returns (PARTINGTON, 1998). This is supported by observations from the Greenland ice sheet by FAHNESTOCK ET AL. (1993). There is no clear surface manifestation of the boundary (the so-called dry snow line) between this and the dry snow radar glacier zone. Single strong snow melt events can move the dry snow line upwards for a time range of several years as studied by RAU ET AL. (2001) based on backscatter modelling.

6.3.3 Wet snow radar zone

During the ablation season, melting increases the liquid water content in the snowpack. As the radar signal is already drastically reduced by small amounts of liquid water, the penetration depth is diminished to the uppermost centimetres. 2 Vol. % of liquid water in the snow cover will reduce the penetration depth to approximately 1 wave length (ULABY ET AL., 1986). HALL (1998) gives a penetration depth of 1-4 cm when the liquid water content rises to 4-5 % in the snowpack. The importance of scattering mechanisms will therefore change from predominately volume scattering to surface scattering with increasing melt. Thus, the development of the wet snow radar zone can be identified by very low backscatter values. The wet snow radar zone is separated from the frozen percolation radar zone by the transient wet snow line which can be also addressed as the actual 0°C isotherm in the snow cover. However, a general gradation of backscatter values with altitude will occur as a result of the decrease in liquid water content. Consequently, the transient wet snow line can not be expected to be detected as a discrete boundary. Moreover, a high moisture

content in deeper layers, as e.g. from previous melt event, will complicate a detection of this boundary line.

6.3.4 Metamorphosed wet snow radar zone (M2 / P2)

In a second stage of snowmelt, high backscatter values comparable to those of a frozen percolation radar zone have been observed at various locations, in particular in highly maritime climates of Alaska and the Canadian Coast Range (SMITH ET AL., 1997; RAMAGE ET AL., 2000). Latter authors attributed the brightness of the return to a roughening of the surface due to metamorphosis of the wet snow. Field measurements determined that suncups (higher-relief undulations in three dimensions) caused this high backscatter in the metamorphosed wet snow zone. For wet snow conditions, surface roughness contributes to a higher-magnitude backscatter coefficient (RAMAGE ET AL., 2000). When the liquid water content of the snow pack increases beyond 3 Vol. %, surface scattering on a roughened surface causes an increase in backscatter (ULABY ET AL., 1986; SHI & DOZIER, 1995) whereas smooth, wet surfaces reveal low backscatter.

6.3.5 Bare ice radar zone

The lower part of a glacier is formed by the bare ice radar zone. Here the total yearly accumulation is lost by ablation. The backscatter signal in the bare ice radar zone is caused by scattering of a rough, dense ice surface, the resulting sigma nought values (-9 to –13 dB) range between the values reported for the wet snow and the frozen percolation radar zone. During melt conditions, the adjacent upper radar zone is formed by the wet snow radar zone, whereas, during freezing conditions, high backscatter from the frozen percolation radar zones facilitates a discrimination of bare glacier ice. As a consequence, the bare ice radar zone can be determined in SAR imagery. The upper boundary of the bare ice radar zones is the transient snow. During winter, the bare glacier is covered by a dry unmetamorphosed snow cover that is almost transparent for the radar signal, and no significant changes in the radar return have to be expected. Therefore, a distinct border between the frozen firn and bare glacier ice can be detected. However, if snow melt occurs during winter months, the backscatter signal of the overlying snow cover will be altered to that of a frozen percolation radar zone and hence cause considerable uncertainty in determining the last year firn line. During summer, the backscatter differences between wet snow and bare glacier ice are sufficiently large to enable a clear separation.

An area of superimposed ice, which is high-density refrozen melt from the previous year's accumulation, can also form between the wet snow and the bare ice radar zone. In a heavy ablation year, this zone may be completely melted away, leaving the firn line equivalent to the equilibrium line (PARTINGTON, 1998). MARSHALL ET AL. (1995) suggested that the superimposed-ice zone is potentially distinguishable in SAR data as a result of its greater degree of smoothness relative to the glacier ice.

However, only concurrent and extensive field observations enabled such an interpretation of the SAR data.

For glaciological and climatological studies, spatially distributed measurements of mass balance parameters are of particular interest. The boundaries between the different radar glacier glacier zones therefore reveal considerable information (RAU ET AL., 2000):

(1) The transient firn line separating bare ice radar zone and wet snow (summer) or frozen percolation radar zone (winter) documents the current spatial extension of the ablation zone. Particularly, the position of the transient firn line at the end of the ablation season is often regarded as the equilibrium line altitude (ELA) which is a key parameter for the glaciers mass balance.

(2) The dynamic wet snow line between the actual wet snow radar zone and frozen percolation radar zone approximately coincides with the position of the actual 0°C isotherm.

Table 6.2: *Overview on SAR backscatter coefficients (C-band) as reported for different study sites.*

Radar glacier zone	σ° [dB]	Study site	Author
Dry snow radar zone	< -8	Greenland	PARTINGTON (1998)
	-20 to -14	Antarctic Peninsula	RAU & SAURER (1998)
	-17	Antarctic Peninsula	WUNDERLE (1996)
	-20 to -14	Antarctic Peninsula	RAU ET AL. (2000)
	< -14	Antarctic Peninsula	RAU & BRAUN (submitted)
Frozen percolation radar zone	-7 to -3	Coast Range, Alaska	SMITH ET AL. (1997)
	-8 to -3	Coast Range, Alaska	RAMAGE & ISACKS (1998), RAMAGE ET AL. (2000)
	≈ -4	Greenland	PARTINGTON (1998)
	-6 to -2	Antarctic Peninsula	RAU & SAURER (1998)
	-3	Antarctic Peninsula	WUNDERLE (1996)
	-8 to 0	Antarctic Peninsula	RAU ET AL. (2000)
	-8 to -3	King George Island	this study
Wet snow radar zone	-22 to-11	Coast Range, BC	SMITH ET AL. (1997)
	-25.5 to -12	Coast Range, Alaska	RAMAGE & ISACKS (1998) , RAMAGE ET AL. (2000)
	< -15	Alaska	PARTINGTON (1998)
	-17	Antarctic Peninsula	WUNDERLE (1996)
	-25 to -15	Antarctic Peninsula	RAU ET AL. (2000)
	-22 to -15	King George Island	this study
phase 2 melt radar zone (P2)	-8 to -6	Coast Range, BC	SMITH ET AL. (1997)
	-7.5 to -3	Coast Range, Alaska	RAMAGE & ISACKS (1998) , RAMAGE ET AL. (2000)
	-8 to -4	King George Island	this study
Bare radar glacier zone	-12 to -10	Coast Range, BC	SMITH ET AL. (1997)
	-12 to -10	Coast Range, Alaska	RAMAGE & ISACKS (1998) , RAMAGE ET AL. (2000)
	-10 to -15	Antarctic Peninsula	RAU ET AL. (2000)
	-9 to -6	Alaska	PARTINGTON (1998)
	-14 to -6	Antarctic Peninsula	RAU ET AL. (2000)
	-13 to -10	King George Island	this study

(3) The dry snow line skirting the dry snow radar zone is an indicator for singular extreme melt events also impacting the uppermost altitudes (RAU ET AL., 2001, RAU & BRAUN, 2000).

6.4 Data processing and data analyses

All ERS-1/2 data used in this study was prepared using processing chains in the ESA SARToolbox and ERDAS Imagine software packages. First, from all 40 images normalised backscatter values (σ°)were calculated using the algorithm based on LAUR ET AL. (1998). A compensation for losses during the analogue-digital conversion and a correction for the replica power variation was included in these procedures. Subsequently, the images were co-registered using a master image from the 18 February 1998 for the descending and an image from 15 July 1997 for the ascending orbit.

To determine the seasonal and inter-annual variation of backscatter coefficients, areas of interest (AOIs) covering about 300 pixels (corresponding to about 7500 m²) were defined on the King George Island ice cap along an altitudinal transect ranging from 85 m a.s.l. to about 650 m a.s.l. The locations of the AOIs are displayed by different symbols in figure 6.5. Averaged backscatter values were calculated for all pixels within an AOI. In order to determine the firn line positions at the end of the ablation season, thresholds of -14 dB and -6 dB (BRAUN & RAU, 2000) were applied to separate bare ice from the wet snow (end of summer) and the frozen percolation radar zone (winter) respectively. Finally, the firn line positions where digitised and superimposed on a digital elevation model (BRAUN ET AL., 2001) to determine the mean elevation of the firn lines. Since the imagery was not corrected for topography, this approach bears errors due to relief induced distortions. However, the resulting errors were deemed small as the AOI transect was located on smooth terrain with slopes less then 5°. Moreover, the variations in the sigma nought values, caused by changes in the liquid water content of the snowpack are considerably higher than those resulting from differences in the local incidence angle.

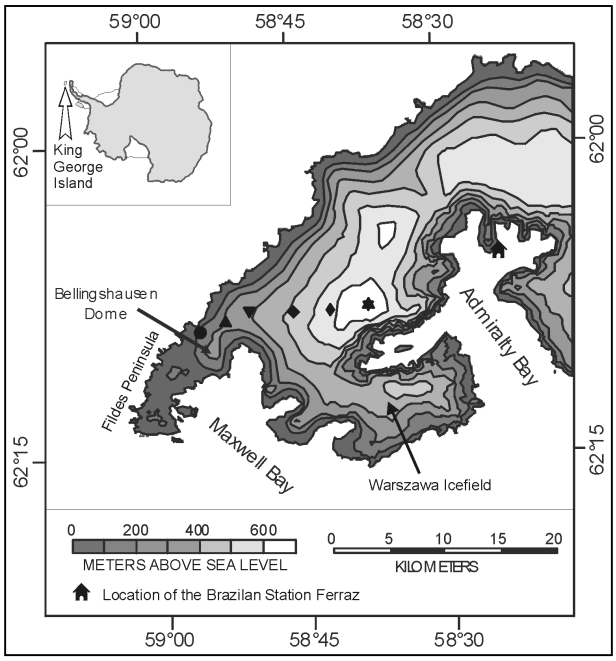

Figure 6.5: *Location of the areas of interest (AOIs) are denoted with the similar symbols as in the figures 7.13 and 7.15.*

7 Snowmelt on the King George Island ice cap

7.1 Surface energy balance calculations at the AWS sites

The results of the surface energy balance computations for the various AWS sites will be presented and discussed in the following subchapters. The calculated fluxes and melt rates for the summer 1997/98 will be linked to large-scale atmospheric circulation and compared to other energy balance studies and ablation measurements in the region of the Antarctic Peninsula. Finally, a sensitivity study of the applied model will be given to estimate possible errors resulting from parameterisation or measuring inaccuracies.

7.1.1 Surface energy balance and ablation during the 1997/98 field season

The course of the individual energy balance terms, the sum of energy fluxes, the calculated hourly melt rates and the snow depletion throughout the measuring period in 1997/98 are shown in figure 7.1. The results obtained from snow depletion observations allowed the division of the entire research period into three major ablation phases:

1) A phase of relatively strong ablation took place from the beginning of the measurements until mid December. Temperatures were well above the freezing point, and high relative humidity values indicate air mass transport over the ice-free Bellingshausen Sea and Drake Passage.

2) A period of almost no snowmelt followed with temperatures below 0 °C until the end of the year. During this phase, cold, dry air masses, originating from the Antarctic continent, dominated the surface energy fluxes over the snow cover on the King George Island ice cap.

3) On New Year's Eve 1997, phase 2 was terminated by an intense snowmelt event lasting until 04 January 1998. Snowmelt continued until the end of the measuring period. In this phase, advection of warm humid air masses caused high ablation rates as in phase 1.

Throughout the measuring period, net radiation provided the major energy input for snowmelt (Table 7.1), although during phase 2 clear sky conditions led to increased nocturnal radiative losses. It can be seen from the modelled hourly snowmelt that the pronounced daily cycle of the radiation balance triggered ablation (Figure 7.1). Regarding the mean value, sensible heat flux was a second energy source, while the latent heat flux did not lead to significant ablation (Table 7.1). The low latent heat flux is caused by averaging since positive and negative values equalise each other over the entire measuring period. Rain heat flux contributed only with 0.3 % to the net energy balance at AWS 1. During the different ablation phases, remarkable features can be observed. In phase 1, turbulent heat fluxes were positive, while in the second phase, sensible heat flux showed the highest positive and negative amplitudes. In phase 2, the heat loss occurred due to evaporation from the snow cover. The turbulent fluxes were therefore characterised as negative. Only at one occasion, in the beginning of January, the contribution of turbulent heat fluxes to snowmelt exceeded that of radiation balance. Phase 3 was similar to phase 1 in terms of the distribution of energy fluxes.

The study shows that on the King George Island ice cap, the major energy input during summer melt is provided by net radiation, with sensible heat flux as a secondary source. On average, latent heat flux did not contribute significantly to ablation. Similar findings were reported by BINTANJA (1995) for Ecology Glacier in Admiralty Bay. The mean distribution of the energy balance components at AWS 1 (85 m a.s.l.) and Ecology Glacier (100 m a.s.l.) coincide well. However, the absolute mean values of the present study only reached half of the energy input measured

Table 7.1: *Mean values of meteorological variables and surface energy balance components at the different AWS sites (02 December 1997 to 12 January 1998).*

Parameter	AWS 1	AWS 2	AWS 3a	AWS 3b
altitude (m a.s.l.)	85	255	385	619
measuring period	01/12/97-12/01/98	01/12/97-12/01/98	06/12/97-17/12/97	19/12/97-11/01/98
air temperature at 2 m (°C)	-0.03	-0.95	-0.63	-3.83
relative humidity at 2 m (%)	92.1	93.1	97.5	97.6
wind speed at 2 m (m s^{-1})	4.9	5.25	3.84	6.0
downward shortwave radiation (W m^{-2})	214.5	248.5	253.9	287.6
upward shortwave radiation (W m^{-2})	176.7	204.4	205.9	248.9
albedo (%)	82.3	82.3	81.1	86.5
net radiation (W m^{-2})	22.5	19.9	16.4	3.0
sensible heat flux (W m^{-2})	9.5	1.5	-3.0	-2.4
latent heat flux (W m^{-2})	-1.1	-3.1	-2.3	-3.2
net energy balance (W m^{-2})	31.0	18.4	11.1	-2.7

during the summer of 1991/92 (BINTANJA, 1995). This may be due to the fact that he measured in a comparably warm year (1,5 K warmer than the average). Although figure 4.7 shows that in January 1998 the mean monthly air temperature also exceeded the long-term monthly mean (1968-2000), the December 1997 was within the long-term mean. The majority of the measuring period reported in this study was in December 1997.

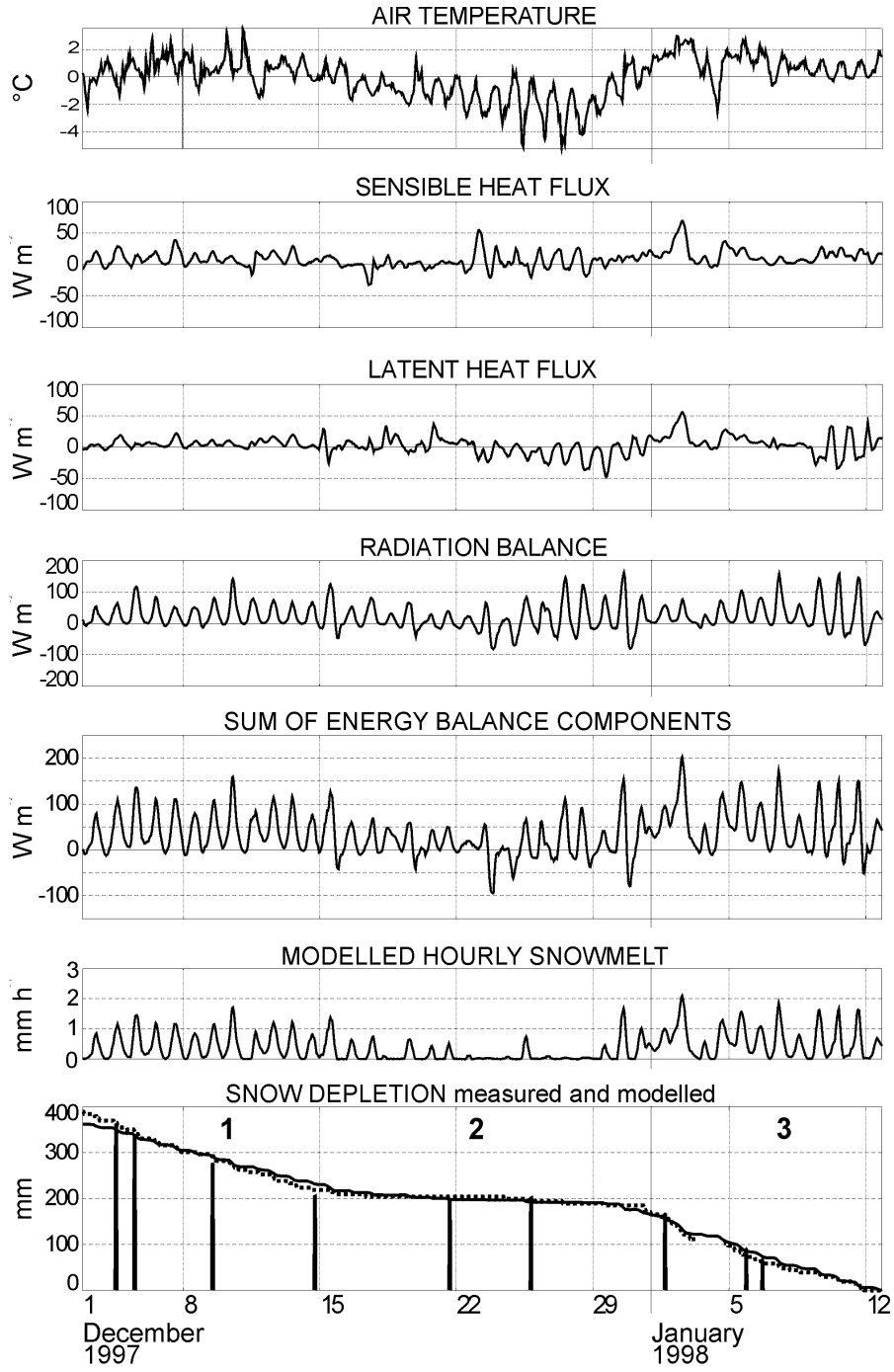

Figure 7.1: *Energy balance components, sum of energy fluxes, modelled hourly snowmelt and snow depletion at AWS 1 for the entire measuring period. Solid line: modelled ablation, dotted line: measured ablation with snow depth sensor, bars: readings of ablation stakes.*

Moreover, the measuring periods covered different time spans (BINTANJA'S, (1995) observations cover 4 weeks versus 6 weeks in the present study). BINTANJA's research period lacked a phase of low temperatures with advection from south or southeast where no ablation was recorded as it was in the present study. Additionally, the study site in Admiralty Bay is generally characterised by higher temperatures and less cloud coverage as outlined in chapter 4.4.2. Furthermore, the occurrence of bare glacier ice at the end of the measuring period at the Ecology test site in 1991/92 may have been another reason for the higher ablation measured by BINTANJA (1995).

The extraordinary agreement between measured and modelled water equivalent decrease indicates that the chosen model is appropriate for the conditions encountered on the ice cap. Generally, snowmelt occurred at lower elevations during almost all synoptic situations, while the highest parts of the King George ice cap were affected only by strong advection events due to meridional air mass transport. The distribution of energy balance components and melt rates differed widely depending on altitude. This corresponds to the findings by KNAP ET AL. (1996) who suggested that an increase or decrease in mean air temperature would affect the lower parts of the ice cap most considerably.

7.1.2 The influence of large-scale synoptic weather patterns on surface energy balance terms and ablation

The results presented in the previous section indicated the dependence of energy balance terms on atmospheric conditions. Therefore, the calculations of local surface energy balance were combined with an analysis of concurrent synoptic-scale weather situations. Four typical synoptic circulation patterns dominating extensive time periods were therefore identified. They were classified according to the subjective criteria of direction of air mass advection. The location of pressure centres and resulting direction of air mass transport were derived from 12-hourly NOAA IR-composites, surface pressure charts with a similar time resolution and the prevailing wind direction at the AWS sites. A verification of the classification was done using the daily radio sounding data available from Bellingshausen station. Mesocyclones were not included in the analysis since their average life span (< 12h) is shorter than the temporal resolution of the available composite data (HEINEMANN, 1995; KING & TURNER, 1997). An example for each synoptic situation is shown in figure 7.2. Accordingly, representative radio sounding data of Bellingshausen station are plotted in figure 7.3 for the four weather situations. Air temperature, sums of energy balance components and hourly melt rates are presented in figure 7.4. Figure 7.5 shows energy balance terms averaged over time and resulting snowmelt rates for all three AWSs.

The classified synoptic circulation patterns are listed in the following in the chronological order of their occurrence during the observation period:

(a) advection from north to northwest

(b) southerly to southeasterly air mass transport

(c) advection from northwest

(d) advection from west to southwest

a) Advection from north to northwest (11-13 December 1997)

From 9 December 1997 on, a synoptic scale low pressure centre moved rapidly eastwards over the Bellingshausen Sea (Figure 7.2a). It slowed down in front of the Antarctic Peninsula and caused the advection of warm, humid air masses from the north. The frontal zone in the satellite image is clearly marked by a cloud band. Behind this strong depression centre, a mesocyclone developed which is not represented in the pressure chart but visible in the NOAA image of 11 December 1997. KING & TURNER (1997) reported that mesocyclones often develop on the lee of synoptic scale depressions near the frontal zone. However, the impact of that mesocyclone on surface energy fluxes was considered negligible for the purpose of this study. With the approach of the depression centre to the Antarctic Peninsula, air temperatures rose above 0°C (Figure 7.4a). In the area of the South Shetland Islands, north to northwesterly air mass transport prevailed (Figure 7.3a) and caused predominantly overcast sky. This led to an almost balanced long-wave radiation balance, and short-wave irradiance caused an intensive daily cycle of snowmelt. Latter could be reproduced by the model runs as shown for AWS 1 (Figure 7.4a). The net energy balance was positive at all three locations (Figure 7.5a) resulting in melt rates between 6 and 9 mm WE per day. This was mainly due to the positive mean radiation balance. Latent heat was found to substantially contribute to the energy balance only at the lowest site (AWS 1), and only at this site a positive sensible heat flux was observed.

b) Advection from southeast along the Antarctic Peninsula (26-30 December 1997)

This synoptic situation was characterised by a depression centre north of the Antarctic Peninsula and high pressure over the Peninsula itself. A further depression centre was located in the northeastern Weddell Sea sector. The chart of sea level pressure and the radio sounding data indicate a southerly to southeasterly flow of air masses (Figure 7.2b, 7.3b). This led to the transport of cold, dry air from the central Antarctic continent along the mountain ridge of the Antarctic Peninsula towards the South Shetland Islands. PARISH (1989) pointed out that air masses originating from the Weddell Sea may play a significant role in the synoptic meteorology of the South Shetland Islands. The barrier winds cannot pass the obstacle of the Antarctic Peninsula due to the strong inversion in the Weddell Sea area. Air masses are deviated along the mountain crest to the north where they spread and sometimes reach the South Shetland Islands. During this situation, air temperatures almost

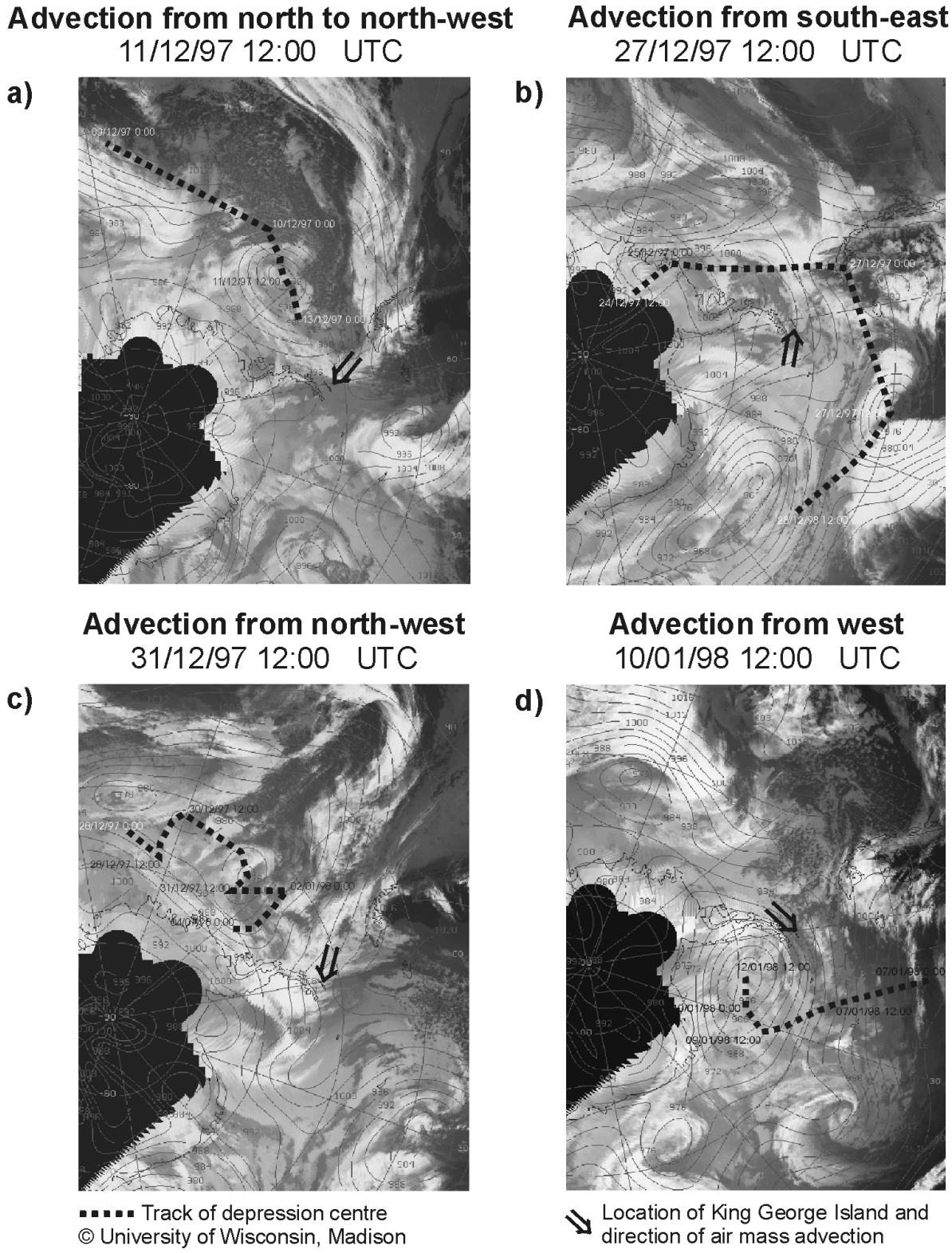

Figure 7.2: *NOAA IR-composites and surface pressure charts for the analysed synoptic situations. The tracks of the major depressions are marked. The following large-scale weather patterns were distinguished regarding the air mass transport to King George Island: (a) advection from north to the north-west, (b) southerly to south-easterly air mass transport, (c) advection from north-west and (d) advection from west to south-west.*

never exceeded 0°C and relative humidity dropped to a mean value of 75%. Such low relative humidity and cloud coverage persisting over several days are not very common in summer for the maritime climate of the South Shetland Islands.

The mean net energy balance was slightly positive only at the two lowermost AWS. In the highest parts of the King George Island ice cap, a mean energy loss of about 20 W m^{-2} was calculated. This can be attributed to a significant heat loss by evaporation as a consequence of the simultaneous occurrence of air temperatures some degrees below the freezing-point, low relative humidity values and an isothermal snow cover at 0°C with a high liquid water content. Negative mean latent heat flux was observed at all AWS, but the average net radiation was negative only at AWS 3. This synoptic situation resulted in significant daily variations of sensible heat flux at AWS site 1 (Figure 7.1). However, the average sensible heat flux does not reveal these daily cycles. Snowmelt was negligible during this synoptic situation. Air temperatures rose above 0°C only at the end of this period due to an approaching

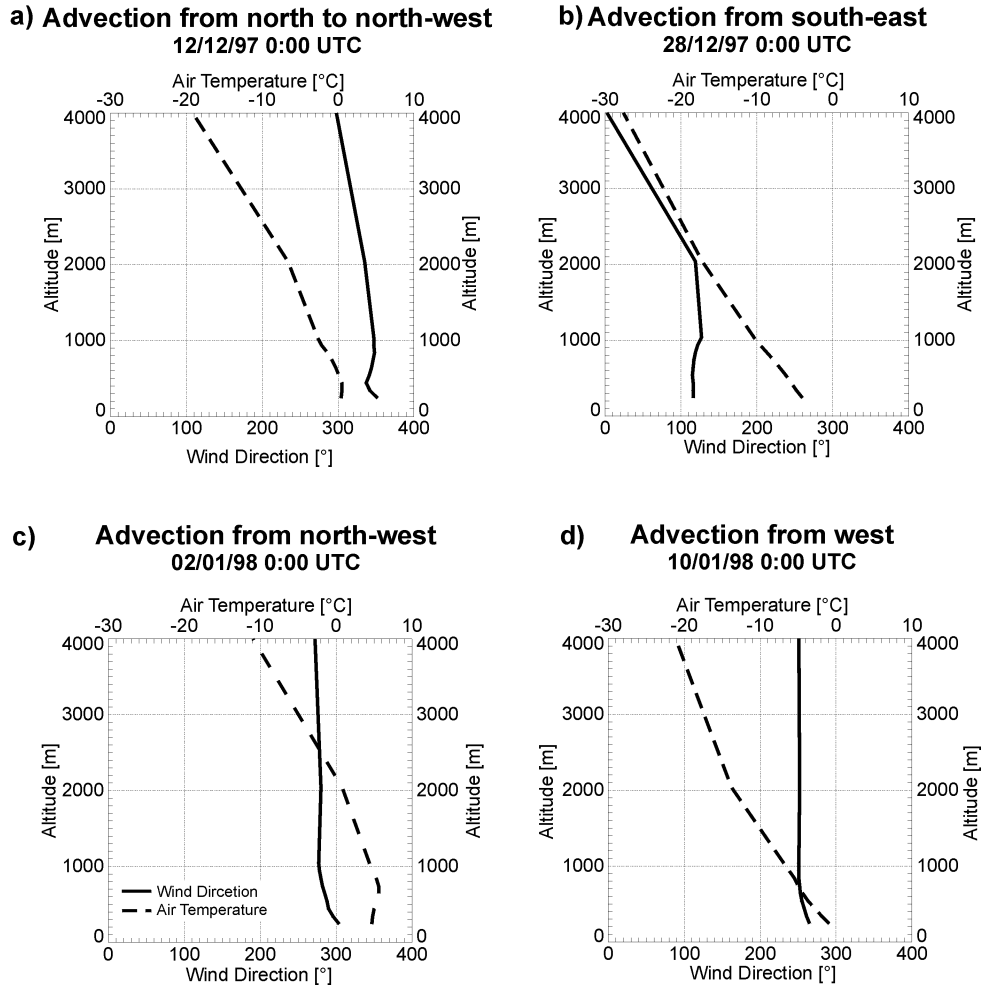

Figure 7.3: *Representative radio sounding profiles from Bellingshausen station during four different synoptic situations showing wind direction (solid line) and air temperature (dashed line): (a) advection from north to the northwest, (b) southerly to southeasterly air mass transport, (c) advection from northwest and (d) advection from west to southwest.*

depression centre in the Bellingshausen Sea (Figure 7.2c). The distribution of energy balance terms with a pronounced negative latent heat flux at the highest AWS corresponds to observations further south in the area of Marguerite Bay and Alexander Island (SCHNEIDER, 1998; JAMIESON & WAGER, 1983). However, in these regions, sensible heat flux provides more energy for snow melt than net radiation.

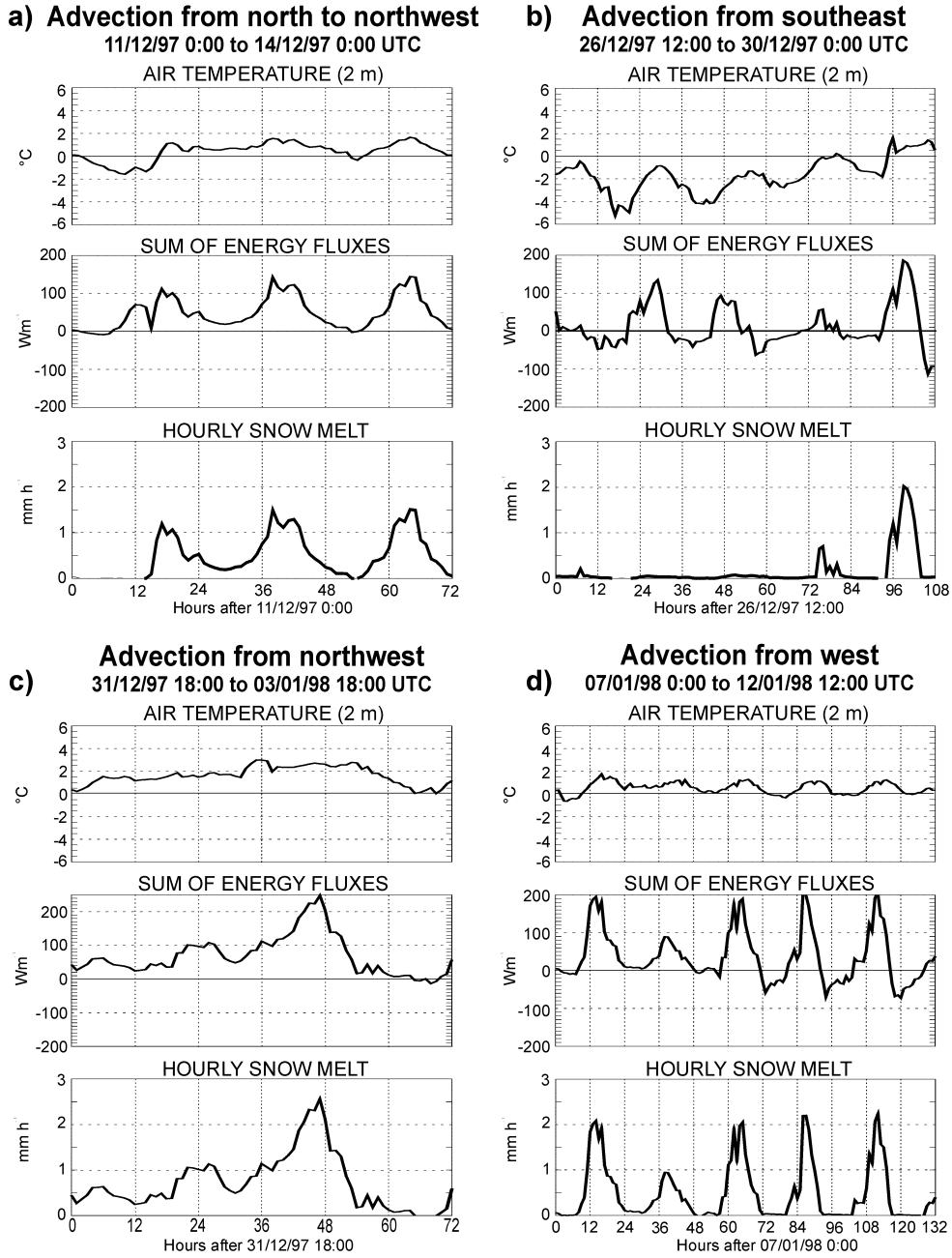

Figure 7.4: *Air temperature, sum of energy fluxes and modelled hourly snowmelt at AWS 1 for different large-scale synoptic circulation patterns: (a) advection from north to the north-west, (b) southerly to south-easterly air mass transport, (c) advection from north-west and (d) advection from west to south-west.*

c) Advection from northwest (31 December 1997 - 03 January 1998)

A centre of low pressure in the Bellingshausen Sea and high pressure over the South American continent caused a strong meridional advection of warm, humid air masses from northwest towards the Antarctic Peninsula. The depression centre was observed for the first time on the composite images on 28 December 1997 at about 135°W and it then moved continuously east-, north- and southwards. On 02 January 1998, it reached its location closest to King George Island and disappeared on 04 January 1998 west of Alexander Island (Figure 7.2c). Radio sounding data show westerly winds at all altitudes up to 4,000 m a.s.l. (Figure 7.3c). As a result of high wind speeds coupled with warm and humid air masses, the energy input from turbulent heat fluxes exceeded the input from net radiation. A daily cycle of snowmelt which could have been induced by solar irradiance was prevented by the dense cloud coverage. Therefore, the warm air masses and the positions of the pressure centres triggered snowmelt during this situation. The highest hourly melt rates of the entire field campaign were observed and modelled with up to 2.5 mm h^{-1} at AWS 1 (Figure 7.4c). No significant altitudinal differentiation in available energy for snowmelt could be detected at this occasion. However, the contribution of net radiation to ablation was more important at higher rather than at lower altitudes (Figure 7.5c). Similarly, HOGG ET AL. (1982) found very high contributions of sensible heat fluxes to the total energy balance on South Georgia. The frequent passage of low pressure centres in that region results in high air temperatures and concurrent high wind speeds. High sensible heat flux is the consequence.

d) Advection from west (07-12 January 1998)

This synoptic situation was characterised by a major depression centre located in the Weddell Sea. This low originated from lower latitudes and moved into the Weddell Sea until 09 January 1998, where it persisted till the end of the measuring period (Figure 7.2d). The stable constellation of pressure centres resulted in a westerly to southwesterly air mass transport from the Bellingshausen Sea to the region of the South Shetland Islands (Figure 7.3d). A strong daily cycle of all meteorological variables was observed (Figure 7.4d). Air temperatures almost never dropped below 0 °C during the night at AWS 1 (Figure 7.4d). However, temperatures at the other AWS sites remained at or below freezing point. This resulted in positive average sensible heat fluxes at the lowermost AWS and negative values for the higher elevations. The predominantly overcast sky (6/8 to 8/8) caused a major energy gain by net radiation at all AWS sites. Overall, heat loss occurred at all AWSs by latent heat flux. This led to moderate snowmelt rates at lower altitudes and almost no snowmelt at AWS 3.

Summarising the outlines above, the variation of energy balance terms and the obvious subdivision in different phases indicate that synoptic scale atmospheric

circulation controls the local surface energy balance terms and therefore ablation on the King George Island ice cap. Northerly and northwesterly air flow lead to the highest ablation rates. These warm humid air masses originate from lower latitudes and are transported over the ice free southern ocean. KEJNA (1993) showed that northerly to northwesterly flow is the dominant air mass transport during his investigated 3-year period (1986-89). However, even within the north to north-

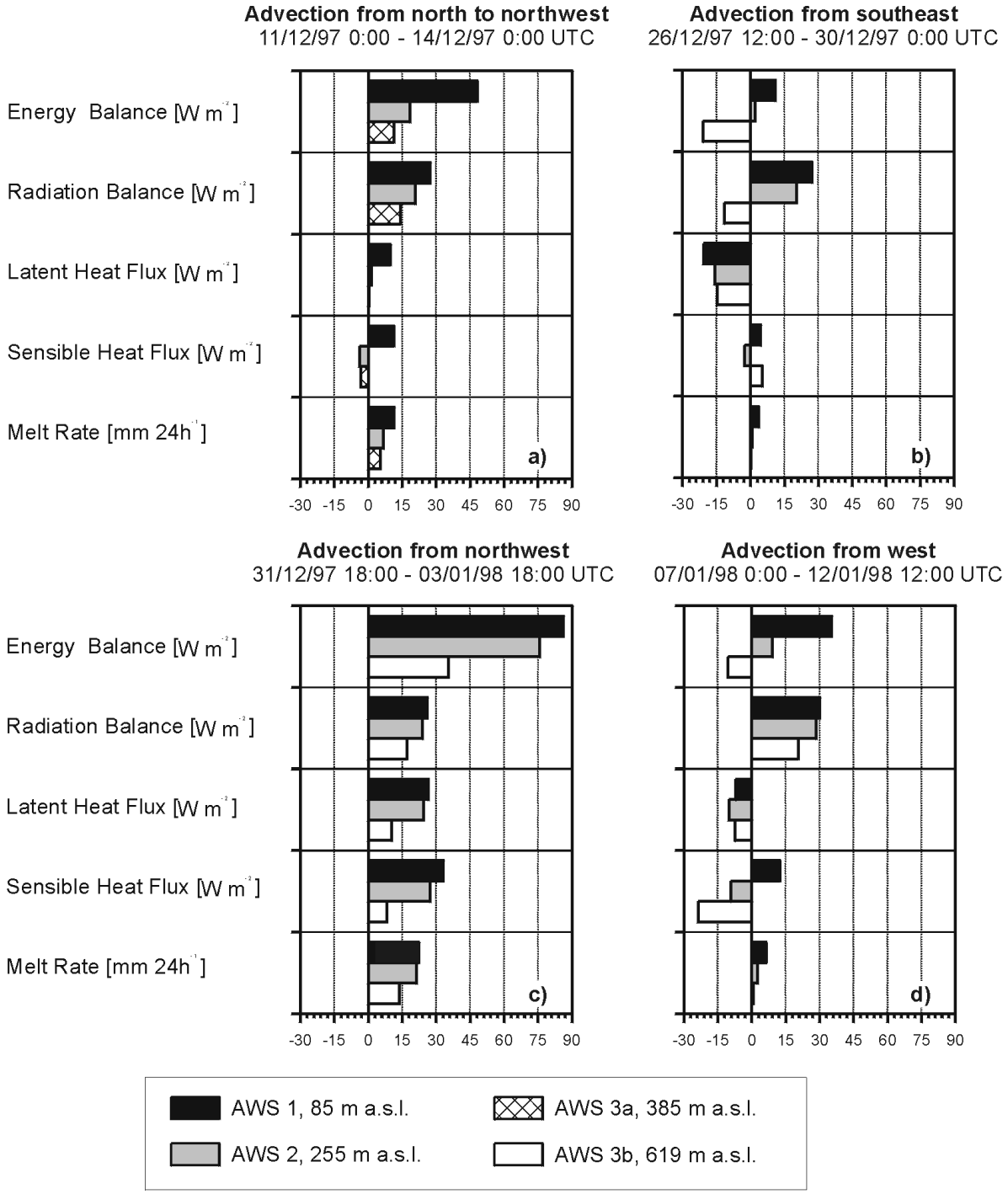

Figure 7.5: *Mean values of energy balance components for the three AWS during different air mass advection: (a) advection from the north to the north-west, (b) southerly to south-easterly air mass transport, (c) advection from the north-west and (d) advection from the west to the south-west.*

westerly advection, considerable differences in energy input and ablation occurred. This was shown by the contrasts of situation a) and c). While very strong pressure gradients caused meridional flow during phase c), synoptic situation a) was characterised by an approaching cyclone. In both situations net radiation balance reached similar values but turbulent fluxes differed greatly. TURNER & LEONARD (1996) also reported a quasi-stationary synoptic-scale low in the Weddell Sea, as in situation c). In their study, the cyclone reached the longest life span recorded during a whole year. KEJNA (1993) states that southerly flow is not very common in summer but more frequent in winter, when depression centres pass further to the north. The cold air leads to a marked decline in ablation and to refreezing of liquid water within the snow pack at higher altitudes on the ice cap. CARLETON (1992) reports that southerly flow from the Weddell Sea is more frequent in El Niño years and causes a marked delay of sea ice disappearance near the South Orkney Islands as was the case in 1997/98. One may speculate, that this unusually long period of southerly and easterly flow is a consequence of these anomalies in the Southern Hemisphere circulation, but more research is needed to collect further conclusive evidence.

A strong dependence of calculated surface energy fluxes and ablation rates on large-scale atmospheric circulation patterns was demonstrated. This is especially interesting since strong indications for changes in the atmospheric circulation in the region of the Antarctic Peninsula to more frequent northerly advection of warm air masses in particular during winter were observed by several authors (e.g. TURNER ET AL. 1997, 1998; KING, 1994; KING & HARANGOZO, 1998; see chaper 1.3). RACHLEWICZ (1997) already showed that warm-air advection can result in extraordinarily high snowmelt during winter on King George Island. Therefore, the ice cap of King George Island seems to be highly sensitive to climatic changes since summer ablation and winter accumulation will be affected by a change in the large-scale circulation pattern to more frequent northerly flow.

The high positive temperature trends along the Antarctic Peninsula were derived from monthly and yearly means. However, the current results indicate that sensitivity studies based on the addition of 1 K to air temperature of a short data set are very limited. A change in the frequency of certain synoptic weather situations does not only result in air temperature increase, but in the modification of other meteorological variables as well. A higher frequency of northerly advection will increase the ablation days, whereas in terms of a sensitivity study, a general increase of 1 K affects only periods where the net energy balance is already positive or nearly balanced. Consequently, the approach of a 1 K addition leads ro a different process modelling than changing the frequency of typical synoptic situations. However, more accurate analyses of synoptic weather patterns and their frequencies over several years are required to base sensitivity studies on this approach.

7.1.3 Sensitivity of the energy balance model and calculated ablation rates

To estimate the influences of measuring errors and the choice of the roughness length as a tuning parameter, a sensitivity analysis of the model was carried out. Table 7.2 shows that the adjustment of roughness lengths is crucial for the magnitude of the calculated turbulent fluxes. However, keeping this parameter to values reported over snow and ice, the general partitioning of the energy balance components remains. Inaccuracies in the temperature measurements mainly influence the sensible heat flux, whereas latent heat flux is less sensitive to changes of this variable. The addition of 1 K to measured values is often used to simulate climate change conditions. The calculations show that sensible heat flux and ablation would increase drastically. However, it should be considered that the alteration of only one variable will not reflect true conditions, e.g. changes in radiation balance and wind conditions are not taken into account. Changes in relative humidity cause only very small variations in the distribution of energy fluxes, since the mean latent heat flux over the observation period is almost negligible. Especially, the increase of humidity values shows low influence. This can be attributed to the fact that measured relative humidity values are frequently close to saturation conditions. The results of this sensitivity analysis permit to deduce at least some general characteristics of energy balance components on the King George Island ice cap from the model runs.

Table 7.2: *Sensitivity analysis of energy balance calculations at AWS 1 (85 m NN). Mean values for the period 02 December 1997 to 12 January 1998. Z_e denotes the varied effective roughness length, AT for air temperature and RH for relative humidity. The mean value of the radiation balance (22.5 W m^{-2}) was not altered in any of the sensitivity runs.*

Varied parameter / variable	Net energy balance [W m^{-2}]	Latent heat flux [W m^{-2}]	sensible heat flux [W m^{-2}]	Modelled ablation [mm]
$z_e=1*10^{-5}$	25.3	-1.8	4.5	309.3
$z_e=1*10^{-4}$	27.8	-1.6	6.8	340.4
$z_e=5*10^{-4}$	***31.0***	***-1.1***	***9.5***	***383.2***
$z_e=1*10^{-3}$	33.9	-0.7	12.0	412.7
$z_e=1*10^{-2}$	54.5	4.0	27.9	646.9
AT -1.0 K	23.0	-2.7	3.1	301.0
AT -0.5 K	27.0	-1.5	5.9	338.9
AT -0.3 K	28.8	-1.2	7.4	356.8
AT -0.1 K	30.6	-1.1	9.1	374.2
AT ± 0.0 K	***31.0***	***-1.1***	***9.5***	***383.2***
AT +0.1 K	32.3	-1.2	10.9	393.2
AT +0.3 K	33.6	-1.6	12.6	410.8
AT +0.5 K	35.7	-1.8	14.9	431.2
AT +1.0 K	41.0	-2.6	20.9	482.7
RH -5 %	28.2	-3.9	9.5	363.4
RH -3 %	29.4	-2.7	9.5	372.6
RH -1 %	30.4	-1.6	9.5	380.0
RH ± 0 %	***31.0***	***-1.1***	***9.5***	***383.2***
RH +1 %	31.3	-0.7	9.5	386.1
RH +3 %	32.0	0.0	9.5	391.0
RH +5 %	32.7	0.7	9.5	394.9

7.1.4 Characteristics of surface energy balance and ablation at various sites on the Antarctic Peninsula and in its vicinity

To enable a grading of the outcomes from the surface energy balance calculation on King George Island, they will be compared to previously published data to show a possible regional differentiation of energy fluxes and processes triggering snowmelt.

In particular, general characteristics between this study and results from a glacier in the inner Marguerite Bay near the Argentine station San Martín (SCHNEIDER, 1998) will be reviewed.

7.1.4.1 Comparison of King George Island and San Martín, Marguerite Bay

Although the two heat balance studies cannot be compared directly, as they were measured during different years, the same energy balance model was applied and the data set was obtained with similar instrumentation.

The mean albedo during the measuring period was 0.82 (snow surface) at the study sites on King George Island and in inner Marguerite Bay. At both sites, the mean air temperatures during the periods of observation were higher than the long-term averages based on data from Bellingshausen station (King George Island) and San Martín station (Marguerite Bay). For example, the mean temperature for San Martín in January 1995 was +3.1°C compared to the long-term average of +2.2°C (1979-1998). The corresponding value for Bellingshausen was +2.4°C in January 1998 and +1.3°C for the long-term average (1944-1998). Unfortunately, there are no long-term observations of the frequency of synoptic situations available to check if the two years were representative. However, the temperature record of Faraday indicates that both years were similar and also close to the mean of the period 1988-1998. The mean air temperature for the months December, January, February were +1.05°C (1994/95), +1.1°C (1997/98) and 1.2°C (mean of the years 1988 - 1998).

Therefore, the magnitude of fluxes will be compared for the two sites in the following. In general the mean of the energy available for snow melt is higher (+63 W m^{-2}, 17 mm WE d^{-1}) on sub-Antarctic King George Island in comparison to Marguerite Bay (+19 W m^{-2}, 6 mm WE d^{-1}) assuming similar large scale synoptic conditions for the two different years. The ratio between net radiation and turbulent heat fluxes is also quite different, with a ratio of approximately 1.5 for King George Island and 0.86 for Marguerite Bay. Additional energy of 5 W m^{-2} is produced by condensation on the South Shetland Islands. For Marguerite Bay however, the latent heat transfer is an energy loss of -25 W m^{-2} due to sublimation and evaporation from the snow cover according to our measurements. This extraordinarily high value and the fact that sensible heat flux is the dominating heat source is remakrable in comparison to all other studies referred to in this work (Table. 5.1, Table, 7.3). The high latent heat flux value might be an overestimation since relative humidity measurements are problematic in cold temperatures. Another possible explanation might be the methodological approach, using gradients between the two levels of air temperature and humidity measurements during negative temperatures. Measuring errors or inaccuracies resulting from insufficient sensor calibration in the San Martín data set may have led to considerable miscalculation in the turbulent heat balance terms.

In order to refine the interpretation of the energy balances of the two study sites, energy balance terms and meteorological readings were classified in respect to the

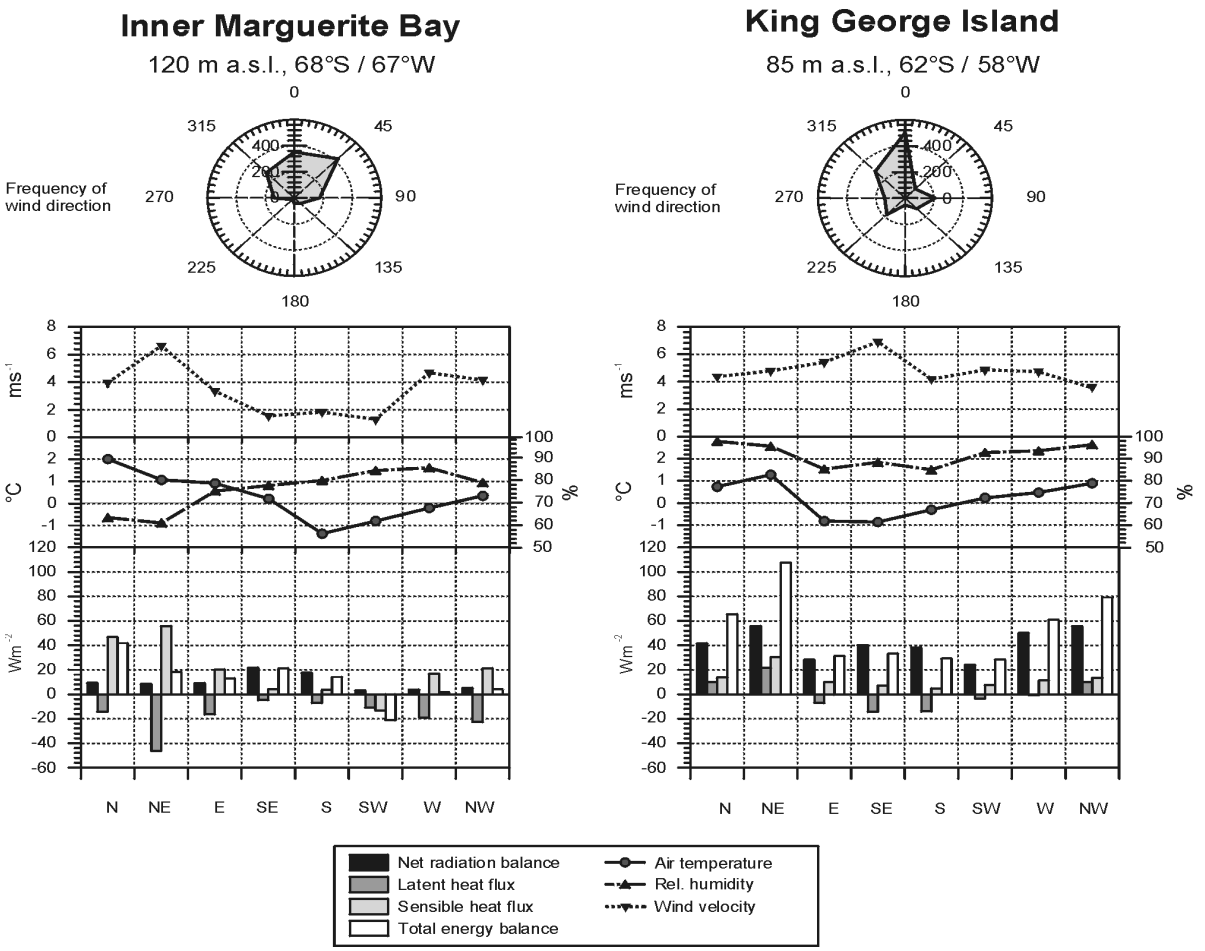

Figure 7.6: *Frequency of wind directions during the research periods on Northeast Glacier (Marguerite Bay) (left) and on King George Island (right). The mean values of wind speed, air temperature, relative humidity and the terms of the energy balance for different wind direction classes during the periods of investigation on Northeast Glacier (left) and on King George Island (right) are presented at the bottom.*

wind direction measured at 2 m above the snow surface at the AWS (Figure 7.6). Due to local topographic effects the measured wind direction does not necessarily coincide with the synoptic scale wind direction. Nevertheless, Figure 7.6 reveals interesting characteristics:

It is obvious that generally air temperatures on King George Island are not much higher than at the Marguerite Bay test site. However, at any wind direction the relative humidity is significantly higher on King George Island. This is in agreement with the different latent heat fluxes at the two study sites.

In Marguerite Bay, wind from northerly directions was most frequently encountered during the observed period. The northeast wind direction reflects foehn-type winds across the mountain chain with high mean wind velocity and low relative humidity. In consequence, the latent heat flux from the isotherm snow pack (0°C) is negative during these situations. The sensible heat flux is enhanced due to the high mean air temperature which results from the adiabatic descent of the air.

Since the study site in Marguerite Bay is protected by an offshore island in the west (Millerand Island, summit at 900 m a.s.l.), westerly air flow is measured as wind from northwest or north at the AWS. During these weather situations, warm air is advected into Marguerite Bay. High sensible heat flux triggers intensive snow melt, whereas the radiation balance is of minor importance for the overall energy balance. Wind from the southern sector with extraordinarily low wind velocities rarely occur. These situations can be attributed to a high pressure ridge over the Antarctic Peninsula. The turnover of the energy balance is small during these situations and the net radiation balance dominates the energy balance.

Wind directions from north and northwest prevail on King George Island. Ablation is very high during these periods because of the advection of warm and moist air masses from lower latitudes as could be demonstrated in chapter 7.1.2. Cold and dry polar air is advected from the south and around the northern tip of the peninsula from the east. The southerly and easterly air flow is a consequence of the cold barrier wind originating in the Weddell Sea. During these periods, latent heat flux shows negative values and the sensible heat flux is very small. The radiation balance contributes the major proportion of the ablation.

7.1.4.2 Comparison to other studies on and near the Antarctic Peninsula

In the following section the results of the studies from King George Island and Marguerite Bay are compared to previously published data for the Antarctic Peninsula (Table 7.3). Again, the interannual variability might limit the conclusions drawn from this comparison.

At a test site on South Georgia, HOGG ET AL. (1982) obtained the largest sensible heat flux (+42 W m^{-2}) published for the Antarctic Peninsula. A possible explanation might be the higher wind speeds and the more northerly location with higher air temperature during the summer months. The radiation balance is comparable to the values obtained on King George Island.

The ratios between turbulent heat fluxes and net radiation are similar in both studies from King George Island. BINTANJA (1995) observed a higher amount of available energy for snowmelt (+96 W m^{-2}) than in the present study. Easterly advection of cold air masses dominated a time period of approximately 10 days in December 1997. This is one reason for the generally lower energy balance in this study when compared to the study of BINTANJA (1995). Furthermore, his test site in Admiralty Bay is characterised by lee side effects leading to a higher mean air temperature. Enhanced input by net radiation is a direct consequence of the lower albedo of bare glacier ice towards the end of his field campaign.

CASASSA (1989) presented an estimation of the surface energy balance for Anvers Island using bulk equations with coefficients derived from Hokkaido, Japan. Anvers Island which has a highly maritime climate is located in an intermediate position between the South Shetland Islands and the Marguerite Bay. This is reflected in the

Table 7.3: *Summary of results from energy balance studies on the Antarctic Peninsula, on the South Shetland Islands and on South Georgia. (Values denoted with [*)] were estimated from figures.)*

Study site	Research period	Radiation balance	Sensible heat flux	Latent heat flux	Sum of energy fluxes	z_0, z_{0H}, z_{0E} [m]
Present study:						
King George Island 62° S / 58° W, 85 m a.s.l.	02/12/97 - 06/02/98	43.5 W m^{-2} 69.1 %	14.7 W m^{-2} 23.4 %	4.7 W m^{-2} 7.5 %	62.9 W m^{-2} 100%	$5*10^{-4}$
Former studies:						
Inner Marguerite Bay 68° S / 67° W, 120 m a.s.l.	20/12/94 - 19/02/95	8.6 W m^{-2} 46.2%	35.5 W m^{-2} 190.8%	-25.5 W m^{-2} -137%	18.6 W m^{-2} 100%	10^{-3}, 10^{-3}, 10^{-5}
South Georgia 54° S / 36 ° W, 375 m a.s.l. HOGG ET AL. (1982)	01/11/73 - 04/04/74	47.5 W m^{-2} 54.8 %	41.6 W m^{-2} 47.9 %	-2.3 W m^{-2} -2.7 %	86.8 W m^{-2} 100 %	$1.3*10^{-3}$, 10^{-5}, 10^{-5}
King George Island 62° S / 58 ° W, 100 m a.s.l. BINTANJA (1995)	17/12/90 - 16/01/91	60.8 W m^{-2} 63.5%	27.4 W m^{-2} 28.7 %	7.4 W m^{-2} 7.8 %	95.6 W m^{-2} 100 %	$1*10^{-3}$
Anvers Island[*)] 64.5° S / 63.5° W, 474 m a.s.l. CASASSA (1989)	05- 16/02/82	14.5 W m^{-2} 32.9 %	4.7 W m^{-2} 10.7 %	24.9 W m^{-2} 56.5 %	44.1 W m^{-2} 100 %	-
Alexander Island[*)] 71° S / 68° W, 250 m a.s.l. JAMIESON & WAGER (1983)	03/11/73 - 31/01/74	8 W m^{-2} 20.5 %	32 W m^{-2} 82 %	-1 W m^{-2} -2.5 %	39 W m^{-2} 100%	$1*10^{-3}$

value of the net radiation balance (+15 W m^{-2}). The ratio of the turbulent fluxes is in contrast to all other studies from the Antarctic Peninsula. A possible explanation might be the use of questionable transfer coefficients in the bulk equations.

JAMIESON & WAGER (1983) measured similar values of radiation balance (+8 W m^{-2}) and sensible heat flux (+32 W m^{-2}) as compared to the Marguerite Bay study. However, their mean value of the latent heat flux was only -1 W m^{-2} for the test site on Alexander Island. Large negative values as calculated from the Marguerite Bay data due to the foehn-type winds were not reported by JAMIESON & WAGER (1983).

Snow melt during the summer is much higher at the test site on the South Shetland Islands than in the Marguerite Bay (e.g. three times higher in our study). At both study sites, the advection from northern directions causes the highest snow melt rates during the summer season. Therefore, the increase of synoptic situations with northerly air flow, as predicted by KING & HARANGOZO (1998), would substantially increase ablation on the Antarctic Peninsula. Precipitation will also be enhanced by higher northerly air flow (TURNER ET AL. 1995, 1997). This could compensate for the predicted increase of ablation.

7.1.5 Interannual variations of ablation rates on King George Island and their relevance in comparison to other directly measured data sets

The data set of the present study comprises comprehensive meteorological and direct ablation measurements from three field campaigns in the late spring to early summer season (December to mid of January) at similar location. Only very few energy balance observations, even outside Antarctica, can rely on such a base. As a consequence thereof, this King George Island data set forms an exceptional base to study the interannual variation of the ratios of energy balance components and the resulting ablation rates. Comparability is slightly reduced by the short operation times of AWS A and B in 1995/96. Comparisons of the calculations at AWS 3b can not be performed as data quality in 1999/2000 did not allow computations of energy fluxes in adequate precision.

Figure 7.7 shows the result of the computed energy balance components as mean values over the entire research periods. The high net radiation values at AWS A in 1995/96 are caused by the disappearance of the snow cover to the end of the measuring period and the exposition of the underlying solid ice layer with a

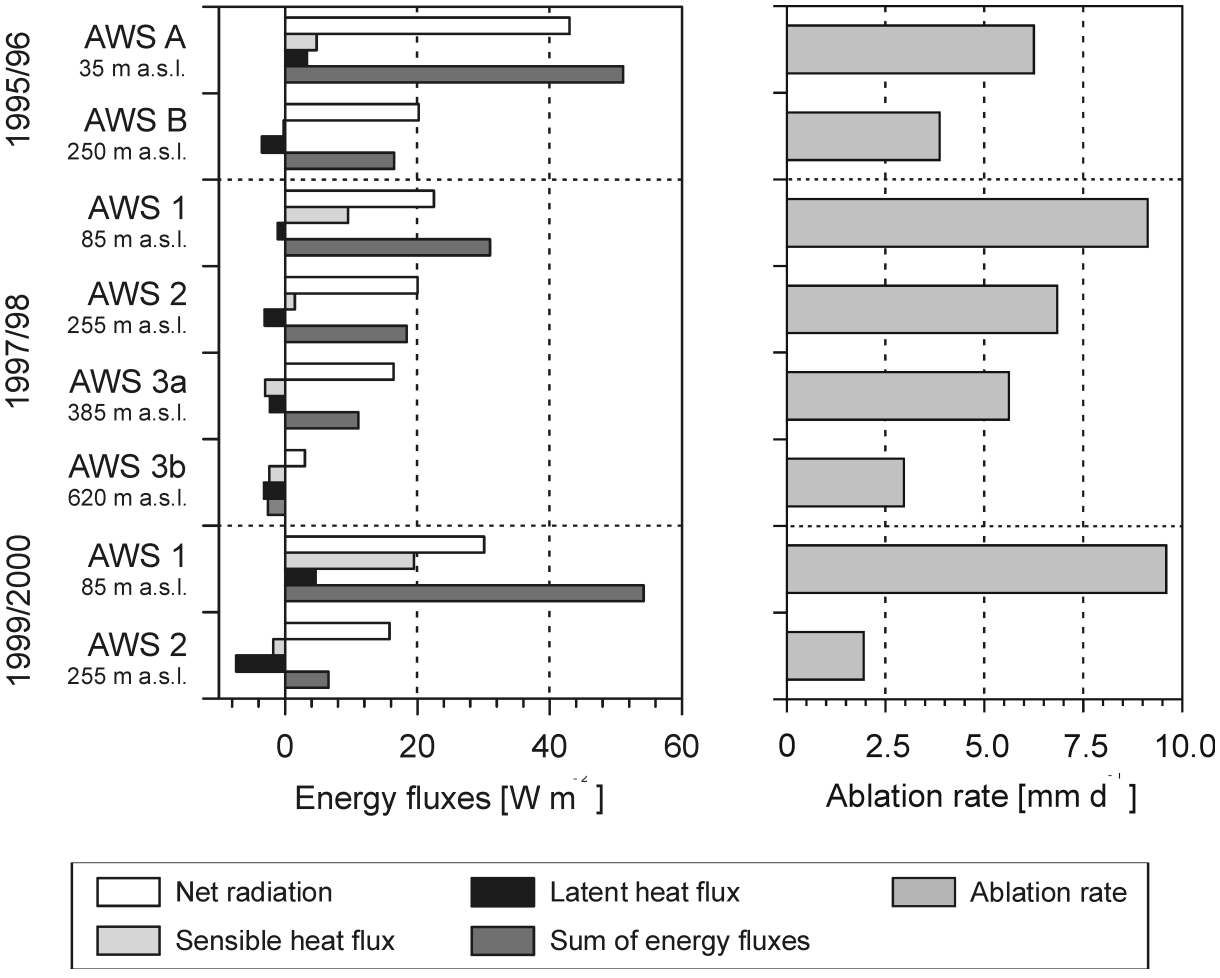

Figure 7.7: *Interannual variations of ablation rates and energy balance components at the AWS sites on the King George Island ice cap.*

considerable reduction of albedo at this periglacial site. Sensible heat flux at the lowermost AWS show drastic differences during each field campaign. This might be first attributed to the choice of roughness lengths, as it would also explain the higher values of the latent heat flux. However, as outlined in section 7.1.3, the variations due to the choice of the roughness length between $5*10^{-4}$ m and $1*10^{-3}$ m led only to changes in sensible heat flux from 9.5 to 12.0 W m^{-2}. Hence, sensible heat flux was higher during the 1999/2000 field campaign at AWS 1. The lower values in 1997/98 are a direct consequence of the occurrence of an extended cold period of almost two weeks in late December 1997. Such a period was absent in the 1999/2000 data set, and thus ablation rates in this year were higher in the lowermost areas. On the other hand, the 1999/2000 season featured frequent snow precipitation occasionally also down to the lower elevations. Each precipitation event led to a considerable increase of albedo for several days after snowfall and hence to a reduction of energy gain by net radiation. This might have compensated for the absence of an extended cold period in this season. As outlined above, the interannual variation of the magnitude of energy balance terms are considerable. However, the portions of the energy fluxes at similar altitudes do not reveal such variations.

Extrapolating the modelled mean ablation rates over an entire ablation season of 120 days, corresponding to a melt season from December to March (see figure 4.12) would result in approximately 750 mm WE a^{-1} in 1995/96 (AWS A) 1100 mm WE a^{-1} in 1997/98 (AWS 1) and 1150 mm a^{-1} in 1999/2000 (AWS 2). If, as suggested by by WEN ET AL. (1998), the ablation season is extended to November for the lowermost areas and assuming constant ablation rates, the total ablation would amount to about 1500 mm WE a^{-1}. It has to be stated that during all field campaigns no ice melt occurred at the AWS sites. However, shortly above AWS 1 ice melt was recorded during all years starting in the end of December or early January. As a consequence, the extrapolated ablation rates for the lowermost areas have to be considered as conservative estimates as albedo reduction due to the appearance of glacier ice would further increase ablation. These ablation rates coincide well with the measurements of Bintanja (1995) who determined a mass loss of 750 mm WE a^{-1} by ablation within a one month period in 1990/91.

The first ablation measurements on King George Island were performed near the former British Base G by NOBEL (1965). He reported lower ablation rates as observed in this study for the generally warmer site in Admiralty Bay (Table 7.4). Only the extrapolated values from the 1995/96 season on Bellingshausen Dome fit to this data. Nobel's measurements were continued some years later by STANSBURY (1961) revealing already considerable year-to-year variation. However, his values are still lower than the extrapolated ablation rates from BINTANJA (1995) who also measured in Admiralty Bay. Due to generally lower air temperatures on the northern and north-western coast and higher degree of cloudiness (see chapter 4.3.2), ablation rates on Bellinghausen Dome are expected to be smaller than those observed on the southern coast. Taking this into account and considering that ice melt had not yet

started in the 1997/98 and 1999/2000 observations, the data of this study is well within the range of the highest ablation rates observed by Bintanja (1995) and STANSBURY (1961a). Only ORHEIM & GOVORUKHA (1982) measured on the same site as this study and obtained only the half of melt during the two seasons 1969/70 and 1970/71. The observed high ablation rates from the 1990s are further supported by indications for an upward shift of the snowline on King George Island since the 1950s and the significant positive air temperature trend detected in the summer air temperature record from Bellingshausen station. In particular, summer air temperatures during the 1990s were extremely high in comparison to the long-term mean (Figure 1.9). Comparing the King George Island ablation rates with values from the Antarctic Peninsula, they remain among the highest so far reported for this region (Table 7.4). Based on new data from only one site, MORRIS (1999) suggested to revise the ablation sensitivity of Antarctic Peninsula ice towards climate change published by DREWRY & MOrris (1992) by a factor of 2 upwards. The ablation rates of this study support this.

***Table 7.4**: Compilation of ablation rates for the Antarctic Peninsula region.*

Year	Site	Ablation rate [mm WE a^{-1}]	Author
1957/58	Flagstaff Glacier, Stenhouse Glacier King George Island	750 assumed to be negligible	NOBLE (1965)
01-04/1959 1959/60	Flagstaff Glacier, King George Island	50 1310	STANSBURY (1961a)
1969-71	Bellingshausen Dome King George Island	750	ORHEIM & GOVORUKHA (1982)
1985-91	Bellingshausen Dome King George Island 45 m a.s.l. 252 m a.s.l.	1430 410	WEN ET AL. (1998)
1963-66	Galindez Ice Cap (65°15'S, 58°15'W)	300	SADLER (1968)
1986-95	Moraine Corrie Glacier Alexander Island (71°03'S/68°20'W)	1200	MORRIS (1999)

7.2 Spatially distributed snowmelt modelling

7.2.1 Ablation rates during the 1997/98 summer season

As was shown in chapter 5.4.2, the distributed energy balance model performed very well in lower areas where data quality and data availability was generally better than in the highest elevations of the ice cap. The agreements between modelled and measured ablation for the AWS 1 site as well as for the various ablation stakes were

extraordinarily high. However, as the validation procedure refers only to point data sets, information on model performance over larger areas was not available. Evidence exists that the model results are of lower quality in higher elevations. This has to be considered when the outcomes are interpreted. Moreover, several assumptions and simplifications had to be used to realise the computation in an adequate time frame. As a consequence, many local effects as e.g. induced by the wind field, cloudiness or small-scale variations of snow depth induced by crevasse patterns, wind drift or topographic effects were not considered. This may be most significant for the initial water equivalent as it triggers the further snowmelt process and determines where bare glacier ice will appear during the course of the season. As data availability only enabled a linear interpolation, these simplifications have to be regarded as the major limitation of the study. It is therefore suggested to consider this distributed model output as an estimation of the surface energy balance and melt which give a first idea of the magnitude and distribution of fluxes rather than absolute values.

The model allows to split the various radiation balance components and turbulent fluxes. Figure 7.8 displays the incoming and outgoing radiation as well as the respective balances. The magnitude of the components is shown in different colours. Details on mean, maxima and minima values of the respective grids are given in table 7.5.

Generally, topographic influence on radiation terms is low as has to be expected from the smooth orography of the island. Only on the steep slopes of Arctowski Icefield towards Ezcurra Inlet and the other northern slopes of the inlets and bays, remarkably smaller amounts of global radiation are computed. This feature shows up again in the shortwave radiation balance and is still visible in the net radiation grid. Longwave incoming radiation shows only weak altitudinal differentiation, and outgoing radiation displays small spatial variance. As a consequence of the lower surface temperatures in higher altitude (Figure 7.9), emitted longwave radiation decreases with increasing elevation. Thus, longwave radiation balance shows the highest values in the central area of the ice cap, whereas at lower elevations with bare ice and a 0°C-isotherm snow cover occur, comparably high radiative energy loss prevail. Exposition of bare glacier ice with low albedo in the course of the model run leads to a distinct higher shortwave radiation balance in this area. This compensates for the smaller longwave

Table 7.5: *Spatial maxima, minima and mean values of the energy balance components [W m^{-2}] and ablation rates averaged over the full period of computation (03 December 1997 to 11 January 1998). I is direct radiation, D diffuse radiation, $L_S^{\downarrow}$ and $L^{\uparrow}$ are incoming and outgoing longwave radiation, Q_N is net radiation, Q_H and Q_E the sensible and latent heat fluxes, respectively, Q_R the heat supplied by rain, Q_M energy available for melt, M is melt [mm WE] and A ablation [mm WE].*

	I	***D***	***I+D***	***I+D (1-α)***	$L_S^{\downarrow}$	$L^{\uparrow}$	Q_N	Q_H	Q_E	Q_R	***A***
Mean	89.1	123.9	213.0	38.7	319.0	306.7	26.4	7.8	-7.6	0.04	261.5
Max	105.4	141.9	238.2	107.8	331.2	312.8	89.6	20.8	-0.6	0.09	1089.3
Min	28.5	123.5	164.7	27.3	304.8	299.6	15.4	0.3	-10.0	0.03	138.3

radiation balance in these areas and is responsible for the higher net radiation at the glacier margins.

Net radiation is the major energy source in all areas of the ice cap (Table 7.5). This is consistent with the findings of the single location calculations (Figure 7.9). The mean values for the sensible heat flux range between 0 and 21 W m^{-2}, which is also in very good agreement with the computations for the AWS sites. Due to the absence of stability correction, latent heat flux is predominantly negative or near balance. Both turbulent fluxes show a strong altitudinal dependence. This is a direct consequence of the input assumptions as only altitudinal lapse rates for air temperature were used. Together with the described spatial patterns of net radiation, these fluxes influence each other by the iterative computation of surface temperature as latter has a direct implication on the longwave outgoing radiation and determines temperature gradient between screen level air temperature and glacier surface. A clear dependence of altitude of the surface temperature is revealed in figure 7.9. The value

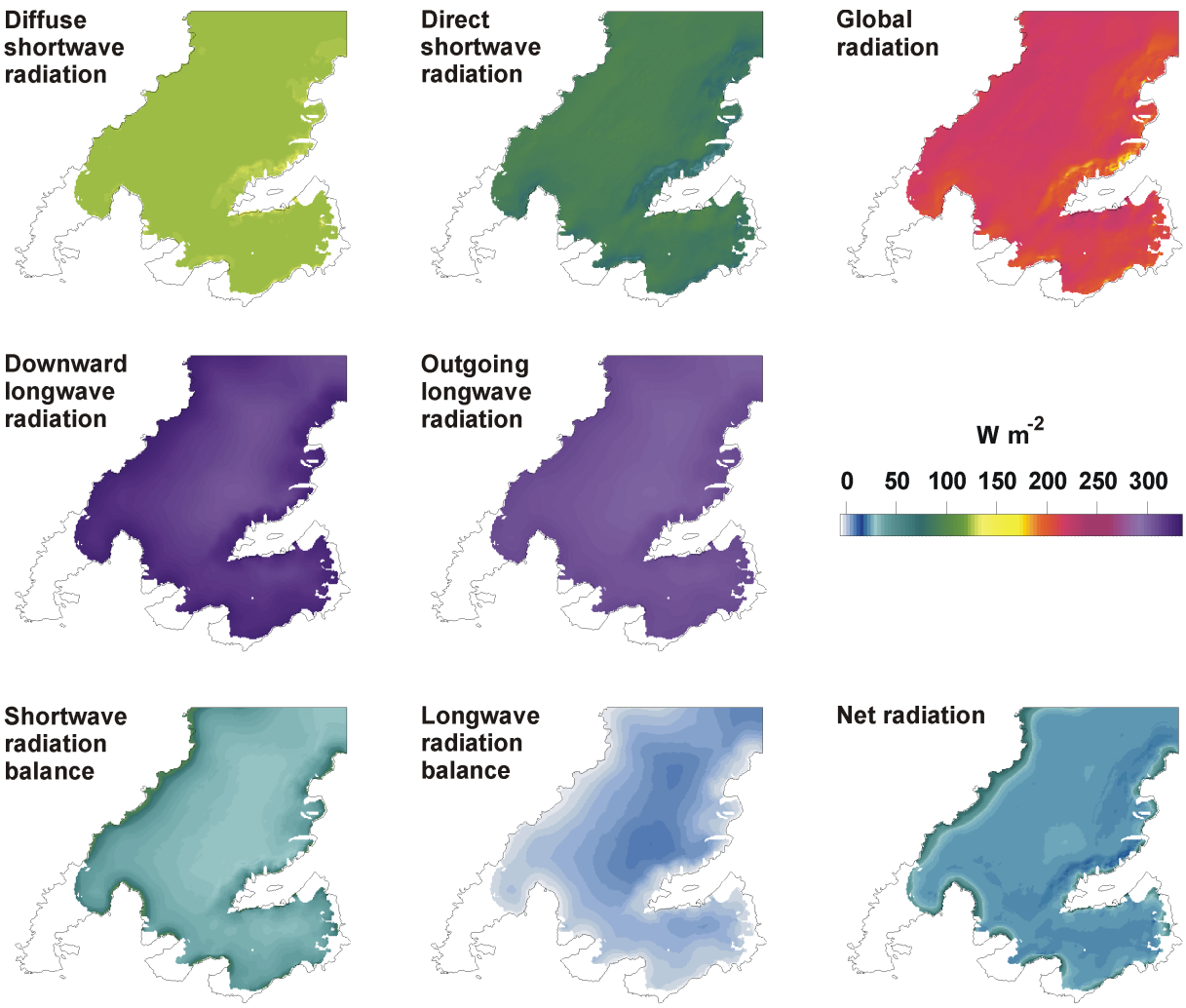

Figure 7.8: *Spatial variations of radiation terms. Shown are means over the entire measuring period (03 December 1997 to 11 January 1998).*

range spans from –0.6 at the glacier margins to –3.6°C on top of the ice cap. This clearly points out the necessity of an adequate parameterisation of surface conditions, in particular of surface temperature. Summarising all fluxes, the dependence of surface energy balance on elevation on King George Island becomes even more obvious. Modelled ablation rates range from 1089 mm WE near sea level to only 138 mm WE on top of the ice cap. Although these model results refer only to surface melt, and the internal melt water transport and routing in the firn layers and glacier are not considered, some general statements can be given in regard to the ablation patterns. Considering the surface temperature distribution, frequent refreezing of melt water at higher elevations has to be expected. In elevations up to about 250 m a.s.l., melt rates for short periods amount to more than 200 mm WE, whereas towards the higher elevations (top of the ice cap included in the model run is at 679 m a.s.l.) melt rates rapidly decrease. These finding are confirmed by the presence of a distinct water table at the snow ice transition and the distribution of internal water inclusions in the glacier (see chapter 4.4.3). Hence, the assumption that all the modelled amount of melt water come to discharge from the ice cap in elevations below 250 m a.s.l. seems to be justified. However, no statement on the percolation and discharge process in the higher areas can be given.

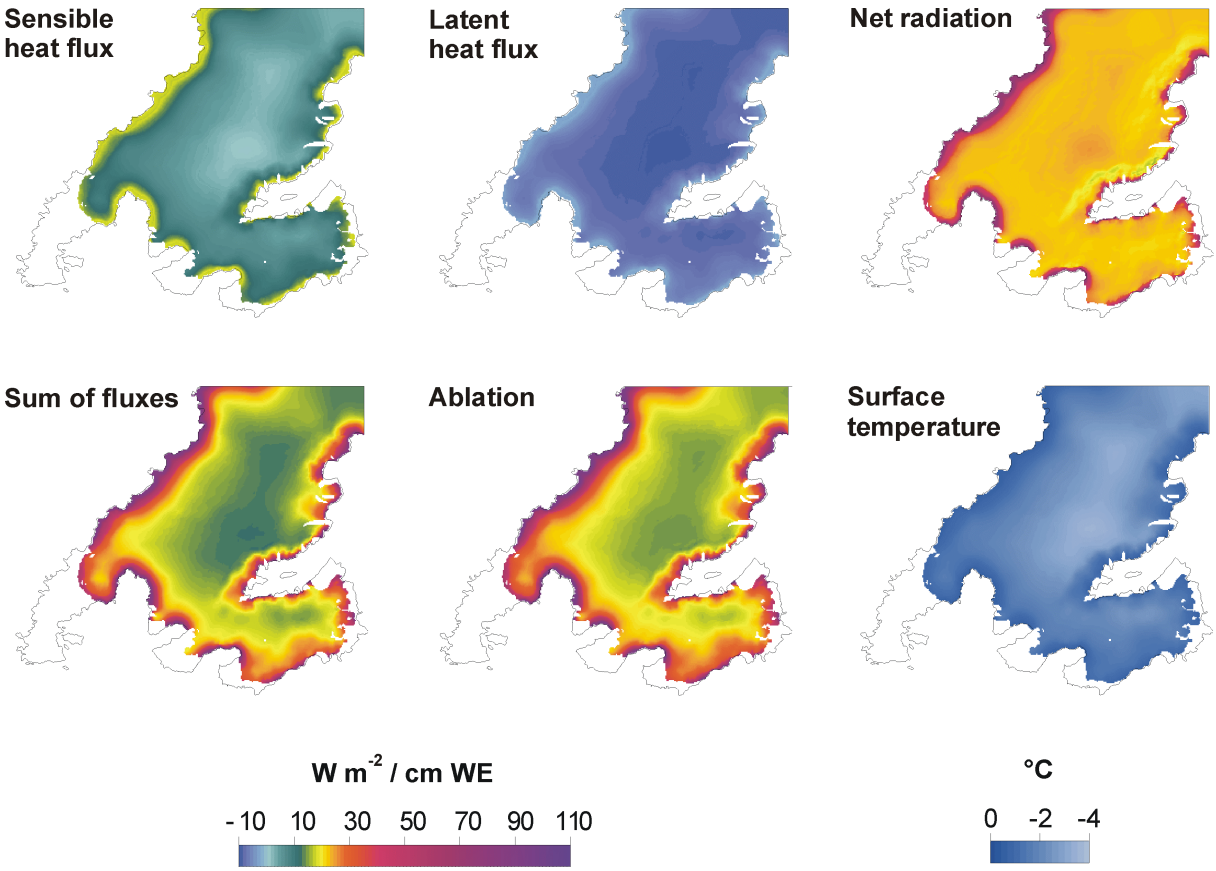

Figure 7.9: *Spatial distribution of surface energy balance components [W m^{-2}], ablation [cm WE] and surface temperature [°C] as means over the entire computation period (03 December 1997 to 11 January 1998).*

As outlined above, bare glacier ice in the lowermost areas starts to be exposed from about the middle of the field campaign onwards. Figure 7.10 shows the surface types to different dates as revealed from the model run. The bare ice areas at the end of the computation period coincide well with the described patterns in shortwave radiation balance and net radiation. During the advection event from 31 December 1997 to 04 January 1998, sufficient snow fall occurred to enable the coverage of the entire glacier with a thin fresh snow layer. However, due to the high energy input by this advection melt event, the new snow rapidly melted. This can also be seen in figure 7.11, where the control run represents the computations referred to in this subchapter. The area of exposed bare ice dropped to 0 km² during two occasions in this period. However, pre-event surface conditions are reached fast after the storm.

Figure 7.10: *Development of bare ice areas during the 1997/98 season as computed by the distributed energy balance model.*

7.2.2 Model sensitivity: influence of roughness length, precipitation, albedo and air temperature lapse rate parameterisations

As has to be expected, the alteration of surface roughness lengths affects the turbulent fluxes most(Table 7.6). However, the mean net radiation also increases considerably when the selected roughness length for snow is significantly larger than the standard values. This leads to a tripling of the sensible heat flux, and, as a consequence, the amount of calculated melt is far too high. The feedback on net radiation can be explained by the exposure of more bare ice due to the much higher melt rates. In contrast to this, variation of the roughness length for ice results in only marginal changes in the model output. This can be attributed to the fact that ice surfaces are restricted to a comparable small area skirting the glacier.

Variations of the precipitation parameterisation has a comparably low influence on the model performance since the amount of precipitation during the computation period was small. Changes in the threshold temperature lead to slightly changed surface conditions and alter the energy fluxes via albedo rather than by a direct effect on the rain-heat flux or snow-water equivalent.

Albedo triggers the radiation terms and indirectly the turbulent heat fluxes via the surface temperature iteration. Consequently, it is a crucial parameter and its appropriate choice is fundamental for a good model performance. Strongest model sensitivities were recorded for snow albedo since more than 85 % of the glacier were snow covered until the end of the modelling period. Importance of ice albedo

Table 7.6: *Sensitivity analysis of the distributed energy balance model. Listed are mean values for Q_N, Q_H, Q_E and T_S as well as cumulated amount of ablation (mm WE) of the entire grid and computation period.*

Varied parameter		Q_N	Q_H	Q_E	A	T_S
Control run	-	26.4	7.8	-7.6	261.5	-2.0
Roughness lengths	$Z_{0,ice}$ = 0.0001 m; $z_{0,snow}$ = 0.0001 m; ratio $z_{0,ice}/z_{0T,E}$ = 1	24.9	3.6	-5.4	232.3	-1.9
	$Z_{0,ice}$ = 0.01 m; $z_{0,snow}$ = 0.01 m; ratio $z_{0,ice}/z_{0T,E}$ = 1	29.7	20.8	-12.1	366.1	-2.1
	$Z_{0,ice}$ = 0.001 m; $z_{0,snow}$ = 0.001 m; ratio $z_{0,ice}/z_{0T,E}$ = 10	25.6	5.3	-6.5	243.1	-2.0
	$Z_{0,ice}$ = 0.001 m; $z_{0,snow}$ = 0.001 m; ratio $z_{0,ice}/z_{0T,E}$ = 100	25.0	3.9	-5.6	234.0	-1.9
	$Z_{0,ice}$ = 0.001 m; $z_{0,snow}$ = 0.01 m; ratio $z_{0,ice}/z_{0T,E}$ = 1	29.7	19.6	-11.5	359.8	-2.1
	$Z_{0,ice}$ = 0.001 m; $z_{0,snow}$ = 0.0001 m; ratio $z_{0,ice}/z_{0T,E}$ = 1	24.9	3.8	-5.5	234.1	-1.9
Precipitation	T_0 = 1.0°C; increase with altitude 10%	27.9	7.4	-7.9	270.8	-2.0
	T_0 = 2.0°C; increase with altitude 10%	25.6	7.9	-7.6	254.7	-2.0
	T_0 = 1.5°C; increase with altitude 30%	23.8	8.8	-6.9	251.8	-2.1
	T_0 = 1.5°C; increase with altitude 0%	29.2	6.5	-8.5	269.2	-1.9
Albedo	α_{snow} = 0.81; α_{ice} = 0.10; α_{firn} = 0.70	28.9	7.7	-7.7	286.5	-2.0
	α_{snow} = 0.81; α_{ice} = 0.60; α_{firn} = 0.70	24.7	7.8	-7.6	244.8	-2.0
	α_{snow} = 0.70; α_{ice} = 0.39; α_{firn} = 0.70	33.8	5.9	-8.9	308.1	-1.9
	α_{snow} = 0.90; α_{ice} = 0.39; α_{firn} = 0.70	13.4	10.7	-5.6	173.8	-2.2
	α_{snow} = 0.81; α_{ice} = 0.39; α_{firn} = 0.60	26.4	7.8	-7.6	261.5	-2.0
	α_{snow} = 0.81; α_{ice} = 0.39; α_{firn} = 0.80	26.4	7.8	-7.6	261.5	-2.0
Air temperature lapse rate	0.2 K per 100 m	22.8	12.2	-5.9	288.8	-1.3
	0.4 K per 100 m	20.8	9.5	-7.6	217.8	-1.6
	0.6 K per 100 m	21.1	7.1	-9.0	180.6	-1.9
	0.8 K per 100 m	22.2	5.1	-9.9	160.8	-2.3
surface temperature	iteration step 0.5 K	26.6	9.3	-6.7	260.0	-2.1

increases with the augmenting exposure of bare glacier ice in the course of the season or in case of climate sensitivity scenarios when a large portion of bare glacier ice has to be expected. Variations in firn albedo are indifferent as firn surface did not appear during the model run. This parameter only becomes important when the snow line retreats beyond the equilibrium line as e.g. the case for climate sensitivity scenarios or extraordinary warm years.

Perhaps most striking is the enormous sensitivity of the model towards the choice of the air temperature lapse rate. As with the roughness lengths, this parameter influences the turbulent fluxes and indirectly the radiation balance. Due to an inappropriate choice of air temperature lapse rate, ablation for the entire period and grid might be underestimated by 40%. Even with a low lapse rate of 0.4 K per 100 m altitude difference, melt is still underestimated. This stresses the already indicated strong dependence of snowmelt and lapse rates on the predominant air mass advection (see chapters 4.3.2.3 and 7.1.2). During cold conditions, lapse rates are high, whereas low lapse rates were observed during the advection of warm humid air masses. Only the employment of actual lapse rates can compensate such fluctuations which are, hence, a prerequisite if ablation is to be estimated accurately. The application of literature values as e.g. summarised in table 4.5 leads to ablation rates which are too low. These lapse rates were statistically derived from station data and represent long-term, averaged conditions rather than short-term advection events. Appropriate lapse rates are particularly required when sensitivity studies with mass balance models via a degree-day approach or estimations of ice mass contribution to future sea level are intended. Otherwise, the errors can only be compensated by the assumption of too high degree-day factors which leads to wrong extrapolation for future scenarios. Finally, the choice of the iteration step for surface temperature reduction does not significantly influence the model results.

7.2.3 Ablation on the King George Island ice cap under changing climatic conditions

It could be shown in the previous chapters 1 and 4, that strong indications for a high sensitivity of the King George Island ice masses towards future warming exist. Glaciers, and in particular small glaciers with short response times, have retreated since the 1950s. A change in surface mass balance has most likely occurred since then and in particular during the last decade with extraordinary warm summer seasons.

As the model performed well for the 1997/98 season and the model sensitivity towards the various parameterisation has been tested, the data set allows a rough estimation of the summer mass balance during increasing air temperatures. The applied scenarios do not include any changes in the frequency of certain weather systems nor changes in the precipitation pattern or radiation feedback processes. Only air temperature is increased based on the data from the 1997/98 season.

Table 7.7: *Effect of further temperature increase on surface energy balance and ablation rates on King George Island based on the data set from 1997/98. Energy balance components are in W m^{-2} and ablation in mm WE.*

Parameter varied		Q_N	Q_H	Q_E	A	T_S
Control run	-	26.4	7.8	-7.6	261.5	-2.0
Air temperature increase	+0.5 K	30.6	7.0	-7.9	292.5	-2.1
	+1.0 K	33.4	7.1	-7.7	326.0	-2.2
	+ 2.0 K	37.5	10.6	-5.7	424.8	-2.0

Moreover, the initial snow cover grid refers to conditions in 1997/98. The spatial variation of snow water equivalent is approximated by a linear regression with altitude. This certainly does not reflect the true conditions in all areas. If too much snow is assumed, the resulting sensitivity would be underestimated, in the opposite case sensitivity would be too high. As a consequence, the values summarised in table 7.7 can only be regarded as a magnitude of what melt rates on the island might look like in a changing climate. The absolute values have to be treated with caution, as a warming is most frequently accompanied by a change in the atmospheric circulation. This modifies many other meteorological parameters like cloudiness, radiation terms, wind conditions, humidity or precipitation.

First of all, it is noticeable that a future warming of +0.5 K would result in only slightly higher ablation rates. This effect is lower than an inappropriate choice of one of the more important parameter sets. However, if air temperature is further increased to +1 K, ablation for the 6 week time period increases by about 25%, in case of +2 K even 62% more melt has to be expected. As net radiation is the energy balance term that shows strongest changes, the increasing ablation can be attributed to changes in the surface conditions, i.e. an increase of the area with bare glacier ice. In fact, that is what figure 7.11 reveals. Displayed is the area of exposed bare glacier ice. The control run refers to the model computations for the unchanged meteorological data set in 1997/98 as described in chapter 7.2.1. Bare ice would appear considerably faster under warming conditions than under present ones. The influence of short-term snow fall events would drop further, and already with +0.5 K, the snow storm event from New Years Eve 1997 would not have lead to a fresh snow cover over the entire glacier. It has therefore to be expected that the divergence of the curves would further increase in the course of the ablation season as the influence of bare ice becomes more important later in the season.

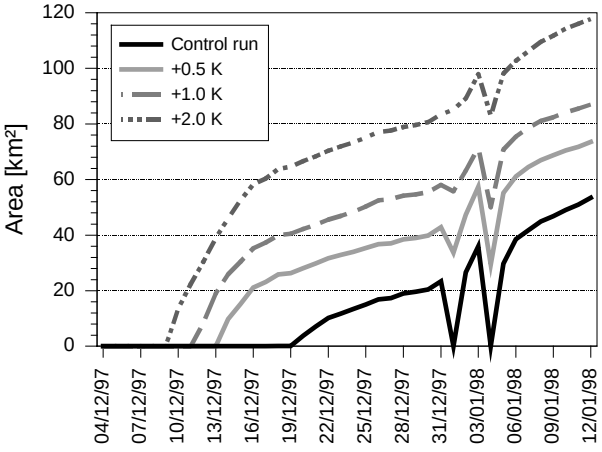

Figure 7.11: *Calculated areas of bare ice to form in dependence of the different climate scenarios. The entire glacerised area covered by the distributed energy balance model runs computations amounts to 418.2 km².*

7.3 Snowmelt dynamics as revealed from SAR remote sensing

7.3.1 Seasonal development of radar glacier zones in 1996/97

A sequence of ERS-2 SAR images, covering almost the entire ablation period in 1996/97, is used to analyse the development of ablation patterns on the King George Island ice cap. Here, all radar glacier zones except for the dry snow radar zone develop over the year depending on the prevailing meteorological conditions and altitude. Based on meteorological records, the dry snow radar zone was calculated to potentially occur above an altitude of approximately 1,950 m a.s.l. at the latitude of King George Island, while the highest elevation on the island is 705 m a.s.l. (WUNDERLE, 1996).

7.3.1.1 Winter conditions

A typical late-winter situation is shown on the ERS-2 image from 19 October 1996 (Figure 7.12a). The entire ice cap appeared bright, with σ°-values ranging between -3 and -8 dB (Figure 7.13). These values are characteristic of a frozen percolation radar zone (Table 6.2).

7.3.1.2 Onset of spring melt

The onset of spring snowmelt can be seen on the second image, which was taken on 04 November 1996 (Figure 7.12). While the frozen percolation zone remained persistent above 530 m a.s.l., an extensive area of low σ°-values developed in the lower parts of the ice cap. Backscatter values ranging from -15 to -18 dB in elevations between sea level and approximately 350 m a.s.l. indicate the existence of a wet snow radar zone (Figure 7.13). Between latter and the frozen percolation radar zones, a transition formed where backscatter values increased with altitude from –15 to –8 dB.

7.3.1.3 Summer situation

The following scenes represent different situations of the King George Island ice cap during the summer ablation season (Figure 7.12c-f, 7.13). In the image taken on 29 January 1997, backscatter values below –18 dB can be attributed to the expansion of the wet snow radar zone over the most of the ice cap excluding the highest areas. At AOI 620 m, the averaged σ°-value decreased to –12 dB. On 1 February 1997, the backscatter value at the AOI 85 m showed a significant increase from –18 to –10 dB. The latter value is characteristic of a bare ice radar zone (Table 6.2). All the other AOIs displayed low variations in their σ°-values referring to the previous acquisition date.

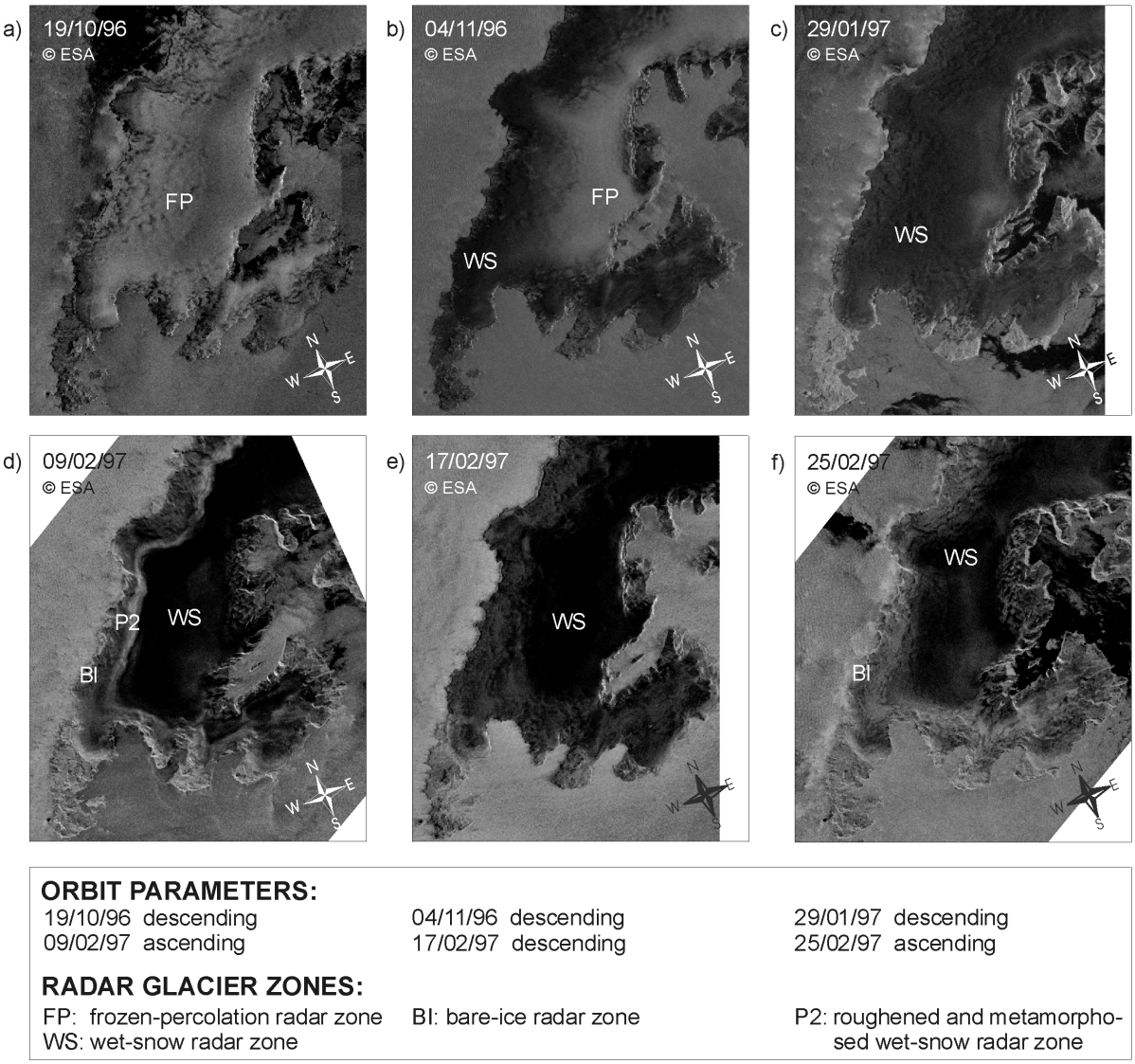

Figure 7.12: *Development of radar glacier zones on King George Island as revealed by ERS-2 SAR images.* ***(a)*** *Winter conditions with a frozen percolation zone covering the entire island,* ***(b)*** *onset of snowmelt,* ***(c-f)*** *development of the different radar glacier zones during summer 1997.*

On 09 February 1997, when the AOI 210 m was included in the bare ice radar zone the situation changed drastically. Between this snow-free area and the wet snow radar zone which meanwhile covered almost the entire upper parts of the ice cap, a well defined bright band with σ°-values ranging between –4 and –8 dB was formed. It skirted the north-western parts of the ice cap and was limited to an altitude of approximately 250 m a.s.l. One week later, the striking bright band disappeared. The backscatter values of almost all AOIs showed a remarkable decrease. All values were below –13 dB.

Backscatter values of almost all AOIs increased again in the image from 25 February 1997. The bare ice zone reached up to approximately 250 m a.s.l., while the upper parts of the ice cap were characterised by σ°-values ranging between –13 and –17 dB.

7.3.1.4 Interpretation of SAR data based on meteorological records

The observed pattern of radar glacier zones is a direct consequence of the prevailing meteorological conditions prior to and during the image acquisition. Therefore, meteorological records from Ferraz station are used for the interpretation of the observed backscatter pattern on the King George Island ice cap (Figure 7.13).

Negative air temperatures dominated the time period prior to the acquisition of the ERS-2 image taken on 19 October 1996. Several minor events with positive air temperatures during this month did not lead to significant melting and therefore did not affect the backscatter behaviour of the snow cover on 19 October. As a consequence, an entirely frozen snowpack can be assumed for the ice cap, which coincides with the observed high backscatter values of a frozen percolation radar zone.

Advection of warm air masses starting on 27 October caused a progressive wetting of the snow surface and significantly reduced the snow cover extent in the ice-free areas of the island (WINKLER ET AL., 1998). Snowmelt was most intense in the lowest areas of the ice cap forming an extended wet snow radar zone up to an altitude of approximately 350 m a.s.l. (Figure 7.12). Decreasing liquid water content resulted in higher backscatter returns with increasing altitude. Applying a mean temperature lapse rate of 6.5 K km^{-1}, the maximum altitude of melting during this event can be

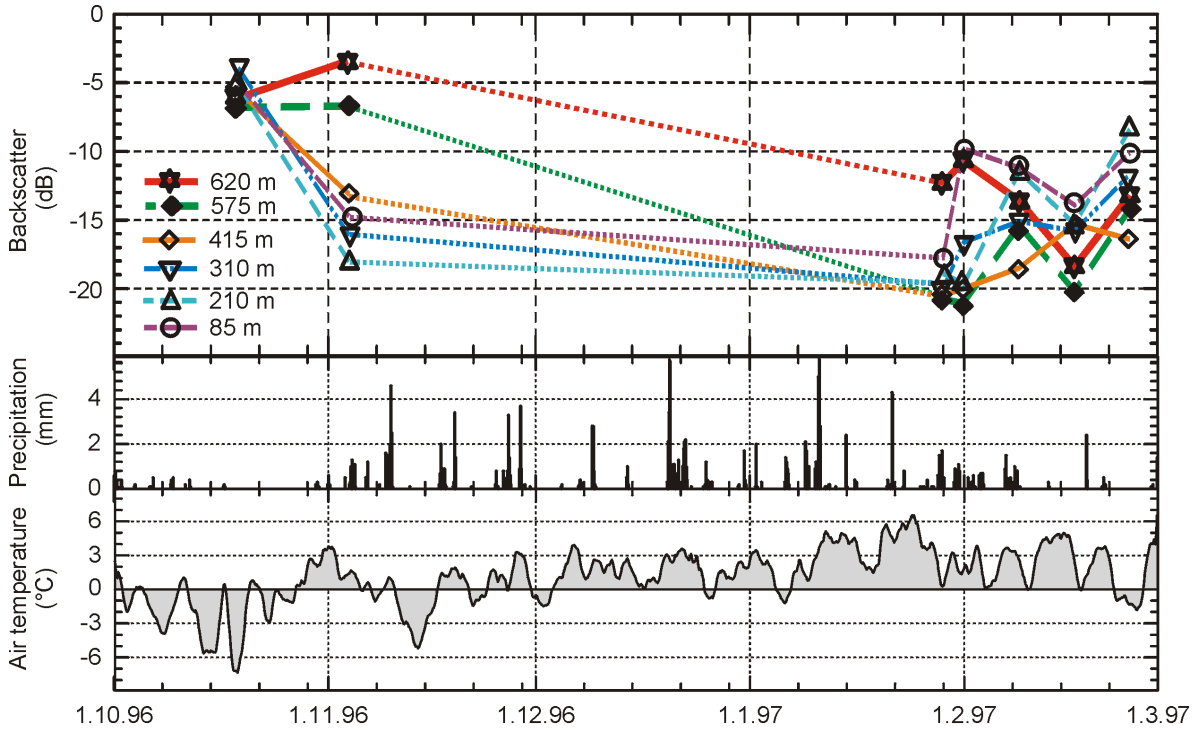

Figure 7.13: *Temporal evolution of backscatter values at the areas of interest (AOI) and meteorological records of Ferraz station during the research period: (a) backscatter signal, (b) precipitation, (c) air temperature. Note, that snowstorm event from 17 February is underrepresented in the precipitation records. No SAR imagery was available between 05 November and 28 January. Hence, the connecting lines in the backscatter graph, do not necessarily coincide with the real backscatter course in the AOI in this period.*

estimated to approximately 540 m a.s.l. on 01 November. This is in good agreement with the observed lower limit of the frozen percolation radar zone on 04 November applying a threshold of – 8 dB for determining the lower boundary of this radar zone (Table 6.2).

This melt event initiated the ablation season of the austral summer 1996/97 on the King George Island ice cap. Although the temperatures again dropped below 0°C in mid-November, positive temperatures prevailed until the end of February. A prolonged, uninterrupted period of high air temperatures was recorded during January (Figure 7.13). It can therefore be concluded from the meteorological records, that during this period the snow cover of the entire ice cap, including the uppermost parts, was intensely wetted. However, short-time refreeze events occurred occasionally during the whole ablation season. Indications for these alternating melt and refreeze cycles can also be found in the SAR images. Prior to the image acquisition on 29 January, air temperatures at Ferraz station dropped to almost 0°C. At the highest elevations of the ice cap, refreezing of the formerly wet snow led to a reduction of the liquid water content in the snowpack and therefore to an increase in backscatter values (AOI 620 m, figure 7.12c, 7.13). Even more evident, such a refreeze event is documented in the air temperature data and the ERS-2 image taken on 25 February (Figure 7.12f, 7.13).

Although no field data is available, the meteorological records suggest that at least the lower parts of the ice cap were snow-free at the end of January 1997. This assumption is supported by comparison of meteorological data and own field observations from 1995/96 and 1997/98. However, in the image taken on 29 January, a homogeneously distributed wet snow radar zone stretches over the ice cap from sea level to approximately 600 m a.s.l. This apparent contradiction can be explained by a snowfall event of 5.4 mm water equivalent accompanied by low temperatures prior to the image acquisition. As a consequence, the formerly exposed glacier ice was covered by wet, fresh snow. In the following days, a drastic increase of σ°-values at AOI 85 m from –17 dB on 29 January to –10 dB on 01 February can be attributed to the removal of this wet snow cover and the re-exposure of bare glacier ice. Due to the continuing high air temperatures and the resulting high ablation rates, the altitude of the transient snowline increased progressively. It can be located above 210 m a.s.l. as indicated by a steep rise of σ°-values at AOI 210 m between 01 February and 09 February. As a result of the high temperatures and the precipitation event prior to the image acquisition on 09 February, the wet snow radar zone remained persistent in the higher parts of the ice cap. The weather conditions give no evidence about the processes leading to the formation of the bright band visible in the SAR image. However, based on the analysis of the meteorological data, a temperature inversion that would have led to a dry, frozen snowpack in lower elevations can be excluded.

On 17 February, temperatures again dropped to the freezing point at Ferraz station, while at the same time a heavy snow storm was reported from the island (WINKLER

pers. com., 1999). A layer of presumably wet, fresh snow explains the observed decrease of backscatter values at all AOIs on this date. Furthermore, the disappearance of the bright band due to the fresh snow cover seems to be plausible.

During a warm period lasting until 22 February, the fresh snow cover could have easily been depleted. Subsequently, a period of three days with negative temperatures preceded the image acquisition on 25 February. Hence, a sequence of a bare ice radar zone covering the lowermost 250 m a.s.l., a wet snow radar zone in intermediate altitudes and a refreezing snow cover in the highest parts of the ice cap can be identified in the SAR image.

7.1.3.5 High radar returns from a wet snowpack?

The observed backscatter values for the different radar glacier zones identified on the King George Island ice cap are in good coincidence with values reported from other regions (Table 6.2). Furthermore, the measured σ°-values agree well with backscatter model results as presented by PARTINGTON (1998), SCHNEIDER ET AL. (1997), SMITH ET AL. (1997) and RAU ET AL. (2001).

The striking bright band on the SAR image taken on 9 February with σ°-values between –8 and –4 dB can be regarded as an extra radar glacier zone. Although these backscatter returns are not unlike those from a frozen percolation radar zone, meteorological records definitely indicate a melting snowpack below 300 m a.s.l. prior to and during the image acquisition. Since heavily dissected, bare glacier ice is absent in this area, multipath scattering from an irregular ice surface can also be excluded as a possible backscatter mechanism. Moreover, high returns from the superimposed ice zone existent on the King George Island ice cap (WEN ET AL. 1998) can be ruled out as a plausible explication. With local slope angles less than 10° in the area of the bright band, the smooth surface of the superimposed ice is expected to cause low backscatter values due to high specular reflection from the surface (MARSHALL ET AL., 1995; PARTINGTON, 1998).

So far, only few studies have observed such a phenomenon (e.g. RAMAGE & ISACKS, 1998; SMITH ET AL., 1997). Latter suggested the term “phase 2 melt radar zone” (P2 or M2) for this high-backscatter area, which is interpreted as a rapidly melting first-year snow cover with a metamorphosed roughened surface. The high backscatter returns are most likely explainable by multipath scattering from a roughened, wet snow surface (RAMAGE & ISACKS 1998; SMITH ET AL., 1997). The appearance of this P2 radar snow zone has only been reported from maritime climates in North America (Coast Range Mountains of Alaska and British Columbia) and now probably on the South Shetland Islands. However, no final answer can be given for the occurrence on the King George Island ice cap, as ground truth data collected simultaneously during image acquisition is missing.

7.3.1.6 The late-summer firn line on the King George Island ice cap 1996/97

For the monitoring of climatic variations and glacier mass balance studies, the knowledge on the equilibrium line altitude (ELA) is of special importance. In agreement with different authors (e.g. MARSHALL ET AL., 1995; SMITH ET AL., 1997; KÖNIG ET AL., 2001b; RAU ET AL., 2001), the late-summer firn line can be regarded as an approximation of the ELA. It has to be mentioned that both, the existence of a superimposed ice zone and the exposure of firn from previous years, generally induce uncertainties in the determination of the ELA from SAR imagery.

On the northwestern parts of the King George Island ice cap, the transient snowline has been determined to an altitude of approximately 250 m a.s.l. at the end of February 1997. Due to the lack of direct field evidence from 1997, no estimation on position differences between the late-summer firn line and the ELA can be given for this year. The obtained value fits well within the altitude range of the ELA given by previous studies from glaciers of the South Shetland Islands summarised in table 4.7.

7.3.2 Interannual variation of snowmelt patterns and firn line elevation

7.3.2.1 Snow cover dynamics and ablation patterns

In figure 7.11 and chapter 7.3.1, the yearly cycle of ablation patterns as revealed by SAR data was presented and discussed for the year 1996/97. Similar snowmelt patterns can be found in the imagery for the preceding and succeeding mass balance years. For the 1997/98 season, during which energy balance calculations were performed, imagery was available only before and after the measuring period. However, the strong signs of refreezing in the uppermost areas of the ice cap were even more pronounced in this year (Figure 7.14). To further determine interannual variations of the ablation patterns from ERS-1/2 SAR imagery, mean backscatter coefficients within 4 AOIs were calculated from all images and plotted in relation to the month of the mass balance year (Figure 7.15).

AOI 85m represents the lowest elevations of the ice cap. This AOI displays a large scatter of the backscatter coefficients with values ranging between –16 and –6 dB. The σ°-values of the winter imagery show a very homogeneous behaviour grouping around –10 dB, which is the typical value range of a bare ice radar zone (RAU ET AL., 2000). A possibly existing fine grained winter snow pack overlying the bare ice is transparent for the radar beam. Similarly, a large amount of the values in the summer months and of the spring imagery are in this range. Values below –15 dB can only be found in AOI 85m during November and January. These low values are caused by a wet snow radar zone covering the bare ice at that time.

AOI 210 m and AOI 415 m show an almost identical distribution of the σ°-values – high backscatter during winter months indicating a frozen coarse grained snow pack (percolation radar zone). The low σ°-values during summer months are caused by the high liquid water content of the snow pack which leads to the absorption of the

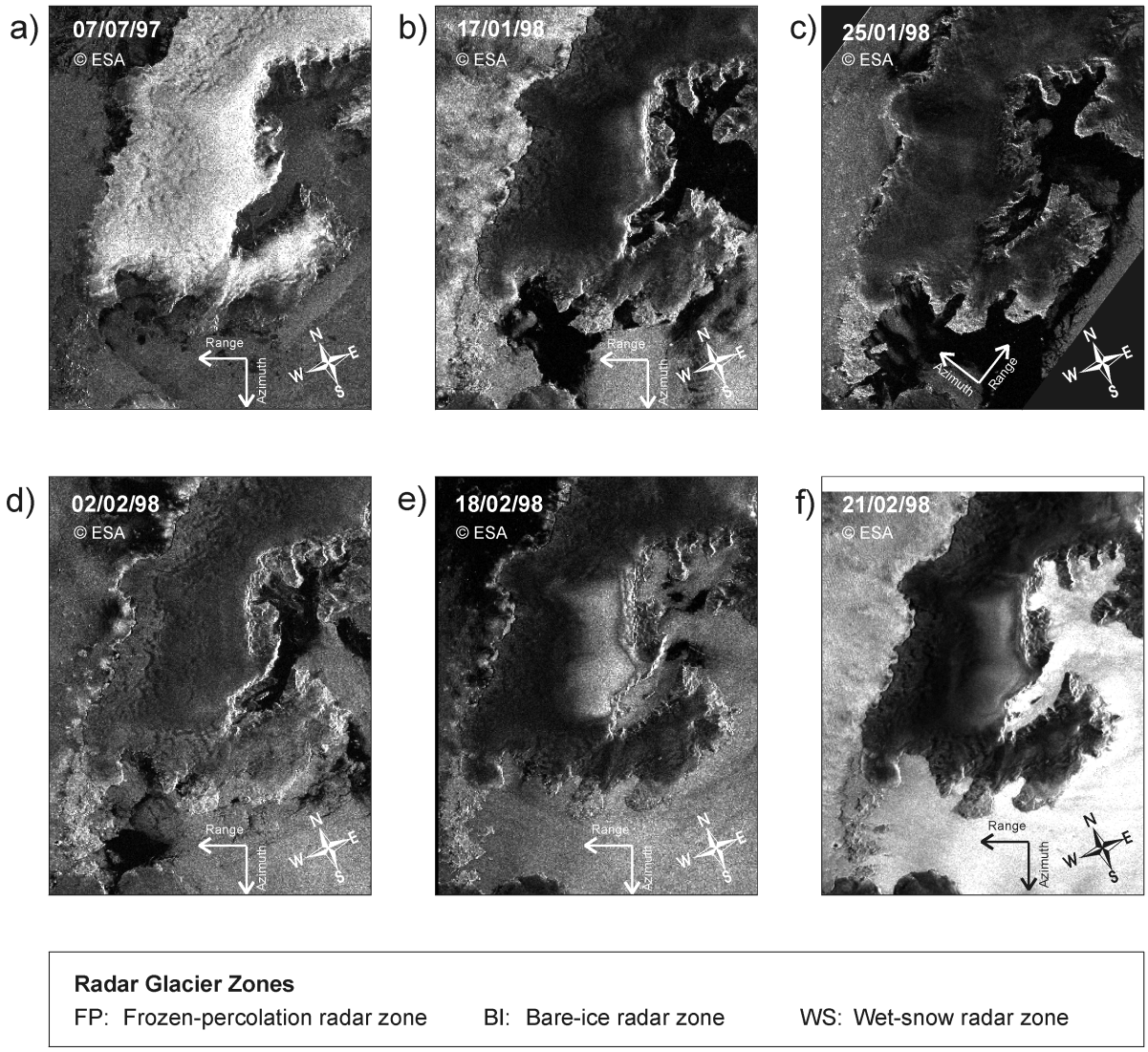

Figure 7.14: *Ablation patterns on the King George Island ice cap as revealed by ERS-2 SAR imagery during the austral summer 1997/98. All images except c) are descending orbit.*

radar signal (wet snow radar zone). A continuous increase of the backscatter values in this wet snow radar zone over time is observed. This phenomenon occurs in all mass balance years. BRAUN ET AL. (2000), RAMAGE & ISACKS (1998) as well as SMITH ET AL. (1997) have reported that increasing surface roughness of a wet snow cover might be responsible for the increased backscatter values. This situation is a consequence of the continuos snow metamorphism at the end of the mass balance year. Therefore, it might be also the reason for the increasing σ°-values in the wet snow radar zone to the end of the ablation season on King George Island.

The backscatter signal from AOI 620 m which is located at the highest elevation of the ice cap shows high values in the winter and early spring images. These back-scatter coefficients are typical for a frozen, strongly metamorphosed snow pack of a frozen percolation radar zone. However, a large scatter of the σ°-values can be found during the summer months. This is attributed to frequent melt and refreeze cycles

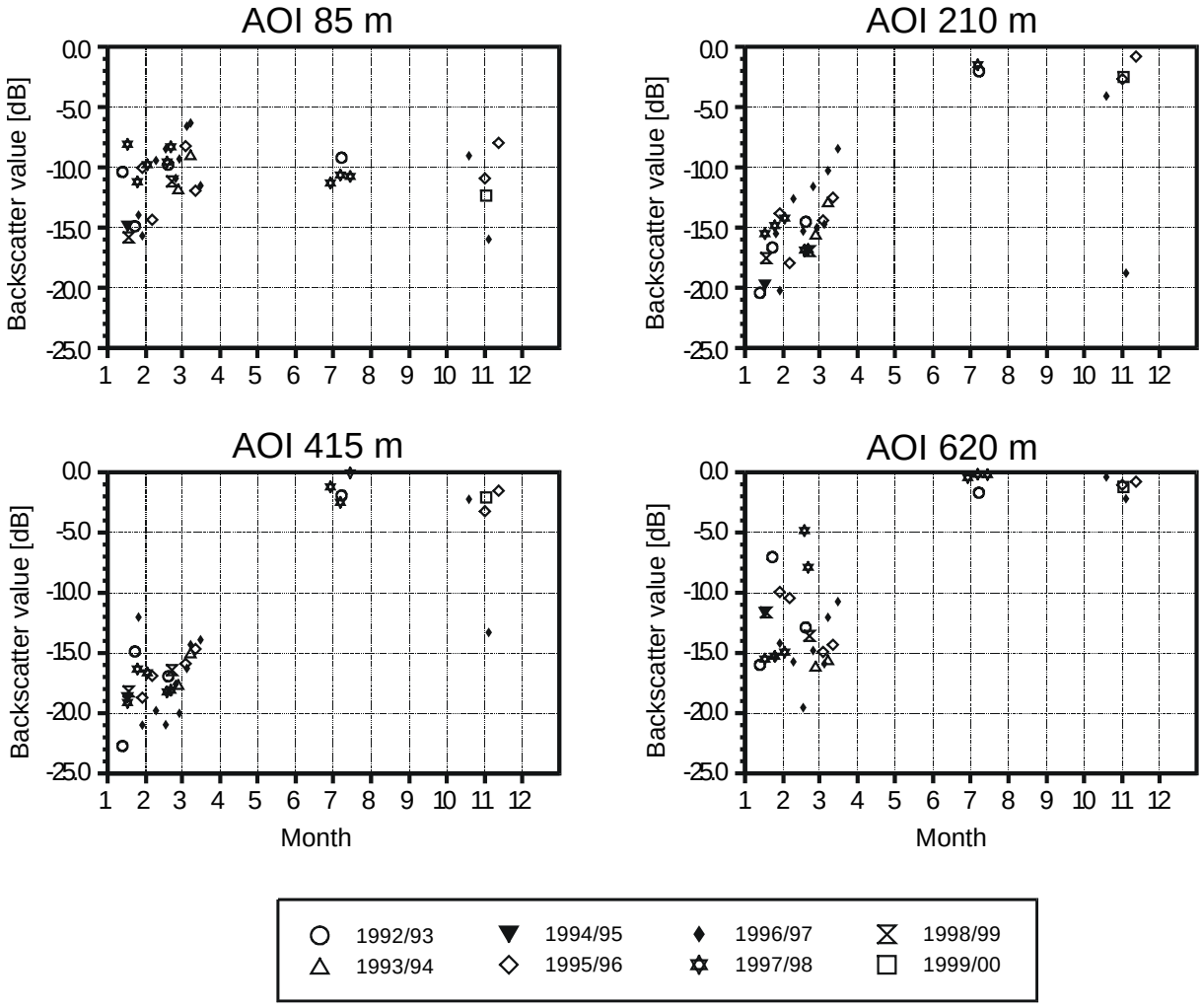

Figure 7.15: *Backscatter values in the four areas of interest (AOIs) of all annualised images (1992-1999). The mass balance seasons are distinguished by different symbols. AOI 85 m is located in the lowermost part of the island, AOI 210 m and AOI 415 m in intermediate elevations while AOI 620 m consists of the highest part of the main ice cap of King George Island.*

that lead to a changing backscatter signal according to the actual liquid water content of the snow pack. It can be assumed that the uppermost layers of the snowpack were completely frozen during image acquisition, sufficient to increase backscatter signal to the value range of that of the frozen percolation radar zone. Damping of the radar signal by wet snow was superimposed by the scattering at the large grain sizes and ice lenses in the snow cover.

7.3.2.2 Firn line positions

The late-summer firn line, separating the bare ice radar zone from the frozen percolation and wet snow radar zone, has been identified as a first approximation of the ELA (RAU ET AL., in press). Moreover, firn line positions (FLP) are a key parameter for snowmelt modelling, as the distinctions in surface albedo of snow and firn lead to a considerable differentiation of the melt rates. Extracting the FLPs from SAR data on a

multi-year basis therefore considerably enhances the knowledge on glacier mass balance. However, a quantitative determination of the firn line altitudes has only rarely been realised.

The backscatter values for the bare ice radar glacier zone published in the literature range widely between -14 and –6 dB. In figure 7.16, the variations of the classification of the bare ice radar zone for the same mass balance year on a subset of Bellingshausen Dome are shown using late summer and winter imagery from both ascending and descending orbit. The backscatter values are classified in a colour scheme between –16 and –6 dB. For this site, information from own ground surveys in the months December to January of the mass balance years 1995/96, 1997/98 and 1999/2000 are available. Furthermore, measured equilibrium line altitudes have been published for several years from the South Shetland Islands (Table 4.7). The small ice cap of Bellingshausen Dome addressed to in the following covers an elevation range from 35 m a.s.l. to 250 m a.s.l..

In order to enable an objective outline of the firn line in all images, the value range between –6 to –16 dB was classified (Figure 7.16). These thresholds were varied to analyze the persistence of the classified area in relation to the threshold value, but no considerable changes in the FLP could be determined. However, influence of the

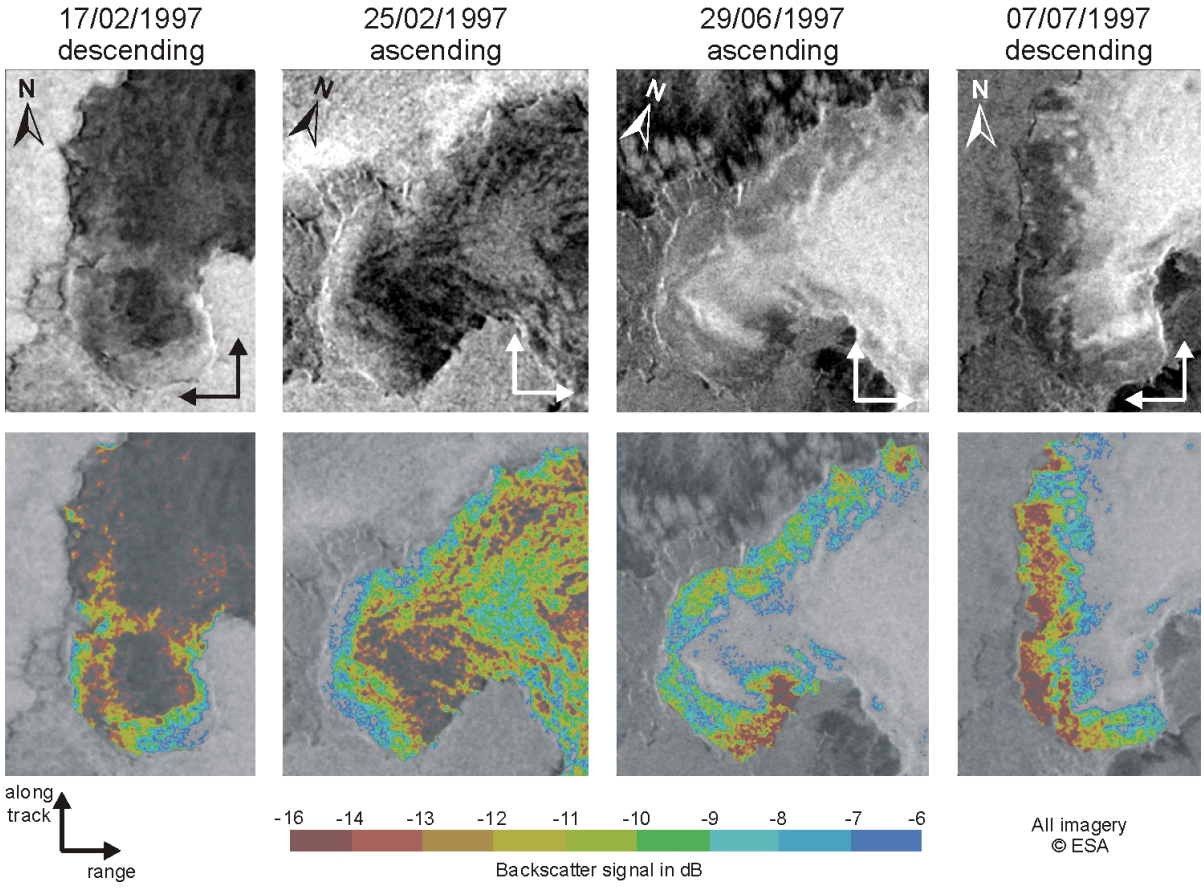

Figure 7.16: *Differences in the determination of the firn line position using winter and summer imagery from the ascending and descending orbit for a subset of Bellingshausen Dome, King George Island. The original ERS-2 SAR images are shown in the upper row, whereas the lower row shows the classified bare ice radar zone using a value range between –16 and –6 dB.*

local incidence angle on the backscatter signal could be recognized although not in a range influencing the result of the classification. The classified bare ice zone agrees well with ground observations from the previous and the following year. In the ascending as well as in the descending orbit, the boundary between bare ice and frozen percolation radar zone is marked by values of about -8 to -6 dB in the winter imagery, whereas in the summer imagery the radar zones are separated by the lowest values of -14 to -16 dB (Figure 7.16). This indicates that different thresholds have to be applied for winter and summer acquisition dates to discriminate the bare ice radar zone

The images from the descending orbit show good agreements regarding the classified bare ice areas. Only in the northern part, minor changes are caused by a snow fall event before 17 February 1997 which partially covered the bare ice. The classification in the ascending image from 26 June 1997 coincides with the results of the descending orbit. However, the ascending image from 25 February 1997, marking the maximum bare ice extend in this season, shows only very little agreements with the other imagery. The maximum elevation of firn line in this image at about 250 m a.s.l. coincides with measurements from the GPR survey in the following year by PFENDER (1999). Consequently, it has to be supposed that the winter images from 1997 do not show the real extend of the bare ice zone at the end of the former ablation season. RACHLEWICZ (1997) stated, that advection of warm humid air masses can lead to a complete disappearance of the snow cover in lower elevations even in winter. It might be the case, that prior to the image acquisition in June 1997 such an advection event completely melted the autumn snow cover in the lower elevations of Bellingshausen Dome and metamorphosed the snow pack in the higher parts. Cold temperatures in the following days and during image acquisition led to the typical backscatter values of a frozen percolation radar zone in the upper and a bare ice radar zone in the lower elevations.

This example demonstrates that timing of image acquisition is of major relevance for the determination of the FLP. However, for regions like King George Island where days with air temperatures above 0°C occur in almost all winter months, the use of late summer imagery is inevitable for the determination of the FLP. Hence, late summer images from ascending and descending orbits were preferred for the following analysis of FLPs.

The analysis of the entire set of ERS-1/2 SAR images revealed no large inter-annual variations of the firn line altitude (Table 7.8). Generally, the values range between

Table 7.8: *Altitudes of the transient firn line as revealed from ERS SAR imagery for Bellingshausen Dome on King George Island. A denotes ascending orbit; D descending orbit*

Glacier mass balance year	Date of Image acquisition	Orbit	Firn line altitude [m]
1991/92	08/07/1992	D	160
1992/93	04/03/1993	D	200
1993/94	08/03/1994	A	200
1995/96	12/03/1996	A	200
1996/97	25/02/1997	A	250-270
1997/98	21/02/1998	D	180-200
1998/99	22/02/1999	D	200-220

160 and 250 m a.s.l. in almost all mass balance years of the 1990s showing considerable interannual variation. The accuracy of the FLA determination is estimated to about 20 m in altitude as a consequence of the precision of the digital elevation model and foreshortening effects. The highest altitude of the firn line could be observed for the mass balance year 1996/97 with about 250 m a.s.l. As stated in chapter 7.3.1, summer air temperatures in this year were well above the long-term average and hence, snowmelt started already in early November. The ground based ELA measurements for the mass balance year 1991/92 on Bellingshausen Dome (Table 4.7) are in good agreement with the observed firn line altitude in the radar imagery. The small differences may be caused by the location of the point measurements and by the fact that satellite derived FLA does not consider superimposed ice. Using the derived FLA as an approximation of the ELA and comparing them with the ELA values of table 4.7, a rise of the ELA/FLA of about 50 m seems to have taken place since the 1970's.

7.4 A synthesis of snow and glacier melt on the King George Island ice cap as revealed from the different approaches

So far the outcomes of the different methods have been discussed separately depending on the approach. This section will give an overview on how the results of this study fit on the climatological and glaciological knowledge about the King George Island ice cap as outlined in chapter 4.

In regard to the melt patterns, the results of all three approaches, SAR remote sensing, energy balance modelling and GPR, coincide. The sequences of SAR images shown in chapter 7.3 clearly indicate that the highest parts of King George Island are subject to frequent melt refreeze cycles which lead to considerable changes of the backscatter characteristics during the ablation season. Moreover, the well defined isochrones and "Raymond bumps" in this part of the ice cap strengthen the hypothesis that there influence by percolating melt water is reduced.

In the lower elevations, the snow cover remains continuously wetted during summer months. This phenomenon can be observed during all years in which SAR data was available. Similar results are indicated by the distributed energy balance modelling, where the highest elevations show low mean surface temperatures (<-2.5°C), whereas the bare ice zone extends up to 100 m a.s.l. during the short modelling period. The modelling reveals a considerable altitudinal gradient of ablation. Ground penetrating radar can observe features that persist over large time periods, e.g. the presence of the water table or changes in the firn structure. Figure 7.17 summarises the results of the extended GPR survey by BLINDOW & PFENDER (unpublished, 1998). Areas below 400 m a.s.l. show strong water inclusions and changes in firn structure. This is in very good agreement with the high melt rates determined by stake measurements and the results of the single location and distributed energy balance modelling.

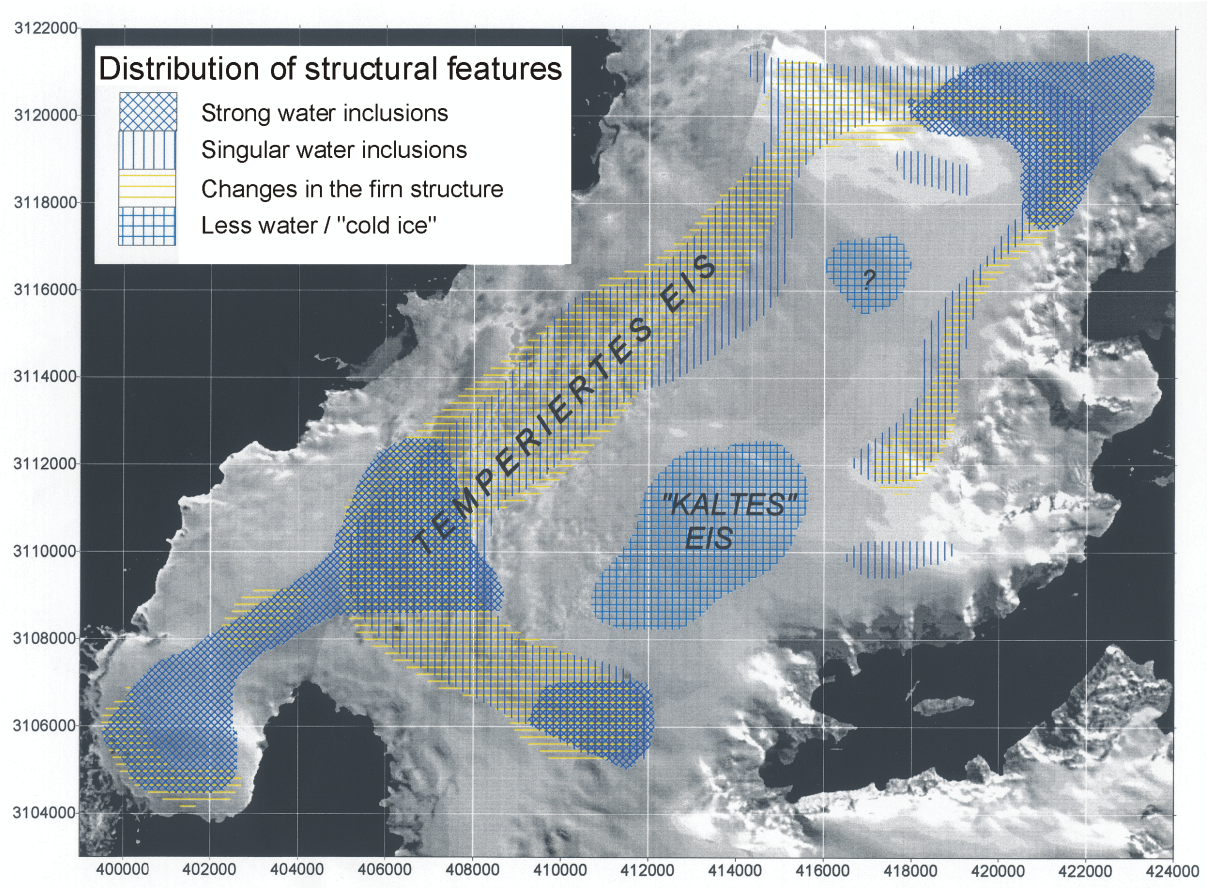

Figure 7.17: *Synthesis map of the ground penetrating radar survey compiled by BLINDOW & PFENDER (1998 unpublished).*

The firn line elevations derived from several late summer and winter ERS-1/2 SAR images are consistent with the results from previous studies. Although the interannual variations are high the present firn lines on Bellingshausen Dome derived from SAR data are considerably higher than in the 1970s. The highest FLP at about 250 m a.s.l. is consistent with the analysis of the GPR data (PFENDER, pers. com 1999). Similar findings are reported from other sites on the South Shetland Islands.

Neither the distributed snowmelt modelling nor the analysis of SAR imagery or the GPR survey could explain the pattern of sediment plumes as observed in the SPOT satellite imagery. However, many of the questions raised in chapter 1 might be answered either by the review of the environmental settings of King George Island and the ongoing climatic changes along the Antarctic Peninsula or by the ablation modelling and the analysis of remote sensing data. It could be shown

- that ablation rates and the energy exchange at the snow surface vary considerably with altitude although the altitudinal range of King George Island extends only between 0 and 705 m a.s.l..
- that large-scale synoptic weather systems trigger the snowmelt process. In particular, advection of warm, humid air masses from the north causes highest melt rates.

- that interannual variations of ablation rates are remarkable. Again the prevailing synoptic conditions are of major importance.
- that the use of concurrent altitudinal air temperature lapse rates for snowmelt modelling in this latitudes is advisable.
- that ablation rates are among the highest so far published for the Antarctic Peninsula.
- that the ablation processes on the ice cap are highly sensitive towards future air temperature increase. Combining this information with the already detectable glacier retreat and indications for a negative mass balance, glaciers on King George Island are considered as very good indicators to detect climatic changes in the region of the Antarctic Peninsula.

8 Outlook

In this work, the present glaciological knowledge of the King George Island ice cap was reviewed and enhanced. During the data compilation and analyses, many ideas developed, where further research could start or where the outcomes of this work could directly be used in subsequent studies. In the following, these possibilities are listed according to the major topics of this thesis.

The ***precision and reliability of the distributed energy balance modelling*** and sensitivity estimates could be improved by a better initial snow cover grid. Here, more detailed snow height surveys on various locations of the ice cap would be necessary. An advanced possibility could be combining this information from test areas on the ice cap with ablation patterns derived from satellite imagery of previous years. MUNRO (1991) pointed out that the position of the equilibrium line is crucial when sensitivity studies are performed as it strongly forces the radiation fluxes as also obvious from the present study results. Additionally, it would be of great interest if the time periods of available SAR and optical satellite data as well as energy balance modelling would be concurrent. The imagery could then be used as a spatially distributed validation set, e.g. surface types from SPOT or approximation of the 0°C-isotherms from SAR data. This could help to determine possible errors resulting from the partially simple approaches used to interpolate the meteorological variables in the distributed energy balance model. A comparison of modelled surface temperatures with concurrent products derived from satellite measurements (e.g. from the LANDSAT ETM+ or ASTER sensor) would point in a similar direction. The precision of the ablation estimates could considerably improved if the distributed model of surface energy balance were combined with snow model treating the water retention and refreeze processes in the snowpack. However, for such an approach, detailed information on the snow structure should be available or at least meteorological data should cover the last years to enable a simulation of the snow cover.

Another major point directly resulting from this study would be to improve the ***link between large-scale synoptic weather patterns and energy balance modelling***, not only for King George Island but also for other sites on the Peninsula. This would follow the suggestions given by NEAL & FITZHARRIS (1997) to increase the understanding of the interaction between synoptic circulation and glacier mass balance parameters. To achieve this objective, energy balance calculations for other locations on the Antarctic Peninsula would have to be performed in order to determine how the different weather systems affect the various sites. The review given in this work showed considerable differences along the Peninsula in regard to the ablation rates and the processes triggering snowmelt. Such a study would require a detailed and complete classification scheme of synoptic weather types in the region and further energy balance studies. Subsequently, frequency statistics of synoptic weather types should be derived from e.g. NCEP or NCAR reanalysis or NOAA data, and the influence of an increase of certain weather situations on ablation rates would have to be analysed. This would certainly be the most elegant way to perform a climate sensitivity study.

A ***validation of GCMs*** with the presented data from King George Island as done e.g. by KING & CONNOLLY (1997) would be helpful, however, it hardly seems suitable due to the large grid size of such global models and the island being surrounded by ocean. These inhomogenities in one grid cell of a GCM will inhibit a direct comparison. Down-scaling of the GCM results and perhaps coupling to a mesoscale model for the Antarctic Peninsula would hence be a prerequisite.

In the chapters 1 and 3, a short overview of actual changes in the climate and glacial systems of King George Island was given. A significant air temperature increase since 1968 is detectable in the climatic records. Moreover, a raise in the number of degree-days was determined for other time series on the Antarctic Peninsula, e.g. Fossil Bluff and the composed Marguerite Bay record (MORRIS, 1999; SMITH ET AL., 1998). Similar statistical analysis should be performed for King George Island using the now available definite time series from Bellingshausen station which reaches back to 1968 (Marshall & Lagun, submitted). The data set comprises air temperature, precipitation, cloudiness and relative humidity. Moreover, these standard meteorological observations enable the run of a ***simple glacier mass balance models for the King George Island ice cap***. A calibration of such a model could either be done using the ablation measurements from various years or using the energy balance calculations of this work. Such a study could show if mass balance changes or dynamic adjustments of the glacier front positions on King George Island were the major reasons for the immense glacier retreat detected on the island (see also Chapter 4.5.1).

A complete ***2D- or 3D-modelling of the King George Island ice masses*** would certainly bring new insights on glacier dynamics. The distributed estimation of ablation rates from energy balance modelling, the observed ablation patterns from ERS-1/2 SAR imagery and the synthesis with the GPR-results could be key input

parameters. The digital elevation model compiled for this study will certainly form a major backbone of such a model application (BRAUN ET AL., 2001). The large amount of available satellite imagery facilitates the derivation of which crevasse patterns and stress zones, the delimitation glacier drainage basins as well as the detailed study of glacier retreat. The meteorological records of King George Island can be extended back to the beginning of the 20th century by the Orcardas time serie. These data set from together with the various glaciological surveys on the island's ice cap a unique database in Antarctica that demands further investigation. Additionally, an exact dating of the isochrones determined in various GPR sections (e.g. Figure 4.14), e.g. by a link to vulcanic eruptions of nearby volcanoes on Deception or Penguin Island, would enable obtaining spatially distributed mass balance data.

Aerial photography, from 1952 up to present (Figure 3.2) are only disposable for very few regions in Antarctica. The database for King George Island is favourable for further studies on glacier retreat and dynamics from a remote sensing perspective. It should be tested if the quality of the imagery and the new ASTER stereo pairs permit calculating digital elevation models for selected areas on King George Island, as e.g. the small cirque glaciers on Keller Peninsula or near Arctowski station, in sufficient precision to study surface lowering and glacier retreat. Is this works, the ***photogrammetric method*** could be applied to **quantify *mass balance changes*** and to **detect of mass losses over a time period of 50 years**. Furthermore, this data could be used to check simple mass balance models and ice dynamic model as mentioned above.

First attempts have been made to use ***SAR interferometry*** to improve the topographic information of the island. Moreover, differential interferometry could provide distributed information on glacier velocities which would be another basic input for glacier modelling. However, the frequent melt events are a major problem as they considerably reduce phase coherence between the acquisition dates. The present ablation modelling may not compensate for that, but it can help to interpret discrepancies in the interferometric results.

The field of possible glaciological activities is wide and only very few of them need further field work. It seems that the database compiled during and for this work is already suitable for the application of various models of different complexity. The new remote sensing satellites, e.g. ASTER, LANDSAT 7 or SPOT 5 in the optical spectra, and ENVISAT and RADARSAT-2 in the radar C-band, will enhance the possibilities to ***monitor glacial changes as well as snow cover and ice dynamics from space*** as e.g. proposed by the international framework Global Land Ice Measurements from Space (GLIMS). In regard to the contribution of the ice masses of central Antarctica and Greenland to global sea level rise, CRYOSAT and ICESAT with their high precision altimeters will provide accurate measurements of surface changes and enable detect of on-going changes. However, the applicability of altimeter data to King George Island is doubtful due to the still present topography in the pixel size of these sensors.

Finally, the work is integrated in the ***SCAR WG-GGI project King George Island GIS (KGIS)***, an international attempt to establish GIS standards for Antarctica with the use of King George Island as a first pilot study. The major input from this study is the topographic database and the various glaciological data sets.

9 References

AMBACH, W. (1977a): Untersuchungen zum Energieumsatz in der Ablationszone des Grönländischen Inlandeises: Nachtrag. In Expedition Glaciologique Internationale au Groenland 4, No. 5, Bianco Lunos, Køpenhavn, 63 p.

AMBACH, W. (1977b): Untersuchungen zum Energieumsatz in der Akkumulationszone des Grönländischen Inlandeises: Nachtrag. In Expedition Glaciologique Internationale au Groenland 4, No. 7, Bianco Lunos, Køpenhavn, 44 p.

AMBACH, W. (1985): Characteristics of the heat balance of the Greenland ice sheet for modelling. *Journal of Glaciology* **31** (107), 3-12.

AMBACH, W. (1986): Nomographs for the determination of melt water from snow- and ice surfaces. *Berichte des naturwissenschaftlich-medizinischen Vereins in Innsbruck* **73**, 7-15.

ANDERSON, E. A. (1976): A point energy and mass balance model of a snow cover. *NOAA Technical Report NWS* **19**, Washington, D.C., 150 p.

ANDERSON, P. S. (1994): A method for rescaling humidity sensors at temperatures well below freezing. *Journal of Atmospheric and Oceanic Technology* 11 (5), 1388-1391.

ANTARCTIC PLACE NAMES COMMITTEE FOREIGN AND COMMONWEALTH (1986): APC Misc 64, South Shetland Islands, Sheet 1 King George Island, 1 : 100 000, 10th edition.

ARISTARAIN, A. J., PINGLOT, J. F. & POURCHET, M. (1987): Accumulation and temperature measurements on the James Ross Island ice cap, Antarctic Peninsula, Antarctica. *Journal of Glaciology* **33** (115), 1-6.

ARISTARAIN, A. J., JOUZEL, J. & LORIUS, C. (1990): A 400 years isotope record of the Antarctic Peninsula climate. *Geophysical Research Letters* **17** (12), 2369-2372.

AWI (1999): Geowissenschaftliche Polarforschung - mittel- bis langfristige Perspektiven der deutschen Polarforschung. Alfred-Wegener-Institut, Bremerhaven.

BAHR, D. B. (1997): Global distributions of glacier properties: A stochastic scaling paradigm. *Water Resource Research* **33** (7), 1669-1679.

BAHR, D. B. & MEIER, M. F. (2000): Snow patch and glacier size distributions. *Water Resource Research* **36** (2), 495-501.

BARSCH D. & MÄUSBACHER, R. (1986a): Beiträge zur Vergletscherungsgeschichte und zur Reliefentwicklung der Südschetland Inseln*. Zeitschrift für Geomorphologie N. F., Suppl.-Bd*. **61**, 25-37.

BARSCH D. & MÄUSBACHER, R. (1986b): New data on the relief development of the South Shetland Islands, Antarctica. *Interdisciplinary Science Reviews* **11** (2), 211-218.

BENN, P.I. & EVANS, D. J. A. (1998): Glaciers and Glaciation. Arnold, 745 p.

BENSON, C. S. (1996): Stratigraphic studies in the snow and firn of the Greenland ice sheet. Snow, Ice and Permafrost Establishment. *Research Report* **70**. (Revised edition of 1962 report).

BERNIER, P.Y. (1987): Microwave remote sensing of snowpack properties: potential and limitations. *Nordic Hydrology* **18**, 1-20.

BETGEN, T. (1998): Wetter und Witterung in Cierva Point (Antarktische Halbinsel) im Südsommer 1996/97. Unveröffentlichte Zulassungsarbeit zum Staatsexamen. Universität Freiburg.

BINDSCHADLER, R. (1998): Monitoring ice sheet behaviour from space*. Reviews of Geophysics*, **36** (1), 79-104.

BINDSCHADLER, R. A., FAHNESTOCK, M.A., SKVARCA, P. & SCAMBOS, T.A. (1994): Surface-velocity field of the northern Larsen Ice Shelf, Antarctica. *Annals of Glaciology* **20**, 319-326.

BINTANJA, R. (1992): Glaciological and meteorological investigations on Ecology Glacier, King George Island, Antarctica (Summer 1990-1991). *Circumpolar Journal* **1-2**, 59-71.

BINTANJA, R. (1995): The local surface energy balance of the Ecology Glacier, King George Island, Antarctica: measurements and modelling. *Antarctic Science* **7** (3), 315-325.

BINTANJA, R. & VAN DEN BROEKE, M. R. (1994): Local climate, circulation and surface-energy balance of an Antarctic blue-ice area. *Annals of Glaciology* **20**, 160-168.

BINTANJA, R. & VAN DEN BROEKE, M. R. (1995): Momentum and scalar transfer coefficients over aerodynamically smooth Antarctic surfaces. *Boundary Layer Meteorology* **74**, 89-111.

BIRKENMAJER, K. (1979a): Age of the Penguin Island Volcano, South Shetland Islands (West Antarctica), by the lichenometric method. *Bulletin Polish Academy of Sciences* **27** (1-2), 69-76.

BIRKENMAJER, K. (1979b): Lichenometric dating of glacier retreat at Admiralty Bay, King George Island (South Shetland Islands, west Antarctica). *Bulletin Polish Academy of Sciences* **27** (1-2), 77-85.

BIRKENMAJER, K. (1980a): New place names introduced to the area of Admiralty Bay, King George Island (South Shetland Islands, Antarctica). *Studia Geologica Polonica* **66**, 67-88.

BIRKENMAJER, K. (1980b): Tertiary volcanic-sedimentary succession at Admiralty Bay, King George Island (South Shetland Islands,Antarctica). *Studia Geologica Polonica* **64**, 8-65.

BIRKENMAJER, K. (1981a): Lichenometric dating of raised marine beaches at Admiralty Bay, King George Island (South Shetland Islands, West Antarctica). *Quaternary Science Reviews, Terre* **29** (29), 119-127.

BIRKENMAJER, K. (1981b): Raised marine features and glacial history in the vicinity of H. Arctowski Station, King George Island (South Shetland Islands, Antarctica). *Quaternary Science Reviews*. **29** (2), 109-117.

BIRKENMAJER, K. (1982a): Late Cenozoic phases of block-faulting on King George Island (South Shetland Islands, West Antarctica). *Bulletin Polish Academy of Sciences, Terre* **30**, 21-32.

BIRKENMAJER, K. (1982b): Pliocene tillite-bearing succession of King George Island (South Shetland Islands, Antarctica). *Studia Geologica Polonica* **74**, 7-72.

BIRKENMAJER, K. (1984): Further new place names for King George Island and Nelson Island, South Shetland Islands (West Antarctica), introduced in 1981. *Studia Geologica Polonica* **79**, 163-177.

BIRKENMAJER, K. (1989): King George Island. In DALZIEL, I.W.D., BIRKENMAJER, K., MPODOZIS, C., RAMOS, V.A. & THOMSON, M.R.A (Leaders): *Tectonics of the Scotia Arc. Antarctica*. Field Trip Guidebook, T 180. *28th International Geological Congress*, Washington, D.C., 144-121.

BIRKENMAJER, K. (1994): Quaternary Geology at Lions Rump (SSSI No. 34), King George Island, South Shetland Islands (West Antarctica). *Bulletin of the Polish Academy of Sciences, Earth Sciences* **42** (3), 207-221.

BIRKENMAJER, K. (1995): Glacier retreat and raised marine beaches at Three Sisters Point, King George Island (South Shetland Islands, west Antarctica*). Bulletin of the Polish Academy of Sciences, Earth Sciences* **43** (2), 135-141.

BIRKENMAJER, K. (1996): Tertiary Glacial/Interglacial Palaeoenvironments and Sea-Level Changes, King George Island, West Antarctica. An Overview. *Bulletin of the Polish Academy of Sciences, Earth Sciences* **44** (3): 157-181.

BIRKENMAJER, K. (1997a): Geology of the northern coast of King George Island, South Shetland Islands (West Antarctica). *Studia Geologica Polonica* **110**, 7-26.

BIRKENMAJER, K. (1997b): Quaternary geology at Arctowski Station, King George Island, South Shetland Islands (West Antarctica). *Studia Geologica Polonica* **110**, 91-104.

BIRKENMAJER, K (1999): Present and past glaciation: a geological perspective. In WETTLAUFER J. S., DASH, J. G. & UNTERSTEINER, N. (eds.)*: Ice Physics and Natural Environment*, Springer-Verlag, Berlin, Heidelberg. *NATO ASI Series*, Vol. I **56**,109-119.

BIRKENMAJER, K. & KELLER, R. A. (1990): Pleistocene age of Melville Peak Volcano, King George Island, West Antarctica, by K-Ar Dating. *Bulletin Polish Academy of Sciences* **38** (1-4), 17-24.

BIRKENMAJER, K., OCHYRA, R., OLOSSON, I. U. & STUCHLIK, L. (1985): Mid-Holocene radiocarbon-dated peat at Admiralty Bay, King George Island (South Shetland Islands, West Antarctica). *Bulletin of the Polish Academy of Sciences* **33** (1-2), 7-13.

BISHOP, M. P., SHRODER JR., J. F. & WARD, J. L. (1995): SPOT multispectral analysis for producing supraglacial debris-load estimates for Batura Glacier, Pakistan. In NELLIS, M. D. (ed.): Remote Sensing Images & Technical Notes. *Geocarto International* **10** (4), 81-90.

BLACKADAR, A. K. (1997): Turbulence and diffusion in the atmosphere. Springer-Verlag, Berlin.

BRAITHWAITE, R. J. & OLESEN, O.B. (1990): Valculation of glacier ablation from air temperature. West Greenland. In OERLEMANS, J. (ed.): *Glacier fluctuations and climatic change*. Dordrecht, Kluver Academic Publishers, 219-233.

BRAITHWAITE, R. J. (1981): On glacier energy balance, ablation, and air temperature. *Journal of Glaciology* **27** (97), 381-391.

BRAITHWAITE, R. J. (1995): Aerodynamical stability and turbulent sensible-heat flux over a melting ice surface, the Greenland ice sheet. *Journal of Glaciology* **41** (139), 562-571.

BRAITHWAITE, R. J., KONZELMANN, T., MARTY, C. & OLESEN, O. B. (1998): Reconnaissance study of glacier energy balance in North Greenland, 1993-94. *Journal of Glaciology* **44** (147), 239-247.

BRAUN, L. N. (1985): Simulation of snowmelt-runoff in lowland and lower alpine regions of Switzerland. *Zürcher Geographische Schriften* **21**, 166 p.

BRAUN, M. & GOßMANN, H. (in press): Glacial changes in the area of Admiralty Bay and Potter Cove, King George Island, Antarctica. In BÖLTER (ed.): *GeoEcology of Terrestrial Antarctic Oases*. Springer Verlag.

BRAUN, M., RAU, F., SAURER, H. & GOßMANN, H. (2000): Development of radar glacier zones on the King George Island ice cap, Antarctica, during the austral summer 1996/97 as observed in ERS-2 SAR-data. *Annals of Glaciology*, **31**, 357-363.

BRAUN, M., SIMÕES, J. C. , VOGT, S., BREMER, U. F., BLINDOW, N., PFENDER, M., SAURER, H., AQUINO, F. E. & FERRON, F. A. (2001): An Improved Topographic Database for King George Island. Compilation, Application and Outlook. *Antarctic Science* **13** (1), 41-52.

BROCK, B. W., WILLIS, I. C., SHARP, M. J. & N. S. ARNOLD (2000): Modelling seasonal and spatial variations in the surface energy balance of Haut Glacier d'Arolla, Switzerland. *Annals of Glaciology* **31**, 53-62.

BRUTSAERT, W. H. (1982): Evaporation into the atmosphere. Reidel Publishing Company, 299 p.

BUDD, W. F. (1991): Antarctica and global change. *Climatic Change* **8**, 271-299.

BUSINGER , J. A., WYNGAARD, J. C., IZUMI, Y. & BRADLEY, E. F. (1971): Flux-profile relationships in the atmospheric surface layer. *Journal of Atmospheric Sciences* **28**, 181-189.

CALVET, J. & CORBERA, J. (1993): Fluctuations of the ice cap on Livingston Island - South Shetland. *Selper* **9** (1/2), 31-35.

CALVET, J., CORBERA, J. & FURDADA, G. (1992): Variación del frente glaciar en Bahía Sur y Punta Siddons entre 956 y 1991, Isla Livingston, Islas Shetland del Sur. In LÓPEZ-MARTINEZ J. (Ed.): *Geologia de la Antartida Occidental. Simposios* T3, III Congreso Geológico de España y VIII Congreso Latinoamericano de Geología, Salamanca, España, 283-292.

CALVET, J., GARCÍA SELLÉS, D. & CORBERA, J. (1999): Fluctuaciones de la extensión del casquete glacial de la isla Livingston (Shetland del Sur) desde 1956 hasta 1996. *Acta Geolgogica Hispanica* **34** (4), 365-374.

CARLETON, A. M. (1988): Sea ice-atmosphere signal of the southern oscillation in the Wedell Sea, Antarctica. *Journal of Climate* **1**, 379-388.

CARLETON, A. M. (1992): Synoptic interactions between Antarctica and lower latitudes. *Australian Meteorological Magazine* **40**, 129-147.

CARLETON, A. M., JOHN, G. & WELSCH, R. G. (1998): Interannual variations and regionality of Antarctic sea-ice-temperature associations. *Annals of Glaciology* **27**, 403-408.

CARRASCO, J. F. & BROMWICH, D. H. (1993): Interannual variations of mesoscale cyclones near the Antarctic Peninsula. *4th International Conference on Southern Hemisphere Meteorology and Oceanography, 29.03. - 02.04.93*, Hobart, Australia, 449-500.

CARRASCO, J. F., BROMWICH, D. H. & LIU, Z. (1997): Mesoscale cyclone activity over Antarctica during 1991. 2. Near the Antarctic Peninsula. *Journal of Geophysical Research* **102** (D12), 13939-13954.

CASASSA, G. (1989): Velocity, heat budget and mass balance at Anvers Island ice cap, Antarctic Peninsula. *Antarctic Record* **33** (3), 341-352.

CERVELLATI, R., RAMORINO, C., SIEVERS, J., THOMSON, J. & CLARKE, D. (2000): A composite gazetteer of Antarctica. *SCAR Bulletin* **138**, 7-14.

CHANG, K. I., JUN, H. K., PARK, G. T. & EO, Y. S. (1990): Oceanographic conditions of Maxwell Bay, King George Island, Antarctica (Austral Summer 1989). *Korean Journal of Polar Research* **1** (1), 27-46.

CHEN, S., ZHANG, L. & LU, C. (1990): Statistical analysis of cyclone tracks in western Antarctic region. *Acta Meteorologica Sinica* **4** (1), 74-80.

CLAPPERTON, C. M. (1990): Quaternary glaciations in the southern ocean and Antarctic Peninsula area. *Quaternary Science Reviews* **9**, 229-252.

CLAPPERTON, C. M. & SUDGEN, D. E. (1988): Holocene glacier fluctuations in South America and Antarctica. *Quaternary Science Reviews* **7**, 185-198.

COMISO, J. C (2000): Variability and trends in Antarctica surface temperatures from in situ and satellite infrared measurements. *Journal of Climate* **13**, 1674-1696.

CONNOLLEY, W. M. & O'FARRELL, S. P. (1998): Comparison of warming trends over the last century around Antarctica from three coupled models. *Annals of Glaciology* **27**, 565-570.

CURL, J. E. (1980): A glacial history of the South Shetland Islands, Antarctica. *Institute of Polar Studies Report,* Columbus, Ohio **63**, 129 p.

DAHE, Q. (ed.) (1989): CHINARE data report No. 5, Glaciological data in the region of the great Wall Station, Antarctica from Dec. 1985 to Feb. 1989. *Antarctic Record* **33** (3).

DALZIEL, I. W. D. (ed.). 1989. Tectonics of the Scotia Arc. Field trip Guidebook T180, Punta Arenas, Chile to Ushuaia, Argetina, January 1- February 1, 1989, American Geophysical Union, Washington, D.C..

DAYTON (1989): Interdecal variation in an Antarctic sponge and its predators from oceanographic climate shifts. *Science* **245**, 1484-1486.

DE LA CASINIÈRE, A. C. (1974): Heat exchange over a melting snow surface. *Journal of Glaciology* **13** (67), 55-72.

DE WOLDE, J. R., HUYBRECHTS, P., OERLEMNS, J. & VAN DE WAL, R. S. W. (1997): Projections of global sea level rise calculated with a 2D energy-balance climate model and dynamic ice sheet models. *Tellus* **49A**, 486-502.

DEL VALLE R. & TATUR, A. (1993): Holocene evolution of landscape and biota on King George Island, Antarctica. *Verhandlungen des Internationalen Vereins für Limnologie* **25**, 1128-1130.

DINGLE, R. V., MCARTHUR, J. M. & VROON, P. (1997): Oligocene and Pliocene interglacial events in the Antarctic Peninsula dated using strontium isotope stratigraphy. *Journal of the Geological Society of London* **154**, 257-264.

DOAKE C. S. M. & VAUGHAN, D. G. (1991): Rapid disintegration of Wordie Ice Shelf in response to atmospheric warming. *Nature* **350**, 328-330.

DOAKE, C. S., CORR, H. F. J., ROTT, H., SKVARKA, P. & YOUNG, N. W. (1998): Breakup and conditions for stability of the northern Larsen Ice Shelf, Antarctica. *Nature* **391**, 778-780.

DOMACK, E. W. (1990): Climatic and oceanographic controls upon antarctic fjord sedimentation: Examples from the Antarctic Peninsula and South Shetlands. *Antarctic Journal of the United States* **25** (5), 59-60.

DOMACK, E. W. & WILLIAMS, C. R. (1990): Fine structure and suspended sediment transport in three Antarctic Fjords. *Antarctic Research Series* **50**, 71-89.

DOMACK, E. W., BUKRLEY, L. A. & WILLIAMS, C. R. (1989): Character of modern glacial marine sediments: Antarctic Peninsula and South Shetland Islands*. Anarctic Journal of the United States* **24** (5), 113-115.]

DOMACK, E. W., MASHIOTTA, T. A., BURKLEY, L. A. & ISHMAN, S. E. (1993): 300-Years cyclicity in organic matter preservation in Antarctic fjord sediments. *Antarctic Research Series* **60**, 265-272.

DOMACK, E. W., LEVENTER, A., GILBERT, R., BRACHFIELD, S., ISHMAN, S., CAMERLENGHI, A., GAVAHAN, K., CARLSON, D. & BARBOUKIS, A. (2000): Cruise reveals history of Holocene Larsen Ice Shelf. *EOS* **82** (2), 13,16-17.

DOWDESWELL, J. A., REES, W. G. & DIAMENT, A. D. (1994): ERS-1 SAR investigations of snow and ice facies on ice caps in the European high arctic. *Proceedings of the ERS-1 Symposium ‚Space at the Service of our Environment'*, Hamburg, Germany, 11-14 October 1993 (ESA SP-361, January 1994), 1171-1176.

DREWRY, D. J. & MORRIS, E. M. (1992): The response of large ice sheets to climate change. *Philosophical Transactions Royal Society of London* **B** (338), 235-242.

DYNKEREKE, P. G. & VAN DEN BROEKE, M. R. (1994): Surface energy balance and katabatic flow over glacier and tundra during GIMEX-91. *Global and Planetary Change* **9** (1/2), 17-28.

ENEMOTO, H. & OHMURA, A. (1990): The influence of atmospheric half-yearly cycle on the sea ice extent in the Antarctic. *Journal of Geophysical Research* **95**, 9497-9511.

FAHNESTOCK, M., BINDSCHADLER R., KWOK, R. & JEZEK, K. (1993): Greenland ice sheet surface properties and ice dynamics from ERS-1 SAR imagery. *Science* **262** (5139), 1530-1534.

FERRIGNO, J.G., WILLIAMS JR. R.S., ROSANOVA, C.E., LUCCHITTA, B.K. & SWITHINBANK, C. (1998): Analysis of coastal change in Marie Byrd Land and Ellsworth Land, Wets Antarctica, using Landsat imagery. *Annals of Glaciology* **27**, 33-40.

FORSTER, R. R., RIGNOT, E. & DAS, S. (1996): Shuttle image radar (SIR-C/X-SAR) reveals near surface properties of the South Patagonian Icefield. *Journal of Geophysical Research* **101** (E10), 23,169-23,180.

FOX, A. J. & COOPER, A. P. R. (1998): Climate change indicators from archival aerial photography of the Antarctic Peninsula region. *Annals of Glaciology* ***27***, 636-642.

GOVORUKHA, L. S., CHUDAKOV, V. I. & SHALYGIN, A. M. (1975): Radar ice sounding on King George (Waterloo) Island. *Information Bulletin of the Soviet Antarctic Expedition* **8** (11), 588-590.

GRAINGER, M. E. & LISTER, H. (1966): Wind speed, stability and eddy viscosity over melting ice surfaces. *Journal of Glaciology* **6**, 101-127.

GREGORY J. M. & OERLEMANS, J. (1998): Simulated future sea-level rise due to glacier melt based on regionally and seasonally resolved temperature changes. *Nature* **391**, 474-476.

GREULL, W. & OERLEMANNS, J. (1987): Energy balance calculations on and near Hintereisferner (Austria) and an estimate of the effect of greenhouse warming on ablation. In OERLEMANNS, J. (ed.): *Glacier fluctuations and climate change, glaciology and quaternary geology*, Dordrecht, 305-323.

GROBE, C. W., RUHLAND, C. T. & DAY, T. A. (1997): A new population of Colobanthus quitensis near Arthur Harbor, Antarctica: Correlating requirement with warmer summer temperatures. *Arctic and Alpine Research* **29** (2), 217-221.

GROENEWEG, W. J. & BEUNGK, F. F. (1992): The petrography and geochemistry of the King George Island Supergroup and the Admiralty Bay Group volcanics, South Shetland Islands. In J. López-Martinez (ed.). *Geología de la Antártida Occidental*, Simposios T3, III Congreso Geológico de España y VIII Congreso Latinoamericano de Geología, Salamanca, España, 43-60.

GURGUL, H. (1993): Description of quantity and dispersion distribution changes of mineral suspensions occurring in the Ezcurra Inlet waters, King George Island within a year cycle. *Korean Journal of Polar Research* **4** (1), 3-14.

HALL, D. K. (1998): Remote sensing of snow and ice. In HENDERSON, F. M. & LEWIS A. J. (1998): Principles and applications of imaging radar. Manual of remote sensing, 3rd edition, Vol. 2. John Wiley & Sons, Inc. New York, Chichester, Weinheim, Brisbane, Singapore, Toronto, 677-703.

HALL, D. K., WILLIAMS JR., R. S., BARTON, J. S., SIGURÐSSON, O., SMITH, L. C. & GARVIN, J. B. (2000): Evaluation of remote-sensing techniques to measure decadal-scale changes of Hofsjökull ice cap, Iceland. *Journal of Glaciology* **46** (154), 375-388.

HALLIKAINEN, M. (1996): Retrieval of sea ice and snow parameters from microwave radiometer and radar data. In RASCHKE, E. (ed.): Radiation and Water in the Climate System: Remote Measurements', *NATO ASI Series* **1** (45), 527-545.

HAN, M. W. & YOON, H. I. (1990): Effect of sea salts in the major anion distribution in an ice core of the Fildes Peninsula ice field: a preliminary study result. *Korean Journal of Polar Research* **1** (2), 17-23.

HAN, J., HUIJUN, J. WEN, J. & SHANG, X. (1995): Temperature distribution of Collins ice cap, King George Island, Antarctica. *Antarctic Research* **6** (2), 57-65.

HAN, J., XIE, Z., DAI, F. & ZHANG, W. (1999): Volcanic eruption recorded in an ice core from Collins Ice cap, King George Island, Antarctica. *Annals of Glaciology* **29**, 121-125.

HARANGOZO, S. A. (2000): A search for ENSO teleconnections in the west Antarctic Peninsula climate in austral winter. *International Journal of Climatology* **20**, 663-679.

HARANGOZO, S. A., COLWELL, S. R. & KING, J. C. (1997): An analysis of a 34-year air temperature record from Fossil Bluff (71°S, 68°W), Antarctica. *Antarctic Science*, **9** (3), 355-363.

HATTERSLEY-SMITH, G. (1949): King George Island Glaciological Report for 1948-49. *Falkland Islands Dependencies Service Report*, unpublished.

HATTERSLEY-SMITH, G. (1991): The history of place-names in the British Antarctic Territory. *British Antarctic Survey Scientific Report* **113**, Vol. I & II.

HAY, J. E. & FITZHARRIS, B. B. (1988): A comparison of the energy-balance and bulk aerodynamic approaches for estimating glacier melt. *Journal of Glaciology* **34** (117), 145-453.

HEINEMANN, G. (1995): Polare Mesozyklonen. *Bonner Meteorologische Abhandlungen* **45**, 157 p.

HEINEMANN, G. & ROSE, L. (1990): Surface energy balance, parameterizations of boundary-layer heihts and the application of resistance laws near an Antarctic ice shelf front. *Boundary-Layer Meteorology* **51**, 123-158.

HENDERSON, F. M. & LEWIS, A. J. (1998): Principles and applications of imaging radar. Manual of remote sensing, 3rd edition, Vol. 2. John Wiley & Sons, Inc. New York, Chichester, Weinheim, Brisbane, Singapore, Toronto.

HINES, K. H., BROMWICH, D. H. & MARSHALL, G. J. (in press): Artificial surface pressure trends in the NCEP/NCAR reanalysis over the southern ocean and Antarctica. *Journal of Climate*.

HJORT, C., BJÖRCK, S., INGÓLFSSON, Ó. & MÖLLER, P. (1998): Holocene deglaciation and climate history of the northern Antarctic Peninsula region: a discussion of correlations between the Southern and Northern Hemisphere. *Annals of Glaciology* **27**, 110-112.

HOCHSCHILD, V. (1995): Geomorphologische Kartierung und Untersuchung der Auftaudynamik mit ERS-1-SAR-Daten im Bereich der Antarktischen Halbinsel. *Bremer Beiträge zur Geographie und Raumplanung* **28**, 160 p.

HOCK, R. (1998): Modelling of Glacier Melt and Discharge. *Zürcher Geographische Schriften* **70**, 126 S.

HOCK, R. (2000): A computer program to calculate melt and discharge in highly glacierized areas. Program documentation and users manual, 64 p.

HOCK, R. & HOLMGREN, B. (1996): Energy balance and ablation of Storglaciären, Northern Sweden. *Geografiskae Annaler* **78 A** (2-3), 121-131.

HOFFMANN, J. A., NÚÑEZ, S. E. & VARGAS, W. M. (1997): Temperature, humidity and precipitation variations in Argentina and the adjacent sub-antarctic region during the present century. *Meteorologische Zeitschrift* **6**, 3-11.

HOFMANN, E. & PRIDDLE, J. (2000): Interannual variability in the southern ocean. Summary report of a workshop Cambridge, United Kingdom, 2-7 August 1999. *SCAR Bulletin* **138** (July 2000), 4-6.

HOGG, I. G. G., PAREN, J. G. & TIMMIS, R. J. (1982): Summer heat and ice balances on Hodges Glacier, South Georgia, Falkland Islands Dependencies. *Journal of Glaciology* **28** (99), 221-238.

HOLMGREN, B. (1971): Climate and energy exchange on a subpolar ice cap in summer. Arctic Institute of North America, Devon Island expedition 1961-63. *Meteorologiska Institutionen, Uppsala Universitet. Meddelanden* **111**, Part A-F.

HONG, G. H., KIM, D. Y., CHUNG, H. & PAE, S. (1991): Coastal and inshore water interaction, mixing and primary productivity in the Bransfield Strait, Antarctica during austral summer 198/90. *Korean Journal of Polar Research* **2** (1), 43-59.

HONG, S.-M. PARK, B.-K., YOON, H.-I.. YAEDONG, K. & OH, J.-K. (1991): Depositional environment in and paleoglacial setting around Marian Cove, King George Island, Antarctica. *Korean Journal of Polar Research* **2** (2), 73-85.

HOUGHTON, J. T., JENKINS, G. J. & EPHRAUMS, J. J. (1990): Climate change. The IPCC scientific assessment. Published for the World Meteorological Organization/United Nations Environemntal Programme Intergovernmental Panel on Climate Change by Cambridge University Press.

HOUGHTON, J. T., MEIRA FILHO, L. G., CALLANDER, B. A., HARRIS, N., KATTENBERG, A. & MASKELL, K. (1996): Climate change 1995. The science of climate change. IPCC report, Cambridge University Press, Cambridge.

HULBE, C. L. (1997): Recent changes to Antarctic Peninsula ice shelves: what lessons have been learned? *Natural Science* **1** (6). (e-Journal)

Iken, K. (1996): Trophische Beziehungen zwischen Makroalgen und Herbivoren in der Potter Cove (King-George-Insel, Antarctica). *Berichte zur Polarforschung* **201**, 201 p.

JACKA, T. H. & BUDD, W. F. (1998): Detection of temperature and sea-ice-extent changes in the Antarctic and Southern Ocean, 1949-96. *Annals of Glaciology* **27**, 553-559.

JAMIESON, A. W. & WAGER, A. C. (1983): Ice, water and energy balances of Spartan Glacier, Alexander Island. *British Antarctic Survey Bulletin* **52,** 155-186.

JANSSEN, I. & HUYBRECHTS, P. (2000): The treatment of meltwater retention in mass-balance parametrizations of the Greenland ice sheet. *Annals of Glaciology* **31**, 133-140.

JAZDZEWSKI, K., JURASZ, W., KITTEL, W., PRESLER, E. & SICINSKI, J. (1986): Abundance and biomass estimates of the benthic fauna in Admiralty Bay, King George Island, South Shetland Islands. *Polish Biology* **6**, 5-16.

JAZDZEWSKI, K., DE BROYER, V. TEODORCZYK, W. & KONOPACKA, A. (1991): Survey and distributional patterns of the amphipod fauna of Admiralty bay, King George Island, South Shetlands. *Polish Polar Research* **12** (3), 461-472.

Jezek, K. C. (1998): Glaciological properties of the Antarctic ice sheet from RADARSAT synthetis aperture radar imagery. *Annals of Glaciology* **29**, 286-290.

JEZEK, K. C., DRINKWATER, M. R., CRAWFORD, J. P., BINDSCHADLER, R. & KWOK, R. (1993): Analysis of synthetic aperture radar data collected over the southwestern Greenland ice sheet. *Journal of Glaciology* **39** (131), 119-132.

JIAWEN, R., DAHE, Q., PETIT, J. R., JOUZEL, J., WENTI, W., CHEN, L., XIAOJUN, W., SONGLIN, Q. & XIAOXIANG, W. (1995): Glaciological studies on Nelson Island, South Shetland Islands, Antarctica. *Journal of Glaciology* **41** (138), 408-412.

JIN Q., F. KUANG, H. RUAN & XING, G. (1983): Island arc vulcanism and magmatic evolution in Fildes Peninsula, King George Island, Antarctica. In*: Antarctic Earth*

Science, Proceedings of the Fourth International Symposium on Antarctic Earth Sciences, Univ. Adelaide, South Australia, 16-20 August 1982, 250-255.

JOHANNESSON, T., RAYMOND, C. & WADDINGTON, E. (1989): Timescale for adjustment of glaciers to changes in mass balance. *Journal of Glaciology* **35**, 345-358.

JOHN, B. S. (1972): Evidence from the South Shetland Islands towards a glacial history of West Antarctica, *Insti. Briti. Geogr. Spec. Publ.* No. **4**, 75-92.

JOHN, B. S. & SUDGEN, D. E. (1971): Raised marine features and phases of glaciation in the South Shetland Islands. *British Antarctic Survey Bulletin* **24**, 45-111.

JONES, D. A. & SIMMONDS, I. (1993): A climatology of Southern Hemisphere extratropical cyclones. *Climate Dynamics* **9**, 131-145.

JONES, D. A. & SIMMONDS, I. (1994): A climatology of Southern Hemisphere anticyclones. *Climate Dynamics* **10**, 333-348.

JONES, P. D. (1990): Antarctic temperatures over the present century – a study from early expedition records. *Journal of Climate* **3**, 1193-1203.

JONES, P. D., MARSH, R., WIGLEY, T. M. L. & PEEL, D. A. (1993): Decadal timescale links between Antarctic Peninsula ice-core oxygen-18, deuterium and temperature*. The Holocene* **3** (1), 14-26.

JONES, P. D., NEW, M., PARKER, D. E., MARTIN, S. & RIGOR, I. G. (1999): Surface air temperature and its changes over the past 150 years. *Reviews of Geophysics* **37** (2), 173-199.

KAROLY, D. J. (1989): Southern Hemisphere circulation features associated with El-Niño events. *Monthly Weather Reviews* **115**, 3133-3145.

KEJNA, M. (1993): Types of atmospheric circulation in the region of H. Arctowski Station (South Shetland Islands) in the xears 1986-1989. In REPELEWSKA-PEKALOWA, J. (ed.): *XX Polar Symposium, Man Impact on Polar Environment*. Lublin, Poland, 369-375.

KEJNA, M (1998): Air temperature in the Admiralty Bay region (King George Island, Antarctica) in the period 1977-1996 according to meteorological data from the H. Arctowski station. Torun. Unpublished report.

KEJNA, M., LÁSKA, K. & CAPUTA, Z. (1998): Recession of the Ecology Glacier (King George Island) in the period 1961-1996. In GLOWACKI, P. & BEDNAREK, J. (eds.) *Polish Polar Studies*. *25th International Polar Symposium*, Warsaw, 1998. Institute of Geophysics of the Polish Academy of Sciences, Warsaw, 121-128.

KELLY, R.E.J., ENGESET, R., KENNETT, M., BARRETT, E.C. & THEAKSTONE, W. (1997): Characteristic snow and ice properties of a Norwegian ice cap determined from complex ERS SAR, in Proceedings of the *3rd ERS Symposium on 'Space at the Service of our Environment'*, pp. 831-836, Florence, Italy.

KING, J. C. (1994): Recent climate variability in the vicinity of the Antarctic Peninsula. *International Journal of Climatology* **14**, 357-369.

KING, J. C. (1996): Longwave atmospheric radiation over Antarctica. *Antarctic Science* **8** (1), 105-109.

KING J. C. & ANDERSON, P. S. (1994): Heat and water vapour fluxes and scalar roughness lengths over an Antarctic ice shelf. *Boundary Layer Meteorology* **69**, 101-121.

KING J. C. & CONNOLLEY, W. M. (1997): Validation of the Surface Energy balance over the Antarctic ice sheets in the U.K. Meteorological Office Unified Climate Model. *Journal of Climate* **10**, 1273-1287.

KING, J. C. & TURNER, J. (1997): Antarctic Meteorology and Climatology. - Cambridge *Atmospheric and Space Science Series*, Cambridge University Press, Cambridge, 409 p.

KING J. C. & HARANGOZO, S. A. (1998): Climate change in the western Antarctic Peninsula since 1945: observations and possible causes. *Annals of Glaciology* **27**, 571-575.

KLÖSER, H. & ARNTZ, W E. (1994): RASCALS (Research on Antarctic Shallow Coastal and Litoral Systems) Untersuchungen zur Struktur und Dynamik eines antarktischen Küstenökosystems. *Polarforschung* **64** (1), 27-41.

KLÖSER, H., FERREYRA, G., SCHLOSS, I., MERCURI, G., LATURNUS, F. & CURTOSI, A. (1994): Hydrography of Potter Cove, a small fjord-like inlet in King George Island (South Shetlands). *Estuarine, Coastal and Shelf Science* **38**, 523-537.

KNAP, W. H., OERLEMANNS, J. & CADÉE, M (1996): Climate sensitivity of the ice cap of King George Island, South Shetland Islands, Antarctica. *Annals of Glaciology* **23**, 154-159.

KÖNIG, M., WINTHER, J.-G. & ISAKSSON, E. (2001a): Measuring snow and glacier ice properties from satellite. *Reviews of Geophysics* **39** (1), 1-27.

KÖNIG, M., WINTHER, J.-G., KNUDSEN, N. T. & GUNERIUSSEN, T. (2001b): Equilibrium- and firn-line detection with multipolarization SAR. First results. In Wunderle & Nagler (eds.): *Proceedings of the 2nd EARSeL Workshop* - Special Interest Group Land Ice and Snow, June 16-17, 2000, Dresden.

KÖNIG-LANGLO, G. & AUGSTEIN, E. (1994): Parametrization of the downward long-wave radiation at the earth's surface in polar regions. *Meteorologische Zeitschrift* **3** (6), 434-347.

KONZELMANN, T. (1994): Radiation conditions on the Greenland ice sheet. *Züricher Geographische Schriften* **56**, 124 p.

KONZELMANN, T. & BRAITHWAITE, R. J. (1995): Variations of ablation, albedo and energy balance at the margin of the Greenland ice sheet, Kronprins Christian Land, eastern north Greenland. *Journal of Glaciology* **41** (137), 174-182.

KOWALSKI, D. & WIEBILSKA, D. (1989): Synoptic features of the severe winter 1986 at Arctowski Station, King George Island, West Antarctica. *Polish Polar Research* **10** (1), 57-71.

KRATKE, J. & WIELBINSKA, D. (1987): Vertical wind profile under small velocity conditions over the Admiralty Bay, King George Island, West Antarctica. *Polish Polar Research* **8** (1), 75-83.

KRAUS, H. (1973): An energy balance model for ablation in mountainous areas. Snow and Ice Symposium (Proceedings of the Moscow Symposium, August 1971), *IAHS Publ*. **104**, 74-78.

KÜHNE, S. (1997): Solitäre Ascidien in der Potter Cove (King George Island, Antarktis). Ihre ökologische Bedeutung und populationsdynamik. *Berichte zur Polarforschung* **252**, 153 p.

LAUR, H., BALLY, P., MEADOWS, P., SANCHEZ, J., SCHAETTLER, B. & LOPINTO, E. (1997): Derivation of the backscattering coefficient σ° in ESA ERS SAR PRI products. *ESA Document no. ES-TN-RS-PM-HL09*, Issue 2, Rev. 4, 39 p.

LEE, D.-Y. (1992): Topographic evidences of raised beaches along the Barton Peninsula, Antarctica. *Korean Journal of Polar Research* **3** (1/2), 71-84.

LEMASURIER W. E. & THOMSON, J. W. (Ed.) 1990. Volcanoes of the Antarctic Plate and Southern Oceans. *Antarctic Research Series* **48**, 322-324.

LEVENTER, A., DOMACK, E. W., ISHMAN, S. E., BRACHFELD, S., MCCLENNEN, C. E. & MANLEY, P. (1996): Productivity cycles of 200-300 years in the Antarctic Peninsula region: understanding linkages among the sun, atmosphere, oceans, sea ice, and biota. *GSA Bulletin* **108** (12), 1626-1644.

LEWIS, K. J., FOUNTAIN, A. G., & DANA, G. L. (1998): Surface energy balance and meltwater production for a Dry Valley glacier, Taylor Valley, Antarctica. *Annals of Glaciology* **27**, 603-609.

LIGOWSKI, R. & KOPCYZYŃSKA, E. E. (1993): Phytoplankton, In: RAKUSA-SUSZCZEWSKI, S., (ed.): *The maritime Antarctic coastal Ecosystem of Admiralty Bay*. Department of Antarctic Biology, Polish Academy of Sciences, Warsaw, 45-48.

LIPSKI, M. (1987), Variations of physical conditions and chlorophyll a contents in Admiralty Bay, King George Island, South Shetland Islands (1979). *Polish Polar Research* **8** (4), 307-332.

LIU, G., CUI, Z. & XIONG, H. (1992): Coastal phenomena and isostatic uplift around Fildes Peninsula of King George Island, South Shetland Islands, Antarctica. *Antarctic Research* **3** (2), 45-55.

LUCCHITA, B.K. & ROSANOVA, C. E. (1998): Retreat of northern margins of George VI and Wilkins Ice Shelves, Antarctic Peninsula. *Annals of Glaciology* **27**, 41-46.

MACHARET, Y. Y. & MOSKALEVSKY, M. Y. (1999): Structure and dynamics of outlet Lange Glacier, King George Island ice cap, South Shetland Islands, Antarctica. *Annals of Glaciology* **29**, 202-206.

MACHERET, Y. Y., MOSKALEWSKY, M. Y., SIMÕES, J. C. & LADOUCH, L. (1997): Study of King George Island ice cap, South Shetland Islands, Antarctica using radio-echo sounding and SPOT, ERS-1 SAR satellite images. *Proceedings of an International Seminar on the use and application of ERS in Latin America*, Vina del Mar, Chile, 25-29 Nov. 1996, 249-254.

MACHERET, Y. Y., MOSKALEWSKY, M. Y., SIMÕES, J. C. & LADOUCH, L. (1998): Structure and regime of King George Island ice sheet, South Shetland Islands, Antarctica, as a typical glacier in the south subpolar region. 4th International Symposium on Glacier Caves and Cryokarst in Polar and High-Mountain Regions. Salzburg, Austria, September 1-7, 1996, *Salzburger Geographische Materialien* **28**, 73-80.

MALE, D. H. & GRANGER, D. M. (1981): Snow surface energy exchange. *Water Resource Research* **17**, 609-627.

MARSHALL, G. J. & LAGUN, V. (submitted): A definite monthly surface temperature series for Bellingshausen station. *Polar Record*.

MARSHALL, G.J. & HARANGOZO, S.A. (in press): An appraisal of NCEP/NCAR reanalysis MSLP viability for climate studies in the South Pacific. *Geophysical Research Letters*.

MARSHALL, G. J., REES, W. G. & DOWDESWELL J. A. (1995): The discrimination of glacier facies using multi-temporal ERS-1 SAR data. In ASKNE, J. (ed.): *Sensors and Environmental Applications of Remote Sensing*. Balkema, Rotterdam, 263-269.

MARSHALL, G. J., TURNER, J. & MINERS, W. D. (1998): Interpreting recent accumulation records through an understanding of the regional synoptic

climatology: an example from the southern Antarctic Peninsula. *Annals of Glaciology* **27**, 610-616.

MARTIANOV, V. & RAKUSA-SUSZCZEWSKI, S. (1989): Ten years of climate observations at the Arctowski and Bellingshausen Station (King George Island, South Shetland Islands, Antarctica). In BIRKENMEYER, A. (ed.): *Global Change Regional research Centres: Scientific Problems and Concept Developments*, Warsaw-Jablonna, IGBP IASA UNESCO PAS Seminar, 80-87.

MARTIN, P. J. & PEEL, D. A. (1978): The spatial distribution of 10m temperatures in the Antarctic Peninsula. *Journal of Glaciology* **20** (83), 311-317.

MARTIN, S. (1975): Wind regimes and heat exchange on Glacier de Sait-Sorlin. *Journal of Glaciology* **14** (70), 91-105.

MÄTZLER, C. (1987): Applications of the interaction of microwaves with the natural snow cover. *Remote Sensing Reviews* 2, 259-387.

MÄTZLER, C., STROUUI, T., WEISE, T., FLORICIOIU & ROTT, H. (1997): Microwave snowpack studies made in the Austrian Alps during the SIR-C/X-SAR experiment. *International Journal of Remote Sensing* **18** (12), 2505-2530.

MAYES, P. R. (1985): Secular variations in cyclone frequencies near the Drake Passage, southwest Atlantic. *Journal of Geophysical Research* **90**, 5829-5839.

MERCER, H. J. (1978): West Antarctic ice sheet and CO_2 greenhouse effect: a threat of disaster. *Nature* **271**, 321-325.

MOORE, P. G. (1977): Inorganic particulate suspensions in the sea and their effects of marina animals. *Oceanography and marine Biology Annual Reviews* **15**, 225-363.

MOORE, R. D. (1983): On the use of bulk aerodynamic formulae over melting snow. *Nordic Hydrology* **14** (4), 193-206.

MORRIS, E. M. (1989): Turbulent transfer over snow and ice. *Journal of Hydrology* 108, 205-223.

MORRIS, E. M. (1999): Surface ablation rates on Moraine Corrie Glacier, Antarctica. *Global and Planetary Change* **22**, 221-231.

MORRIS, E.M. & HARDING, R. J. (1991): Parametrization of turbulent transfer between glaciers and the atmosphere. *International Association of Hydrological Sciences* (IAHS) *Publication* 208, 543-549.

MORRIS, E. M. & VAUGHAN, D. G. (1992): Snow surface temperatures in west Antarctica. In MORRIS, E. M. (ed.): *The contribution of Antarctic Peninsula ice to sea level rise*. *British Antarctic Survey Ice & Climate Special Report* **1**, 17-24.

MORRIS, E. M., ANDERSON, P.S., BADER, H.-P., WEILEMANN, P. & BLIGHT, C. (1994): Modelling mass and energy exchange over polar snow using the DAISY model. *Snow and Ice Cover: Interactions with Atmosphere and Ecosystems* (Proceedings of Yokohama Symposia J2 and J5, July 1993), *IAHS Publ*. **223**, 53-60.

MOTOI, T., KITOH, A. & KOIDE, H. (1998): Antarctic Circumpolar wave in a coupled ocean-atmosphere model. *Annals of Glaciology* **27**, 483-487.

MUNRO, D. S. & J. A. DAVIES (1977): An experimental study of the glacier boundary layer over melting ice. *Journal of Glaciology* **18** (80), 425-436.

MUNRO, S. (1989): Surface roughness and bulk heat transfer on a glacier: comparison with eddy correlation. *Journal of Glaciology* **35** (121), 343-348.

MUSER, D. (1995) Der Gletscherrückzug auf King George Island, South Shetland Islands zwischen 1956 und 1992. Eine digitale Auswertung von Karten, Luftbildern und Satellitendaten. Unpublished thesis, Albert-Ludwigs-Universität Freiburg, 82 p.

NEAL, S. M. & FITZHARRIS, B. B. (1997): Energy balance and synoptic climatology of a melting snowpack in the southern alps, New Zealand. *International Journal of Climatology* **17**, 1595-1609.

NELLIS, M. D., HARRINGTON JR., J. A. & WU, J. (1998): Remote sensing of temporal and spatial variations in pool size, suspended sediment, turbidity, and Secchi depth in Tuttle Creek Reservoir, Kansas: 1993. *Geomorphology* **21**, 281-293.

NESJE, A. & DAHL, S. O. (2000): Glaciers and environmental change. Arnold. London. 203 p.

NOBEL, H. M. (1959): Report on Glaciological Observations at Admiralty Bay, King George Island, South Shetland Islands, 1957-58. *Falkland Islands Dependencies Survey I.G.Y. Glaciological Report*, unpublished.

NOBLE, H. M. (1965): Glaciological observations at Admiralty Bay, King George Island, in 1957-58. *British Antarctic Survey Bulletin* **5** (41), 1-11.

O'FARRELL, S. P. & CONNOLLEY, W. M. (1998): Comparison of warming trends predicted over the next century around Antarctica from two coupled models. *Annals of Glaciology* **27**, 565-570.

OERLEMANNS, J. (1993): Modelling of glacier mass balance. In PELTIER, W. R. (ed.), Ice in the climate system. Berlin, Springer Verlag, *NATO ASI Series I: Global Environemntal Change*, 101-116.

OERLEMANNS, J. (1994): Quantifying global warming from the retreat of glaciers. *Science* **264**, 243-245.

OERLEMANNS, J. (2000): Analysis of a 3 year meteorological record from the ablation zone of Moteratschgletscher, Switzerland: energy and mass balance. *Journal of Glaciology* **64** (155), 571-579.

OERLEMANNS, J. & Reichert, B. K. (2000): Relating glacier mass balance to meteorological data by using a seasonal sensitivity characteristic. *Journal of Glaciology* **46** (152), 1-6.

OERLEMANNS, J., ANDERSON, B., HUBBARD, A., HUYBRECHTS, P., JOHANNESSON, T., KNAP, W. H., SCHMEITS, M., STROEVEN, A. P., VAN DE WAL, R. S. W., WALLINGA, J. & ZUO, Z. (1998): Modelling the response of glaciers to climate warming. *Climate Dynamics* **14**, 267-274.

OHMURA, A., KONZELMANN, T., ROTACH, M., FORRER, J., WILD, M., ABE-OUCHI, A. & TORITANI, H. (1994): Energy balance for the Greenland ice sheet by observation and model computation. *Snow and Ice Covers: Interactions with the atmosphere and ecosystems* (Proceedings of Yokohama Syposia J2 and J5, July 1993, *IAHS Publ.* **223**, 85-94.

OKE, T. (1987): Boundary layer climates. Routledge, London, New York, 435 p.

ORHEIM, O. (1972): A 200 year record of glacier mass balance at Deception Island, southwest Atlantic Ocean, and its bearing on model of global climatic change. *Dissertation Abstracts International* **B 33** (4), 1620.

ORHEIM, O. & GOVORUKHA, L. S. (1982): Present-day glaciation in the South Shetland Islands. *Annals of Glaciology* **3**, 233-238.

ORHEIM, O., BULL, C. & SCHYTT, V. (1972): Glaciological studies of past climatic variations in the South Shetland Islands. *Antarctic Journal of the United States* **7** (4), 99-100.

PANKHURST, R. J. & SMELLIE, J. L. (1983): K-Ar geochronology of the South Shetland Islands, Lesser Antarctica: apparent lateral migration of Jurrassic to Quaternary island arc volcanism. *Earth and Planetary Science Letters* **66**, 214-222.

PARISH, T. R. (1983): The influence of the Antarctic Peninsula on the wind field over the western Weddell Sea. *Journal of Geophysical Research* **88** (C4), 2684-2692.

PARK, B.-K., CHANG, S.-K., YOON, H. I. & CHUNG, H. (1998): Recent retreat of ice cliffs, King George Island, South Shetland Islands, Antarctic Peninsula. *Annals of Glaciology* **27**, 633-635.

PARKINSON, C. L. (1994): Spatial patterns in the length of sea ice season in the Southern Ocean. 1979-1986. *Journal of Geophysical Research* **99** (16), 16237-16339.

PARTINGTON, K. C (1998): Discrimination of glacier facies using multi-temporal SAR data. *Journal of Glaciology* **44** (146), 42-53.

PATERSON, W. S. B. (1994): The physics of glaciers. Third edition. Oxford, etc., Elsvier.

PAULO A. & TOKARSKI, A. K. (1982): Geology of the Turrent Point – Three Sisters Point area, King George Island (South Shetland Islands, Antarctica). *Studia Geologica Polonia* **74**, 81-103.

PECHERZEWSKI (1980): Distribution and quantity of suspended matter in Admiralty Bay (King George Island, South Shetland Islands). *Polish Polar Research* **1** (1), 75-82.

PEDDERSEN, O. B., CHRISTIANSEN, C. & LAURUS, M. B. (1995): Wind-induced long term increase and short term fluctuations of shallow water suspended matter and nutrient concentrations, Ringkbing Fjord, Denmark. *Ophelia* **41**, 273-287.

PEEL, D. A. (1992a): Spatial temperature and accumulation rate variations in the Antarctic Peninsula. In MORRIS, E.M*. (ed.): The contribution of Antarctic Peninsula ice to sea level rise. British Antarctic Survey Ice & Climate Special Report* **1**, 11-15.

PEEL, D. A. (1992b): Ice core evidence from the Antarctic Peninsula region. In BRADLEY, R. S. & P. D. JONES (eds.): *Climate Since A.D. 1500*. London, Routledge, 549-570.

PEEL, D. A., MULVANEY, R., PASTEUR, E. C. & CHENERY, C. (1996): Climate changes in the Atlantic sector of Antarctica over the past 500 years from ice-core and other evidence. In JONES, P.D., BRADLEY, R.S. & JOUZEL, J. (eds.): *Climate Variations and Forcing Mechanisms*. *NATO ASI Series 141*, 243-262.

PEPPER, J. (1954): The meteorology of the Falkland Island and Dependencies 1944-1950. C. F. Hidgson and son LTD, London.

PFENDER, M. (1999): Topographie und Glazialhydrologie von King George Island, Antarktis. Unpublished Diploma Thesis, University of Münster.

PLATT, H. M. (1979): Ecology of the King Edward Cove, South Georgia: macrobenthos and the benthic environment. *British Antarctic Survey Bulletin* **49**, 231-238.

PRANDTL, L. (1934): The mechanics of viscous fluids (Aerodynamic theory). In DURAND (ed.): Vol. 3, Division G, Berlin.

PROŠEK, P., JANOUCH, M. & KRUSZEWSKI, G. (1996): Components of the radiation balance and their regime in the summer of 1994/95 at H. Arctowski station (the South Shetlands). *Komitet Badań Polarnych Polskiej Akademii Nauk*. Komisja Meteorologii i Klimatologii, Gdynia, 107-135.

PROŠEK, P., JANOUCH, M. & LÁSKA, K. (2000): Components of the energy balance of the ground surface and their effect on the thermics of the substrata of the vegetation oasis at Henryk Arctowski station, King George Island, South Shetland Islands. *Polar Record* **26**, 3-18.

PUDSEY C: F., P. F. BAKER & LARTER, R. D. (1994): Ice shelf retreat from the Antarctic Peninsula shelf. *Continental Shelf Research* **14** (15), 1647-1675.

RACHLEWICZ, G. (1995): Ablation of Ecology Glacier, King George Island (South Shetland Islands) in the year 1991. *XXII Sympozjum Polarne*, Wroclaw - Ksiaz.

RACHLEWICZ, G. (1997): Mid-winter thawing in the vicinity of Arctowski Station, King George Island. *Polish Polar Research* **18** (1), 15-24.

RACK, W., ROTT, H., SIEGEL, A. & SKVARCA, P. (1999): The motion field of northern Larsen Ice Shelf derived from satellite imagery. *Annals of Glaciology* **29**, 261-266.

RACK, W., ROTT, H., SIEGEL, A., DOAKE, C. S. M. & SKVARCA, P. (2000). Interferometric Analysis of the Deformation Pattern of the northern Larsen Ice Shelf, Antarctic Peninsula, compared to Field measurements and Numerical Modeling. *Annals of Glaciology* **31**, 205-210.

RAKUSA-SUSZCZEWSKI, S. (1993): The maritime Antarctic coastal Ecosystem of Admiralty Bay. Department of Antarctic Biology, Polish Academy of Sciences, Warsaw, 216 p.

RAKUSA-SUSZCZEWSKI, S. (1995): The hydrography of Admiralty Bay and its inlets, coves and lagoons (King George Island, Antarctica). *Polish Polar Research* **16** (1/2), 61-70.

RAKUSA-SUSZCZEWSKI, S. (in press): Landscape, climate and geoecosystem changes in Admiralty Bay, South Shetland Islands, Maritime Antarctic. In BÖLTER, M. (ed.),: *GeoEcology of Terrestrial Antarctic Oases*. Springer Verlag.

RAKUSA-SUSZCZEWSKI, R.; BATTKE, Z. & CISAK, J., (1993), Morphometry of the Admiralty Bay shores and basins. In RAKUSA-SUSZCZEWSKI, S. (ed.) (1993), *The maritime Antarctic coastal Ecosystem of Admiralty Bay*. Department of Antarctic Biology, Polish Academy of Sciences, Warsaw, 27-30.

RAMAGE, J. M. & ISACKS, B. L. (1998): Seasonal changes in Alaskan Radar Glacier Zones. *Proceedings of the final RADARSAT Application Development and Research Opportunity (ADRO) Symposium*, 13-15th of October 1998, Montreal. CD-ROM.

RAMAGE,J. M., ISACKS, B. I. & MILLER, M. M. (2000): Radar glacier zones on southeast Alaska, U.S.A.: field and satellite observations. *Journal of Glaciology*, **46** (153), 287-296.

RAMOS, A., SOBRINO, I., GILDE SOLA, L. & PIÑERO, C (1987): Un examen general del macrobentos de los archipelagos del arco de escotia, encontrados durante la campaña „Antartida 8611“. *Actas del segundo symposium español de estudias antarticos, Consejo superior de investigaciones cientificas*, Madrid, 353-364.

RAU, F. & SAURER, H. (1998): Investigations into snow cover dynamics on two glaciers in the central Marguerite Bay (Antarctic Peninsula) using ERS and RADARSAT SAR imagery. *Proceedings of the Final RADARSAT Application Development and Research Opportunity (ADRO) Symposium*, 13-15th of October 1998, Montreal. CD-ROM.

RAU, F. & BRAUN, M. (submitted): The regional distribution of the dry snow zone on the Antarctic Peninsula north of 70° South. *Annals of Glaciology* **34**.

RAU, F., BRAUN, M., FRIEDRICH, M., WEBER, F. & GOßMANN, H. (2001): Radar glacier zones and their boundaries as indicators of glacier mass balance and climatic variability. In Wunderle & Nagler (eds.*): Proceedings of the 2nd EARSeL Workshop - Special Interest Group Land Ice and Snow*, June 16-17, 2000, Dresden, CD-ROM.

RAU, F., BRAUN, M., SAURER, H., GOßMANN, H., KOTHE, G., WEBER, F., EBEL, M. & BEPPLER, D. (2000): Monitoring multi-year snow cover dynamics on the Antarctic Peninsula. *Polarforschung* **67** (1/2), 27-40.

RAUSCHERT, M. (1991): Ergebnisse der faunistischen Arbeiten im Benthal von King George Island (Süd Shetland Inseln, Antarktis). *Berichte zur Polarforschung* **76**, 75 p.

REIJMERS, C., GREULL, W. & J. OERLEMANNS (1999): The annual cycle of meteorological variables and the surface energy balance on Berkner Island, Antarctica. *Annals of Glaciology* **29**, 49-54.

REINIGER, K.-D. & ZIMMER, A. (2000): The German Antarctic receiving station within the international ground segment for remote sensing. *Polarforschung* **67** (1/2), 3-6.

REISWIG (1971): In situ pumping activities of trpoical Demospongiae. *Martime Biology* **9**, 38-50.

REN, J. (1990): Temperature regime of the glaciers in the neighbourhood of Great Wall Station, Antarctica. *Antarctic Research* **2** (2), 22-27.

REYNOLDS, J. M. (1981): The distribution of mean annual temperatures in the Antarctic Peninsula. *British Antarctic Survey Bulletin* **54**, 123-133.

ROTT, H. & MÄTZLER, C. (1987): Possibilities and limits of synthetic aperture radar for snow and glacier surveying. *Annals of Glaciology* **9**, 195-199.

ROTT, H. & NAGLER, T. (1993): Snow and glacier investigations by ERS-1 SAR. First results. *Proceedings of the 1st ERS-1 Symposium, Space at the Service of our Environment*, Cannes, France, 4-6 November 1992, ESA SP-359 (March 1993), 577-852.

ROTT H., SKVARCA, P. & NAGLER, T. (1996): Rapid Collapse of Northern Larsen Ice Shelf. *Science*, **271**, 788-792.

ROTT, H., RACK, W., NAGLER, T. & SKVARCA, P. (1998): Climatically induced retreat and collapse of northern Larsen Ice Shelf, Antarctic Peninsula. *Annals of Glaciology* **27**, 86-92.

SADLER, I. (1968): Observations on the ice cap of Galindez and Skua Islands, Argetine Islands. 1960-66. *British Antarctic Survey Bulletin* **17**, 21-49.

SÁIZ-SALINAS, J. I., RAMOS, A., GARCÍS, F. J., TRONCOSO, J. S., SAN MARTIN, G., SANZ, C. & PALACIN, C. (1997): Quantitative analysis of macrobenthic soft-bottom assemblages in South Shetland waters (Antarctica). *Polish Biolology* **17** (4), 393-400.

SAMSON, J. (1989): Antarctic Surface temperature time series. *Journal of Climate* **2**, 1164-1172.

SAURER, H., WUNDERLE, S., & GOSSMANN, H. (1998): Radarfernerkundung der Antarktischen Halbinsel. *Geographische Rundschau* **50**, 71-77.

SCAMBOS, T. A., HULBE, C., FAHNESTOCK, M. & BOHLANDER, J. (2000): The link between climate warming and break-up of ice-shelves in the Antarctic Peninsula. *Journal of Glaciology* **46** (154), 516-530.

SCAR, Scientific Committee on Antarctic Research (1993): The role of Antarctica in Global Change, An International Plan for a Regional Research Programme.

SCHLOSS I., FERREYRA G. & KLÖSER, H. (1998): Seasonal variation of the conditions for phytoplankton growth in Potter Cove. *Berichte zur Polarforschung* **299**, 59-66.

SCHLOSS, I., KLÖSER, H., FERREYRA, G., CURTOSI, A., MERCURI, G. & PENOLA, E. (1997): Factors governing phytoplancton and particulate matter variation in Potter Cove, King George Island (Antarctica). In BATTAGLIA, B., VALENCIA, J. & WALTON, D. W. H. (eds.): *Antarctic Communities.* Cambridge University Press, 135-141.

SCHMIDT R., MÄUSBACHER, R. & MÜLLER, J. (1990): Holocene diatom flora and stratigraphy from sediment cores of two Antarctic lakes (King George Island). *Journal of Paleolimnology* **3**, 55-74.

SCHNEIDER, C. (1998): Zur raumzeitlichen Differenzierung der Energiebilanz und des Zustandes der Schneedecke auf zwei Gletschern der Marguerite Bay, Antarktische Halbinsel. *Freiburger Geographische Helfte* **56**, 251 p.

SCHNEIDER, C. (1999): Energy balance estimates during the summer season of glaciers of the Antarctic Peninsula. *Global and Planetary Change* **22**, 117-130.

SCHNEIDER, C. & GOßMANN, H. (1999): Klima und Klimawandel am Rande der Antarktis - Die Antarktische Halbinsel. *Geographische Rundschau* **51** (9), 469-476.

SCHNEIDER C., WUNDERLE, S. & FRIEDRICH, M. (1997): Snow cover investigations by means of ground truth, modelling and ERS-SAR imagery. In WUNDERLE, S. (ed.): *Proceedings of the EARSeL workshop 'Remote Sensing of Land Ice and Snow'*, University of Freiburg, Germany, 17.-18. April 1997, Paris, 95-102

SCHWERDTFEGER, W. (1970): The climate of the Antarctic. In: ORVIG, S. (ed.): Climates of the Polar Regions, *World Survey of Climatology* **14**, Elsevier Publishing Company, Amsterdam – London - New York, 253-369.

SCHWERDTFEGER, W. (1975): The effect of the Antarctic Peninsula on the temperature regime of the Weddell Sea. *Monthly Weather Review* **103**, 45-51.

SCHWERDTFEGER, W. (1976): Changes of temperature field and ice conditions in the area of the Antarctic Peninsula. *Monthly Weather Review* **104**, 1441-1443.

SCHWERDTFEGER, W. (1984): Weather and climate of the Antarctic. Amsterdam, Elsvier Scientific Publishers.

SHI, J. & DOZIER, J. (1993): Measurements of snow- and glacier-covered areas with single-polarization SAR. *Annals of Glaciology* **17**, 72-76.

SHI, J. & DOZIER, J. (1995): Inferring snow wetness using C-band data from SIR-C's polarimetric synthetis aperture radar. *IEEE Transactions on Geoscience and Remote Sensing* **33** (4), 905-914.

SICINSKI, J., RÓŻYCKI, O. & KITTEL, W. (1996): Zoobenthos and sooplankton of Herve Cove, King George Island, South Shetland Islands, Antarctic. *Polish Polar Research* **17** (3/4), 221-238.

SIEVERS, J. & THOMSON, J. (1995): Adopting one name per feature on maps of Antarctica: an experimental application - Topographic Map (Satellite Image Map) 1:250 000 Trinity Peninsula SP21-22/13. *Polarforschung* **65** (3), 123-131. (published in 1998).

SIMMONDS, I. & JONES, D. A. (1998): The mean structure and temporal variability of the semiannual oscillation in the southern extratropics. *International Journal of Climatology* **18**, 473-504.

SIMMONDS, I. & WU, X. (1993): Cyclone behavious to changes in winter southern hemisphere sea-ice concentration. *Quaternary Journal of the Royal Meteorological Society* **119** (513), 1121-1148.

SIMMONDS, I., JONES, D. A. & WALLAND, D. J. (1998): Multi-decadal climate variability in the Antarctic region and global change. *Annals of Glaciology* **27**, 617-621.

SIMÕES, J. C. & DANI, R. (1994): Levantamento e monitoramento de geleiras de pqeueno porte: Península Keller, Ilha Rei Jorge, Antártica*. Boletim de reumos Expandidos, 38° Congreso Brasileiro de Geologia*, 349-351..

SIMÕES, J. C. & BREMER, U. F. (1995): Investigation of King George Island ice cover using ERS1 SAR and SPOT imagery. Symposium “La Antarctica: un continente relevado”, Ushuaia, 1995. *Selper* **11** (1/2), 56-60.

SIMÕES, J. C., BREMER, U. F., AQUINO, F. E. & FERRON, F. A. (1999): Morphology and variations of glacial drainage basins in the King George Island ice field, Antarctica. *Annals of Glaciology* **29**, 220-224.

SINCLAIR, M. R. (1994): An objective cyclone climatology for the southern hemisphere. *Monthly Weather Review* **122**, 2239-2256.

SINCLAIR, M. R. (1996): A climatology of anticyclones and blocking for the Southern Hemisphere. *Monthly Weather Reviews* **124**, 245-263.

SKVARCA, P. (1993): Fast recession of the northern Larsen Ice Shelf monitored by space images. *Annals of Glaciology* **17**, 317-321.

SKVARCA, P. (1994): Changes and surface features of the Larsen Ice Shelf, Antarctica, derived from Landsat and Kosmos mosaics. *Annals of Glaciology* **20**, 6-12.

SKVARCA, P., RACK, W., ROTT, H. & IBARZÁBAL Y DONÁNGELO, T. (1998): Evidence of recent climatic warming on the eastern Antarctic Peninsula. *Annals of Glaciology* **27**, 628-632.

SKVARCA, P., RACK, W. & ROTT, H. (1999a): 34 year satellite time series to monitor characteristics, extent and dynamics of Larsen B Ice Shelf, Antarctic Peninsula. *Annals of Glaciology* **29**, 255-260.

SKVARCA, P., RACK, W., ROTT, H. & IBARZÁBAL Y DONÁNGELO, T. (1999b): Climatic trend, retreat and disintegration of ice shelves on the Antarctic Peninsula: an overview. *Polar Research* **18** (2), 151-157.

SMELLIE J. L., PANKHURST, J., THOMSON, M. R. A. & DAVIES, R. E. S. (1984): The geology of the South Shetland Islands: VI. Stratigraphy, geochemistry and evolution. *British Antarctic Survey Scientific Reports* **87**, 85 p.

SMITH, A. M., VAUGHAN, D. G., JOHNSON, A. C. & DOAKE, C. S. M. (1998): Surface lowering of Rothera Point ice ramp in response to regional climate change: *Annals of Glaciology* **27**, 113-118.

SMITH, I. N., BUDD, W. F. & REIS, P. (1998): Model estimates of Antarctic accumulation rates and their relationship to temperature changes. *Annals of Glaciology* **27**, 246-250.

SMITH, R. C. & STEARNS, C. R. (1993): Antarctic pressure and temperature anomalies surrounding the minimum in the Southern Oscillation Index. *Journal of Geophysical Research* **98** (D7), 13071-13083.

SMITH, L. C., FORSTER, R. R., ISACKS, B. I. & HALL, D. K. (1997): Seasonal climatic forcing of alpine glaciers revealed with orbital synthetic aperture radar. *Journal of Glaciology*, **43** (145), 480-448.

SMITH, R. C., STAMMERJOHN, S. E. & BAKER, K. S. (1996): Surface air temperature variations in the western Antarctic Peninsula region. *Antarctic Research Series* **70**, 105-121.

SMITH, R. I. L. (1990): Signy Island as a paradigm of biological and environmental change in Antarctic terrestial ecosystems. In KERRY, K. R. & HEMPEL, G. (eds.): *Antarctic Ecosystems. Ecological Change and Conservation*. Springer-Verlag, Berlin, 32-50.

SPLETTSTOESSER, J. (1992): Antarctic Global Warming? *Nature* **355**, 503.

STAMMERJOHN, S. E. & SMITH, R. C. (1996): Spatial and temporal variability of western Antarctic Peninsula sea ice coverage. - IN: ROSS, R. M., E. E. HOFMANN; L. B. QUETIN (eds.): *Foundations for Ecological Research West of the Antarctic Peninsula*, Washington, D.C., 81-104.

STAMMERJOHN, S. E. & SMITH, R. C. (1997): Opposing southern climate pattern as revealed by trends in regional sea ice coverage. *Climate Change* **37**, 617-639.

STANSBURY, M. J. (1961a): Glaciological observations at Admiralty Bay (Lat. 62°05'S, Lon. 58°24'W), King George Island, South Shetland Islands, 1959-60. *Falkland Islands Dependencies Survey, Preliminary Glaciological Report* **4**, 45 p. (BAS Archives Document Reference: AD6/2/1961/S5).

STANSBURY, M. J. (1961b): Glaciological observations upon two cirque glaciers in the Falkland Islands Dependencies. Master thesis, University of Birmingham, unpublished.

STARK, P. (1994): Climatic warming in the central Antarctic Peninsula area. *Weather* **49**, 215-220.

STRETEN, N. A. & TROUP, A. J. (1973): A synoptic climatology of satellite observed cloud vortices over the Southern Hemisphere. *Quarterly Journal of the Royal Meteorological Society* **99**, 56-72.

STRETEN, N. A. & WENDLER, G. (1968): The midsummer heat balance of an Alaskan maritime glacier. *Journal of Glaciology* **7** (53), 431-440.

STROZZI, T. & MÄTZLER, C. (1995): In-situ backscattering measurements of snowcover with coherent scatterometers at 5.3 and 35 GHz. *Proceeding of IGARSS'95*, Firenze, IEEE Catalogue Nr. 95CH35777, 1502-1504.

SVERDRUP, H. U. (1936): the eddy conductivity of the air over a smooth snow field. *Geofysiske Publikasjoner* **11**, 5-69.

TAKEUCHI, Y., NARUSE, R., SATOW, K. & ISHIKAWA, N. (1999): Comparison of heat balance characteristics at five glaciers in the Southern Hemisphere. *Global and Planetary Change* **22**, 201-208.

THOMPSON, L. G., PEEL, D. A., MOSLEY-THOMPSON, E., MULVANEY, R., DAI, J., LIN, P. N., DAVIS, M. E. & RAYMOND, C. F. (1994): Climate since AD 1510 on Dyer Plateau, Antarctic Peninsula: evidence for recent climate change. *Annals of Glaciology* **20**, 420-426.

TOKARSKI A. K. (1987): Structural events in the South Shetland Islands (Antarctica). III. Barton Horst, King George Island. *Studia Geologica Polonica* **40**, 7-37.

TOKARSKI, A. K. (1984): Structural events in the South Shetland Islands (Antarctica). II. Tertiary volcanics and sediments south of Ezcurra Fault, King George Island. *Studia Geologica Polonica* **79**, 131-162.

TURNER, J. & ROW, M. (1989): Mesoscale vortices in the British Antarctic Territory. In TWITCHELL, P. F. & RASMUSSEN, E. A. (eds.): *Polar and Arctic lows*. A. DEEPAK Publishing, 347-356.

TURNER, J. & THOMAS, J. P. (1994): Summer-season mesocale cyclones in the Bellingshausen-Wedell region of the Antarctic and links with the synoptic-scale environment. *International Journal of Climatology* **14**, 871-894.

TURNER, J. & COLWELL, C. R. (1995): Temporal variability of precipitation over the western Antarctic Peninsula. *Preprints of the fourth conference on Polar Meteorology and Oceanography*. American Meteorological Society, Boston, 113-116.

TURNER J. & LEONARD, S. (1996): Synoptic scale weather systems around the Antarctic Peninsula from satellite imagery and model fields. *8th Conference on Satellite Meteorology and Oceanography*, January 28 - February 02 1996, Atlanta, Georgia, 574-577.

TURNER, J., COLWELL, C. R. & HARANGOZO, S. (1997): Variability of precipitation over the western Antarctic Peninsula from synoptic observations. *Journal of Geophysical Research* **102** (D12), 13999-14007.

TURNER, J., LEONARD, S., LACHLAN-COPE, T. & MARSHALL, G. J. (1998a): Understanding Antarctic Peninsula precipitation distribution and variability using a numerical weather prediction model. *Annals of Glaciology* **27**, 591-956.

TURNER, J., MARSHALL, G. J. & LACHLAN-COPE, T. A. (1998b): Analysis of synoptic-scale low pressure systems within the Antarctic Peninsula sector of the circumpolar trough. *International Journal of Climatology* **18**, 253-280.

ULABY, F. T., MOORE, R. K. & FUNG, A. K. (1986): Microwave remote sensing, active and passive. Vol. III., Addison-Wesley Publishing Company.

VAN DEN BROEKE, M. R. (2000a): The semiannual oscillation and Antarctic climate. Part 1: influence on near surface temperatures (1957-79). Antarctic Science 10 (2), 175-184.

VAN DEN BROEKE, M. R. (2000b): The semiannual oscillation and Antarctic climate. Part 2: recent changes. *Antarctic Science* **10** (2), 184-191.

VAN DEN BROEKE, M. R. (2000c): The semiannual oscillation and Antarctic climate,. Part 3: the role of near-surface wind speed and cloudiness. *International Journal of Climatology* **20**, 117-130.

VAN DEN BROEKE, M. R. (2000d): The semiannual oscillation and Antarctic climate,. Part 4: a note on sea ice cover in the Amundsen and Bellingshausen Seas. *International Journal of Climatology* **20**, 455-462.

VAN DEN BROEKE, M. R. (2000e): The semi-annual oscillation and Antarctic climate,. Part 5: impact on the annual temperature cycle as derived from NCEP/NCAR re-analysis. *Climate Dynamics* **16**, 369-377.

VAN DEN BROEKE, M. R. (in press): On the interpretation of Antarctic temperature trends. *Journal of Climate*.

VAN LOON, H. & SHEA, D. J. (1987): The southern Oscillation, VI. Anomalies of sea level pressure on the Southern Hemisphere and of Pacific sea surface temperatures during the development of a warm event. *Monthly Weather Reviews* **115**, 370-379.

VARELA, L. (1998): Hydrology of Matías and Potter Creeks. *Berichte zur Polarforschung* **299**, 33-39.

VAUGHAN, D. G. (1992): The ice shelves of the Antarctic Peninsula: changing climate and sea level. In MORRIS, E. M. (ed.): The contribution of Antarctic Peninsula ice to sea level rise, British Antarctic Survey, *Ice & Climate Special Report* **1**, BAS, Cambridge, 35-44.

VAUGHAN, D. G. & DOAKE, C. S. M. (1996): Recent atmospheric warming and retreat of ice shelves on the Antarctic Peninsula. *Nature* **379**, 328-331.

VAUGHAN, D. G., MANTRIPP, D. R., SIEVERS, J. & DOAKE, C. S. M. (1993): A synthesis of remote sensing data on Wilkins Ice Shelf, Antarctica. *Annals of Glaciology* **17**, 211-218.

VILAPLANA, J. M. & PALLÀS, R. (1994): Características y evolución del manto nivoso en Isla Livingston. In CACHO J. & D. SERRAT (eds.), *Actas del V Simposio Español de Estudios Antárticos,* Madrid, Comisión Interministerial de Ciencia y Tecnología, 279-290.

WÄGELE, J. W. & BRITTO, T. A. (1990): Die sublitorale Fauna der maritimen Antarktis. *Natur und Museum* **120** (9), 269-282.

WARREN, C. R. (1992): Iceberg calving and the glaciomarine record. *Progress in Physical Geography* **16** (3), 253-282.

WARREN, D. E. & TURNER, J. (1989): Studies of Antarctic mesoscale systems using satellite imagery and sounder data. In TWITCHELL, P. F. & E. A. RASMUSSEN (eds.*): Polar and Arctic lows*. A. DEEPAK Publishing, 389-400.

WARREN, S. G. (1982): Optical properties of snow. *Reviews of Geophysics and Space Physics* **20** (1), 67-89.

WCRP, World Climate Research Programme (1998): Climate and Cryosphere (CLIC), Organization of Internationally Co-ordinated Research Into Cryosphere and Climate. WMO/TD no. 867.

WEATHERLY, J. W., WALSH, J. E. & ZWALLY, H. J. (1991): Antarctic sea ice variations and seasonal air temperature relationships. *Journal of Geophsical Research* **96** (C8), 15119-15130.

WEIDICK, A. & MORRIS, E. M. (1998): Local glaciers surrounding the continental ice sheets. In HAEBERLE, W., HOELZLE, M. & SUTER, S. (eds.): *Into the second century of world-wide glacier monitoring – prospects and strategies*. UNESCO, Paris, *Studies and Reports in Hydrology* **56**, 197-207.

WEISCHET, W. (1979): Einführung in die allgemeine Klimatologie. Teubner Stuedienbücher, 256 p.

WELLER, G. (1992): Antartica and the detection of environmental change. *Philosophical Transactions of the Royal Society of London* **338**, 201-208.

WELLER, G. (1998): Regional impacts of climate change in the Arctic and Antarctic. *Annals of Glaciology* **27**, 543-552.

WELLER, G. & SCHWERDTFEGER, P. (1970): Thermal properties and heat transfer processes of snow of the central Antarctic plateau. *IAHS Publ.* **86**, 284-298.

WEN, J., KANG, J., XIE, Z., HAN, J. & LLUBERAS, A. (1994): Climate, mass balance and glacial changes on small dome of Collins ice cap, King George Island, Antarctica. *Antarctic Research* **5** (1), 52-61.

WEN, J., KANG, J., HAN, J., XIE, Z., LIU, L. & WANG, D. (1998): Glaciological studies on King George Island ice cap, South Shetland Islands, Antarctica. *Annals of Glaciology* **27**, 105-109.

WENDLER, G. & ISHIKAWA, N. (1973): Experimental study of the mount of ice melt using three different methods: A contribution to the International Hydrological decade. *Journal of Glaciology* **12** (66), 399-410.

WHITE, W. B. & PETERSON, R. (1996): An Antarctic circumpolar wave in surface pressure, wind, temperature and sea-ice extent. *Nature* **380**, 699-702

WIELBINSKA, D. & SKRZYPCZAK, E. (1988): Mean air temperatures at definite wind directions at Arctowski station, King George Island, West Antarctica. *Polish Polar Research* **9** (1), 133-145.

WIGLEY, T. M. L. & RAPER, S. C. B. (1995): A heuristic model for sea level rise due to the melting of small glaciers. G*eophysical Research Letters* **22**, 2749-2752.

WILLIAMS JR., R. S., HALL, D. K. & BENSON, C. S. (1991): Analysis of glacier facies using satellite techniques. *Journal of Glaciology* **37** (125), 120-128.

WINKLER, B., SCHULZ, F. & KAPPEN, L. (1998): Seasonal variations of abiotic factors in terrestrial habitats. *Berichte zur Polarforschung* **299**, 28-32.

WORKING GROUP OF GEODESY & GEOGRAPHIC INFORMATION (1999): Composite Gazetteer of Antarctica, Ver. 02/1999. http://www.pnra.it/SCAR_GAZE.

WUNDERLE, S. & GOSSMANN, H. (1995): Investigación de la dinámica de la capa de nieve de King George Island y de una región costera de Marguerite Bay (Antártica) por medio imágenes SPOT y ERS-1. *Selper* **11** (1/2), 65-71.

WUNDERLE, S. (1996): Die Schneedeckendynamik der Antarktischen Halbinsel und ihre Erfassung mit aktiven und passiven Fernerkundungsverfahren. - *Freiburger Georgaphische Hefte* **48**, 172 p.

WUNDERLE, S. & SCHMIDT, J. (2000): Fluctuations and ice-flow velocity of the Northeast and McGlary Glaciers on the Antarctic Peninsula derived from remote sensing data and SAR interferometry. *Polarforschung* **67** (1/2), 41-52.

XIE, Y. & CUI, Z. (1992): The environmental events on King George Island since the last glaciation. *Antarctic Research* **3** (2), 56-68.

YAN, M. (1997): A preliminary study on oxigen isotop of ice cores of Collins ice cap, King George Island, Antarctica. *Chinese Journal of Polar Science* **8** (1), 65-71.

YOON, H. I., KIM, Y., CHOE, M. Y. & NAM, S. H. (1994): Glaciomarine sedimentation and paleoglacial settings of Marian Cove, King George Island, Antarctica.

KORDI Research Papers (Korean Ocean Research & Development Institute) **11**, 1023-1030.

ZAMORUYEV, V. V. (1972): Results of glaciological observations at Bellingshausen station in 1968. *Sovetskaya Antarkticheskaya Ekspeditsiya Trudy* **55**, 135-144.

ZHANG, W., LIU, J. & WANG, C. (1997): Characteristics of major minerals in volcanic ash in ice core from Collins ice cap, King George Island, Antarctic. *Chinese Science Bulletin* **42** (10), 845-850.

ZHENG, X. & LIU, X. (1990): Geology of Fildes Peninsula, King George Island, West Antarctica. A Study on the stratigraphy and vulcanism. *Antarctic Research* **1** (1), 8-19.

ZHU, G., JING, X., HAN, J. & XINSHENG, G. (1994): Radar sounding and study of the bedrock topography on Collins ice cap. *Antarctic Research* **6** (2), 40-45.

ZUO, Z. & OERLEMANS, J. (1997): Contribution of glacier melt to sea-level rise since AD 1865: a regionally differentiated calculation. *Climate Dynamics* **13**, 835-845.